INFLUENCES OF BIOLOGICAL AND PHYSICAL HETEROGENEITIES ON MICROBIAL TRANSPORT THROUGH POROUS MEDIA

by
Jessica A. Lawson

A dissertation submitted to Johns Hopkins University in conformity with the requirements for the degree of Doctor of Philosophy

Baltimore, Maryland
September, 2015

Abstract

Although enhanced virus transport has been observed in anoxic aquifers, little is known about the effects of biological heterogeneity – including microbially-induced zonation of terminal electron-acceptor processes – on microbial transport in groundwater. An improved understanding of the influence of heterogeneities of physical and biological origin on microbial transport would benefit water supply and water reuse applications, including riverbank filtration (RBF).

Laboratory studies of planktonic *S. oneidensis* MR-1 cultures confirmed the influence of metabolic state, represented by electron acceptor conditions and growth phase, on transport-relevant surface properties of the organism. Discernible differences in zeta potential and apparent hydrophobicity (as measured by the MATH test) were detected between aerobic and anaerobic cultures. Zeta potentials were generally in the range of -4 to -10 mV. Results of EPS analysis were in qualitative agreement with the electrokinetic findings that nitrate-reducing cultures had lower net surface charge than aerobic cultures at log phase. However, similar qualitative agreement between the results of cell surface characterization by MATH and electrokinetic analyses was not observed. Our results confirm previous reports that charge, non-polar interactions, and steric factors contribute to adhesion and attachment behavior in complex ways, and further demonstrate that redox conditions can affect transport-relevant properties.

Stochastic modeling studies in one and three dimensions explored the influences of physical and biological heterogeneity on microbial transport. Both models showed the potential for heterogeneity to adversely impact system performance. The 1D model

demonstrated that correlations between biological and physical heterogeneities can influence virus breakthrough in complex, varied, and sometimes counterintuitive ways. The 3D study, based on a novel dimensionless framework to describe an RBF flow field, separated the contribution of the pumping-induced distribution of flow path lengths from the overall filtration behavior of the system. While a less linear flow field improves removals and apparent filtration efficiency, heterogeneity in hydraulic conductivity hurts filtration performance on average; physical and flow heterogeneities thus counteract each other. Our results further underscored how a failure to fully account for correlations between physical/flow heterogeneities and attachment processes can produce artificial scale dependency in macroscale estimates of attachment parameters.

Readers:

Edward J. Bouwer (Advisor)
Abel Wolman Professor of Environmental Engineering
Chair, Department of Geography and Environmental Engineering

Kai Loon Chen
Assistant Professor
Department of Geography and Environmental Engineering

Ciaran J. Harman
Assistant Professor
Department of Geography and Environmental Engineering

Charles C. Young
Assistant Research Professor
Johns Hopkins University Applied Physics Laboratory

Preface and Acknowledgements

The late M. Gordon Wolman (1924-2010), universally esteemed by those who had the good fortune to call him a colleague or teacher, was well-known among Ph.D. students in the Department of Geography and Environmental Engineering for asking interesting questions during qualifying exams. During my own departmental exam, he asked me whether I thought we – environmental engineers and scientists, loosely speaking – had learned anything from the environmental missteps of the 20th century. Confronted with the environmental challenges of the 21st century, were we doomed to repeat mistakes like DDT and MTBE? Was I optimistic or pessimistic? Surely the personal viewpoint of a young doctoral candidate is of little import; I hardly recall my own reply.

The true value of Reds's question is that it directs our attention outwards. It asks that we consider our research projects, our individual fields of expertise, our collective discipline, in larger context. And to do so, we must at least be aware of that larger context, of which a DoGEE education makes sure. The successful navigation of environmental issues exacerbated by changing demographics, land use, and climate will require the integration of multiple viewpoints and the participation of many actors. The water resources challenges of the 21st century will likely need both top-down and bottom-up approaches, an amalgam of engineering principles and more dynamic processes.

In that spirit, the work in this dissertation attempted to draw connections between disciplines as disparate as colloid chemistry and groundwater hydrology. The three main projects described in the following pages took three different approaches to the same underlying question: how does heterogeneity of physical or biological origin affect microbial transport? Through laboratory studies characterizing microbial surface properties, an exploration of biological heterogeneity in a 1D model system, and simulations of filtration in a heterogeneous 3D riverbank filtration setting, this thesis sought to contribute to the understanding of microbial transport through porous media in a drinking water supply context.

The work presented here was funded in part by Johns Hopkins University Dean's and Departmental Fellowships, and by a grant from the National Science Foundation Graduate Research Fellowship Program. I am fortunate to have done my graduate work in a department that nurtures a culture of rigorous inquiry, intellectual freedom, and social responsibility. Above all, I am grateful for the patient support of my advisor, my committee and the department; of many fellow students current and former; and of my friends and family.

JAL
September 2015

Table of Contents

List of Tables

List of Figures

1 Introduction and literature review

1.1 Motivation

Interactions between surface water and groundwater are essential to many modern water resources management strategies. Advances incited by water scarcity and enabled by modern technology have brought us beyond naturally-infiltrated groundwater pumped from hand-dug wells sunk below the water table to large-scale engineered systems that exploit the interconnectivity between groundwater and surface water.

Inseparable from the question of water supply is the matter of water quality. The mixing of surface water and groundwater, be it during natural infiltration or in an engineered system, provides an opportunity for transfer of natural and anthropogenic contaminants. Researchers have focused on the subsurface fate of compounds including nutrients [1, 2], agrochemicals [3, 4], pharmaceuticals [5-7], fuel components [8] and xenobiotics from landfill or waste-site leachate [9]. This dissertation investigates the transport of microbial contaminants, taking both laboratory and computer modeling approaches.

Microbial contamination of groundwater typically involves organisms of fecal origin. Infiltrating rainwater can wash organisms from sources in the unsaturated zone (e.g., agricultural operations and septic drain fields) into the aquifer below. Surface waters may be contaminated through release of insufficiently treated sewage, runoff from agricultural operations, or even from pets and wildlife. When these surface waters infiltrate to the subsurface in natural or engineered systems, groundwater may become contaminated.

Demonstrated sources for microbial groundwater contaminants are numerous. Groundwater sampling down gradient from a swine lot controlled animal feeding operation (CAFO) found fecal indicator organism concentrations that were four to twenty times higher than up-gradient samples [10]. Researchers studying a sewage-impacted, unconfined sandy aquifer have measured coliphage contamination originating from fecal matter in an overlying septic tank drain field [11]. Onsite sewage treatment and disposal systems for individual homes may pose a particular risk in coastal areas and other locations where seasonal high water table events can saturate septic drain fields, facilitating transport of sewage contaminants [12]. And shallow aquifer contamination has frequently been traced to leaky sewer lines, including incidents that have resulted in illness when the aquifer is a source of drinking water [13]. Several pathways for microbial contamination of groundwater are sketched in Figure 1-1.

Approximately 242 million Americans (about 85% of the entire U.S. population) depend on the public water supply, and 37% of the water in the public water supply comes from groundwater [14]. In spite of water quality regulations that apply in these systems, including mandated 4-log removal of viruses [15], microbial risk remains. For the 2009-10 reporting period, the most recent for which data is available, the CDC identified 28 drinking-water-borne disease outbreaks in public supply systems that sickened 980 people, killing eight of them [16]. Ten of those outbreaks were caused by deficiencies that occurred at a point under the jurisdiction of the water utility, i.e., in the source water, during treatment, or in the distribution system; and six of them involved microbial contamination in untreated or insufficiently treated groundwater. Furthermore,

in these ten instances, the source water was invariably groundwater or groundwater mixed with surface water.

In the previous reporting period (2007-08), there were 36 disease outbreaks associated with drinking water, causing 4,128 illnesses and three deaths [17]. Sixteen of these outbreaks were traced to deficiencies that fell under the jurisdiction of the water utility, 13 of which were associated with untreated or insufficiently treated groundwater. For the 2005-06 reporting period, three of 20 drinking-water-borne outbreaks were attributed to viruses, and norovirus was suspected in both of the outbreaks for which the etiology was officially unknown [18]. The combination of unknown etiologies and underreporting means that overall disease burden due to microbial contamination of drinking water is probably higher than CDC statistics suggest.

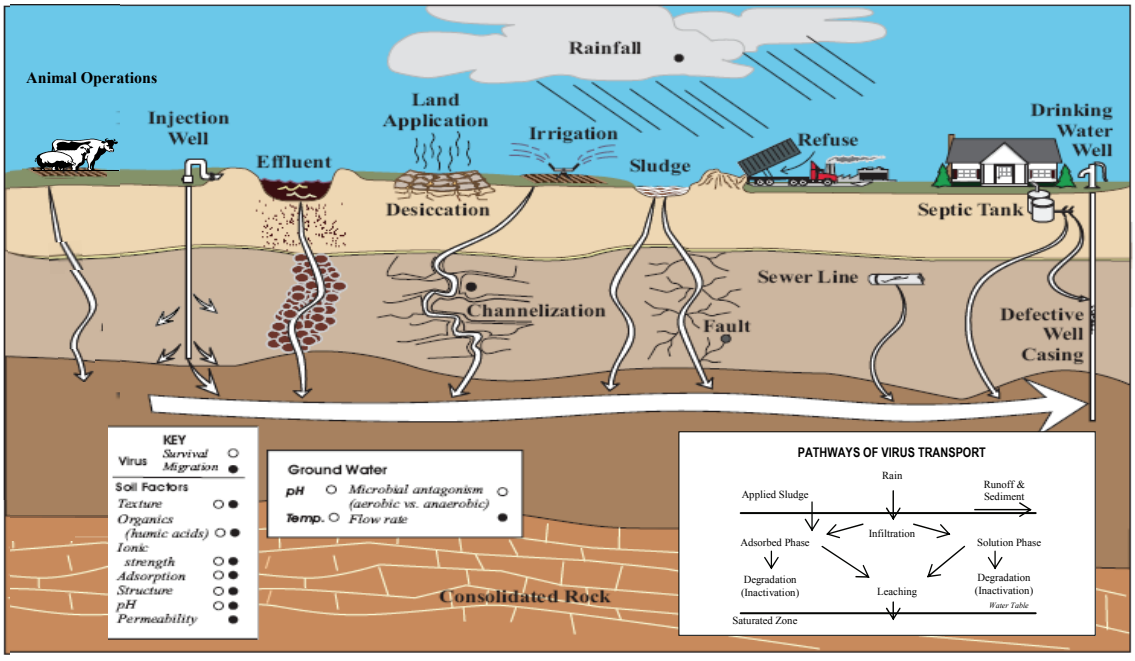

Figure 1-1: Pathways for microbial contamination of groundwater. Adapted from [19].

Another ~44 million Americans (the remaining 15% of the U.S. population) have their own drinking water source [14]. Their unregulated, private supplies range from springs or individual wellheads to community wells serving fewer than 25 individuals or 15 connections. The vast majority of these systems depend on groundwater and have little or no treatment. CDC summaries reported five drinking-water-borne disease outbreaks in private, unregulated systems in both 2009-10 and 2007-08 [16, 17]. For both periods, four of the five outbreaks were attributed to untreated groundwater. During the 2001-02 reporting period, nine of 23 groundwater-associated outbreaks occurred in private, unregulated wells [20].

Even deep groundwater in confined formations is not necessarily safe from pathogen contamination. A recent study conducted by the U.S. Geological Survey monitored six deep municipal drinking water supply wells in Madison, Wisconsin for enteroviruses, adenoviruses, rotavirus, hepatitis A virus (HAV), and noroviruses [21]. Every one of the wells tested positive multiple times during the 18-month sampling period, and many of the samples showed not only virus presence but also virus infectivity. Simultaneous sampling of local sewage and lake water suggested that leaky sewers were the most likely contamination source, and that transport into the groundwater was much faster than had been previously suspected.

Chlorine disinfection is an effective barrier against bacterial and viral contaminants, but when disinfection is absent, or in the event of treatment train failures, problems can arise. Beyond American borders, disinfection is not universal. Some countries, notably The Netherlands, do not disinfect groundwater that is to be used for drinking water [22], and in parts of the developing world, disinfection may be the

exception rather than the rule. The United Nations Environment Program [23] has estimated that as many as 2.75 billion people worldwide may depend on groundwater as their source of drinking water. More than half of the world's megacities (population over 10 million) used groundwater for at least 25% of the drinking water supply in the year 2000. Estimated groundwater contributions to drinking water supply range from 15% in Australia to 99% in Austria [24], with a European average around 75%. Over 50% of the potable supply in India and China comes from groundwater [24]. Little data is available for the African continent. Research that contributes to understanding of microbial transport in groundwater systems, particularly focusing on situations where enhanced pathogen transport may occur, has obvious relevance to engineering and water resources management decisions with public health implications in the US and abroad.

1.1.1 The structure of this dissertation

The work described in this thesis aimed to advance scientific understanding of factors influencing microbial transport in groundwater systems, particularly the influence of physical and biological heterogeneities. A combination of laboratory analyses and computer simulations were conducted, each focusing on a different dimension of the problem.

- The present introductory chapter reviews a wide range of background topics and literature that motivate and inform the work.
- The second chapter describes laboratory investigations undertaken to characterize the transport-relevant surface properties of a model microorganism, *Shewanella oneidensis*, grown under different terminal electron acceptor conditions. We demonstrate that a single organism can exhibit different characteristics as a

function of its metabolic state, which may in turn affect its potential for transport through porous media. We further pilot the development of a biofilm reactor with the aim of measuring similar changes in bulk surface properties of attached microbial growth.

- The third chapter presents a sensitivity analysis of filtration theory as a predictor for microbial transport and removal in aquifer settings, with a focus on the relative importance of those factors likely to exhibit biological or physical heterogeneity in natural systems. We then apply a simple 1D model to explore the potential influence of correlated biological and physical heterogeneities on microbial removal performance, with an application to a small field dataset.
- The fourth chapter proposes a framework for further investigation of the influences of coupled physical and biological heterogeneities when the simplifying assumption of 1D flow is not realistic. Using a more sophisticated, 3D model system, we demonstrate the application of this framework to a set of hypothetical riverbank filtration installations to analyze the relative importance of flow field heterogeneity and physical aquifer heterogeneity on microbial removals.
- The final chapter summarizes our findings and presents concluding remarks. It is followed by an appendix describing some method tests performed with MS2 bacteriophage, a common model organism for microbial transports studies in lab and field settings.

1.2 Groundwater systems of interest

1.2.1 General characteristics

When infiltrating surface waters pass through the unsaturated zone and farther into the saturated subsurface, physicochemical processes result in varying degrees of removal for a range of particulate contaminants, including bacteria, viruses, parasites, and suspended materials. Biological and geochemical processes can bring about the immobilization, degradation and/or transformation of organic matter and chemical contaminants such as pesticides, metals, and nitrogen species. Bacteria and other potentially pathogenic microbial contaminants can furthermore be inactivated by changing chemical conditions or simply by long subsurface travel times [25].

These physicochemical, biological, and geochemical processes largely result in a reduction of contaminant concentrations compared to the raw surface water, thus improving water quality if and when the infiltrated water is subsequently recovered. Dilution of the infiltrating water with (generally higher-quality) groundwater can bring about further reductions in the concentrations of surface-derived contaminants. A variety of water supply and management systems, discussed later in this section, are designed to exploit these beneficial processes.

1.2.1.1 Redox zonation, or zonation of terminal electron accepting processes (TEAPs)

As surface water moves into an aquifer, native soil microorganisms break down the organic matter present, using it as a substrate and carbon source, and transferring the electrons released during their metabolic processes to a terminal electron acceptor, thus linking the oxidation of organic carbon to the redox chemistry of the aquifer [26, 27].

Microbes deplete the most energetically-favorable electron acceptor first: oxygen. If they are metabolically able to do so, they then turn to the next-most energetically favorable. Otherwise they give way to different species that can derive energy by degrading the substrate under anaerobic conditions. The process continues until the substrate is depleted. When the oxygen present in infiltrating waters is insufficient to degrade all the organic matter, characteristic zonation of microbially-induced terminal electron acceptor processes develops [28]. These zones are depicted in a schematic in Figure 1-2, with simplified example reactions for the microbial oxidation of organic matter with each sequential electron acceptor.

Redox zone	**Oxidation-reduction reaction**	**ΔG^o(w) kJ/eq**
Aerobic respiration	$CH_2O + O_2 = CO_2(g) + H_2O$	-119
Nitrate reduction	$CH_2O + 4/5\ NO_3^- + 4/5\ H^+ = 2/5\ N_2(g) + CO_2(g) + 7/5\ H_2O$	-113
Manganese reduction	$CH_2O + 2MnO_2(s) + 4H^+ = 2Mn^{2+} + CO_2(g) + 3H_2O$	-96.9
Iron reduction	$CH_2O + 4Fe(OH)_3(am) + 8H^+ = 4Fe^{2+} + CO_2(g) + 11H_2O$	-46.7
Sulfate reduction	$CH_2O + 1/2\ SO_4^{2-} + 1/2\ H^+ = 1/2\ HS^- + CO_2(g) + H_2O$	-20.5

Free energies reported for pH=7 at 25°C [29]. Concentrations 1 M except $[Mn^{2+}] = [Fe^{2+}] = 10^{-6}$ M.

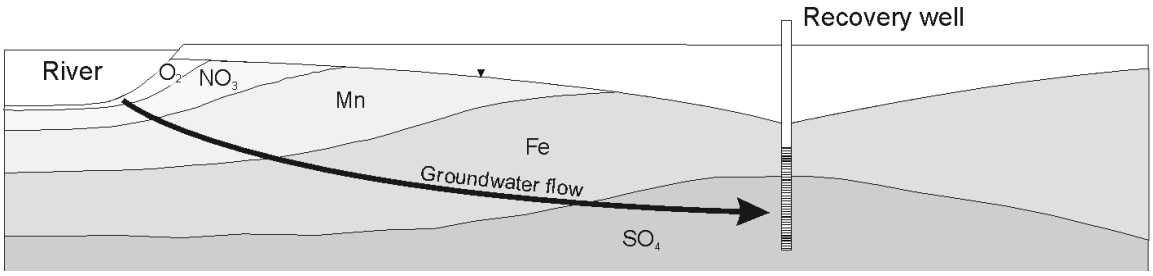

Figure 1-2: Microbially-induced redox zonation can develop when available dissolved oxygen is insufficient to degrade the organic material present. Adapted with permission from reference [30].

This "redox zonation" varies in space and time [31]. It has long been recognized, because it can be problematic when reduction of iron- and manganese minerals in anoxic zones causes increased levels of dissolved iron and manganese in the abstracted water [32-35]. These species must often be removed by subsequent treatment processes to avoid aesthetic problems (taste, color, staining).

Researchers have studied transport in aquifers nominally aerobic or anaerobic. However, to our knowledge, no one has yet analyzed the influence of redox zonation (specific TEAP regimes) on pathogen transport.

1.2.2 Riverbank filtration (RBF)

1.2.2.1 Operational characteristics

In Europe, riverbank filtration has been used for drinking water production for over a century [25]. In the U.S., interest in riverbank filtration (RBF) in the last 15-20 years has reflected water suppliers' attention to options for improving source-water quality [36], particularly in the period leading up to the finalization of the Long Term 2 Enhanced Surface Water Treatment Rule in 2006. The principle of RBF is simple. Rather than treating surface water directly, a set of production wells is installed adjacent to the river. Pumping from these wells induces flow from the river, through the banks and alluvial aquifer system, and into the well, with the subsurface materials acting as a "natural" filter. Lake bank filtration is a variant but similar system. A typology of RBF settings is shown in Figure 1-3. The configuration at the top left corner is believed to be the most common [37]. Unsaturated conditions below the river (center right) are unusual, representing a pumping rate that is mismatched with the hydraulic conductivity of the

riverbed. Many different lateral configurations are possible for horizontal collector wells (bottom right).

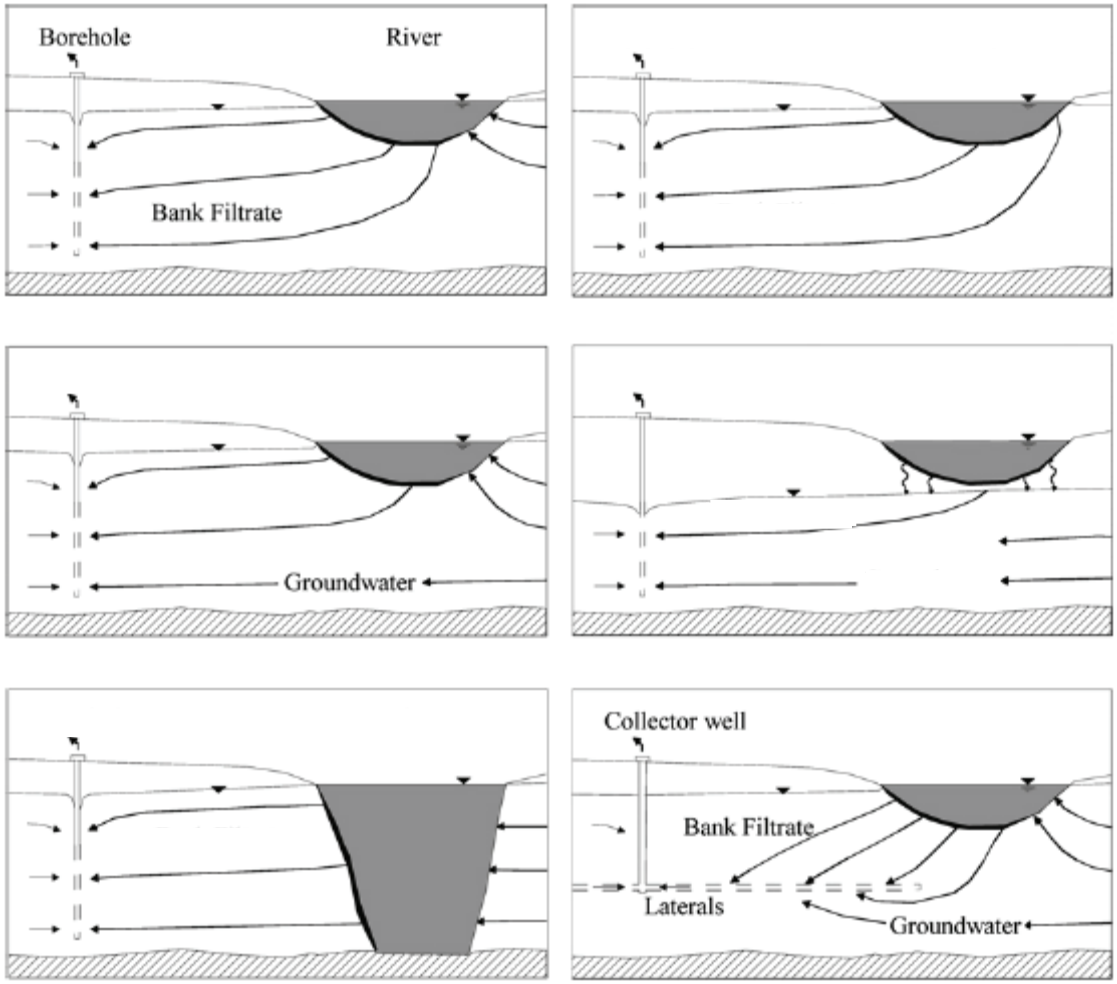

Figure 1-3. A typology of RBF settings. Reprinted from [37] with permission from Elsevier.

Riverbank filtration systems are typically installed in alluvial aquifers that have granular, water-bearing formations hydraulically connected to the riverbed. These formations are unconsolidated deposits of sand, clay, silt, pebbles, and larger size fractions. Fractured rock and coarse gravel aquifers are generally not appropriate as RBF sites because of the potential for high-velocity preferential flow paths to develop, along which little filtration would take place [38, 39]. The long-term presence of biologically

active zones around losing streams enhances attenuation processes, so RBF siting on losing reaches promotes the effective removal of organics and the establishment of stable water quality in the well [40].

A typical RBF well is 20 to 40 m deep and set back from the river by 20 to 300 m [41]. Wells in the U.S. are often on the shorter end of this range, whereas wells in Europe tend to be farther from the river. Subsurface residence times can vary from 5 to over 100 days, and are in practice a mix of values [25]. Hydraulic conductivities are generally on the order of 10^{-4} to 10^{-2} m/s (~10-100 m/d), and the European RBF experience suggests that average infiltration rates below ~0.2 m^3/d per m^2 of riverbed enhance system stability [40]. RBF wells are either standard vertical installations or horizontal wells. Horizontal wells have one or more radial collector arms arranged horizontally around a central vertical well shaft. These laterals may project beneath the riverbed itself, in which case travel times are greatly reduced and yields increase. Pumping rates vary enormously: one study of an RBF installation in Bolivia reported a sustainable pumping rate under 800 m^3/d for one well [42], while the horizontal collector well field located on islands in the Danube upstream of Budapest, Hungary has a production capacity of ~$1x10^6$ m^3/d, with individual wells that yield in excess of 10,000 m^3/d [39]. The six radial wells at the Russian River RBF site in Sonoma County, California are reported to provide a system capacity of 14,500 m^3/hr, corresponding to an average yield of 58,000 m^3/d per well [43].

1.2.2.2 Microbial performance characteristics

Monitoring results from existing RBF installations show that the technology can be effective in removing pathogens. Researchers in the Netherlands have reported that an

RBF system on the Meuse River achieves 5-log removal efficiency for pathogenic bacteria, viruses, and parasites under steady-state conditions [44]. The average groundwater residence time is 2 weeks. In this study, viruses of different sorts were present in surface water at 0.11 – 14 L^{-1}, *Giardia* cysts were present at 0.1-12 count/L, and *Cryptosporidium* oocysts were present at 0.3-26 count/L. However, no enteric viruses or protozoan (oo)cysts were ever detected in the water extracted from the pumping well, although well samples did occasionally test positive for other viruses, bacterial spores, and bacteria. Other researchers obtained similar results in studies of pathogen removal at RBF facilities on the Rhine in Germany [45].

Monitoring of an RBF site on the Ohio River at Louisville, KY has also shown good removal of bacteria. Over the course of a 7-month study period, total coliform removal ranged from 0.9 to >4.5 log removal with an average removal of 3.1 logs. Of the few well-water samples that did test positive for total coliforms, most were at the detection limit of 1 MPN (most probable number) per 100 mL [46].

One of the challenges in establishing removal efficiencies for pathogens, particularly protozoan pathogens, in RBF systems is that concentrations in surface water are generally low and analytical detection methods are not straightforward. These difficulties motivate the use of surrogates to establish microbial removals, despite concern over and continuing research into the merits of using e.g., bacterial spores, algae or diatoms to represent pathogen transport behavior [47]. Nonetheless, good removal of surrogates may be generally indicative of the performance of the RBF system, and many researchers do report surrogate removals. For example, the Louisville, KY study [48] reported >3-log reductions in total aerobic (bacterial) spores in the RBF system. This

removal compares favorably to the removal achieved by conventional or slow-sand filtration.

Another observational study of an RBF system in the U.S., this one on the Great Miami River in Ohio, showed good removal of protozoan pathogens. In fact, over 10 years of sporadic sampling, no *Cryptosporidium* oocysts or total coliforms were ever detected in well-water samples. A 3.6-log reduction in *Crytposporidium*-sized particles (a size-based surrogate) was observed over the flow path from the river to the well [49].

Lest the above removal performance statistics leave the impression that RBF systems are invariably reliable for pathogen removal, it should be mentioned that a number of outbreaks of cryptosporidiosis have also been associated with RBF in alluvial aquifers. As summarized by Schijven *et al.* [50], these outbreaks occurred in the 1990s in England, Canada, and Japan, and none of them were unequivocally linked to failure of the RBF system. Indeed it is often difficult to establish the precise cause of a waterborne disease outbreak.

Still, there is some evidence that RBF systems may be most susceptible to pathogen breakthrough when infiltration rates change, particularly during flood or high-flow conditions. In the Flehe Waterworks on the Rhine, high microbial counts in RBF filtrate were only observed at the beginning of flood periods. The researchers concluded that breakthrough was due to non-steady state conditions in newly saturated regions, which then quickly "adapted" [45]. In general, there is concern that the combination of increased infiltration rates and potentially shortened flow paths during flood conditions could adversely affect RBF system performance. In rivers where a significant "clogging layer" of fine silt and sediment is present in the riverbed, flood scour could disturb this

layer, and this too could make the RBF system more susceptible to pathogen breakthrough [50, 51].

1.2.2.3 Global relevance of RBF

Studies since the 1980s have investigated hydraulic and attenuation processes at U.S. and European RBF sites [1, 49, 52-57]. RBF serves in many cases as a pre-treatment technology with advantages over direct treatment of surface water for drinking water production, although use of RBF as a primary treatment technology is also possible [58]. European concerns have generally focused on mobilized inorganics and chemical pollutants present in river water (including, more recently, trace organics), while American investigations have focused on the removal of pathogens and, to a lesser extent, disinfection byproduct precursors.

A 2002 ES&T feature on bank filtration noted the potential for RBF to provide inexpensive quality improvements for poor-quality raw surface water [36]. That RBF is low-tech and low-capital compared to construction and operation of a conventional treatment plant, as well as being often more sustainable than pure groundwater withdrawal, makes the technology more attractive. Taking scientific publications as an indicator, the last decade has seen greatly increased interest in RBF beyond European and U.S. borders. Published studies of prospective, new, and existing RBF sites in southeast Asia (e.g., India [59-62], Bangladesh [63], Malaysia [64-66]), South America (e.g., Brazil [67, 68], Bolivia [42], Columbia [69]), Africa (e.g., Zimbabwe [70], Egypt [71]), Asia (e.g., China [72], Korea [73], Thailand [74]), and the Middle East (e.g., Jordan [75]) – to name a few – testify to the global relevance of RBF research. In some places, these RBF

wells provide the primary or only treatment between source and consumer. Researchers have also turned their attention to the potential effects of climate change on RBF system performance [76-78]. Clearly, an improved understanding of the underlying processes that govern RBF system performance – as distinct from accumulated, site-specific, operational expertise – will benefit water resources management worldwide.

1.2.3 Other relevant engineered systems

Insights about microbial transport gleaned from RBF are likely to be applicable in a number of other engineered groundwater management schemes, and vice versa. Despite differences in implementation and hydraulic characteristics – pumping vs. natural gradients, saturated vs. unsaturated conditions, the quality of the recharge water – these systems share a deliberate exploitation of subsurface passage to generate water quality improvements and/or water resource management benefits. The terminology used to refer to these systems and their many variants is somewhat fluid. Collectively, engineered aquifer recharge technologies have been hailed as essential to water reuse to meet current and future demands on water resources [79], although a number of challenges remain, including public perception, regulatory issues, and knowledge gaps related to contaminant transport. A schematic of several of the systems explained in the following paragraphs appears in Figure 1-4.

Dune filtration, best known in The Netherlands, uses a shallow infiltration ditch in a sandy, dune-like formation to retain surface water at higher elevation, thus supplementing infiltration. The artificially elevated water table induces groundwater flow through the highly permeable sand towards a down-gradient location where the water seeps out into an abstraction canal and is recovered as surface water [80]. A

subterranean drain system often helps capture infiltrated water and direct it towards the abstraction canals.

Managed Aquifer Recharge (MAR) is the deliberate and actively managed recharge of water to aquifers for subsequent recovery and use or environmental benefit [81]. Many MAR configurations are possible, but in the most general sense, non-potable water is retained behind a dam or in infiltration galleries situated in high-permeability soils. After sufficient time in operation, a "mound" of groundwater forms under the recharge area, raising the local water table. These schemes are sometimes termed "artificial recharge" or "induced infiltration," and may be implemented to counter the adverse effects (ecological damage, shallow wells run dry) of a water table depleted by drought or overuse. Subsurface residence times of the recharged water reflect the relatively shallow nature of these systems – weeks to months, depending on the distance between the infiltration basins and the point of withdrawal. Australia has made significant advances implementing the technology [82]. As a general term, MAR can also include aquifer storage and recovery (ASR) and soil aquifer treatment (SAT), which are each discussed below.

Aquifer storage and recovery (ASR) is a specific type of MAR that involves the injection of high-quality water into a confined aquifer so that it may be pumped out again at a later time [83]. Water, often treated to drinking water standards, is pumped down a well, typically into a deep formation, where it is banked for future withdrawal from the injection point. When water is instead withdrawn at a down-gradient well, the system is sometimes called aquifer storage, transport, and recovery (ASTR). AS(T)R offers advantages as a water storage technology – the ability to bank water seasonally and to

hold large volumes without the significant footprint or evaporative losses of surface reservoirs. Additionally, the outlet/withdrawal point can be at some distance from the inlet/injection without the need for any infrastructure to connect them. But ASR is often incorporated into water reuse strategies for other reasons, as well. Time underground and mixing with groundwater breaks the perceived "toilet-to-tap" pathway to overcome the yuck factor many consumers associate with direct potable reuse. The combination of dilution, biogeochemical transformations, and the absorptive capacity of the subsurface likely also reduces concentrations of anthropogenic trace compounds that are neither removed during wastewater treatment nor measured in drinking water standards. Typical residence times are highly variable, but are often engineered at months to years. Opportunities for pathogen transport are largely limited to accidental contamination through e.g., leaky boreholes or treatment deficiency in injected water, although contamination from natural sources cannot be ruled out. ASR has been widely implemented in arid areas, including the American southwest [84].

Soil aquifer treatment exploits the purifying capacity of soil processes to remove wastewater contaminants. Treated sewage, usually secondary effluent, is intermittently released into large, shallow basins and allowed to infiltrate naturally [83]. Alternate wetting and drying cycles with periodic scraping of the basin floor help to prevent clogging and maintain an elevated infiltration rate. A type of MAR, SAT can raise the local water table, but unlike MAR galleries that focus primarily on recharge, SAT is not operated to create a groundwater mound with fully saturated flow paths between the infiltration basin and the local water table. Due to the use of reclaimed water, the opportunity does exist for transport of pathogens and other anthropogenic contaminants

into the groundwater aquifer below an SAT site, although operation is generally optimized to reduce the risk of such transfers, and field studies have shown good SAT performance [85].

Septic drainfields serve to spread and infiltrate liquid waste from septic tanks that receive all the sewage and grey water from households that lack a connection to a municipal sanitary sewer. Solids settle out and anaerobic biological transformations reduce the organic content of the waste during its time in the underground septic tank, from which the liquid fraction flows out through buried, perforated pipes into a shallow gravel leachfield [86]. Similar to SAT, properly functioning septic drainfields maintain an unsaturated zone between the infiltration area and the water table below. However, poorly-installed systems, shallow or unusually high water tables, and flooding can all cause conditions conducive to the direct transfer of sewage-derived contaminants into an unconfined aquifer below. A number of contamination events and waterborne disease outbreaks have been traced to pathogens transported into local groundwater from septic drainfields [87, 88].

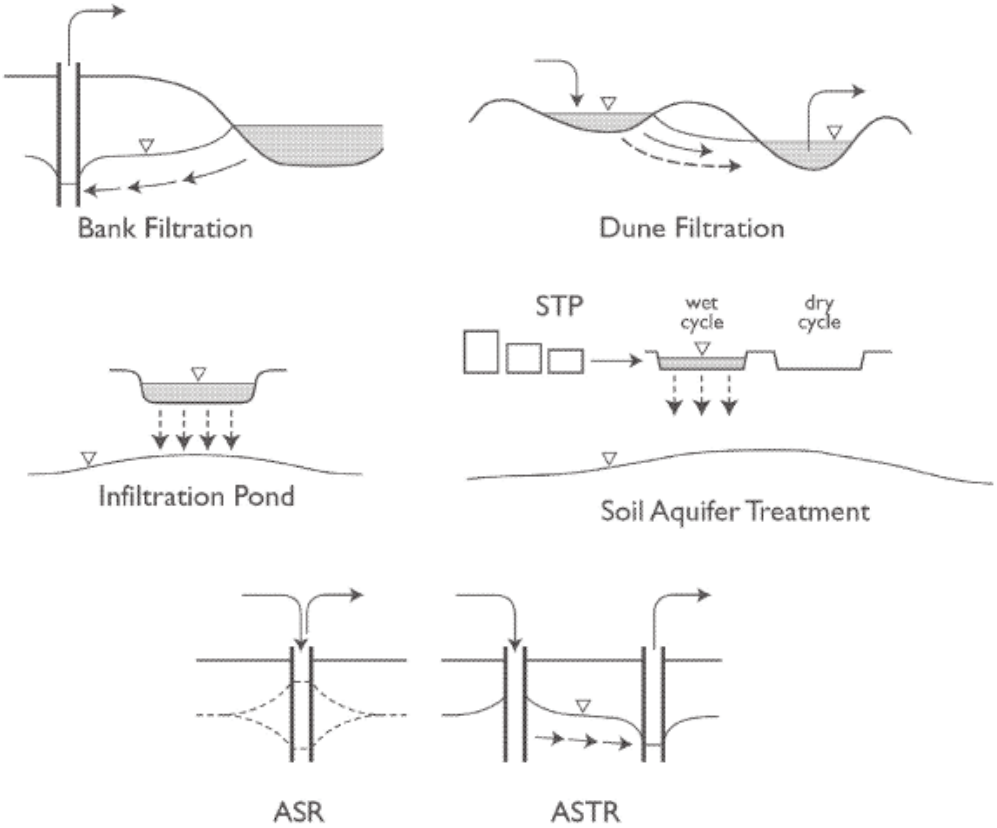

Figure 1-4. Cartoon of several related engineered systems for artificial supplementation of groundwater recharge. Adapted from Figure 1 in reference [89] with kind permission from Springer Science and Business Media.

1.3 Microbial transport and inactivation

1.3.1 Physicochemical principles of microbial transport in porous media

Pathogen removal in RBF systems is generally described by filtration theory. Viruses, bacteria, and protozoan (oo)cysts are treated as particles moving through saturated porous media. The advection-diffusion equation which was developed for packed beds [90] is frequently cited to describe the movement of particles and their interactions with the aquifer material:

$$\frac{dC}{dt} + \vec{v}_p \nabla C = D\nabla^2 C + \left(1 - \frac{\rho}{\rho_p}\right)\frac{mg}{3\pi\mu d_p}\frac{dC}{dz}. \qquad \text{(Eqn 1-1)}$$

Here, C is the concentration of suspended particles, $\vec{v}_p$ is the local flow velocity, t is time, D is particle diffusion coefficient, ρ and ρ_p are the respective densities of water and the particles, m and d_p are the particle mass and diameter, μ is the viscosity of water, g is the gravitational constant, and z is the coordinate axis in the direction of the gravitational force. The first term on the left describes the change in concentration over time at a given point. The second term describes the contribution of advection. On the right, the first term describes diffusion and the second gravitational settling. Interception of a particle by collision with the media is included in the boundary conditions. The equation cannot be solved analytically.

The attachment of a microorganism to a grain surface requires that the two come in contact with each other, and that this "collision" result in the microorganism "sticking" onto the collector surface. Using this conceptualization to simplify the advection-diffusion equation, filtration theory expresses the rate of (microbial or colloidal) particle attachment in terms of a "single collector efficiency" η_0 and a "collision efficiency" α. The concentration of particles as a function of the travel distance L through the porous media can then be expressed as [90]:

$$\ln\frac{C_L}{C_O} = -\frac{3}{2}(1-\varepsilon)\eta_0\alpha\left(\frac{L}{d_c}\right), \qquad \text{(Eqn. 1-2)}$$

where ε is the porosity and d_c is the grain size of the filter medium (i.e., the aquifer material). Herein lies a first obvious difficulty in applying filtration theory to natural systems: in many aquifers, neither porosity nor grain size is likely to be homogeneous.

A number of different researchers have solved the advection-diffusion equation numerically to give empirically fitted relations for the single collector efficiency based on

theoretical formulations. One of the most recent of these is the T&E equation, which builds on earlier work, improving previous fits [91 and references therein]:

$$\eta_0 = 2.4 A_s^{1/3} N_R^{-0.081} N_{Pe}^{-0.715} N_{vdW}^{0.052} + 0.55 A_s N_R^{1.675} N_A^{0.125} + 0.22 N_R^{-0.24} N_G^{1.11} N_{vdW}^{0.053}$$

where (Eqn. 1-3)

$N_R = \frac{d_p}{d_c}$	aspect ratio, with d_c as the diameter of the collector (media)
$N_{Pe} = \frac{U d_c}{D}$	ratio of advective to diffusive transport, U is flow velocity and D is Einstein's diffusion coefficient
$N_{vdW} = \frac{A}{kT}$	van der Waals number, A is the Hamaker constant, k is the Boltzman constant, and T is the temperature in Kelvin
$N_A = \frac{A}{12\pi\mu a_p^2 U}$	attraction number, where a_p is the particle radius
$N_G = \frac{2}{9}\frac{a_p^2(\rho_p - \rho)g}{\mu U}$	gravity number, ratio of Stokes settling velocity to fluid velocity
$A_s = \frac{2(1-\gamma^5)}{2-3\gamma+3\gamma^5-2\gamma^6}$	Happel's porosity-dependent parameter for the effects of neighboring grains where $\gamma = (1-\varepsilon)^{1/3}$.

The first composite term in the equation for η_0 describes the contribution of convective (Brownian) diffusion to overall particle deposition and takes into account both hydrodynamic forces and van der Waals forces. The second composite term describes the contribution of interception to particle deposition. The third composite term describes the contribution of gravity (i.e., particle settling). Due to the small size of viral particles, Brownian diffusion is the dominant mechanism responsible for bringing about collisions between viruses and media grains. Interception and gravity forces are more

important for larger particles like protozoan (oo)cysts. Removal by straining is omitted from classical filtration theory, although a few recent studies (e.g., reference [92]) have suggested that it may factor into removal for the largest microbial particles (*Giardia* cysts, $d_p \sim 10$ μm) even in the absence of fine sedimentary materials ($d_c < 200$ μm). It is of note that filtration theory predicts the fewest collisions (and hence potentially the greatest transport) for bacteria-sized particles ($d_p \sim 1$ μm) [36].

The above theory describing the frequency of collisions has proven reasonably accurate. On the other hand, attempts at describing the proportion of collisions which result in attachment of the particle to a grain of porous media are less successful. The collision efficiency α depends on interactions between the charged particle surface and the charged surface of the porous media grains. These interactions are in turn dependent on solution chemistry and the properties of the surfaces involved, and have often been explained at least qualitatively by DLVO theory (see the following subsection).

Ultimately, particle-media interactions are dependent on the surface properties of both the particles and the porous media, and are very sensitive to system chemistry. This makes it difficult to predict collision efficiencies. As a result, the quantitative prediction of pathogen transport is somewhat uncertain business.

1.3.1.1 DLVO interactions

The physicochemical interactions reflected in α are often considered in terms of DLVO theory (e.g. [93, 94]). It describes the potential energy profile between two surfaces in aqueous solution as a balance between attractive (van der Waals) and repulsive (electrostatic double-layer) forces. The repulsive forces originate from the accumulation of counter-ions (having opposite charge) and depletion of co-ions (having

the same charge) near the surface of a charged particle. Sketches of example DLVO profiles are shown in Figure 1-5.

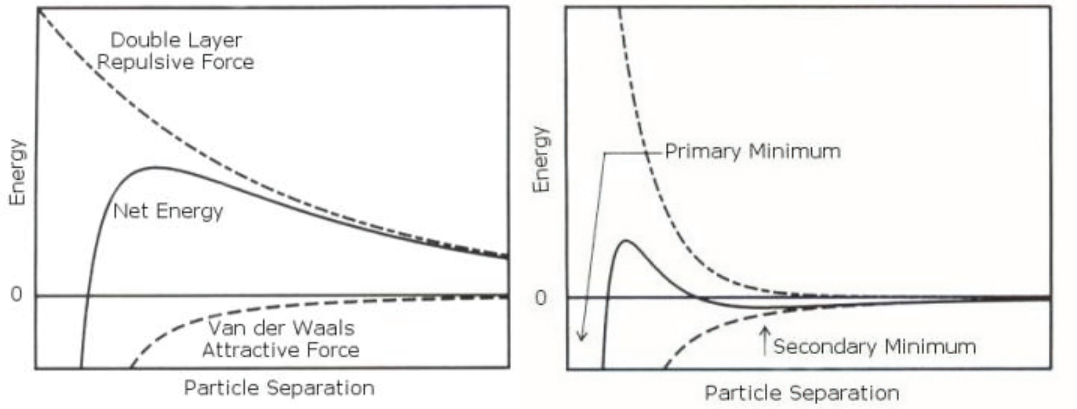

Figure 1-5. Hypothetical DLVO energy profiles for repulsive conditions at lower (left) and higher (right) ionic strength. The minimum separation distance shown is not zero, and the infinite repulsive energy of interaction at zero separation distance is not shown.

Moving away from the particle, counter-ion concentrations decrease asymptotically to bulk solution concentration, while co-ion concentrations increase. Overlapping of the ionic "atmospheres" of like-charged particles gives rise to repulsive forces described as electrostatic. With increasing particle separation, typical profiles for DLVO potential energy of interaction in the presence of repulsive forces include a deep primary well, a primary energy barrier due to electrostatic repulsion, and possibly a shallow secondary minimum. As ionic strength (I) increases, compression of the double-layer and corresponding shielding of repulsive forces mean that inter-particle separation distances must decrease for the particles to experience interaction forces of similar magnitude. The potential energy in the primary minimum shifts towards increasingly attractive interactions, the height of the primary energy barrier is reduced, and a secondary minimum appears where attractive forces also dominate. The secondary minimum and primary barrier subsequently disappear entirely as I increases even further.

Of course, electrostatic repulsive forces are absent for particles with zero surface charge (or with opposite charge), and attachment/aggregation is favored. Van der Waals attractive forces are unaffected by changes in solution chemistry. If the primary barrier is not too high or if no primary barrier exists, the energy of collision between a particle and a media grain can result in attachment in the primary minimum. Such attachment is often assumed to be irreversible without major perturbation of solution chemistry, since the average thermal energy of the attached particle is too small to escape the primary well. The secondary well, however, may be shallow enough that the energy required for detachment is only a few kT [95].

In the most general case, that of particle transport through homogeneous, clean quartz sand, both the media and particles (viruses, bacteria, etc) have negative surface charge. These conditions are considered "unfavorable" to deposition. Nonetheless, the large primary well exists at very close separation distance, and if the energy of the particle colliding with the surface is sufficient to overcome the energy barrier, the particle will be irreversibly deposited (attached) to the media surface. At higher ionic strength, the energy barrier is lower, and deposition is favored. Smaller particles are more easily deposited in the primary well.

When the secondary minimum is present, reversible attachment may occur. Recent research indicates that deposition in the secondary minimum may be an important part of particle transport through porous media [94, 96]. Deposition in the secondary minimum is favored at higher ionic strength and for larger particle sizes. This has

important implications for transport, because it means that attached particles could later be released if the ionic strength decreased (or the pH increased, etc).

Many other factors are likely to come into play in a field situation, where perfectly clean, homogeneous quartz sand is unlikely. The presence of positively-charged iron oxide coatings on aquifer materials favors particle attachment [97]. However, negatively-charged natural organic matter (NOM) can compete for surface-binding sites. At the same time, NOM has hydrophobic groups which might provide favorable binding sites for hydrophobic groups in virus, oocyst, or bacteria surface coatings [98]. Certainly, physical and chemical heterogeneity have the potential to significantly affect transport [99], a idea explored in depth throughout this dissertation.

1.3.1.2 Non-DLVO interactions

Researchers generally observe qualitative agreement between observed attachment behavior and what would be expected based on DLVO-type considerations: changes in deposition behavior tend to occur around the pH_{pzc} (point of zero charge) of the particles and surfaces involved, and screening of surface charge or competition for surface sites generally has the expected effect on attachment. DLVO theory is, however, insufficient to explain deposition of biological particles quantitatively, even under controlled conditions, and researchers have invoked steric factors, charge heterogeneity, and hydrophobic/hydrophilic interactions [100-102] to account for the discrepancies. A smaller body of literature has also focused on improving upon the shortcomings of zeta potential calculations used in DLVO-type analyses of "soft" particles [103, 104]. The concept of zeta potential assumes a shear plane in the double-layer charge distribution at

a clearly-defined, hard, impermeable surface, but no such surface exists for a biological particle.

Controlled laboratory investigations of bacterial deposition on glass and Teflon surfaces and clean porous media [102] found that DLVO-type repulsive interactions inhibited deposition at low ionic strength, but that steric interactions dominated at high *I*. The effective range for DLVO interactions fell at separation distances between the location where the DLVO energy barrier exceeded 5kT and the location of the secondary minimum. At $I < 0.001$M this range was more than 100 nm, so only very long polymers could bridge to access the primary well and cause irreversible attachment. On the other hand, steric interactions seemed to dominate at $I = 0.1$M, where the effective range of DLVO interactions was only 10nm. Interpreting deposition in terms of the dominant surface polymers (anionic polysaccharides, amphiphilic molecules, non-polysaccharide proteins/lipids) for the different bacterial strains observed, researchers concluded that polymers either promoted deposition by bridging or inhibited it by steric hindrance, depending on the nature of the polymer and the surface. In a separate study, comparison of deposition profiles for three *Pseduomonas aeruginosa* strains (mucoid, nonmucoid, and EPS-deficient) with similar surface charge characteristics revealed the importance of steric interactions between EPS polymers and media grains [105].

Properties of planktonic *E. coli* including cell size, surface charge, hydrophobicity and zeta potential (calculated from electrophoretic mobility measurements) have been shown to fluctuate as a function growth phase [106, 107], cell starvation [108], or oxygen tension [109]. *Burkholderia cepacia* properties have been observed to vary depending on nutrient conditions [110]. All these changes have been correlated with changes in

deposition behavior in porous media. For example, compared to cells grown under aerobic conditions, *E. coli* O157:H7 cells grown under anaerobic conditions were less spherical, had greater negative surface charge, and exhibited enhanced transport in clean sand columns (α = 0.59 vs. α = 0.9 for aerobic organisms). However, parallel investigations with another pathogen, *Yersinia enterocolitica*, gave nearly opposite results [109].

In light of these results, it likely that these same physicochemical properties will continue to be relevant to particle deposition in the "reverse" system, where the biological material is not necessarily the attaching particle, but rather the porous media itself, coated with biofilm. Since biofilms respond metabolically and morphologically to environmental conditions, the surface properties of a biofilm may also change with the metabolic state of the organisms in the biofilm. If so, it is hypothesized that such changes could affect particle attachment to the biofilm.

1.3.2 Virus filtration behavior in field and column studies

As reviewed by Fong [111], low infective doses and slow die-off rates relative to bacteria contribute to the health risks of groundwater contamination by viral pathogens like Norovirus or Rotavirus. Practical considerations including safety and culturability have led researchers studying viral transport to work primarily with surrogates, including bacteriophages such as PRD1, MS2, ϕX174, and Qβ.

As presented in detail in the preceding sections, the removal of microorganisms by passage through porous aquifer materials is often considered in terms of colloid filtration theory. We briefly summarize and restate that formulation here in the context of the interpretation of laboratory and column data. The attachment of a microorganism

to a grain surface requires that the two come in contact with each other, and that this "collision" result in the microorganism "sticking" onto the collector surface. The collision itself depends on the particle's approach to a collector, described as a theoretical single-collector efficiency (η_0), while the probability of a collision resulting in attachment, or collision efficiency (α), depends on physicochemical interactions between the particle and the collector surface. The parameter η_0 may be evaluated from a correlation such as the T&E equation (Eqn. 1-3, reference [91]) by summing the contributions of gravity, interception, and Brownian motion. The parameter α is extracted from transport data [91]:

$$\alpha = -\frac{2}{3}\frac{d_c}{(1-\varepsilon)L\eta_0}\ln(C/C_0)\,, \qquad \text{(Eqn. 1-4)}$$

where d_c is the diameter of the collector grain, ε is the porosity, C_0 is the influent concentration, and C is the concentration at length L from the influent location.

Large-scale field studies of virus transport are relatively rare, but they contribute valuable data. The physical and (bio)geochemical heterogeneity of natural aquifer materials can be difficult to reproduce meaningfully in laboratory studies. Longer travel distances and residence times make it easier to extract relevant collision efficiencies and surface-associated inactivation rates from field data as compared to laboratory column data, especially when removals are low, although bulk attenuation rates or "filtration factors" may be more meaningful than attempts to interpret field data from heterogeneous natural systems in terms of classical filtration theory [112].

Work at the USGS Cape Cod Toxic Waste Research Site has demonstrated the combined importance of geochemical heterogeneity and groundwater chemistry [97, 113-

115]. The physical and chemical characteristics of the quartz sand and fine gravel aquifer there have been characterized extensively and a number of injection studies performed. A portion of the aquifer is contaminated by a sewage plume. Comparing removal of injected PRD1 in contaminated vs. uncontaminated zones, researchers consistently observe greater attenuation in the uncontaminated area, concentrated over the first meter or so of travel. Low levels of phage persist in both zones over long travel distances (a phenomenon often termed "tailing"), regardless of groundwater chemistry. Enhanced virus mobility in the contaminated zone has been attributed to blocking of favorable (oxy)hydroxide mineral attachment sites by sewage-derived phosphate and organic matter [114]. Complex relations have also been observed between the influences of iron hydroxide minerals, organic matter, and grain size on bacterial retention in field and laboratory sediments [116, 117]. Dissolved organic carbon can block bacterial attachment, particularly under aerobic conditions [118].

Research of phage transport in sandy aquifers in deep well injection [119] and dune recharge [120] systems in The Netherlands has also demonstrated higher initial removal followed by long tailing. Typical collision efficiencies extracted from field data in these studies were lower than those in the Cape Cod aquifer. Data from the deep well injection study also indicate the importance of iron hydroxide mineral coatings: clogging and oxidation of pyrite to iron oxyhydroxides in the aerobic zone around the injection well contributed to significantly higher phage removal in the first few meters compared to the rest of the anoxic aquifer. The authors of a study on MS2 and ϕX174 transport in another anoxic Dutch aquifer attributed the comparatively low collision efficiencies and removal rates they observed to anoxic conditions, suggesting that they might affect iron

oxyhydroxide mineral coatings, thus reducing the availability of favorable attachment sites [121].

The importance of iron (oxy)hydroxide mineral coatings to microbial retention has been confirmed repeatedly in laboratory column studies with glass beads and quartz sand. At pH conditions when mineral coatings are positively-charged (pH_{pzc} 7.5-9 [122]), they provide favorable deposition sites for negatively-charged bacteria and viruses. PRD1 attached under such conditions can be detached by a subsequent increase in pH above the point where the mineral coating takes on a net negative charge [95]. Abudalo *et al.* [122] observed decreasing PRD1 breakthrough in quartz sand columns (from 62.1% to 0.02%) as the fraction of ferric oxyhydroxide-coated surface increased from 0 to 0.12 at pH ~5.7. Corresponding α values rose from 0.0071 to 0.13, in agreement with a previously published model developed from experiments with colloidal silica and indicating that α should be approximately equal to the fraction of positively-charged surface coverage [123]. In separate studies, addition of dissolved organic matter [124] or phosphate [125] reduced PRD1 and *E. coli* attachment, respectively, an effect that was attributed to blocking of positively-charged mineral coatings by competition from these species.

Observed pH dependence of MS2 removal has also been explained in terms of Derjaguin-Landau-Verwey-Overbeek (DLVO) type interactions with quartz and feldspar minerals in the absence of metal hydroxide coatings: attenuation and retardation of MS2 breakthrough in a 1 m model aquifer at pH 6.1 (vs. pH 7.5 or 8.1) was attributed to a combination of reversible secondary minimum attachment to feldspar (pH_{iep} 5-6) and irreversible primary minimum attachment to quartz (pH_{iep} 2.5-3) [126].

The influence of other parameters on phage transport has also been investigated. MS2 transport in tap water through columns packed with natural sandy soil was unaffected by the addition of 40 mg/l dissolved organic matter from biosolids [127], but mineral associated organic matter or NOM promoted MS2 transport in phosphate buffered saline through sand and natural soil columns [128]. Retention of indigenous coliphage in columns simulating soil aquifer treatment of sewage effluent depended on soil type and percolation rate. Interestingly, retention dropped in columns where aerobic respiration was inhibited by addition of sodium azide [129].

The apparently contradictory, or at least inconsistent, nature of results like these highlights the complexity of microbial transport in the presence of biogeochemical heterogeneity and indicates a need for further characterization of these systems under conditions relevant to the natural subsurface environment.

1.3.3 Inactivation of viruses and bacteriophages

Two processes, attachment and inactivation, are generally considered to contribute to virus removal in porous media. Inactivation rates may differ between attached and solution-phase viruses. Attached viral inactivation rates are relevant only if viruses may later detach, i.e., if some attachment is reversible. The difficulty of establishing infectivity for a surface-associated viral particle makes it hard to distinguish between detachment rates and surface inactivation rates [130]. Consequently, most inactivation studies have focused on solution-phase inactivation rates, while estimates of attached-phase inactivation rates are generally extracted from a model fit of lab or field transport data, if they are estimated at all.

When infectivity decays exponentially over time, the inactivation rate k_{inact} is often calculated as

$$k_{inact} = -\frac{1}{t}\ln\frac{C}{C_0} = -\frac{2.3}{t}\log\frac{C}{C_0}, \qquad \text{(Eqn. 1-5)}$$

where C is the concentration of infective virus at time t, and C_0 the concentration at $t = 0$. Researchers have also reported "biphasic" inactivation that does not fit this first order model, with a faster initial activation rate followed by a long period when low levels of active viruses persist [131-133]. Biphasic inactivation is often attributed to supposed viral subpopulations with different inactivation rates.

1.3.3.1 Factors influencing inactivation

Some strains of viruses retain infectivity longer than others [134, 135]. An extensive tabulation of published inactivation studies [136] found that the inactivation rate constants (k_{inact}) for a range of pathogenic human viruses (coxsackieviruses B, echoviruses 7, poliovirus 1, hepatitis A) and bacteriophage surrogates (ϕX174, MS2, PRD1) fall in the range of 0.01 - 0.04 d^{-1} at typical cool groundwater temperatures of 10-12°C. These coefficients correspond to a range of 57 to 230 days required for l-$\log_{10}$ removal by inactivation. However, echovirus 1 inactivation at 12°C was reported to be ten times greater, as were a number of the inactivation coefficients tabulated from studies conducted with various organisms at warmer temperatures, 13-30°C. The tabulation excluded studies which had reported "zero" or insignificant inactivation, although a consideration of detection limits and study duration should have made it possible to put an upper limit on the inactivation rate coefficients for those systems.

Temperature [137, 138], pH [139], mineral surfaces [115, 131], organic matter [115, 124, 140], oxygen tension [133, 134], soil saturation [141], buffer composition, and presence of microorganisms [133, 142, 143] have all been examined as factors affecting viral inactivation rates, although the different studies have variously concluded that these factors are – or conversely, are not – "significant."

These results are not as contradictory as they first seem: different viruses exhibit different inactivation rates and sensitivities; different study durations, conditions, and techniques yield results not directly comparable; and the apparent "significance" of a given factor depends partially on the perspective lent by the researcher's particular application. Previous authors have noted the difficulty of comparing and interpreting inactivation data from different studies [19, 144]. On average, warmer temperature and the presence of native microorganisms seem to increase viral inactivation, but reviewers have highlighted the need for research into interactive factors affecting virus survival, notably the linked effects of native microorganisms, dissolved oxygen levels, and mineral matrices [144].

1.3.3.2 Mechanism of virus inactivation, solution vs. attached

A viral particle consists of a shell-like, protein capsid housing the virus's genetic material (as DNA or RNA) and, in some cases, a few viral enzymes. The capsid may be surrounded by a membrane-like outer envelope. Infection depends upon successful integration of viable genetic material from the virus into a host cell, which in turn depends on highly specific recognition-site interactions between proteins on the exterior of the viral envelope or capsid and receptors expressed on the surface of the host cell [145]. Researchers have often considered two pathways to viral inactivation:

capsid/envelope damage that affects the recognition site or allows the nucleic acid to escape from the capsid, and degradation of viral nucleic acid within the capsid [130]. These processes may occur in solution or when the virus is attached to a surface. Time, temperature, and physicochemical conditions may contribute more to solution-phase inactivation via nucleic acid degradation or recognition-site damage, while damage to the structural integrity of the capsid may require relatively stronger surface forces such as those experienced by the virion during irreversible or even reversible attachment [115, 130, 146].

1.3.3.3 O_2 and virus inactivation

Examining early field data, researchers proposed two explanations for an observed strong positive influence of dissolved oxygen on inactivation of several polio and echovirus strains [134]: that the capsid might be oxidized directly, or that oxygen might play an indirect role through its influence on microbial growth. Without categorically ruling out the former, other experimental evidence seems to support the latter.

Comparing anoxic and aerobic, sterile and nonsterile groundwater microcosms, Gordon and Toze [133] found that MS2 phage inactivation was indeed slower under anoxic as compared to aerobic conditions, but that the difference was statistically significant only in non-sterile systems. Hurst [142] ran similar experiments under unsaturated conditions and found a two- to three-fold increase in poliovirus type I inactivation rates when aerobic microorganisms were present, compared to sterile or anaerobic systems. These rate differences were significant at the $p = 0.01$ level, and the author concluded that aerobic microorganisms (and/or their exudates) adversely affected

viral survival either directly, or by reducing viral attachment to surfaces, (attachment was assumed to be protective). Note however, that if microbial activity contributes to increased viral inactivation, then we might expect to see the difference between sterile and nonsterile inactivation rates be not only more pronounced but also more statistically significant at temperatures most favorable to microbial growth. This was not observed in the poliovirus study.

1.4 Biofilms in the context of microbial transport

1.4.1 Biofilm characteristics

The microorganisms responsible for redox zonation in the subsurface exist primarily in biofilm communities, since the high specific surface area of porous aquifer materials and the relatively low nutrient conditions in groundwater often favor attached over planktonic growth. Biofilms form when bacterial cells colonize a surface, generally at a solid-liquid interface. The cells excrete extracellular polymeric substances (EPS) that encapsulate them, fill the interstitial spaces in between cells, and provide structural architecture to the entire biofilm, affecting its morphology and helping to attach it to the substratum [105].

Microorganisms are most numerous (10^9-10^{10} cells/g) in the shallowest sediments, where nutrients and organic matter are more readily available, whereas deeper aquifer materials usually have less microbial growth (10^4-10^8 cells/g). In light of this range of cell counts, biofilms may cover ~$8x10^{-6}$ % to 8% of the porous media in a saturated system, with the higher surface coverages in shallower and more nutrient-rich environments [147]. These coverage estimates do not account for the area occupied by

EPS, which can represent 50-90% of the organic matter in the biofilm, and potentially several times the volume of the cells [148, 149].

Biofilms are dynamic, living systems. A biofilm begins as isolated micro-colonies, which later grow together into a heterogeneous layer that continues to evolve over time in response to environmental conditions. Different bacterial populations may predominate at different depths and locations in the biofilm at different times, and the physiological state of the organisms varies as well [150]. Mature biofilms in nutrient-rich systems can reach millimeter thicknesses, exhibiting ripples, mushroom-like structures, or long "streamers." Recent research confirms the influence of the hydrodynamic regime, but indicates that biofilm structure may be controlled by biological (non-physical) factors as well [151].

The EPS matrix includes various secreted proteins, glycoproteins, carbohydrates, glycolipids, and nucleic acids, as well as cellular debris, and exogenous substances like humic acids, multivalent cations, and other colloidal or dissolved compounds, with a potentially significant [152, 153] mineral fraction. It is gel-like, highly hydrated, and exhibits great local variation in charge and in hydrophobicity due to the presence of macromolecules containing, e.g., carboxylic functional groups or hydrophobic amino acids [148]. Redox and pH zonation as a function of depth within a biofilm has likewise been observed [154]. The distribution of charged and hydrophobic/hydrophilic regions on EPS macromolecules contributes to EPS structure and to the sorption properties of microbial aggregates.

Biofilms respond metabolically and morphologically to changing environmental conditions, notably with changes in EPS content and composition in response to low

dissolved oxygen [155]. Aerobic *Shewanella oneidensis* biofilms have shown particular morphological sensitivity to oxygen tension [156] and to the presence of an alternate electron acceptor [157].

1.4.2 Particle-biofilm interactions

Studies intended to elucidate biofilm structure have simultaneously shed light on particle-biofilm interactions. Sectioning and subsequent image analysis reveal that carboxyl-functionalized latex microspheres (diameters 0.5-10 μm) rapidly penetrate single-species (*Pseudomonas aeruginosa*) [158] and wastewater [159] biofilms. These particles enter the biofilm by diffusion or liquid-phase advection into water-filled pores and channels, where those retained are subsequently "buried" if continuing growth fills the pore, or they may be trapped by attachment- or adhesion-type interactions [158, 160, 161].

A variety of factors have been demonstrated to be relevant to particle-biofilm interactions, including bulk-scale biological characteristics, physicochemical characteristics, solution chemistry, and particle properties. Each of these is discussed in more detail in the following paragraphs.

Bulk-scale properties related to biofilm structure influence biofilm-particle interactions: older *P. aeruginosa* biofilms – thicker and rougher, with more and deeper pores – retained more microspheres [158] and clay-like colloids [162]. Similarly, drinking water biofilms exhibiting a more mature, aggregated structure retained more particles, as did biofilms challenged under higher-shear conditions [163]. However, other researchers found no correlation between drinking water biofilm thickness or cell density and microsphere or phage retention [164]. Biofilms in the latter study were only 8 weeks

old, while those in the former study were 7-10 mos. old. Though the maximum biofilm thickness was similar in both cases (~10 μm), the younger biofilms may not have had time to develop the mature, aggregated structure that was observed to retain particles.

Bulk-scale biofilm heterogeneity is relevant even for virus-sized particles. Fluorescence correlation spectroscopy measurements of phage diffusion in biofilms revealed slower diffusion rates for phage and nanospheres (carboxylated latex beads, d=110 nm) in the more homogeneous regions of a biofilm, attributed to local compaction and increased viscosity of the EPS layer there [165, 166]. Researchers investigating dextran and silver nanoparticles also confirmed the influence of biofilm density on particle diffusion [167]. In another study, more viruses attached to a thicker wastewater biofilm than to a thinner drinking water biofilm [168].

Physicochemical characteristics of the biofilm are also likely to influence particle-biofilm interactions. Higher protein content in the EPS layer can correlate with higher particle retention in biofilms [162]. Analyses based on contact angle measurements revealed positive correlations between adhesion of carboxyl-functionalized polystyrene microspheres (d = 2.5 μm) and the electron acceptor and van der Waals components of biofilm surface energy [169]. In another study, carboxylate-modified polystyrene nanospheres (d = 50 nm) were shown to diffuse less freely into a monoculture biofilm after the strain was genetically altered to suppress expression of a major wall-anchored proteinase, thus switching the organism's cell wall from strongly hydrophobic to very hydrophilic [170]. The structure of the biofilm was not altered.

Solution chemistry is likewise important in particle-biofilm interactions. Divalent cations, particularly calcium, are involved in bridging and stabilization of EPS polymers

like alginate [148], so they affect mechanical and visco-elastic properties of biofilms, generally making them more stable [171] and thus better-able to retain particles that are entrapped in them, even during subsequent perturbations of solution chemistry. The influence of solution chemistry was demonstrated in column transport studies of a model colloid [162]: biofilms conditioned by flushing with $CaCl_2$ electrolyte in a concentration decreasing from 70 to 0 mM prior to a challenge with laponite RD retained the model colloid, while those conditioned with 70 to 0 mM NaCl did not.

Not surprisingly, the identity and properties of the particle also matter. In one study, MS2 attached more to a drinking-water biofilm than did ϕX174 and poliovirus, a difference that was partly attributed to MS2's lower isoelectric point. But general surface charge considerations were not sufficient to explain attachment behavior: *Cryptosporidium parvum* and *Giardia lamblia* have pH_{iep}s at least as low as MS2's, and yet they attached less [168], possibly because their larger size made some portions of the rough biofilm surface inaccessible to them. Furthermore, studies comparing deposition of polystyrene and *E. coli* on a drinking water biofilm found large differences, despite similar size and electrophoretic mobility [163]. The researchers surmised that the greater hydrodynamic permeability of "soft" *E. coli* cells plays a role in their adhesion behavior.

Research on the role of particle hydrophobicity in biofilm interactions has come to contradictory conclusions. One study compared deposition of carboxylate-modified and sulfate-modified polystyrene microspheres on drinking water biofilm coupons and observed greater deposition of hydrophilic (carboxylate-modified) microspheres [164]. Other researchers observed different behavior: a wastewater biofilm grown on clay beads

removed hydrophobic (latex) and hydrophilic (carboxylate-modified polystyrene) microbeads equally [172].

1.4.3 Biofilms and (0xy)hydroxide minerals

Iron and manganese (oxy)hydroxide mineral phases have low solubilities under the circumneutral pH conditions typical of natural systems. These positively-charged minerals represent favorable deposition sites for negatively-charged microorganisms, so it is not surprising that researchers who have studied bacteria capable of using Fe(III) or Mn(III,IV) as a terminal electron acceptor find that the bacterial cells are generally surface-associated, though not necessarily in direct contact with the mineral phase [35]. Anoxic groundwater conditions favor the growth of these metal-reducing organisms, which presumably form biofilms on the mineral-coated portions of aquifer materials. Dissolution of iron oxyhydroxide mineral coatings exposed to the dissimilatory iron reducing bacterium *Shewanella oneidensis* has been demonstrated and studied in the laboratory [154, 173]. In anoxic aquifers with developed redox zonation, metal-reducing biofilms may well cover and even dissolve the very same mineral coatings that researchers have demonstrated to be important for retention of viruses and other pathogens.

1.5 Modeling microbial transport in porous media

Mathematical modeling approaches to the study of microbial transport can complement laboratory and field experiments, particularly to explore complex interactions and heterogeneity effects that may be experimentally intractable. Modeling approaches can also help to bridge the gap between (a) laboratory work that may not be

directly relevant or scalable to engineered systems and natural processes, and (b) field studies which, while more relevant and appropriately scaled, are often site-specific and difficult to generalize. Modeling transport in porous media starts with a set of assumptions and a conceptualization of flow, transport behavior, microbial attachment and detachment, and inactivation. These ideas are then structured in a mathematical framework. The full complexity of a dynamic natural system – including physical, chemical, and biological heterogeneities – cannot truly figure into a model as we do not have a complete conceptualization (let alone a fully developed understanding) of these factors, some of which may be interdependent. A recent review summarized the state of the science very succinctly: "There is presently no consensus on the best model formulation, and no single model is expected to accurately simulate all scenarios" [174].

1.5.1 Conventional modeling approaches

Conventional models unite a representation of flow through porous media with the advection-dispersion equation, derived from a mass balance on the contaminant of interest and presented here in one-dimension for simplicity

$$\frac{\partial C}{\partial t} = D\frac{\partial^2 C}{\partial x^2} - v\frac{\partial C}{\partial x}, \qquad \text{(Eqn. 1-6)}$$

where C is the aqueous concentration at distance x and time t, D is the hydrodynamic dispersion coefficient, and v the pore water velocity.

The simplest and most common approach adds microbial attachment, and only microbial attachment [175], despite a great number of factors that can affect the fate and transport of microbes in the subsurface [19, 176]. With S as the concentration of attached

microbes, and ρ_B and n as the respective bulk density and porosity of the porous medium, the expanded mass balance reads:

$$\frac{\partial C}{\partial t} + \frac{\rho_B}{n}\frac{\partial S}{\partial t} = D\frac{\partial^2 C}{\partial x^2} - v\frac{\partial C}{\partial x}. \qquad \text{(Eqn. 1-7)}$$

In some conventional models (e.g., [177, 178]), attachment has been represented as equilibrium adsorption. For an assumed linear adsorption isotherm ($S = K_D C$), the mass balance may be rewritten in terms of a retardation factor, R:

$$R\frac{\partial C}{\partial t} = D\frac{\partial^2 C}{\partial x^2} - v\frac{\partial C}{\partial x} \quad \text{with} \quad R = 1 + \frac{\rho_B K_D}{n}. \qquad \text{(Eqn. 1-8)}$$

Other conventional models conceptualize attachment as a kinetic process [179], with mass transport to the surface of an aquifer grain followed by physicochemical interactions that may result in retention at the grain surface. In this formulation, Eqn. 1-7 is coupled with a kinetic description of the attached microbe concentration S, expressed in terms of attachment and detachment rate constants k_{att} and k_{det}:

$$\frac{\rho_B}{n}\frac{\partial S}{\partial t} = k_{att} C - \frac{\rho_B}{n} k_{\mathrm{det}} S. \qquad \text{(Eqn. 1-9)}$$

Clean-bed filtration theory (CBFT), presented in section 1.3.1 of this chapter, is often used to parameterize k_{att} (as reviewed in references [174, 175, 179] with many examples therein). This is nothing more than a specific case of the kinetic adsorption approach, which may also be simplified by the omission of detachment.

As a final addition, conventional models sometimes include a term describing microbial inactivation or die-off, usually as first-order decay. Eqn. 1-7 then becomes:

$$\frac{\partial C}{\partial t} + \frac{\rho_B}{n}\frac{\partial S}{\partial t} = D\frac{\partial^2 C}{\partial x^2} - v\frac{\partial C}{\partial x} - k_{inact}C\,. \qquad \text{(Eqn. 1-10)}$$

As reviewed extensively in reference [175], experimental and field evidence indicate that the equilibrium adsorption model is an inadequate conceptualization of microbial transport in the subsurface. However, CBFT fails to predict attachment rates quantitatively under repulsive conditions [96, 180], and two of the key parameters – η_0 and α – are complicated. Furthermore, the influences of surface biomacromolecules and microbial dynamics are ignored, non-CBFT removal mechanisms (e.g., straining [92, 181]) are omitted, inactivation is uncertain (see section 1.3.3 in this chapter), and detachment, if it is included, is often little more than a fitting parameter.

Many of the assumptions embedded in the conventional approach are born of convenience: linear equations have analytical solutions, and first-order rate constants may be easily obtained from log-linear plots. These assumptions include the idea that microbes behave like dissolved solutes and therefore move at average porewater velocity, exhibit Fickian dispersion, and are not excluded from any of the porespace accessible to a conservative tracer. Both CBFT and the advection-dispersion mass balance approach assume that microbes and their potential accumulation in the porous media have no affect on flow. Finally, conventional models assume that the aquifer system and the microbes of interest can be represented by effective or average values, as if they were homogeneous.

1.5.2 Alternate models

A number of alternate and more complex models have been developed to address some of the shortcomings of the conventional approach and to explore various aspects of microbial transport in more detail. As described in a recent review [174], these expansions and improvements have included consideration of factors such as settling, chemotaxis, and pore exclusion, which would all alter the trajectory of an individual microbe in the flow field. They have also integrated microbial growth (often represented with Monod kinetics), temperature-dependent inactivation, and clogging of the porous media due to microbial growth and/or retention of fine particles. Several non-equilibrium transport models exist. These include the mobile-immobile and dual-porosity models, both of which posit two water fractions, one that flows and one that doesn't, with diffusive and perhaps advective exchange between the two. A fourth option, the dual-permeability model, uses separate flow and transport equations to describe a fast regime (e.g., flow in fractures) and a slow regime (e.g., exchange in the porous matrix). Similar two-region, non-equilibrium models have been developed to parameterize the actual sorption or attachment interaction between microbes and mineral grains. Other researchers have altered the CBFT-based representation of attachment to try to account for non-exponential deposition profiles by considering factors such as blocking, ripening, heterogeneous microbial populations, and a distribution of kinetic attachment/detachment rates).

Many of the more complex alternate models require some sort of parameter estimation to establish values for model coefficients [174]. In other words, a fitting or

"inversion" technique is applied to determine one or more unknown model parameters, effectively calibrating the model to a specific site or a particular laboratory data set.

1.5.3 Model-derived insights

A conventional 1D applied to the dune recharge experiments [120] previously described (see section 1.3.2) used a kinetic formulation of attachment and detachment, but was unable to match observed virus tailing in monitoring wells. A similar 1D model applied to microbial transport data from the South Oyster Focus Site [117] found apparent decreases in α with increasing transport distance, a phenomenon which has been documented repeatedly when conventional models are applied to field data [182]. However, alternative modeling approaches [183] have demonstrated that this apparent scale-dependency of attachment behavior can in fact be an artifact of approximating the aquifer as homogeneous in a conventional, 1D model. Numerical simulations have further revealed the difficulty of inferring attachment and detachment parameters from conventional models applied to field and laboratory datasets without careful consideration of tailing in aqueous breakthrough curves [179] and, in many cases, full deposition profiles [184].

Stochastic models address uncertainty about appropriate values and potential system heterogeneities by adopting a distribution of parameter values [185]. The value of a stochastic parameter that is used for a particular location, point in time, microbial property, or model realization (depending on the particular implementation) is selected at random based on a probability distribution with user-defined statistical characteristics. Model simulations of virus and bacterial deposition at column scale have demonstrated sensitivity to the particular distribution that was chosen for heterogeneity in attachment

behavior, but when the results were applied to experimental data, no single distribution (normal, log-normal, bimodal normal or power law) was able to represent all of the observations [184].

Other researchers have considered the representation of physical, rather than biological, heterogeneity [186, 187]. Stochastic simulations of a hypothetical solute plume moving through a 10km aquifer with local heterogeneities in hydraulic conductivity K demonstrated the impact of heterogeneity structure on solute transport [187]. Gaussian, truncated Gaussian, and non-Gaussian "facies" models were compared to represent heterogeneous K fields, with significant differences in resulting predictions of plume migration. The results implied that inadvertently overlooking extreme K values in field characterizations – the equivalent of using a truncated Gaussian K field in a model simulation – would result in significant underestimation of contaminant transport.

Coupled consideration of physical heterogeneity, flow, spatially-variable attachment/detachment processes, and biological heterogeneity is of particular interest to the topic of microbial transport, but studies in this area are limited. Bacterial transport data from the South Oyster site has been reanalyzed with a fully 3D flow model [183]. The aquifer was represented using both homogeneous and heterogeneous K fields, and transport predictions compared with kinetic attachment parameterized as using either a constant coefficient, a CBFT-derived coefficient calculated locally from flow and hydraulic conductivity, or a randomly heterogeneous coefficient. This approach demonstrated the pitfalls of overlooking potential correlations between attachment and physical/flow heterogeneity in model studies. Another research group has taken a similar approach to model a hypothetical virus contamination event for an artificial recharge

operation in Orange County, CA [188] and to reinterpret bacterial transport results from the Cape Cod study [189]. Unlike the 3D South Oyster model, these two simulations incorporated a spatially heterogeneous α based on a previously-published empirical correlation with K [190]. More recently, a microbial risk assessment model demonstrated significantly different results for bacterial transport with correlations between physical heterogeneity and CBFT-type attachment vs. conventional, spatially-constant CBFT [191]. The model further suggested that even slow inactivation of attached microbes could alter pathogen retention [192].

1.5.3.1 Modeling artifacts

Estimating parameters from field data is a model-based exercise. The quality of the result depends in part on the quality of the original field data. The inversion method or fitting algorithm is also significant, and represents an area of active research (e.g., references [193, 194]). But the basic conceptualization of the system is equally important, for inaccuracies in fixed parameters and model formulation may be partially compensated by the flexibility of fitted parameters. Thus, as mentioned above for the case of scale-dependency in apparent α [183], modeling studies can introduce artifacts that may be mistaken for meaningful transport phenomena. Modeling studies like reference [195], which sought to determine when a single-rate sorption parameter could reasonably be applied to systems with heterogeneous sorption rates, can also help establish the extent of inaccuracies introduced by the use of "effective" or "apparent" values to represent heterogeneous systems.

1.6 Knowledge gaps

The extent of microbial transport through porous media is determined by the survival of the particle in the subsurface and by the rate of deposition of the particle on subsurface collector grains. The presence of biofilms in this system might affect particle transport on three separate levels.

On the first level, biofilm coatings on media grains could provide an alternate collector surface for particle deposition. Parameters that influence biofilm structure or "adhesion properties" are expected to affect particle attachment [163]. The physical and chemical properties of biofilms - the amount of biofilm present, the structure of that biofilm, the composition of the EPS layer, the viscosity of the EPS layer, the surface energy of the biofilm, etc. – matter in particle-biofilm interactions, though the precise nature of their effects is not always clear. Changes in solution chemistry that affect the biofilm properties by altering electrostatic interactions, the structure/protonation of biomacromolecules, or the metabolic state of the biofilm would therefore be relevant to particle capture/release by biofilms.

Changes in metabolic state are of particular interest and complexity. Not only do microorganisms respond dynamically to nutrient, carbon source, electron-donor and electron-acceptor conditions in the surrounding groundwater, they also affect these very same conditions and other aspects of groundwater chemistry through their own metabolic processes. It is hypothesized that the physical and chemical properties of a biofilm are different (e.g., structure, EPS composition, expression of macromolecules on cell surfaces) under different nutrient and electron-acceptor conditions, and that furthermore, these changes are relevant to particle-biofilm interactions.

On a second level, biofilm microbial activity might affect bioparticle survival. While it seems unlikely that changes in oxygen tension would affect the structure of a viral capsid in such a way as to cause inactivation, changes in DO levels, particularly those that are microbially induced, are likely to correlate with other changes in groundwater composition and microbial activity that may be relevant to virus inactivation and transport.

Notably, microbial activity may mobilize iron and manganese (oxy)hydroxides. The biologically-induced reductive dissolution of (oxy)hydroxide mineral deposits on sand grains could remove positively-charged sites favorable for attachment of negatively-charged biocolloids. These sites may also be coated by anaerobic biofilms, blocking attachment there. It is therefore possible that biofilm microbial activity could affect particle transport on a third level: it could alter media properties in a way that could enhance transport of pathogens in aquifers, particularly in anaerobic systems under iron- or manganese-reducing conditions.

The actual influence of this biological heterogeneity on particle transport through porous media has not been systematically analyzed. The relative importance of effects at each of the three levels is unknown, and the degree of correlation that may exist between biological factors and the physical (abiotic) characteristics of natural aquifer materials is extremely uncertain.

1.7 References

1. Doussan, C., E. Ledoux, G. Poitevin, and M. Detay, *River - Groundwater Relationships and Bank Filtration - an Emphasis on Nitrogen Species Behavior and Evolution.* Houille Blanche - Revue internationale de l'eau, 1995. 50(8): p. 16-21.
2. Rivett, M.O., S.R. Buss, P. Morgan, J.W.N. Smith, and C.D. Bemment, *Nitrate attenuation in groundwater: A review of biogeochemical controlling processes.* Water Research, 2008. 42(16): p. 4215-4232.
3. Hildebrandt, A., M. Guillamon, S. Lacorte, R. Tauler, and D. Barcelo, *Impact of pesticides used in agriculture and vineyards to surface and groundwater quality (North Spain).* Water Research, 2008. 42(13): p. 3315-3326.
4. Kolpin, D.W., J.E. Barbash, and R.J. Gilliom, *Occurrence of pesticides in shallow groundwater of the United States: Initial results from the National Water-Quality Assessment Program.* Environmental Science & Technology, 1998. 32(5): p. 558-566.
5. Heberer, T., A. Mechlinski, B. Fanck, A. Knappe, G. Massmann, A. Pekdeger, and B. Fritz, *Field studies on the fate and transport of pharmaceutical residues in bank filtration.* Ground Water Monitoring and Remediation, 2004. 24(2): p. 70-77.
6. Massmann, G., J. Greskowiak, U. Dunnbier, S. Zuehlke, A. Knappe, and A. Pekdeger, *The impact of variable temperatures on the redox conditions and the behaviour of pharmaceutical residues during artificial recharge.* Journal of Hydrology, 2006. 328(1-2): p. 141-156.
7. Yu, J.T., E.J. Bouwer, and M. Coelhan, *Occurrence and biodegradability studies of selected pharmaceuticals and personal care products in sewage effluent.* Agricultural Water Management, 2006. 86(1-2): p. 72-80.
8. Da Silva, M.L.B., G.M.L. Ruiz-Aguilar, and P.J.J. Alvarez, *Enhanced anaerobic biodegradation of BTEX-ethanol mixtures in aquifer columns amended with sulfate, chelated ferric iron or nitrate.* Biodegradation, 2005. 16(2): p. 105-114.
9. Nay, M., A.J.B. Snozzi, and A.J.B. Zehnder, *Fate and behavior of organic compounds in an artificial saturated subsoil under controlled redox conditions: The sequential soil column system.* Biodegradation, 1999. 10(1): p. 75-82.
10. Sapkota, A.R., F.C. Curriero, K.E. Gibson, and K.J. Schwab, *Antibiotic-resistant enterococci and fecal indicators in surface water and groundwater impacted by a concentrated swine feeding operation.* Environmental Health Perspectives, 2007. 115(7): p. 1040-1045.
11. DeBorde, D.C., W.W. Woessner, B. Lauerman, and P.N. Ball, *Virus occurrence and transport in a school septic system and unconfined aquifer.* Ground Water, 1998. 36(5): p. 825-834.
12. Meeroff, D.E., F. Bloetscher, T. Bocca, and F. Morin, *Evaluation of water quality impacts of on-site treatment and disposal systems on urban coastal waters.* Water Air and Soil Pollution, 2008. 192(1-4): p. 11-24.

13. Bishop, P.K., B.D. Misstear, M. White, and N.J. Harding, *Impacts of sewers on groundwater quality.* Journal of the Chartered Institution of Water and Environmental Management, 1998. 12(3): p. 216-223.
14. Hutson, S.S., N.L. Barber, J.F. Kenny, K.S. Linsey, D.S. Lumina, and M.A. Maupin, *Estimated Use of Water in the United States in 2000*. 2000, U.S. Geological Survey Circular 1268.
15. EPA, *Ground Water Rule: A Quick Reference Guide*. 2008, Office of Water (4606M).
16. Hilborn, E.D., T.J. Wade, L. Hicks, L. Garrison, J. Carpenter, E. Adam, B. Mull, J. Yoder, V. Roberts, and J.W. Gargano, *Surveillance for Waterborne Disease Outbreaks Associated with Drinking Water and Other Nonrecreational Water -- United States, 2009-2010.* MMWR Surveillance summaries: Morbidity and mortality weekly report. Surveillance summaries / CDC, 2013. 62(35): p. 714-720.
17. Brunkard, J.M., E. Ailes, V.A. Roberts, V. Hill, E.D. Hilborn, G.F. Craun, A. Rajasingham, A. Kahler, L. Garrison, L. Hicks, J. Carpenter, T.J. Wade, M.J. Beach, and J.S. Yoder, *Surveillance for Waterborne Disease Outbreaks Associated with Drinking Water -- United States, 2007-2008.* MMWR Surveillance summaries: Morbidity and mortality weekly report. Surveillance summaries / CDC, 2011. 60(SS12): p. 38-68.
18. Yoder, J., V. Roberts, G.F. Craun, V. Hill, L.A. Hicks, N.T. Alexander, V. Radke, R.L. Calderon, M.C. Hlavsa, M.J. Beach, and S.L. Roy, *Surveillance for waterborne disease and outbreaks associated with drinking water and water not intended for drinking--United States, 2005-2006.* MMWR Surveillance summaries: Morbidity and mortality weekly report. Surveillance summaries / CDC, 2008. 57(9): p. 39-62.
19. Azadpour-Keeley, A., B.R. Faulkner, and J.-S. Chen, *Movement and Longevity of Viruses in the Subsurface, EPA/540/S-03/500*. 2003, US EPA National Risk Management Research Laboratory, Cincinnati, Ohio. p. 24.
20. Blackburn, B.G., G.F. Craun, J.S. Yoder, V. Hill, R.L. Calderon, N. Chen, S.H. Lee, D.A. Levy, and M.J. Beach, *Surveillance for waterborne-disease outbreaks associated with drinking water--United States, 2001-2002.* MMWR Surveillance summaries: Morbidity and mortality weekly report. Surveillance summaries / CDC, 2004. 53(8): p. 23-45.
21. Bradbury, K.R., M.A. Borchardt, M. Gotkowitz, S.K. Spencer, J. Zhu, and R.J. Hunt, *Source and Transport of Human Enteric Viruses in Deep Municipal Water Supply Wells.* Environmental Science & Technology, 2013. 47(9): p. 4096-4103.
22. Smeets, P.W.M.H., G.J. Medema, and J.C. Van Dijk, *The Dutch secret: How to provide safe drinking water without chlorine in the Netherlands.* Drinking Water Engineering and Science, 2009. 2(1): p. 1-14.
23. Morris, B.L., A.R.L. Lawrence, P.J.C. Chilton, B. Adams, R.C. Calow, and B.A. Klinck, *Groundwater and its Susceptibility to Degradation: A Global Assessment of the Problem and Options for Management.* 2003, United Nations Environment Programme, Nairobi, Kenya.
24. Howard, G., J. Bartram, S. Pedley, O. Schmoll, I. Chorus, and P. Berger, *Groundwater and public health*, in *Protecting groundwater for health: managing*

the qualityof drinking-water sources, O. Schmoll, et al., Editors. 2006, IWA Publishing: London. p. 3-19.
25. Kuehn, W. and U. Mueller, *Riverbank filtration - An overview.* Journal American Water Works Association, 2000. 92(12): p. 60-69.
26. Hunter, K.S., Y.F. Wang, and P. Van Cappellen, *Kinetic modeling of microbially-driven redox chemistry of subsurface environments: coupling transport, microbial metabolism and geochemistry.* Journal of Hydrology, 1998. 209(1-4): p. 53-80.
27. Lovley, D.R. and E.J.P. Phillips, *Novel mode of microbial energy metabolism: organic carbon oxidation coupled to dissimilatory reduction of iron or manganese.* Applied & Environmental Microbiology, 1988. 54(6): p. 1472-1480.
28. Chapelle, F.H., *Ground-water Microbiology and Geochemistry*. 2nd ed. 2001, New York: Wiley and Sons. 477.
29. Morel, F.M.M. and J.G. Hering, *Principles and Applications of Aquatic Chemistry*. 1993, John Wiley & Sons: New York. 588.
30. Greskowiak, J., *Reactive transport processes in artificially recharged aquifers - Field and modelling studies*. 2006, Humboldt University: Berlin.
31. Barcelona, M.J., T.R. Holm, M.R. Schock, and G.K. George, *Spatial and temporal gradients in aquifer oxidation-reduction conditions.* Water Resources Research, 1989. 25(5): p. 991-1003.
32. Bize, J., B. Grenet, and H. Maneglier, *Le pouvoir épurateur du complexe alluvial en bordure de rivière.* Techniques, Sciences, Méthodes - L'Eau, 1981. 76(7): p. 393-401.
33. Bourg, A.C.M. and C. Bertin, *Biogeochemical Processes During the Infiltration of River Water into an Alluvial Aquifer.* Environmental Science & Technology, 1993. 27(4): p. 661-666.
34. Kedziorek, M.A.M. and A.C.M. Bourg, *Electron trapping capacity of dissolved oxygen and nitrate to evaluate Mn and Fe reductive dissolution in alluvial aquifers during riverbank filtration.* Journal of Hydrology, 2009. 365(1-2): p. 74-78.
35. Lovley, D.R., D.E. Holmes, and K.P. Nevin, *Dissimilatory Fe(III) and Mn(IV) reduction*, in *Advances in Microbial Physiology*. 2004. p. 219-286.
36. Tufenkji, N., J.N. Ryan, and M. Elimelech, *The promise of bank filtration.* Environmental Science & Technology, 2002. 36(21): p. 422A-428A.
37. Hiscock, K.M. and T. Grischek, *Attenuation of groundwater pollution by bank filtration.* Journal of Hydrology, 2002. 266(3-4): p. 139-144.
38. Berger, P., *Removal of Cryptosporidium Using Bank Filtration*, in *Riverbank Filtration: Understanding Contaminant Biogeochemistry and Pathogen Removal*, C. Ray, Editor. 2002, Kluwer Academic Publishers: Dordrecht. p. 85-121.
39. Grischek, T. and C. Ray, *Bank filtration as managed surface - Groundwater interaction.* International Journal of Water, 2009. 5(2): p. 125-139.
40. Grischek, T., J. Schubert, J.L. Jasperse, S.M. Stowe, and M.R. Collins. *What is the appropriate site for RBF?*, in *Management of Aquifer Recharge for Sustainability: Proceedings of the 6th International Symposium on Managed Artificial Recharge of Groundwater (ISMAR6)*. 2007. Phoenix, Arizona: Acacia Publishing. p. 466-474.

41. Hunt, H., J. Schubert, and C. Ray, *Operation and Maintenance Considerations*, in *Riverbank Filtration: Improving Source-water Quality*, C. Ray, G. Melin, and R.B. Linsky, Editors. 2002, Kluwer Academic Publishers: Dordrecht, the Netherlands. p. 61-70.
42. Blavier, J., M.A. Verbanck, F. Craddock, S. Liégeois, D. Latinis, L. Gargouri, G. Flores Rua, F. Debaste, and B. Haut, *Investigation of riverbed filtration systems on the Parapeti river, Bolivia.* Journal of Water Process Engineering, 2014. 1: p. 27-36.
43. Metge, D.W., R.W. Harvey, G.R. Aiken, R. Anders, G. Lincoln, and J. Jasperse, *Influence of organic carbon loading, sediment associated metal oxide content and sediment grain size distributions upon Cryptosporidium parvum removal during riverbank filtration operations, Sonoma County, CA.* Water Research, 2010. 44(4): p. 1126-1137.
44. Medema, G.J., M.H.A. Juhasz-Holterman, and J.A. Luijten. *Removal of micro-organisms by bank filtration in a gravel-sand soil*, in *International Riverbank Filtration Conference*. 2000. Dusseldorf, Germany: IAWR. p. 161-168.
45. Schubert, J., *Water-Quality Improvements with Riverbank Filtration at Dusseldorf Waterworks in Germany*, in *Riverbank Filtration: Improving Source-water Quality*, C. Ray, G. Melin, and R.B. Linsky, Editors. 2002, Kluwer Academic Publishers: Dordrecht, the Netherlands. p. 267-277.
46. Wang, J.Z., R. Song, and S. Hubbs. *Particle removal through riverbank filtration process*, in *International Riverbank Filtration Conference*. 2000. Dusseldorf, Germany: IAWR. p. 161-168.
47. Baveye, P., P. Berger, J. Schijven, and T. Grischek, *Research Needs to Improve the Understanding of Riverbank Filtration for Pathogenic Microorganism Removal*, in *Riverbank Filtration: Improving Source-water Quality*, C. Ray, G. Melin, and R.B. Linsky, Editors. 2002, Kluwer Academic Publishers: Dordrecht, the Netherlands. p. 311-319.
48. Wang, J.Z., *Riverbank filtration case study at Louisville, Kentucky*, in *Riverbank Filtration: Improving Source-water Quality*, C. Ray, G. Melin, and R.B. Linsky, Editors. 2002, Kluwer Academic Publishers: Dordrecht, the Netherlands. p. 117-145.
49. Gollnitz, W.D., J.L. Clancy, B.L. Whitteberry, and J.A. Vogt, *RBF as a microbial treatment process.* Journal American Water Works Association, 2003. 95(12): p. 56-66.
50. Schijven, J., P. Berger, and I. Miettinen, *Removal of Pathogens, Surrogates, Indicators, and Toxins Using Riverbank Filtration*, in *Riverbank Filtration: Improving Source-water Quality*, C. Ray, G. Melin, and R.B. Linsky, Editors. 2002, Kluwer Academic Publishers: Dordrecht, the Netherlands. p. 73-116.
51. Ray, C., T. Grischek, J. Schubert, J.Z. Wang, and T.F. Speth, *A perspective of riverbank filtration.* Journal American Water Works Association, 2002. 94(4): p. 149-160.
52. Darmendrail, D., *Processus biogeochimiques susceptibles d'etre impliques dans l'effet filtre des berges lors de l'alimentation des nappes par les cours d'eau Biogeochemical processes possibly involved in the filtering effect of riverbanks during the supply of aquifers by river watercourses.* Hydrogeologie, 1988(3): p. 187-195.

53. Schlosser, U., *Sanitary Aspects of the Obtaining of Drinking-Water from Bank Filtration and Groundwater Recharge.* Acta Hydrochimica Et Hydrobiologica, 1991. 19(3): p. 319-326.
54. Weiss, W.J., E.J. Bouwer, R. Aboytes, M.W. LeChevallier, C.R. O'Melia, B.T. Le, and K.J. Schwab, *Riverbank filtration for control of microorganisms: results from field monitoring.* Water Research, 2005. 39(10): p. 1990-2001.
55. Weiss, W.J., E.J. Bouwer, W.P. Ball, C.R. O'Melia, M.W. Lechevallier, H. Arora, and T.F. Speth, *Riverbank filtration - fate of DBP precursors and selected microorganisms.* Journal American Water Works Association, 2003. 95(10): p. 68-81.
56. Schubert, J., *Hydraulic aspects of riverbank filtration - field studies.* Journal of Hydrology, 2002. 266(3-4): p. 145-161.
57. Henzler, A.F., J. Greskowiak, and G. Massmann, *Modeling the fate of organic micropollutants during river bank filtration (Berlin, Germany).* Journal of Contaminant Hydrology, 2014. 156: p. 78-92.
58. Ray, C., *Worldwide potential of riverbank filtration.* Clean Technologies and Environmental Policy, 2008. 10(3): p. 223-225.
59. Boving, T.B., B.S. Choudri, P. Cady, A. Cording, K. Patil, and V. Reddy, *Hydraulic and Hydrogeochemical Characteristics of a Riverbank Filtration Site in Rural India.* Water Environment Research, 2014. 86(7): p. 636-648.
60. Singh, P., P. Kumar, I. Mehrotra, and T. Grischek, *Impact of riverbank filtration on treatment of polluted river water.* Journal of Environmental Management, 2010. 91(5): p. 1055-1062.
61. Dash, R.R., E.V.P.B. Prakash, P. Kumar, I. Mehrotra, C. Sandhu, and T. Grischek, *River bank filtration in Haridwar, India: Removal of turbidity, organics and bacteria.* Hydrogeology Journal, 2010. 18(4): p. 973-983.
62. Sharma, B., D.P. Uniyal, R. Dobhal, P.C. Kimothi, and T. Grischek, *A sustainable solution for safe drinking water through bank filtration technology in Uttarakhand, India.* Current Science, 2014. 107(7): p. 1118-1124.
63. Hoque, M.A., J.M. McArthur, P.K. Sikdar, J.D. Ball, and T.N. Molla, *Tracing recharge to aquifers beneath an Asian megacity with Cl/Br and stable isotopes: The example of Dhaka, Bangladesh.* Hydrogeology Journal, 2014. 22(7): p. 1549-1560.
64. Othman, S.Z., M.N. Adlan, and M.R. Selamat, *A study on the potential of riverbank filtration for the removal of color, iron, turbidity and E.Coli in Sungai Perak, Kota Lama Kiri, Kuala Kangsar, Perak, Malaysia.* Jurnal Teknologi, 2015. 74(11): p. 83-91.
65. Shamsuddin, M.K.N., W.N.A. Sulaiman, S. Suratman, M.P. Zakaria, and K. Samuding, *Groundwater and surface-water utilisation using a bank infiltration technique in Malaysia.* Hydrogeology Journal, 2014. 22(3): p. 543-564.
66. Shamsuddin, M.K.N., W.N.A. Sulaiman, S. Suratman, M.P. Zakaria, and K. Samuding, *Conjunctive use of surface water and groundwater via the bank infiltration method.* Arabian Journal of Geosciences, 2014. 7(9): p. 3731-3753.
67. Freitas, D.A., J.J.S.P. Cabral, A.L.R. Paiva, and R.J.R. Molica, *Application of bank filtration technology for water quality improvement in a warm climate: A*

case study at Beberibe River in Brazil. Journal of Water Supply: Research and Technology - AQUA, 2012. 61(5): p. 319-330.
68. Romero, L.G., B.S. Pizzolatti, M.B.D. Soares, D.C.G.S. Michelan, and M.L. Sens. *Bank filtration: Application in rural areas. Case studies in Santa Catarina, Brazil*, in *ASABE - 21st Century Watershed Technology: Improving Water Quality and Environment 2010*. 2010. p. 378-384.
69. Jaramillo, M., *Riverbank filtration: An efficient and economical drinking-water treatment technology.* DYNA (Colombia), 2012. 79(171): p. 148-157.
70. Mutsvangwa, C., B. Mutaurwa, M. Mazhandu, and M. Kubare, *Application of Harvey-Garabedian model for describing bacterial removal in Sand Abstraction Systems associated with ephemeral rivers.* Journal of Contaminant Hydrology, 2006. 88(1-2): p. 55-68.
71. Hamdan, A.M., M.M. Sensoy, and M.S. Mansour, *Evaluating the effectiveness of bank infiltration process in new Aswan City, Egypt.* Arabian Journal of Geosciences, 2013. 6(11): p. 4155-4165.
72. Wang, C., P.F. Wang, and X. Hu, *Removal of CODCr and nitrogen in severely polluted river water by bank filtration.* Environmental Technology, 2007. 28(6): p. 649-657.
73. Lee, S.I. and S.S. Lee. *Site suitability analysis for riverbank filtration in the Han River, Korea*, in *Advances in Water Resources and Hydraulic Engineering - Proceedings of 16th IAHR-APD Congress and 3rd Symposium of IAHR-ISHS*. 2009. p. 236-239.
74. Pholkern, K., K. Srisuk, T. Grischek, M. Soares, S. SchÃ¤fer, L. Archwichai, P. Saraphirom, P. Pavelic, and W. Wirojanagud, *Riverbed clogging experiments at potential river bank filtration sites along the Ping River, Chiang Mai, Thailand.* Environmental Earth Sciences, 2015. 73(12): p. 7699-7709.
75. Blanford, W., T. Boving, Z. Al-Ghazawi, M. Shawaqfah, J. Al-Rashdan, I. Saadoun, J. Schijven, and Q. Ababneh. *River bank filtration for protection of Jordanian surface and groundwater*, in *World Environmental and Water Resources Congress 2010: Challenges of Change - Proceedings of the World Environmental and Water Resources Congress 2010*. 2010. p. 776-781.
76. von Rohr, M.R., J.G. Hering, H.P.E. Kohler, and U. von Gunten, *Column studies to assess the effects of climate variables on redox processes during riverbank filtration.* Water Research, 2014. 61: p. 263-275.
77. Eckert, P., R. Lamberts, and C. Wagner, *The impact of climate change on drinking water supply by riverbank filtration*, in *Water Science and Technology: Water Supply*. 2008. p. 319-324.
78. Sprenger, C., G. Lorenzen, I. Hülshoff, G. Grützmacher, M. Ronghang, and A. Pekdeger, *Vulnerability of bank filtration systems to climate change.* Science of the Total Environment, 2011. 409(4): p. 655-663.
79. Missimer, T.M., J.E. Drewes, R.G. Maliva, and G. Amy, *Aquifer Recharge and Recovery: Groundwater Recharge Systems for Treatment, Storage, and Water Reclamation.* Ground Water, 2011. 49(6): p. 771-771.
80. Piet, G.J. and B.C.J. Zoeteman, *Organic water quality changes during sand bank and dune filtration of surface waters in the Netherlands.* J. AM. WATERWORKS ASSOC., 1980. 72(7 , Jul. 1980): p. 400-404.

81. Dillon, P., S. Toze, D. Page, J. Vanderzalm, E. Bekele, J. Sidhu, and S. Rinck-Pfeiffer, *Managed aquifer recharge: Rediscovering nature as a leading edge technology.* Water Science and Technology, 2010. 62(10): p. 2338-2345.
82. Dillon, P., P. Pavelic, D. Page, H. Beringen, and J. Ward, *Managed Aquifer Recharge: An Introduction*. 2009, Commonwealth of Australia, National Water Commission Waterlines Report No. 13. p. 65.
83. National Research Council (NRC), *Prospects for Managed Underground Storage of Recoverable Water*. 2008, National Academies Press: Washington, D.C.
84. Swiezckowski, D., S. Morris, and T. Carpenter. *An Overview of Arizona's Recharge Program*, in *Proceedings of the 6th International Symposium on Managed Artificial Recharge of Groundwater (ISMAR6)*. 2007. Phoenix, Arizona: Acacia Publishing. p. 366-378.
85. Fox, P., K. Narayanaswamy, A. Genz, and J.E. Drewes, *Water quality transformations during soil aquifer treatment at the Mesa Northwest Water Reclamation Plant, USA*, in *Water Science and Technology*. 2001. p. 343-350.
86. Beal, C.D., E.A. Gardner, and N.W. Menzies, *Process, performance, and pollution potential: A review of septic tank-soil absorption systems.* Australian Journal of Soil Research, 2005. 43(7): p. 781-802.
87. Gunnarsdottir, M.J., S.M. Gardarsson, and H.O. Andradottir, *Microbial contamination in groundwater supply in a cold climate and coarse soil: case study of norovirus outbreak at Lake Myvatn, Iceland.* Hydrology Research, 2013. 44(6): p. 1114-1128.
88. Scandura, J.E. and M.D. Sobsey, *Viral and bacterial contamination of groundwater from on-site sewage treatment systems.* Water Science and Technology, 1997. 35(11-12): p. 141-146.
89. Dillon, P., *Future management of aquifer recharge.* Hydrogeology Journal, 2005. 13(1): p. 313-316.
90. Yao, K.M., M.M. Habibian, and C.R. O'Melia, *Water and Waste Water Filtration - Concepts and Applications.* Environmental Science & Technology, 1971. 5(11): p. 1105-1112.
91. Tufenkji, N. and M. Elimelech, *Correlation equation for predicting single-collector efficiency in physicochemical filtration in saturated porous media.* Environmental Science & Technology, 2004. 38(2): p. 529-536.
92. Tufenkji, N., G.F. Miller, J.N. Ryan, R.W. Harvey, and M. Elimelech, *Transport of Cryptosporidium oocysts in porous media: Role of straining and physicochemical filtration.* Environmental Science & Technology, 2004. 38(22): p. 5932-5938.
93. McDowell-Boyer, L.M., J.R. Hunt, and N. Sitar, *Particle-Transport through Porous-Media.* Water Resources Research, 1986. 22(13): p. 1901-1921.
94. Hahn, M.W. and C.R. O'Melia, *Deposition and Reentrainment of Brownian Particles in Porous Media under Unfavorable Chemical Conditions: Some Concepts and Applications.* Environmental Science & Technology 2004. 38(1): p. 210-220.
95. Loveland, J.P., J.N. Ryan, G.L. Amy, and R.W. Harvey, *The reversibility of virus attachment to mineral surfaces.* Colloids and Surfaces a-Physicochemical and Engineering Aspects, 1996. 107: p. 205-221.

96. Tufenkji, N. and M. Elimelech, *Breakdown of colloid filtration theory: Role of the secondary energy minimum and surface charge heterogeneities.* Langmuir, 2005. 21(3): p. 841-852.
97. Ryan, J.N., M. Elimelech, R.A. Ard, R.W. Harvey, and P.R. Johnson, *Bacteriophage PRD1 and silica colloid transport and recovery in an iron oxide-coated sand aquifer.* Environmental Science & Technology, 1999. 33(1): p. 63-73.
98. Schijven, J., *Virus Removal by Soil Passage at Field Scale and Groundwater Protection*, in *Riverbank Filtration: Understanding Contaminant Biogeochemistry and Pathogen Removal*, C. Ray, Editor. 2002, Kluwer Academic Publishers: Dordrecht. p. 55-84.
99. Bhattacharjee, S., J.N. Ryan, and M. Elimelech, *Virus transport in physically and geochemically heterogeneous subsurface porous media.* Journal of Contaminant Hydrology, 2002. 57(3-4): p. 161-187.
100. Penrod, S.L., T.M. Olson, and S.B. Grant, *Deposition kinetics of two viruses in packed beds of quartz granular media.* Langmuir, 1996. 12(23): p. 5576-5587.
101. Walker, S.L., J.A. Redman, and M. Elimelech, *Role of cell surface lipopolysaccharides in Escherichia coli K12 adhesion and transport.* Langmuir, 2004. 20(18): p. 7736-7746.
102. Rijnaarts, H.H.M., W. Norde, J. Lyklema, and A.J.B. Zehnder, *DLVO and steric contributions to bacterial deposition in media of different ionic strengths.* Colloids and Surfaces B-Biointerfaces, 1999. 14(1-4): p. 179-195.
103. Langlet, J., F. Gaboriaud, C. Gantzer, and J.F.L. Duval, *Impact of chemical and structural anisotropy on the electrophoretic mobility of spherical soft multilayer particles: The case of bacteriophage MS2.* Biophysical Journal, 2008. 94(8): p. 3293-3312.
104. Ohshima, H., *Electrophoresis of soft particles.* Advances in Colloid and Interface Science, 1995. 62(2-3): p. 189-235.
105. Liu, Y., C.H. Yang, and J. Li, *Influence of extracellular polymeric substances on Pseudomonas aeruginosa transport and deposition profiles in porous media.* Environmental Science & Technology, 2007. 41(1): p. 198-205.
106. Walker, S.L., J.E. Hill, J.A. Redman, and M. Elimelech, *Influence of growth phase on adhesion kinetics of Escherichia coli D21g.* Applied and Environmental Microbiology, 2005. 71(6): p. 3093-3099.
107. Walker, S.L., J.A. Redman, and M. Elimelech, *Influence of growth phase on bacterial deposition: Interaction mechanisms in packed-bed column and radial stagnation point flow systems.* Environmental Science & Technology, 2005. 39(17): p. 6405-6411.
108. Haznedaroglu, B.Z., C.H. Bolster, and S.L. Walker, *The role of starvation on Escherichia coli adhesion and transport in saturated porous media.* Water Research, 2008. 42(6-7): p. 1547-1554.
109. Castro, F.D. and N. Tufenkji, *Role of Oxygen Tension on the Transport and Retention of Two Pathogenic Bacteria in Saturated Porous Media.* Environmental Science & Technology, 2008. 42(24): p. 9178-9183.

110. Walker, S.L., *The role of nutrient presence on the adhesion kinetics of Burkholderia cepacia G4g and ENV435g.* Colloids and Surfaces B-Biointerfaces, 2005. 45(3-4): p. 181-188.
111. Fong, T.T. and E.K. Lipp, *Enteric viruses of humans and animals in aquatic environments: Health risks, detection, and potential water quality assessment tools.* Microbiology and Molecular Biology Reviews, 2005. 69(2): p. 357-371.
112. Pang, L.P., M. Close, M. Goltz, M. Noonan, and L. Sinton, *Filtration and transport of Bacillus subtilis spores and the F-RNA phage MS2 in a coarse alluvial gravel aquifer: Implications in the estimation of setback distances.* Journal of Contaminant Hydrology, 2005. 77(3): p. 165-194.
113. Blanford, W.J., M.L. Brusseau, T.C.J. Yeh, C.P. Gerba, and R. Harvey, *Influence of water chemistry and travel distance on bacteriophage PRD-1 transport in a sandy aquifer.* Water Research, 2005. 39(11): p. 2345-2357.
114. Pieper, A.P., J.N. Ryan, R.W. Harvey, G.L. Amy, T.H. Illangasekare, and D.W. Metge, *Transport and Recovery of Bacteriophage PRD1 in a Sand and Gravel Aquifer: Effect of Sewage-Derived Organic Matter.* Environmental Science and Technology, 1997. 31(4): p. 1163-1170.
115. Ryan, J.N., R.W. Harvey, D. Metge, M. Elimelech, T. Navigato, and A.P. Pieper, *Field and laboratory investigations of inactivation of viruses (PRD1 and MS2) attached to iron oxide-coated quartz sand.* Environmental Science & Technology, 2002. 36(11): p. 2403-2413.
116. Dong, H.L., T.C. Onstott, M.F. Deflaun, M.E. Fuller, T.D. Scheibe, S.H. Streger, R.K. Rothmel, and B.J. Mailloux, *Relative dominance of physical versus chemical effects on the transport of adhesion-deficient bacteria in intact cores from South Oyster, Virginia.* Environmental Science & Technology, 2002. 36(5): p. 891-900.
117. Dong, H.L., T.D. Scheibe, W.P. Johnson, C.M. Monkman, and M.E. Fuller, *Change of collision efficiency with distance in bacterial transport experiments.* Ground Water, 2006. 44(3): p. 415-429.
118. Hall, J.A., B.J. Mailloux, T.C. Onstott, T.D. Scheibe, M.E. Fuller, H. Dong, and M.F. DeFlaun, *Physical versus chemical effects on bacterial and bromide transport as determined from on site sediment column pulse experiments.* Journal of Contaminant Hydrology, 2005. 76(3-4): p. 295-314.
119. Schijven, J.F., G. Medema, A.J. Vogelaar, and S.M. Hassanizadeh, *Removal of microorganisms by deep well injection.* Journal of Contaminant Hydrology, 2000. 44(3-4): p. 301-327.
120. Schijven, J.F., W. Hoogenboezem, S.M. Hassanizadeh, and J.H. Peters, *Modeling removal of bacteriophages MS2 and PRD1 by dune recharge at Castricum, Netherlands.* Water Resources Research, 1999. 35(4): p. 1101-1111.
121. Van der Wielen, P., W. Senden, and G. Medema, *Removal of Bacteriophages MS2 and Phi X174 during transport in a sandy anoxic aquifer.* Environmental Science & Technology, 2008. 42(12): p. 4589-4594.
122. Abudalo, R.A., Y.G. Bogatsu, J.N. Ryan, R.W. Harvey, D.W. Metge, and M. Elimelech, *Effect of ferric oxyhydroxide grain coatings on the transport of bacteriophage PRD1 and Cryptosporidium parvum oocysts in saturated porous media.* Environmental Science & Technology, 2005. 39(17): p. 6412-6419.

123. Elimelech, M., M. Nagai, C.H. Ko, and J.N. Ryan, *Relative insignificance of mineral grain zeta potential to colloid transport in geochemically heterogeneous porous media.* Environmental Science & Technology, 2000. 34(11): p. 2143-2148.
124. Foppen, J.W.A., S. Okletey, and J.F. Schijven, *Effect of goethite coating and humic acid on the transport of bacteriophage PRD1 in columns of saturated sand.* Journal of Contaminant Hydrology, 2006. 85(3-4): p. 287-301.
125. Appenzeller, B.M.R., Y.B. Duval, F. Thomas, and J.C. Block, *Influence of phosphate on bacterial adhesion onto iron oxyhydroxide in drinking water.* Environmental Science & Technology, 2002. 36(4): p. 646-652.
126. Schulze-Makuch, D., H. Guan, and S.D. Pillai, *Effects of pH and geological medium on bacteriophage MS2 transport in a model aquifer.* Geomicrobiology Journal, 2003. 20(1): p. 73-84.
127. Cheng, L., A.S. Chetochine, I.L. Pepper, and M.L. Brusseau, *Influence of DOC on MS-2 bacteriophage transport in a sandy soil.* Water Air and Soil Pollution, 2007. 178(1-4): p. 315-322.
128. Zhuang, J. and Y. Jin, *Virus retention and transport as influenced by different forms of soil organic matter.* Journal of Environmental Quality, 2003. 32(3): p. 816-823.
129. Quanrud, D.M., S.M. Carroll, C.P. Gerba, and R.G. Arnold, *Virus removal during simulated soil-aquifer treatment.* Water Research, 2003. 37(4): p. 753-762.
130. Harvey, R.W. and J.N. Ryan, *Use of PRDI bacteriophage in groundwater viral transport, inactivation, and attachment studies.* Fems Microbiology Ecology, 2004. 49(1): p. 3-16.
131. Anders, R. and C.V. Chrysikopoulos, *Evaluation of the factors controlling the time-dependent inactivation rate coefficients of bacteriophage MS2 and PRD1.* Environmental Science & Technology, 2006. 40(10): p. 3237-3242.
132. Collins, K.E., A.A. Cronin, J. Rueedi, S. Pedley, E. Joyce, P.J. Humble, and J.H. Tellam, *Fate and transport of bacteriophage in UK aquifers as surrogates for pathogenic viruses.* Engineering Geology, 2006. 85(1-2): p. 33-38.
133. Gordon, C. and S. Toze, *Influence of groundwater characteristics on the survival of enteric viruses.* Journal of Applied Microbiology, 2003. 95(3): p. 536-544.
134. Jansons, J., L.W. Edmonds, B. Speight, and M.R. Bucens, *Survival of Viruses in Groundwater.* Water Research, 1989. 23(3): p. 301-306.
135. Keswick, B.H. and C.P. Gerba, *Viruses in Groundwater.* Environmental Science & Technology, 1980. 14(11): p. 1290-1297.
136. Pedley, S., M. Yates, J.F. Schijven, J. West, G. Howard, and M. Barrett, *Pathogens: Health relevance, transport and attenuation*, in *Protecting Groundwater for Health: Managing the Quality of Drinking-water Sources*, O. Schmoll, et al., Editors. 2006, World Health Organization, IWA Publishing: London. p. 49-80.
137. Allwood, P.B., Y.S. Malik, C.W. Hedberg, and S.M. Goyal, *Survival of F-specific RNA coliphage, feline calicivirus, and Escherichia coli in water: a comparative study.* Applied and Environmental Microbiology, 2003. 69(9): p. 5707-5710.

138. Hurst, C.J., C.P. Gerba, and I. Cech, *Effects of Environmental Variables and Soil Characteristics on Virus Survival in Soil.* Applied and Environmental Microbiology, 1980. 40(6): p. 1067-1079.
139. Feng, Y.Y., S.L. Ong, J.Y. Hu, X.L. Tan, and W.J. Ng, *Effects of pH and temperature on the survival of coliphages MS2 and Q beta.* Journal of Industrial Microbiology & Biotechnology, 2003. 30(9): p. 549-552.
140. Chattopadhyay, D., S. Chattopadhyay, W.G. Lyon, and J.T. Wilson, *Effect of surfactants on the survival and sorption of viruses.* Environmental Science & Technology, 2002. 36(19): p. 4017-4024.
141. Blanc, R. and A. Nasser, *Effect of effluent quality and temperature on the persistence of viruses in soil.* Water Science and Technology, 1996. 33(10-11): p. 237-242.
142. Hurst, C.J., *Influence of aerobic microorganisms upon virus survival in soil.* Canadian journal of microbiology, 1988. 34(5): p. 696-9.
143. Nasser, A.M., R. Glozman, and Y. Nitzan, *Contribution of microbial activity to virus reduction in saturated soil.* Water Research, 2002. 36(10): p. 2589-2595.
144. John, D.E. and J.B. Rose, *Review of factors affecting microbial survival in groundwater.* Environmental Science & Technology, 2005. 39(19): p. 7345-7356.
145. Madigan, M.T., J.M. Martinko, and J. Parker, eds. *Brock Biology of Microorganisms*. 10th ed. 2003, Prentice Hall: Upper Saddle River, NJ. 1019.
146. Grant, S.B., E.J. List, and M.E. Lidstrom, *Kinetic-Analysis of Virus Adsorption and Inactivation in Batch Experiments.* Water Resources Research, 1993. 29(7): p. 2067-2085.
147. Bouwer, E.J., H.H.M. Rijnaarts, A.B. Cunningham, and R. Gerlach, *Biofilms in Porous Media*, in *Biofilms II: Process Analysis and Applications*, J.D. Bryers, Editor. 2000, Wiley-Liss: New York. p. 123-158.
148. Flemming, H.C., J. Wingender, C. Mayer, V. Korstgens, and W. Borchard, *Cohesiveness in biofilm matrix polymers*, in *Community structure and co-operation in biofilms*, D.G. Allison, et al., Editors. 2000, Cambridge University Press: Cambridge. p. 87-105.
149. Nielsen, P.H., A. Jahn, and R. Palmgren, *Conceptual model for production and composition of exopolymers in biofilms.* Water Science and Technology, 1997. 36(1): p. 11-19.
150. Stewart, P.S. and M.J. Franklin, *Physiological heterogeneity in biofilms.* Nature Reviews Microbiology, 2008. 6(3): p. 199-210.
151. Besemer, K., G. Singer, R. Limberger, A.K. Chlup, G. Hochedlinger, I. Hödl, C. Baranyi, and T.J. Battin, *Biophysical controls on community succession in stream biofilms.* Applied and Environmental Microbiology, 2007. 73(15): p. 4966-4974.
152. Cao, B., L.A. Shi, R.N. Brown, Y.J. Xiong, J.K. Fredrickson, M.F. Romine, M.J. Marshall, M.S. Lipton, and H. Beyenal, *Extracellular polymeric substances from Shewanella sp HRCR-1 biofilms: characterization by infrared spectroscopy and proteomics.* Environmental Microbiology, 2011. 13(4): p. 1018-1031.
153. D'Abzac, P., F. Bordas, E. Joussein, E. Van Hullebusch, P.N.L. Lens, and G. Guibaud, *Characterization of the mineral fraction associated to extracellular polymeric substances (EPS) in anaerobic granular sludges.* Environmental Science and Technology, 2010. 44(1): p. 412-418.

154. Babauta, J.T., H.D. Nguyen, and H. Beyenal, *Redox and pH microenvironments within Shewanella oneidensis MR-1 biofilms reveal an electron transfer mechanism.* Environmental Science and Technology, 2011. 45(15): p. 6654-6660.
155. Kim, H.Y., K.M. Yeon, C.H. Lee, S. Lee, and T. Swaminathan, *Biofilm structure and extracellular polymeric substances in low and high dissolved oxygen membrane bioreactors.* Separation Science and Technology, 2006. 41(7): p. 1213-1230.
156. Thormann, K.M., R.M. Saville, S. Shukla, and A.M. Spormann, *Induction of rapid detachment in Shewanella oneidensis MR-1 biofilms.* Journal of Bacteriology, 2005. 187(3): p. 1014-1021.
157. McLean, J.S., P.D. Majors, C.L. Reardon, C.L. Bilskis, S.B. Reed, M.F. Romine, and J.K. Fredrickson, *Investigations of structure and metabolism within Shewanella oneidensis MR-1 biofilms.* Journal of Microbiological Methods, 2008. 74(1): p. 47-56.
158. Drury, W.J., W.G. Characklis, and P.S. Stewart, *Interactions of 1 μm Latex-Particles with Pseudomonas-Aeruginosa Biofilms.* Water Research, 1993. 27(7): p. 1119-1126.
159. Okabe, S., H. Kuroda, and Y. Watanabe, *Significance of biofilm structure on transport of inert particulates into biofilms.* Water Science and Technology, 1998. 38(8-9): p. 163-170.
160. Drury, W.J., P.S. Stewart, and W.G. Characklis, *Transport of 1 μm Latex-Particles in Pseudomonas-Aeruginosa Biofilms.* Biotechnology and Bioengineering, 1993. 42(1): p. 111-117.
161. Reichert, P. and O. Wanner, *Movement of solids in biofilms: Significance of liquid phase transport.* Water Science and Technology, 1997. 36(1): p. 321-328.
162. Morales, C.F.L., M. Strathmann, and H.C. Flemming, *Influence of biofilms on the movement of colloids in porous media. Implications for colloid facilitated transport in subsurface environments.* Water Research, 2007. 41(10): p. 2059-2068.
163. Paris, T., S. Skali-Lami, and J.C. Block, *Probing young drinking water biofilms with hard and soft particles.* Water Research, 2009. 43(1): p. 117-126.
164. Langmark, J., M.V. Storey, N.J. Ashbolt, and T.A. Stenstrom, *Accumulation and fate of microorganisms and microspheres in biofilms formed in a pilot-scale water distribution system.* Applied and Environmental Microbiology, 2005. 71(2): p. 706-712.
165. Briandet, R., P. Lacroix-Gueu, M. Renault, S. Lecart, T. Meylheuc, E. Bidnenko, K. Steenkeste, M.N. Bellon-Fontaine, and M.P. Fontaine-Aupart, *Fluorescence correlation spectroscopy to study diffusion and reaction of bacteriophages inside biofilms.* Applied and Environmental Microbiology, 2008. 74(7): p. 2135-2143.
166. Lacroix-Gueu, P., R. Briandet, S. Leveque-Fort, M.N. Bellon-Fontaine, and M.P. Fontaine-Aupart, *In situ measurements of viral particles diffusion inside mucoid biofilms.* Comptes Rendus Biologies, 2005. 328(12): p. 1065-1072.
167. Peulen, T.O. and K.J. Wilkinson, *Diffusion of Nanoparticles in a Biofilm.* Environmental Science & Technology, 2011. 45(8): p. 3367-3373.
168. Helmi, K., S. Skraber, C. Gantzer, R. Willame, L. Hoffmann, and H.M. Cauchie, *Interactions of Cryptosporidium parvum, Giardia lamblia, vaccinal poliovirus*

type 1, and bacteriophages phi X174 and MS2 with a drinking water biofilm and a wastewater biofilm. Applied and Environmental Microbiology, 2008. 74(7): p. 2079-2088.
169. Briandet, R., J.M. Herry, and M.N. Bellon-Fontaine, *Determination of the van der Waals, electron donor and electron acceptor surface tension components of static Gram-positive microbial biofilms.* Colloids and Surfaces B-Biointerfaces, 2001. 21(4): p. 299-310.
170. Habimana, O., K. Steenkeste, M.P. Fontaine-Aupart, M.N. Bellon-Fontaine, S. Kulakauskas, and R. Briandet, *Diffusion of Nanoparticles in Biofilms Is Altered by Bacterial Cell Wall Hydrophobicity.* Applied and Environmental Microbiology, 2011. 77(1): p. 367-368.
171. Körstgens, V., H.C. Flemming, J. Wingender, and W. Borchard, *Influence of calcium ions on the mechanical properties of a model biofilm of mucoid Pseudomonas aeruginosa.* Water Science and Technology, 2001. 43(6): p. 49-57.
172. Eisenmann, H., I. Letsiou, A. Feuchtinger, W. Beisker, E. Mannweiler, P. Hutzler, and P. Arnz, *Interception of small particles by flocculent structures, sessile ciliates, and the basic layer of a wastewater biofilm.* Applied and Environmental Microbiology, 2001. 67(9): p. 4286-4292.
173. Zhang, M., J.R. Dale, T.J. DiChristina, and A.G. Stack, *Dissolution morphology of iron (Oxy)(Hydr)Oxides exposed to the dissimilatory iron-reducing bacterium shewanella oneidensisMR-1.* Geomicrobiology Journal, 2009. 26(2): p. 83-92.
174. Bradford, S.A., Y.S. Wang, H. Kim, S. Torkzaban, and J. Simunek, *Modeling Microorganism Transport and Survival in the Subsurface.* Journal of Environmental Quality, 2014. 43(2): p. 421-440.
175. Tufenkji, N., *Modeling microbial transport in porous media: Traditional approaches and recent developments.* Advances in Water Resources, 2007. 30(6-7): p. 1455-1469.
176. Yates, M.V. and S.R. Yates, *Virus Survival and Transport in Ground-Water.* Water Science and Technology, 1988. 20(11-12): p. 301-307.
177. Harter, T., S. Wagner, and E.R. Atwill, *Colloid transport and filtration of Cryptosporidium parvum in sandy soils and aquifer sediments.* Environmental Science & Technology, 2000. 34(1): p. 62-70.
178. Powelson, D.K., C.P. Gerba, and M.T. Yahya, *Virus transport and removal in wastewater during aquifer recharge.* Water Research, 1993. 27(4): p. 583-90.
179. Schijven, J.F. and S.M. Hassanizadeh, *Removal of viruses by soil passage: Overview of modeling, processes, and parameters.* Critical Reviews in Environmental Science and Technology, 2000. 30(1): p. 49-127.
180. Johnson, W.P., M. Tong, and X. Li, *On colloid retention in saturated porous media in the presence of energy barriers: The failure of alpha, and opportunities to predict eta.* Water Resources Research, 2007. 43(12).
181. Bradford, S.A., S. Torkzaban, and S.L. Walker, *Coupling of physical and chemical mechanisms of colloid straining in saturated porous media.* Water Research, 2007. 41(13): p. 3012-3024.
182. Pang, L.P., *Microbial Removal Rates in Subsurface Media Estimated From Published Studies of Field Experiments and Large Intact Soil Cores.* Journal of Environmental Quality, 2009. 38(4): p. 1531-1559.

183. Scheibe, T.D., H.L. Dong, and Y.L. Xie, *Correlation between bacterial attachment rate coefficients and hydraulic conductivity and its effect on field-scale bacterial transport.* Advances in Water Resources, 2007. 30(6-7): p. 1571-1582.
184. Tufenkji, N., J.A. Redman, and M. Elimelech, *Interpreting deposition patterns of microbial particles in laboratory-scale column experiments.* Environmental Science & Technology, 2003. 37(3): p. 616-623.
185. Refsgaard, J.C., S. Christensen, T.O. Sonnenborg, D. Seifert, A.L. Højberg, and L. Troldborg, *Review of strategies for handling geological uncertainty in groundwater flow and transport modeling.* Advances in Water Resources, 2012. 36: p. 36-50.
186. Baratelli, F., M. Giudici, and G. Parravicini, *Single- and Dual-domain Models of Solute Transport in Alluvial Sediments: the Effects of Heterogeneity Structure and Spatial Scale.* Transport in Porous Media, 2014. 105(2): p. 315-348.
187. Siirila-Woodburn, E.R. and R.M. Maxwell, *A heterogeneity model comparison of highly resolved statistically anisotropic aquifers.* Advances in Water Resources, 2015. 75: p. 53-66.
188. Maxwell, R.M., C. Welty, and A.F.B. Tompson, *Streamline-based simulation of virus transport resulting from long term artificial recharge in a heterogeneous aquifer.* Advances in Water Resources, 2003. 26(10): p. 1075-1096.
189. Maxwell, R.M., C. Welty, and R.W. Harvey, *Revisiting the Cape Cod Bacteria Injection Experiment Using a Stochastic Modeling Approach.* Environmental Science & Technology, 2007. 41(15): p. 5548-5558.
190. Rehmann, L.L.C., C. Welty, and R.W. Harvey, *Stochastic analysis of virus transport in aquifers.* Water Resources Research, 1999. 35(7): p. 1987-2006.
191. Molin, S., V. Cvetkovic, and T.A. Stenstrom, *Microbial risk assessment in heterogeneous aquifers: 2. Infection risk sensitivity.* Water Resources Research, 2010. 46.
192. Molin, S. and V. Cvetkovic, *Microbial risk assessment in heterogeneous aquifers: 1. Pathogen transport.* Water Resources Research, 2010. 46.
193. Massoudieh, A., N.X. Lu, X.M. Liang, T.H. Nguyen, and T.R. Ginn, *Bayesian process-identification in bacteria transport in porous media.* Journal of Contaminant Hydrology, 2013. 153: p. 78-91.
194. Hari Prasad, K.S., D.N. Ratha, and C.S.P. Ojha, *Identification of virus transport parameters in groundwater: Data errors and bias.* Journal of Hydro-environment Research, 2012. 6(1): p. 41-50.
195. Maraqa, M.A. and S.A. Khashan, *Modeling solute transport affected by heterogeneous sorption kinetics using single-rate nonequilibrium approaches.* Journal of Contaminant Hydrology, 2014. 157: p. 73-86.

2 Surface properties of Shewanella oneidensis MR-1 cultured under aerobic, NO3-- and Fe(III)-reducing conditions, and development of a biofilm reactor for surface characterization analyses

2.1 Background and Motivation

A recent Dutch field study [1] demonstrated enhanced transport in an anoxic aquifer for the bacteriophage MS2, a common surrogate for pathogenic viruses. The results suggested that The Netherlands' sixty day requirement for subsurface travel or residence time may not be sufficient to protect drinking water abstraction wells located in anoxic aquifers from viral contamination.

Anoxic conditions in shallow aquifers are the result of microbial activity. As surface water moves into an aquifer, native soil microorganisms break down the organic matter present, using it as a substrate and carbon source, and transferring the electrons released during their metabolic processes to a terminal electron acceptor, thus linking the oxidation of organic carbon to the redox chemistry of the aquifer [2, 3]. When the oxygen present in infiltrating waters is not sufficient to degrade all the organic matter, the aquifer becomes anoxic [4].

The microorganisms responsible for anoxic conditions in the subsurface exist primarily in biofilm communities. The bacterial populations and the physiological states of the organisms present in the biofilm vary over both space and time [5] as the biofilm develops and responds to ambient conditions. However, our understanding of these dynamics is insufficient to allow evaluation of the potential impacts on the transport of microbial pathogens and other bioparticles.

2.1.1 Biofilm EPS

The cells in a biofilm are anchored by a gel-like matrix of extracellular polymeric substances (EPS) that includes various secreted proteins, glycoproteins, carbohydrates, glycolipids, and nucleic acids, as well as cellular debris, and exogenous substances like humic acids, multivalent cations, and other colloidal or dissolved compounds, with a potentially significant mineral fraction [6, 7]. It is highly hydrated and locally charged. As reviewed by Flemming *et al.* [8], carboxyl functional groups can contribute significant negative charge to EPS polysaccharides (e.g., uronic acids) and EPS proteins (aspartic and glutamic amino acids), while phosphate-containing nucleotides also contribute negative charge to the EPS layer. High alanine, leucine, and glycine content in EPS proteins can contribute significant hydrophobicity. Hydrophobic interactions, cross-linking with divalent cations, and tangled biopolymers provide stability [9]. The distribution of charged and hydrophobic/hydrophilic regions on macromolecules contributes to EPS structure and to the sorption properties of the biofilm.

While the hydrodynamic regime undoubtedly influences biofilm morphology, biofilm structure is also controlled by biological (non-physical) factors [10]. Increased EPS has been observed in *Pseudomonas* biofilms under starvation conditions, at least in the short term [11]. Low dissolved oxygen conditions can correlate with increased EPS production and lower protein content [12], and with a decrease in carboxylated lipopolysaccharides [13]. *Shewanella oneidensis* biofilms grown aerobically disintegrate quickly when media flow stops, with detachment observed in as little as 5 minutes. It was demonstrated that the effect was due to rapid depletion of dissolved oxygen [14] and the resulting decrease in energy availability as intracellular ATP concentrations fell [15].

Another study of aerobic *Shewanella* biofilms [16] showed distinct morphological differences (Figure 2-1) when they were deprived of fumarate, an alternate electron acceptor used when oxygen is unavailable. The changes were attributed to anaerobic conditions in the deeper layers of the biofilms.

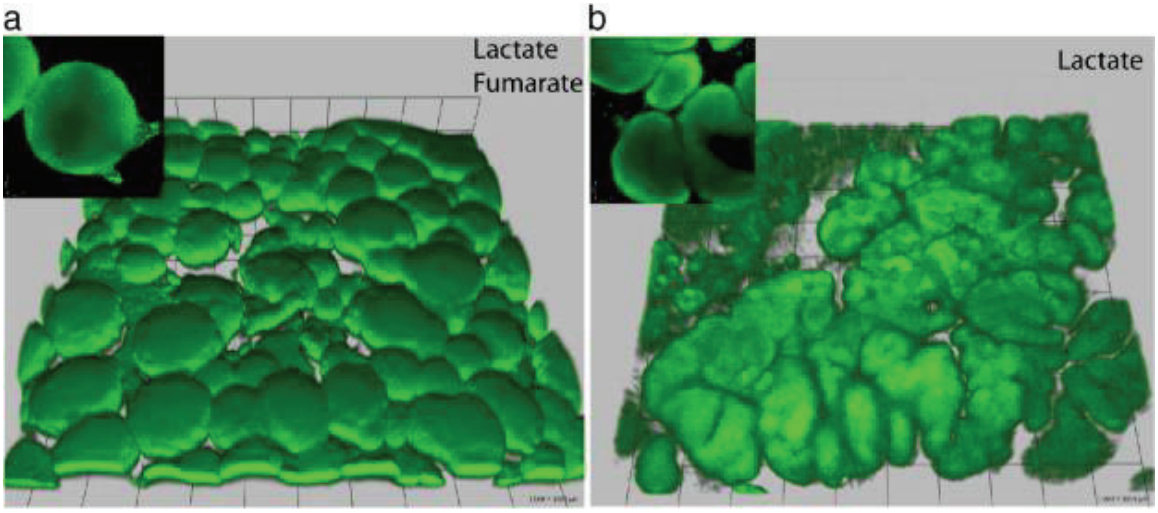

Figure 2-1: *Shewanella oneidensis* grown with a lactate carbon source under aerobic conditions (a) with or (b) without fumarate, an alternate electron acceptor used under anaerobic conditions. Differences in morphology are attributed to metabolic differences in the depths of the biofilm where oxygen is depleted. Figure reprinted from [16] with permission from Elsevier.

2.1.2 Biofilms and particle transport

As reviewed in the introductory chapter, a variety of factors affect particle-biofilm interactions, including bulk-scale biological characteristics of biofilms, physicochemical characteristics of biofilms, solution chemistry, and particle properties. Several recent colloid deposition studies with biofilm-coated media have provided more specific insights on the importance and role of biofilm effects on particle transport.

The complexity of these systems was highlighted in one of the earliest studies on the topic [17], which compared the transport of *E. coli* in columns coated with two different *P. aeruginosa* strains, non-mucoid PAO1 and mucoid PDO300. The mucoid

biofilm improved *E. coli* retention in the column, while the non-mucoid biofilm had a comparatively small impact on *E. coli* removal. The researchers found that surface hydrophobicity and polymeric interactions between the biofilm and the *E. coli* were controlling factors for bacterial transport.

Challenge experiments in quartz sand columns colonized with *E. coli* extended the early evidence for biofilm effects down to the nanoscale size range: the deposition of fullerene particles (d = 85nm) was enhanced by the presence of biofilm across all ionic strengths (1-25 mM NaCl and 0.1-5 mM $CaCl_2$) and flow conditions (4-8 m/d) tested [18]. Although trends were in qualitative agreement with DLVO theory, the attachment-enhancing effects of biofilm roughness were suggested as an additional factor that could help explain observed removals.

Indeed, a later study in a very different system [19] corroborated the idea that biofilm roughness is an important factor influencing particle transport. Groundwater biofilms of various ages grown on PVC coupons were inserted into a parallel-plate flow chamber where the rate constants for *E. coli* and microsphere deposition on the biofilm were determined under various experimental conditions. Young biofilms (2 weeks old) covered the PVC coupon only incompletely, and their physical and community structures had not yet stabilized. *E. coli* deposition on these biofilm coupons was controlled by ionic strength, in agreement with the electrostatic and van der Waals forces described by classic DLVO theory. But as the biofilms matured from 8 wks (when the biofilms achieved complete surface coverage of the PVC coupon) to 16 weeks (when the physical and community structures stabilized), deposition rate constants correlated with biofilm

roughness rather than with solution chemistry. Further comparison of E. coli and microsphere deposition data suggested that steric factors were also in play.

Additional studies have consistently reported that biofilm enhances particle removal in column transport experiments. Another project with *P. aeruginosa* reported that the removal of oocysts and comparably-sized microspheres was at least 2-log greater in biofilm-coated glass bead columns as compared to sterile controls, provided that the biofilms were at least 2-3 weeks old [20]. Comparisons of nano- and microsphere transport showed that when *P. aeruginosa* biofilms were allowed to grow in the sand-packed columns, particle retention increased significantly in all cases [21], but the observed attachment behavior could not be explained by any single dominant process.

A final investigation of colloid deposition in biofilm-coated media evoked additional considerations, relevant for aquifer systems but often unaddressed in laboratory experiments. Transport studies in a 2-D sandbox (45 x 55 x 1 cm) found that clean sand retained 9% of the *E. coli* in an injection test, while retention was 47% in sand coated with a biofilm of groundwater organisms. After a 10 day "starvation" period during which flow of amended groundwater was turned off, flushing the system with sterile groundwater mobilized significant levels of viable *E. coli*, due in part to starvation-induced sloughing of attached biofilm and corresponding release of previously trapped *E. coli* cells [22]. The researchers also reported that the biological activity in the sandbox was sufficient to drive the system anaerobic, although the groundwater feed was O_2-saturated.

The complex interplay of physicochemical and specific interactions controlling particle deposition behavior in these studies highlights the importance of understanding

biofilm-(bio)particle interactions in order to assess the potential for bacterial and pathogen movement in the subsurface environment.

2.1.3 Research needs

Biofilm coatings on media grains could provide an alternate collector surface for deposition of viruses and other biological particles. The very presence of biofilm has been demonstrated to impact particle retention [17, 21]. Parameters that influence biofilm structure or "adhesion properties" are expected to affect particle attachment [23]. The physical and chemical properties of biofilms – e.g., the amount of biofilm present, the structure of that biofilm, the composition of the EPS layer, the viscosity of the EPS layer, and the surface energy of the biofilm – matter in particle-biofilm interactions, though the precise nature of their effects is not always clear.

Changes in biofilm metabolic state are of particular interest and complexity. The Dutch field data [1] suggest that aerobic biofilms might be "stickier" and better at trapping viruses than anaerobic ones, either inherently or due to the effects of solution chemistry on biofilm and EPS properties. Although the anoxic Dutch aquifer showed enhanced virus transport, and although those anoxic conditions were undoubtedly due to the metabolic activity of native subsurface biofilms, little is known about the effects of microbially-induced zonation of terminal electron-acceptor processes (TEAPs) on bioparticle transport and inactivation in groundwater. An improved understanding of the relationship between metabolic state and physicochemical surface properties (e.g., structure, EPS composition, expression of macromolecules on cell surfaces) would help advance the analysis of microbial transport in porous media.

2.2 Objectives

The laboratory investigations described in this chapter sought to contribute to understanding of the role of microbially-induced redox conditions and the influence of biofilms on the extent of transport of biological particles through porous media, with a focus on three specific objectives:

- To characterize the properties of planktonic cultures grown under different redox conditions
- To characterize the properties of biofilms grown under different redox conditions (unachieved)
- To evaluate whether changes in biologically-induced redox conditions may have implications for filter behavior in aquifer-type settings.

2.3 Materials and Methods

2.3.1 Organisms

Although the natural subsurface environment is host to a diverse microbial community, experiments in this project focused on pure cultures to reduce uncontrolled and unquantifiable variability and to ensure that any differences observed under different redox regimes were in fact due to metabolically-linked changes in the properties of the organism, rather than to shifts in community structure or culture bias.

Shewanella oneidensis strain MR-1 was originally selected for study. Although *Shewanella* species have been identified in a variety of subsurface environments where Fe(III) and Mn(IV) reduction occurs, they are probably not significant contributors to manganese and iron reduction in groundwaters, in part because they cannot derive energy

from acetate [24]. Nonetheless, *Shewanella* species figure prominently in the literature on microbial reduction of metals because the organism is not only easy to manipulate and fast-growing, it also exhibits great metabolic flexibility. Critically, it has the ability to exploit a large number of terminal electron acceptors in addition to oxygen: nitrate and nitrite [25], Fe(III) and Mn(IV) [26], sulfite and thiosulfate [27], elemental sulfur [28], as well as other metals and organics, including humic substances.

As reviewed above, previous research has demonstrated that *Shewanella* biofilms are sensitive to sudden changes in oxygen tension [14], making the organism particularly relevant to this work. Furthermore, our laboratory had previous experience with *S. oneidensis* and was in possession of wild type MR-1 (ATCC strain 700550).

Pseudomonas aeruginosa (strain ATCC #27853) was obtained from the JHU Clinical Microbiology Laboratory for the purpose of further biofilm studies. *P. aeruginosa* is the standard laboratory organism for biofilm study [9]. Most mucoid *Pseudomonas* strains, including this one, are extremely active biofilm formers, attaching effectively to a wide variety of surfaces and producing large quantities of extracellular polymeric substances (EPS), particularly alginates [29]. An opportunistic pathogen of environmental origin, *Pseudomonas* has been documented in biofilms in natural and engineered systems [30, 31] and is frequently used as a model organism in biofouling studies (e.g., [32]). Like *S. oneidensis*, *P. aeruginosa* is a facultative anaerobe. It can use nitrate as a terminal electron acceptor, but not ferric iron [33]. Previous research reviewed by Spormann [34] has indicated that *Pseudomonas* biofilm morphology is sensitive to changes in metabolic state, particularly to the availability of a carbon source.

2.3.2 Culture medium

A rich culture medium such as Luria-Bertani (LB) broth provides ample nutrition and supports the rapid growth of a wide variety of bacterial species. It is composed of a mixture of 1.0% (w/v) tryptone (a mixture of peptides yielded by digesting casein with the protease trypsin), 0.5% (w/v) yeast extract, and 1.0% (w/v) NaCl, and adjusted to pH 7. It is easy and inexpensive to prepare, but is chemically undefined, and is not a realistic medium for simulating oligotrophic conditions. Furthermore, the large quantity of undefined organic material may be problematic if "clean" bacterial cells are required for later analyses.

Conversely, a minimal broth such as M1 medium [35] has a defined composition, requiring the addition of many individual metals and trace elements plus necessary macronutrients. Defined media may be designed to simulate particular environmental conditions, e.g., a groundwater, and concerns about sorption of unknown organics from the growth medium onto bacterial cell surfaces may be avoided. However, it can be difficult to formulate a defined medium that contains all the compounds necessary to the growth of a particular bacterial strain at a practical rate and yield.

Since this work intended to investigate the potential significance of metabolic state – more specifically, of the terminal electron accepting process – for parameters relevant to microbial transport in aquifers or during the infiltration of surface waters, a rich growth medium was not appropriate. The growth medium for this study therefore needed to be pH neutral and low in ionic strength, since typical surface waters range from I of 1 μM to 5 mM, while potable groundwaters are usually in the ionic strength range of 1 – 20 mM. Furthermore, the carbon source needed to be provided at a low enough

concentration that the terminal electron acceptor (be it oxygen for aerobic conditions, or nitrate or ferric iron for anaerobic conditions) would not be limiting. At the same time, a carbon-limited, low-nutrient medium would not support sufficient microbial growth for these studies to be practical, even if that meant using a medium with a DOC higher than the 0.1-10 mg/L typically found in groundwaters [36]. Acetate is commonly provided as carbon source for simulated natural systems, but one of the two potential study organisms, *S. oneidensis*, prefers lactate [37]. *S. oneidensis* also requires significant supplementation of metals and amino acids [38], if it is to grow well in defined medium [35]. Furthermore, we wished to avoid phosphate buffers. Iron(III) oxides are extremely insoluble at neutral pH, so the ferric iron provided as a terminal electron acceptor needed to be in coordinated form and yet remain sufficiently bioavailable. The media needed to be as similar as possible regardless of the terminal electron acceptor provided.

After testing various formulations in an effort to reconcile these conflicting demands, we settled on several small modifications to an undefined broth known as Yeast Extract Peptone medium. By halving the quantities of yeast extract and peptone in the original recipe used in previous studies [39, 40] of *S. oneidensis*, we achieved an appropriately weak medium that still contained the trace elements and amino acids necessary to support sufficient growth for our purposes. We supplemented it with 0.5 mM lactate as a carbon source. This medium will henceforth be referred to as "reduced Yeast Extract Peptone" (rYEP) medium. Anaerobic rYEP medium was prepared with the addition of an alternate electron acceptor: nitrate was provided as $NaNO_3$ for nitrate-reducing cultures, and ferric iron was provided as Fe(III)-citrate for iron-reducing cultures. The software package Visual MINTEQ (KTH, Sweden, based on US EPA's

MINTEQA2) was used to estimate equilibrium speciation, the effects of pH adjustment, and the amount of NaCl that should be added to each medium to maintain an ionic strength of I ~ 0.0125. It was not possible to consider the contributions of yeast extract or peptone in these calculations. The general composition and specific recipe for the rYEP medium used in these studies are reported in Table 2-1.

Table 2-1: Composition and recipe for rYEP medium

rYEP Medium

100 mg/l yeast extract
50 mg/l peptone
10 mM HEPES buffer
10 mM $NaHCO_3$
0.5 mM lactate
[1 mM $NaNO_3$]*
[5 mM Fe(III)-citrate]*
pH ~ 7.01, I ~ 0.015
*anaerobic medium only

To make 1 liter final volume:

	Aerobic	**Nitrate-reducing**	**Iron-reducing**
5% (w/v) yeast extract	2 ml	2 ml	2 ml
5% (w/v) peptone	1 ml	1 ml	1 ml
3M NaCl	0.667 ml	0.333 ml	-
0.5 M $NaNO_3$	-	2 ml	-
Fe(III)-citrate	-	-	1.2247 g
milliQ water	924 ml	924 ml	924 ml
0.5 M HEPES, filter sterilized	20 ml	20 ml	20 ml
0.2 M $NaHCO_3$, filter sterilized	50 ml	50 ml	50 ml
0.5 M lactate, filter sterilized	1 ml	1 ml	1 ml

Yeast extract (Bacto), peptone (Difco) and NaCl (J.T. Baker) were added to the appropriate volume of Milli-Q water in a large Erlenmeyer flask. For anaerobic medium, $NaNO_3$ (J.T. Baker) or Fe(III)-citrate (Sigma) was added along with a stir bar and sparge line. The resulting solution was autoclaved on a liquid cycle with sterilization time

adjusted as per the volume prepared and then cooled to room temperature. The buffers HEPES (Fisher) and $NaHCO_3$ (J.T. Baker) were added from stocks that had been previously sterilized by passage through a 0.22 μm polyethersulfone (PES) filter (Millipore). Lactate was added as a carbon source from a similarly filter-sterilized stock prepared from a 60% solution of lactate sodium salt (Fisher). The pH of the aerobic medium was adjusted down from ~7.3 to 7.02±0.02 with 6N HCl (Fisher, trace metals grade), while that of anaerobic medium was adjusted up from ~6.5 to 7.02±0.02 with 10N NaOH (Riedel-de-Haen, extra pure), as measured with an Orion Star 5-Star multimeter (Thermo Scientific). If the medium was anaerobic, cooling and all subsequent steps on the bench took place under N_2 or 80/20 N_2/CO_2 sparge with an oxygen trap (Restek) and a sterile 0.45 μm PFTE filter (Nalgene) inserted into the sparge line to prevent contamination. Standard practices of sterile technique were observed at all times.

2.3.3 Planktonic culture techniques

A small chunk of frozen bacterial stock was used to inoculate a 50 ml "preculture" of *S. oneidensis* or *P. aeruginosa* and grown overnight in Luria-Bertani (LB) broth on an incubator-shaker at 25°C and 125 rpm. The purpose of this preculture was simply to revive the bacterial stock, which had been stored at -80°C with 20% glycerol as a cryoprotectant. A small volume (40 μl) of the overnight preculture was then used to inoculate each 50 ml "experimental" culture. The cells grown in experimental cultures were intended for subsequent analysis, so these cells were grown in reduced yeast extract peptone (rYEP) medium with 0.5 mM lactate. Aerobic cultures were prepared in standard Erlenmeyer flasks with foam stoppers. Anaerobic cultures were prepared differently: anaerobic culture medium was pipetted into 50 ml polypropylene centrifuge

tubes from a freshly-prepared stirred stock under sterile N_2 or 80/20 N_2/CO_2 sparge. While these tubes were being filled, they, too, were under sterile sparge. They were capped immediately upon being filled, and were sparged every time it was necessary to open the tubes (e.g., to inoculate them). Once inoculated, all cultures were incubated at 25°C and 175 rpm, with at least one sterile control per experiment. Gentle shaking was not strictly necessary for the anaerobic cultures; their capped tubes had neither the oxygen transfer nor the swirling motion that took place in the aerobic Erlenmeyer flasks, but this way all cultures were prepared in as uniform a manner as possible. Tubes containing rYEP medium with Fe(III) citrate added were incubated in the dark to avoid photochemical reactions.

To establish typical growth behavior in our experimental medium, growth compared to a sterile control was monitored by optical density (OD) at 600 nm using a UV-visible spectrophotometer (Amersham Biosciences Ultraspec 3100 Pro). Anaerobic tubes opened for growth curve sampling were sacrificed to avoid any effects that the introduction of oxygen would likely have on subsequent growth. Once growth behavior had been established, it was no longer necessary to sacrifice anaerobic cultures; a single, final OD measurement was simply taken at the expected time to confirm that the desired phase of growth had been reached before proceeding directly with further analysis.

For aerobic and nitrate-reducing cultures, attainment of desired "redox" (terminal electron acceptor) conditions was assessed by adding resazurin (Alfa Aesar) to select tubes at a working concentration of ~5 mg/l. Resazurin is blue in solution under aerobic conditions but turns pink under nitrate-reducing conditions, providing simple visual

confirmation of the metabolic state of the culture. Demonstrating attainment of iron-reducing conditions required more sophisticated analysis and is discussed separately.

2.3.4 Modified ferrozine assay

To demonstrate dissimilatory iron reduction, significant elevation of Fe(II) in active, anaerobic cultures must be observed over the course of a growth experiment compared to a sterile (uninoculated) control. It is thus necessary to detect Fe(II) in a growth medium that initially contains 5 mM Fe(III) and which presumably contains a constant 5 mM citrate for the duration of the experiment. Separate tests demonstrated that the addition of citrate does not enhance the growth of *S. oneidensis* in rYEP medium, indicating that there should be no significant biological removal of citrate over the course of a 36-hour growth experiment.

Following Haas *et al.* [41], Fe(II) was quantified using Viollier's modifications [42] to the ferrozine assay [43]. Briefly, the principle is that Fe(III) can interfere with the development of the colored Fe(II)-ferrozine complex. A mixture with initial dissolved iron concentrations $C_{Fe(II)}$ and $C_{Fe(III)}$ reacting with ferrozine will have the following absorbance:

$$A_1 = \varepsilon_{Fe(II)} l C_{Fe(II)} + \varepsilon_{Fe(III)} l C_{Fe(III)}$$

where $\varepsilon_{Fe(II)}$ and $\varepsilon_{Fe(III)}$ are the absorptivities (M^{-1} cm^{-1}) of the Fe(II)-ferrozine and Fe(III)-ferrozine complexes, respectively. For cuvettes with a 1 cm path length, l, the variable drops from the equation.

After addition of a reducing agent, the absorbance of the sample, A_2, is due entirely to the Fe(II)-ferrozine complex, adjusted for the dilution, α, that occurred during reagent addition:

$$A_2 = \varepsilon_{Fe(II)} l \alpha \left(C_{Fe(II)} + C_{Fe(III)} \right).$$

By measuring A_1 and A_2 of a series of ferric iron standards, $\varepsilon_{Fe(II)}$ and $\varepsilon_{Fe(III)}$ may be found. By measuring A_1 and A_2 of an unknown sample, initial concentrations $C_{Fe(II)}$ and $C_{Fe(III)}$ may then be calculated. Viollier *et al.* [42] report $\varepsilon_{Fe(II)} \sim 22900$ M^{-1} cm^{-1} and and $\varepsilon_{Fe(III)} \sim 300$ M^{-1} cm^{-1} derived from ferric chloride standards.

The following reagents for the ferrozine assay were prepared using acid-washed glassware and milli-Q water, and stored in acid-washed plastic bottles: 10 mM ferrozine (Fluka) in 0.1 M ammonium acetate (Aldrich, 99.999% metals basis), 1.4 M hydroxylamine hydrochloride reducing agent (Alfa Aesar) in 2 M HCl (Fisher, trace metals grade), 10 M ammonium acetate buffer adjusted to pH 9.1 with 28-30% ammonium hydroxide (Fisher, trace metals grade). Standards were prepared with Fe(III)-citrate (Sigma) in concentrations ranging from 0 to 250 μM in anaerobic rYEP medium with 0.5 mM lactate. Samples and standards were filtered through a 0.22 μm PES filter (Millipore); samples from anaerobic cultures were analyzed at a 1:50 dilution.

2.3.5 Preparation of *S. oneidensis* cells for surface analyses

S. oneidensis cells were harvested from experimental cultures, and the residual growth medium was carefully washed away before the cells were concentrated into a smaller volume of electrolyte in preparation for hydrophobicity and electrokinetic analyses. These analyses were invariably performed in triplicate, meaning that a minimum of three identical, independent experimental cultures were inoculated and grown up simultaneously as described in the "Culture Techniques" section. Each was subsequently harvested, prepared, and analyzed in parallel. Hydrophobicity and

electrokinetic analyses were carried out on cells harvested from both log phase and stationary phase cultures.

Cells grown to log phase before analysis were grown as triplicate 50 ml cultures. The time required to reach mid-log phase depended on the growth regime: approximately 4.5 hours for aerobic cultures, 9 hours for nitrate-reducing cultures, and 14 hours for iron-reducing cultures. Each one of the triplicate cultures was then harvested by centrifugation for 15 minutes at 4200 rpm and 4°C. The centrifugate was discarded, the pellet was gently washed with 12 mls of cold KCl, and the resulting suspension recentrifuged. This washing procedure was then repeated a second time and the resulting pellet was resuspended in 2-14 ml of cold KCl and placed on ice until further analysis. To minimize the exposure of cells grown anaerobically to aerobic solutions, the KCl used to wash the pellets from anaerobic cultures was previously de-aerated by heating and then cooled under N_2 sparge.

Cells grown to stationary phase were grown with a larger number of initial 50 ml cultures, thus providing a larger quantity of cells for analysis. Six 50 ml aerobic (15.75 hr) or nitrate-reducing (15.7 hr) cultures were prepared, and then pairs of cultures were combined to yield three independent samples so that analysis could proceed in triplicate. Similarly, nine or twelve 50 ml iron-reducing (19.7 hr) cultures were prepared, and groups of three or four were combined to provide three independent samples for triplicate analysis. The washing procedure was the same as that used for log phase cells; the final resuspension volume was 5 ml. To help reduce the possibility of iron-containing precipitates being included in the cell pellet harvested from iron-reducing cultures, each

was carefully pipetted to a fresh centrifuge tube before the first spin, leaving the bottom ~0.5 ml undisturbed.

All washing and resuspension of stationary phase cultures was done in 10 mM KCl. A few of the log phase cultures were washed with KCl at an ionic strength other than the standard 10 mM. This was not ideal, but time considerations did not permit for all the log phase experiments to be repeated using exclusively 10 mM KCl for washing and final resuspension.

2.3.6 Surface Analyses

2.3.6.1 EPS analysis

Extracellular polymeric substances (EPS) were extracted from *S. oneidensis* cells grown under aerobic and nitrate-reducing conditions by ultracentrifugation, which has been shown to release loosely-bound EPS from the cell surface [44, 45]. Triplicate cultures grown to log phase as previously described were centrifuged at 40000 x *g* for 2 hrs at 10°C (Beckman L8-80 centrifuge, Ti55.2 rotor). Sterile controls containing uninoculated growth medium were processed in parallel. The supernatant containing the EPS was filtered through a 0.22 μm cellulose acetate filter (Millipore Stericup®) to remove any remaining cells. The resulting solution was held on ice for subsequent protein and carbohydrate analysis, with all measurements completed within 8 hours.

Protein content was quantified using a Micro BCA Protein Assay Kit #23235 (Thermo Fisher Scientific) according to the manufacturer's instructions. Standards of bovine serum albumin were prepared in concentrations ranging from 0 to 200 μg/mL. A 1:20 dilution of each sample was mixed in 1:1 ratio with the kit's "working reagent" in a polypropylene microcentrifuge tube, and the solutions were incubated for one hour at

60 °C. The absorbance of samples and standards at 562 nm was then measured with a spectrophotometer relative to that of milli-Q water. Each sample or standard was analyzed in triplicate for a total of nine experimental measurements for both aerobic and nitrate-reducing cultures (triplicate analyses of triplicate cultures) and three measurements of each standard.

Carbohydrate content was quantified using the Phenol-Sulfuric Acid method [44, 46, 47]. Briefly, 0.5 mls of a 5% (w/v) phenol (Fluka) solution was added to 0.5 mls of a 1:20 dilution of each sample or standard in a disposable polypropylene centrifuge tube, followed by a second addition of 2.5 mls H_2SO_4 (Fisher, trace metals grade). Tubes were mixed, held for 10 min in a 22 °C water bath, incubated for 15 min in a 30 °C bath, and cooled for 5 min in the 22 °C bath. The absorbances at both 480 and 490 nm were then recorded relative to milli-Q water, corresponding to neutral and acidic carbohydrates, respectively. Careful attention was paid to avoid contamination with cellulose fibers from paper towels and laboratory bench protectors. Again, each sample or standard was analyzed in triplicate for a total of nine experimental measurements for both aerobic and nitrate-reducing cultures (triplicate analyses of triplicate cultures) and three measurements of each standard.

Standards were prepared from Xanthan gum powder (MP Biomedicals) [46] in concentrations ranging from 0 to 300 μg/ml. Preparation of a homogeneous stock, with complete dissolution and without gummy lumps, was achieved by slowly adding 30 mg of powder to a beaker containing 100 mls Milli-Q water under the maximum amount of stirring that could be achieved without introducing bubbles (~730 rpm). The solution was stirred for 30 minutes at room temperature, followed by 30 minutes with gentle

heating (covered with parafilm to prevent evaporative losses), followed by another 30 to 45 minutes without heat until the solution returned to room temperature.

2.3.6.2 MATH assay

The classic microbial adhesion to hydrocarbons (MATH) assay [48, 49] is often used to provide a measure of the apparent hydrophobicity of the surface of bacterial cells [46, 50-52]. A microbial suspension is vortexed with a liquid hydrocarbon, and the bacterial cells may adhere to the surfaces of the resulting oil droplets. The fraction of cells adhering to the oil-water interface is assessed by comparing the initial optical density of the microbial suspension to that after a period of undisturbed phase separation post-mixing.

S. oneidensis was cultured under aerobic, nitrate-reducing or iron-reducing conditions as described in the "Culture Techniques" section and harvested and washed in cold 10 mM KCl as described in the section on preparation of cells for surface analysis, with the last resuspension in 5 ml of cold 10 mM KCl. We once again had three independent samples for analysis.

The spectrophotometer was zeroed on 10 mM KCl and the initial OD of each suspension was measured three times at 600 nm (nine measurements in total). The optimal OD for MATH analysis is 0.3, and initial cell densities should be comparable in all samples, as changes in the initial cell density may affect removal kinetics [53]. The initial OD_{600} of the aerobic samples was in the range of 0.35-0.45 and was deemed acceptable without further adjustment. The nitrate-reducing samples all required the addition of ~2 ml of 10 mM KCl to bring the initial OD_{600} into the same range. There

were fewer cells in the iron-reducing samples, and the initial OD_{600} readings were in the range of 0.25-0.3.

Borosilicate glass tubes were prepared by an acetone rinse, followed by washing in distilled water, overnight acid washing in 5N HNO_3, and thorough rinsing with milli-Q water. Detergents were not used to avoid surfactant contamination. For the MATH assay, four mls of culture suspension were added to a borosilicate glass tube containing 1 ml of n-dodecane (Alfa Aesar, 99+%). The tube was capped and vortexed for 2 minutes at maximum speed. After 15 minutes of undisturbed phase separation, the OD_{600} of the aqueous phase was measured [54]. The blank was prepared similarly, using four mls of 10 mM KCl in the place of the culture suspension. Triplicate samples of triplicate cultures were analyzed, for a total of nine final OD measurements.

The percentage of partitioning to the organic-water interface was then calculated as

$$\% \ partitioning = \frac{initial \ OD - final \ OD}{initial \ OD} * 100 .$$

2.3.6.3 Electrokinetic analysis

A ZetaPALS Zeta Potential Analyzer (Brookhaven Instruments Corporation, Holstville, NY) was used to measure the electrophoretic mobility of *S. oneidensis* cells grown to log or stationary phase under aerobic, nitrate-reducing, or iron-reducing conditions and prepared for surface analysis as previously described. Each reported measurement represents a minimum of nine samples (triplicate cultures sampled in triplicate on the same day) analyzed at a given ionic strength.

The ZetaPALS analyzer applies voltage with alternating polarity across the electrode in the measurement cell and records the velocity of the particles in the resulting electric field by analyzing the phase shift of scattered laser light. An increasing number of "cycles" (polarity changes) increases the time required for a single "run" or measurement, but reduces the relative residual of the curve-fitting process by which the instrument's software calculates the velocity and thus the electrophoretic mobility. A relative residual below 0.02 to 0.03 % is desirable, and was maintained for these measurements. The ZetaPALS software performs multiple, sequential runs to demonstrate the reproducibility of the measurement. These results may then be averaged to report the electrophoretic mobility of the sample. At high ionic strength, oxidation of the electrode can contribute particulate matter that adversely affects the measurement. To side-step this problem, one reduces the number of cycles and runs and compensates partially by increasing the number of samples. Electrophoretic mobility measurements made in 1 and 10 mM KCl were generally collected for three samples of a given culture with 8-10 runs at 17-20 cycles, while those made in 85 mM KCl or higher were generally collected for five samples with 3 runs at 15 cycles. Zeta potential was calculated from electrophoretic mobility by the Smoluchowski equation [55]. The manufacturer reports the instrument quantification range as ±6-100 mV, corresponding to mobilities of ±0.5-8 $(\mu m/s)(V/cm)^{-1}$; the data collected in these experiments was at the very lower limit of its range.

Bubbles in the measurement cell adversely affect electrokinetic results, and the temperature of the sample is relevant to the electrophoretic mobility calculation. Bacterial cell suspensions must be stored on ice until analysis, but the measurement is

taken at a controlled 25°C. To avoid the formation of bubbles during the longer temperature equilibration that would be required to warm a large volume of cold sample, 200 to 300 µl of ice-cold bacterial cell suspension were mixed with 1.5 to 1.8 ml of 25°C electrolyte to provide the desired ionic strength and cell density in the final sample. The mixed sample was loaded into ZetaPALS and allowed 3 minutes of temperature equilibration. The electrolyte used to dilute suspensions of cells that had grown anaerobically was de-aerated and N_2 sparged, as described previously. The electrode was thoroughly rinsed between each sample, and when relative residual rose too high it was cleaned with 70% ethanol and re-conditioned in 150 mM NaCl until the measured conductance exceeded 32000 µS.

2.3.7 Biofilm reactor redesign, setup, and sampling

2.3.7.1 Description

The CDC reactor (model CBR90) from Biosurface Technologies (Bozeman, MT) is specified in ASTM protocol E2562 to assess the impact of solution conditions or coupon (substratum) material on *P. aeruginosa* biofilm formation. Researchers in a wide variety of applications, from biomedical to environmental, have adapted it to study biofilm growth [56, 57]. The original reactor has eight rod-shaped coupon holders, each of which accommodates three disc-shaped coupons that are 12.7 mm in diameter and slightly over 3 mm thick. The coupon holders are suspended from a lid in a 1-liter glass vessel with a side discharge port. Liquid growth media is pumped in through a port in the lid, and mixing is provided with a stir vane assembly rotated by a magnetic stir bar.

These coupons in the original reactor were too small and too thick for our purposes; we needed to replace them with standard microscope slides to facilitate

imaging and streaming potential analysis of the biofilms. We redesigned and rebuilt the reactor accordingly with six rod-shaped coupon holders, each accommodating a single microscope slide (75 x 25 x 1 mm), shown in Figure 2-2.

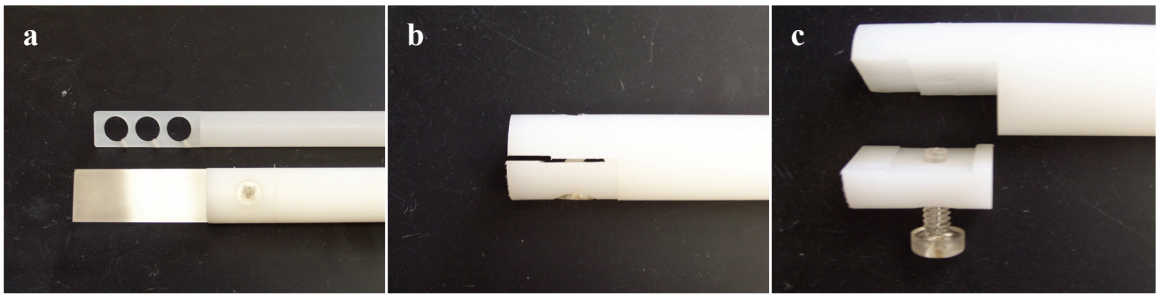

Figure 2-2: Redesigned coupon holders for the biofilm reactor, showing (a) the original triple coupon holder compared to the redesigned holder with a microscope slide in place, (b) side view of the redesigned holder clamping mechanism, (c) side detail, disassembled.

The lid and the six coupon-holder rods of the redesigned reactor were polypropylene. The lid ports were stainless steel tubing. The gasket was self-leveling silicone. PEEK screws to hold the coupons in place were later replaced with nylon screws that proved more resistant to repeated autoclave sterilization. The stir vanes were teflon, and the stir bars were teflon-encased. All plastics were from McMaster-Carr (Princeton, NJ). The 1-liter glass reactor vessels were tall form Berzelius beakers (Kimax #14020, Kimble-Chase, Vineland, NJ) with fritted glass effluent ports custom-blown at approximately the 400 ml mark by Quark Glass (Vineland, NJ).

A peristaltic pump (Ismatec IP, Switzerland) was used to circulate media through the reactor. All influent tubing was PharMed® BPT tubing purchased from Upchurch Scientific/IDEX Health & Science LLC (Oak Harbor, WA). The material was selected for its biocompatibility, durability, and autoclavability. The internal diameter of the two-stop pump tubing itself was 1.29 mm (the flow rate is determined by the combination of this internal diameter and the pump speed). The rest of the connecting tubing had an

internal diameter of 2.79 mm, to accommodate connections to the stainless steel ports on the bioreactor lid and to a glass in-line flow break (Biosurface Technologies) that prevented organisms in the active bioreactor from moving up the influent line towards the supply of sterile growth medium. One of the ports on the bioreactor lid served as an air vent, and was fitted with a 0.45 μm PFTE Filter (Nalgene) to prevent contamination. Critically, the entire reactor assembly was autoclave-sterilizeable with the exception of the two-stop pump tubing, which was bleach-sterilized separately and rinsed with sterile media immediately before use.

2.3.7.2 Operation

Autoclave-sterilized reactor assemblies were filled with sterile rYEP medium and inoculated with 1 ml of pre-culture, either *S. oneidensis* or *P. aeruginosa*, grown to log or stationary phase in LB broth. After an inoculation period in batch mode, the liquid culture in the reactor was discarded and replaced with sterile growth medium. The effluent port was unclamped and the pump turned on to feed fresh media through the influent port at a steady rate for the duration of the biofilm growth period. We tested both low (130 rpm) and high (230 rpm) stir rates during the growth period, with stir controlled by a multi-position digital stir plate (Variomag Poly, Thermo Scientific). Each experiment involved one or two active growth reactors plus a sterile control reactor, all run in parallel.

In an attempt to optimize initial attachment and promote subsequent biofilm growth, several shear conditions were tested during the inoculation period: no stir, low stir, high stir, and combinations of 1 minute at low stir followed by no stir, 1 minute at high stir followed by no stir, and 1 minute at high stir followed by low stir. We also

varied the inoculation period from 12-18 hours. Several pumping rates were tested for the active growth period, corresponding to approximate hydraulic residence times in the reactor from 2.75 to 11 hours.

Microscope slides used as biofilm coupons were standard soda lime glass (Fisher Scientific). They were sonicated for 10 minutes in dilute Alconox detergent, rinsed with distilled water, acid washed overnight in 5N HNO_3, rinsed in MilliQ water, air-dried, and visually inspected for cleanliness (lack of dust, streaking, etc.) Some slides were engraved with a unique identifier and massed before use to facilitate gravimetric determination of dry biomass accumulation. We also tested "polysine" slides (Thermo-Fisher) pre-coated by the manufacturer with poly-L-lysine to give them a positive surface charge that is purported to improve the adhesion of typically negative cytological samples. Poly-L-lysine slides were visually inspected for cleanliness, but were not sonicated in detergent or acid washed.

Biofilm coupons were removed throughout the growth period to assess biofilm development. The sampling protocol was as follows. Working on the bench near an open flame with careful sterile technique, a coupon-holding rod was withdrawn from the reactor. The screw securing its microscope slide (the "coupon") in place was loosened with a flame-sterilized screwdriver and the slide was allowed to drop into a 50-ml conical tube containing non-sterile Q water. The slide was then immediately removed from this rinse by gripping the screw end with a pair of tweezers, being careful not to disturb the active biofilm region, and transferred to an empty 50-ml conical tube where it was allowed to air dry. The coupon-holding rod, still sterile, was reloaded with a sterile "recharge" slide and replaced into the reactor. The recharge slide served merely to

maintain consistent fluid motion in the stirred reactor. The sterility of the control reactor was also assessed at each sampling point by spreading ~ 0.3 ml of liquid dripped directly from the sampled slide and coupon-holding rod assembly onto an LB agar plate. Plates were incubated at 30°C for at least 24 h before checking for visible colony formation.

2.3.8 Biofilm image collection

Air-dried slides were viewed on a Nikon Eclipse E600 light microscope at 10x and 40x magnification in Aperture mode. Digital slide images were acquired with IP Lab software (Becton, Dickinson and Company, Franklin Lakes, NJ). A minimum of three photos of different areas of the biofilm, spaced approximately evenly around the slide, were taken at 10x with the Phase 3 ring and an NCB11 filter. The last of these regions was also photographed at 10x and 40x in Phase 1 with both NCB11 and ND32 filters. Post-processing was done with ImageJ [58].

2.4 Results and Discussion

2.4.1 Growth of planktonic cultures

Typical growth curves of *S. oneidensis* MR-1 under our culture conditions are presented in Figure 2-3. Aerobic cultures have an OD_{600} of ~0.04-0.06 at mid-log phase after about 5 to 6 hours, and reach stationary phase after about 12 hours, at an OD_{600} of ~0.08. Nitrate-reducing cultures grow with similar kinetics, reaching an OD_{600} of ~0.04 after about 7 hours. The cell density at stationary phase is somewhat lower, OD_{600} ~0.07, again after about 12 hours. Iron-reducing cultures grow more slowly and at lower yield: the OD_{600} of a mid-log culture is 0.02-0.03 after about 10 hours, and the culture reaches a stationary phase OD_{600} ~0.04 after some 18 hours. Some interday variability is visible in

these growth curves. Anaerobic cultures grew markedly faster on 7/7 and 7/9. Building climate control problems on those hot summer days led the labs to be unusually warm. The shaker has no cooling capacity, and its motor generates some heat, so while the standard culture temperature was 25°C, these cultures grew at closer to 27°C.

The influence of our modifications to the original yeast extract peptone medium are shown in Figure 2-4. Halving the yeast extract and peptone to a combined total of 150 mg/l essentially halved the final cell density in aerobic culture, an effect that was offset by about a third with the addition of 0.5 mM (44.5 mg/l) lactate, suggesting that the system is limited by the availability of a carbon source, or at least that of an electron donor. Aerobic cultures with resazurin added as a redox state indicator stayed blue, so they were not oxygen limited.

The addition of 5 mM disodium citrate to aerobic cultures reduced growth notably, as shown in Figure 2-5. If citrate can serve as a carbon source at all, the energetic benefits are clearly offset by another process. Citrate is a mild chelating agent and may sequester trace metals, thus limiting their bioavailability.

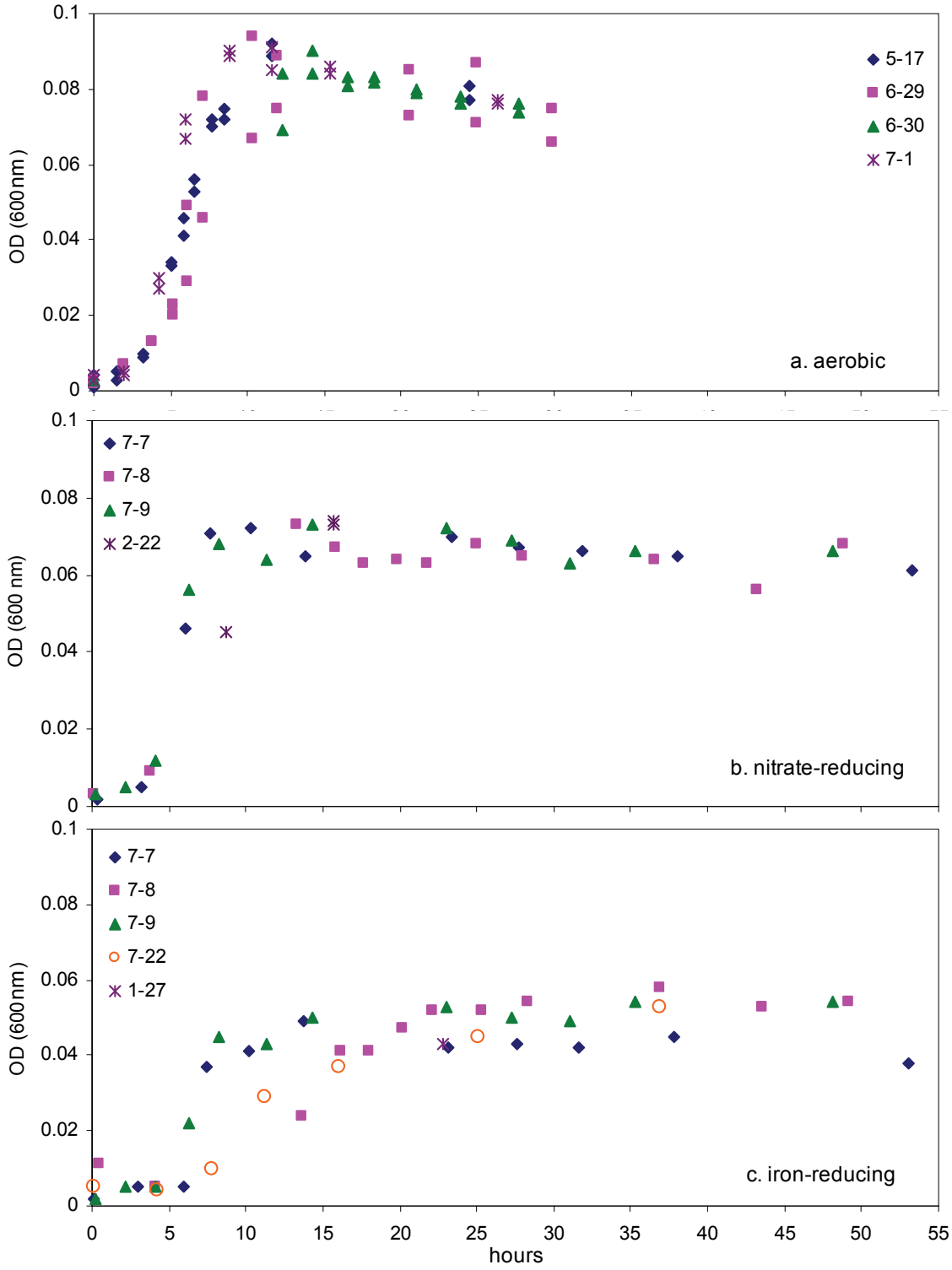

Figure 2-3. Planktonic growth curves for *S. oneidensis* MR-1 under (a) aerobic, (b) nitrate-reducing, and (c) iron-reducing conditions at 25°C and 175 rpm in rYEP medium.

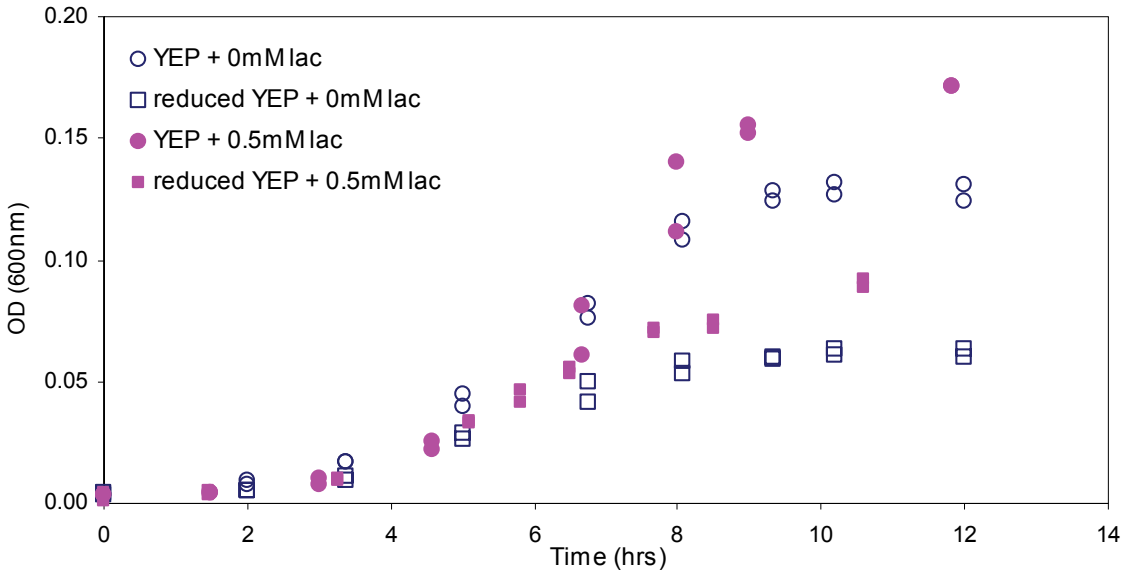

Figure 2-4. Influence of yeast extract, peptone and lactate content of medium on *S. oneidensis* growth at 25°C and 175 rpm.

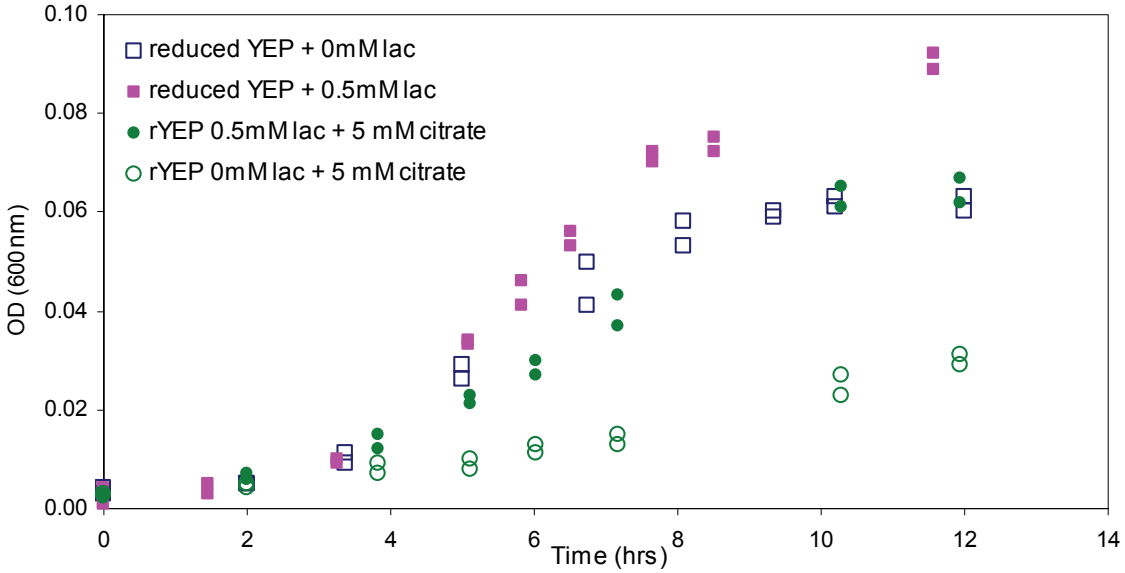

Figure 2-5. Influence of citrate on *S. oneidensis* growth at 25°C and 175rpm in rYEP medium.

2.4.2 Use of the modified ferrozine assay to demonstrate dissimilatory iron reduction

The importance of matrix effects in the modified ferrozine assay cannot be exaggerated. If standards are not prepared in a matrix similar to that of experimental samples, it may be extremely difficult to detect the production of Fe(II) by dissimilatory iron reduction. For example, standards prepared with Mohr's salt (ferrous ammonium sulfate) in MilliQ water and analyzed with the modified ferrozine assay [42] yielded a molar absorptivity, $\varepsilon_{Fe(II)}$, of the Fe(II)-ferrozine complex of 28300 $M^{-1}cm^{-1}$, in close agreement with the standard literature value of 27900 $M^{-1}cm^{-1}$ reported for the original ferrozine assay [43]. The addition of 5 mM citrate to these standards reduced $\varepsilon_{Fe(II)}$ by about twenty percent, to ~ 23200 $M^{-1}cm^{-1}$ (data not shown). Other researchers have noted that citrate does complex ferrous iron as well as ferric iron, and that the kinetic lability of the Fe(II)-citrate complex may be a factor in the rate of formation of the ferrous-ferrozine complex [59].

The absorbance A_1 of ferric standards before the addition of a reducing agent is plotted for various matrices in Figure 2-6a. The molar absorptivity of the ferric-ferrozine complex, $\varepsilon_{Fe(III)}$, may be extracted from the slope of these curves by linear regression analysis. Standards prepared with ferric chloride gave $\varepsilon_{Fe(III)}$ ~360 $M^{-1}cm^{-1}$, similar to the reported value of 300 $M^{-1}cm^{-1}$ [42]. However, the addition of 5 mM disodium citrate to these ferric chloride standards reduced $\varepsilon_{Fe(III)}$ to ~120 $M^{-1}cm^{-1}$. Standards prepared with Fe(III)-citrate in MilliQ water gave $\varepsilon_{Fe(III)}$ of ~950 $M^{-1}cm^{-1}$, while those prepared with

Fe(III)-citrate in sterile, anaerobic rYEP medium had $\varepsilon_{Fe(III)}$ ~120 $M^{-1}cm^{-1}$ with a y-intercept a full order of magnitude higher than that of other standard curves.

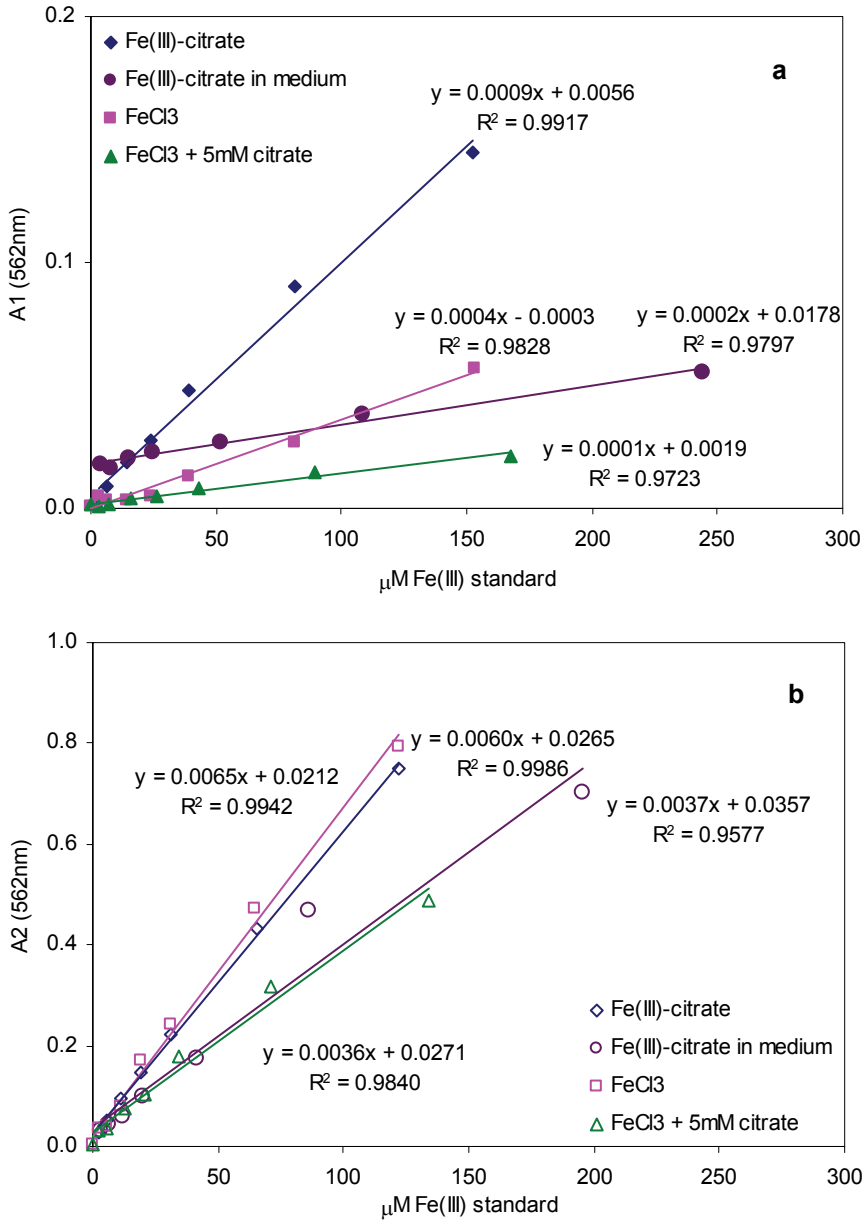

Figure 2-6. Matrix effects on the absorbance of ferric standards in the modified ferrozine assay; (a) A_1 measured before reductant addition; (b) A_2 measured after reductant addition

The absorbance A_2, measured after the addition of a reducing agent and plotted in Figure 2-6b, permitted calculation of $\varepsilon_{Fe(II)}$, which was 600-650 $M^{-1}cm^{-1}$ in the absence of citrate and ~360 $M^{-1}cm^{-1}$ in the presence of citrate, regardless of whether the standards

were prepared from ferric chloride or ferric citrate, in MilliQ water or in growth medium. By contrast, Viollier observed $\varepsilon_{Fe(II)}$ ~22900 $M^{-1}cm^{-1}$ for standards prepared from ferric chloride in water. The low A_2 value we saw for our own ferric chloride standards in MilliQ water may have been due to an improperly prepared buffer solution; color development of the Fe(II)-ferrozine complex is pH dependent [43].

To duplicate as closely as possible the solution chemistry of the cultures for which speciation analysis was required, standards for evaluation of dissimilatory iron reduction in microbial cultures (Figure 2-7) were prepared from ferric citrate in sterile, anaerobic rYEP medium with fresh buffer.

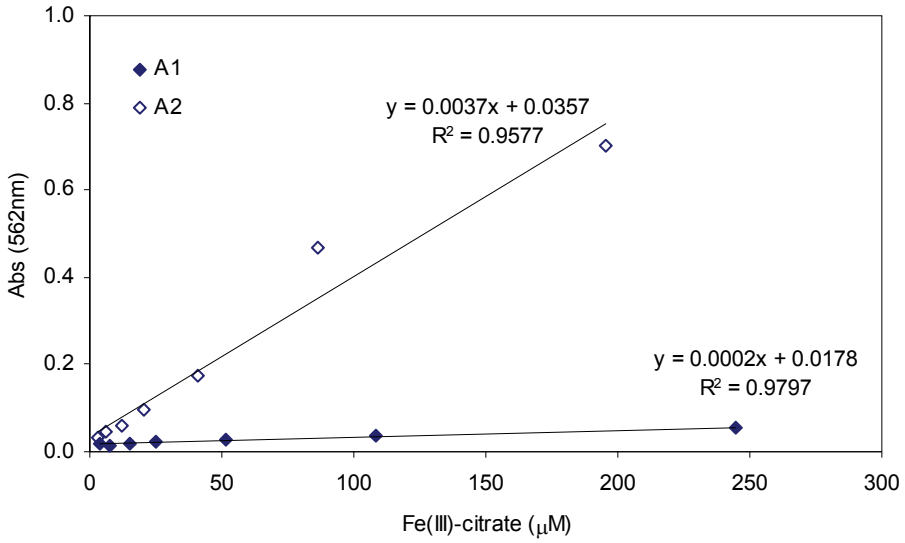

Figure 2-7. Standard curves prepared from ferric citrate in rYEP medium for the assessment of iron speciation in active *Shewanella* cultures

Iron speciation analysis for active anaerobic cultures supplied with Fe(III)-citrate as a terminal electron acceptor is plotted in Figure 2-8. An Fe(II) peak grows in over time in step with the increasing optical density of the culture. This peak is entirely absent from sterile controls, which were generally below the method detection limit of ~3 μM Fe [42], demonstrating that iron reduction was achieved. The fluctuation of the mass

balance on total iron in the sterile control is the direct result of the variability in the ferric iron quantification. The apparent increase in total iron in the active cultures is due to the seeming persistence of ferric iron even as Fe(II) levels rise. As there was no iron source in these cultures, these data suggest that changes in composition of the medium as it supported microbial growth resulted in reduced interferences and correspondingly higher molar absorptivity of the ferric-ferrozine complex compared to the standards and sterile controls.

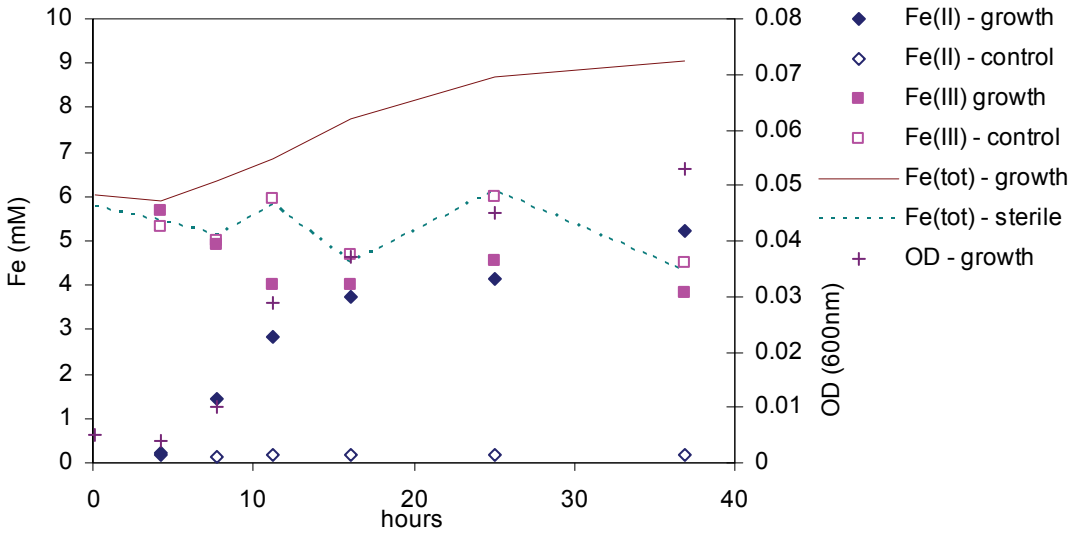

Figure 2-8. Iron speciation analysis of an actively growing *S. oneidensis* culture compared to sterile control

2.4.3 Surface characterizations

2.4.3.1 EPS

The protein and carbohydrate content of EPS extracted from log phase *S. oneidensis* cultures is reported in Figure 2-9 as difference from sterile control. Protein concentrations decreased compared to sterile controls, indicating that the cells assimilated proteins from the growth medium to a greater extent than they exuded them in EPS. Conversely, the carbohydrate content of *Shewanella* EPS more than outweighed

assimilation. Differences between aerobic and nitrate-reducing cultures were not statistically significant, although it is possible that carbohydrates exuded by nitrate-reducing cultures may have been less acidic.

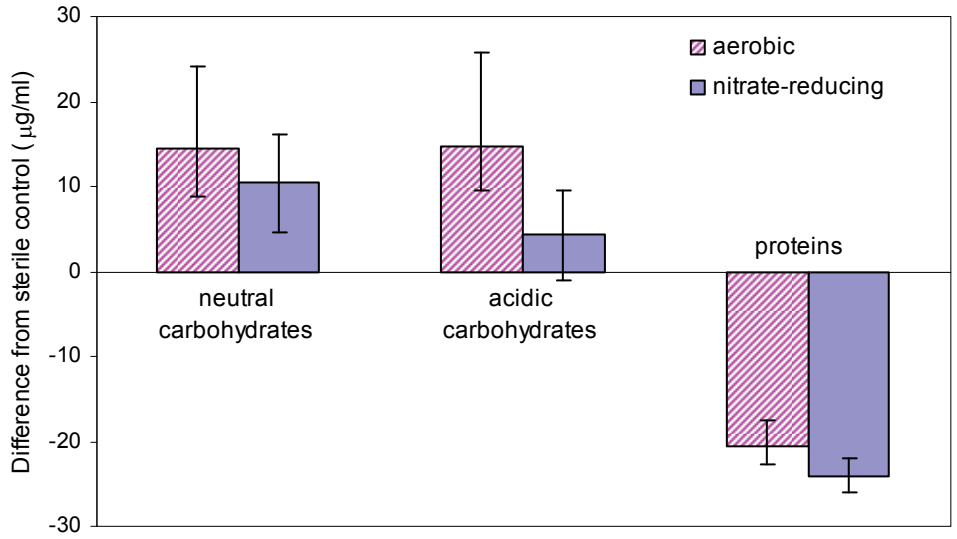

Figure 2-9. Protein and carbohydrate analysis of EPS from aerobic and nitrate-reducing cultures of *S. oneidensis*

The inconclusive nature of these EPS data reflect shortcomings of the method. A gentle physical extraction method was preferred over harsher, chemical extraction of EPS because chemical methods can alter the composition of the EPS itself [54]. For example, extractions with formaldehyde are commonly used in cell surface characterizations that complement attachment studies [60, 61], but formaldehyde extraction underestimates protein content [6]. Furthermore, harsher extractions access EPS that is more tightly affiliated with the cell surface, but the loosely-bound outermost EPS components are perhaps more relevant to the apparent surface properties of the cell. However, gentler physical extraction methods have comparatively low EPS yields, as little as 1 μg/g of cells [6], and a previous study had reported that up to 50% of the total carbohydrate yield could be lost in washing [62]. These concerns led us to omit any washing step prior to

the EPS extraction by ultracentrifugation. Consequently, the cells were not harvested by low-speed centrifugation and washed several times in an electrolyte solution to remove traces of growth medium before proceeding with EPS extraction. This proved problematic, as the extracted EPS could not then be separated from residual organics from the growth medium. It is for this reason that we present our results as changes from the sterile controls.

Biofilms generally contain far more EPS as a percent of total biomass than do planktonic cultures, with EPS contributing up to 90% of the organic matter in a biofilm [63], so low EPS yields are less likely to be problematic in biofilm studies. Furthermore, extensive pelleting and washing protocols are not required to separate biofilms from their growth medium, since the biofilm coupon may simply be removed from the liquid medium. Rather than proceeding to refine the EPS extraction and analysis protocol for liquid cultures, or indeed repeating it for iron-reducing conditions, we considered these results a useful groundwork for future analysis of biofilm EPS.

2.4.3.2 MATH Assay

This assay of the apparent hydrophobicity of the cell surface reveals the relevance of metabolic state to the surface properties for *S. oneidensis*. Percent adhesion at the hydrocarbon interface for various culture conditions is displayed in Figure 2-10. For cultures assessed in exponential phase, nitrate-reducing cells adhered the least at the hydrocarbon interface (12.5 ± 4.8%) and iron-reducing cells the most (45.6 ± 3.1%), with aerobic cells in between (29.4 ± 8.5%). For cultures assessed in stationary phase, aerobic cells adhered less (16.7 ± 5.6%) than the anaerobic ones, but no significant differences were observed between nitrate (30.3 ± 6.0%) and iron-reducing cells (28.5 ± 4.5%).

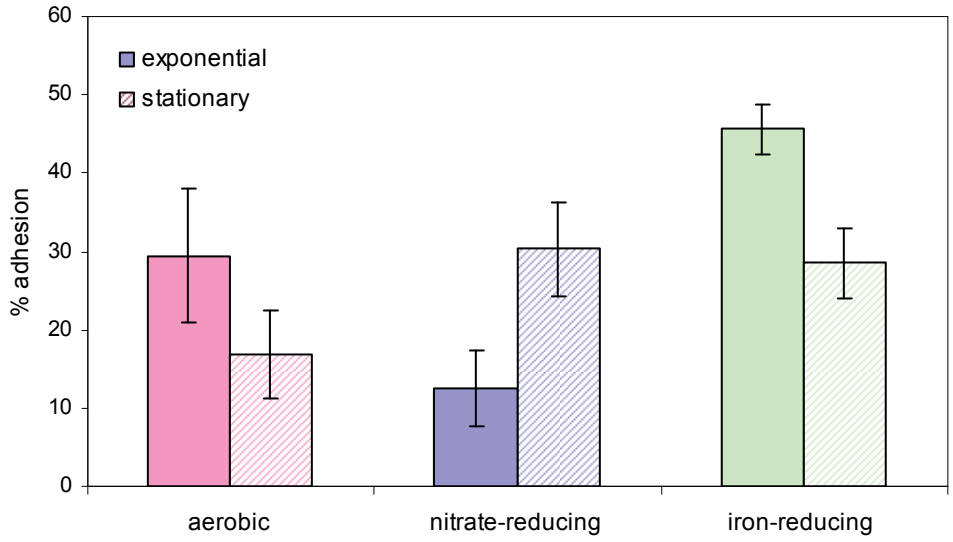

Figure 2-10. MATH assay of exponential and stationary phase *Shewanella* cultures under aerobic, nitrate-reducing and iron-reducing conditions

Although we are not aware of other reports of the effects of growth phase or electron acceptor on the apparent hydrophobicity of *S. oneidensis*, studies of *E. coli* and other organisms have documented marked differences in adhesion in the MATH assay as a function of growth phase [51] and nutrient availability [61]. Increased hydrophobicity is sometimes associated with high polysaccharide content in capsular EPS [61], at least when negatively charged uronic acids are not a significant EPS consitituent. An EPS layer rich in neutral sugars such as glucose and mannose may shield negatively-charged functional groups on lipopolysaccharides and proteins that are associated with the cell membrane [64].

Researchers studying a different *Shewanella* strain, *S. putrefaciens* CIP 8040, have reported a strong pH effect in a MATH assay with octane [65]: they observed nearly 100% adhesion at the aqueous-hydrocarbon interface at pH 4 but less than 10% adhesion at pH 10, regardless of ionic strength. At pH 7, a moderate ionic strength effect was evident, with about 20% adhesion at 1 mM KNO_3 compared to 40% at 100 mM. Results

such as these suggest that the physical interpretation of the MATH assay merits closer attention.

Although the MATH test is widely referred to as a "hydrophobicity" assay, adhesion of bacterial cells at the aqueous-hydrocarbon interface cannot be attributed entirely to non-polar interactions. Researchers have demonstrated that the assay measures the net effect of a variety of forces, including electrostatic forces and Van der Waals interactions [66]. It has therefore been suggested that the assay quantifies hydrophobicity only if it is performed at a pH equal to the isoelectric point [67], where the cells have no net surface charge. However, even these test conditions do not ensure that the MATH assay will measure hydrophobic interactions, as experimental evidence [68] has demonstrated that the interface between water and a nonionic substance can be negatively charged. This phenomenon has been attributed to physisorption of hydroxide ions caused by the ordering of water molecules at the interface [69], an effect which should be more pronounced at high pH. The author of the original MATH method has recently recommended performing it at high ionic strength [70], where double-layer compression will effectively screen surface charge and minimize the contributions of electrostatic interactions, but such conditions are conducive to aggregation of cells in the aqueous phase.

The aforementioned study of *S. putrefaciens* [65] determined that the isoelectric point of the strain was below pH 3 for all relevant experimental conditions. At low ionic strength, the electrophoretic mobility was increasingly negative at higher pH, indicating a more negative surface charge. Thus the decrease in apparent hydrophobicity as pH rose may be partially explained by the deprotonation of EPS functional groups and an

increasing negative charge at the hydrophobic interface. However, these electrostatic interactions caused by the charge contributions of dissociable functional groups should be well-screened at high ionic strength, masking the pH dependence of apparent hydrophobicity. The fact that this was not the case indicates that other factors contribute to adhesion behavior in the MATH test. Supplementary electrokinetic analysis and atomic force measurements led the researchers to postulate that intermolecular forces at high pH led to swelling of the cell membranes and polymeric fringe and thus increased their water permeability, a phenomenon which could explain the decrease in apparent hydrophobicity at pH 10 even under high ionic strength conditions.

Other researchers have also observed qualitative disagreement between adhesion results in the MATH assay and behavior predicted from DLVO theory and measured physicochemical properties of the organisms and hydrocarbons tested [67]. Model calculations suggested that steric factors may explain the discrepancies.

2.4.3.3 Electrokinetic analysis

The results of electrokinetic analysis are plotted in Figure 2-11. During the log phase of growth (Figure 2-11a and c), *S. oneidensis* cells grown aerobically are markedly more negatively charged than those grown anaerobically. Nitrate and iron-reducing cultures have similar surface charge; differences between them were not statistically significant. The surface charge of aerobic and nitrate-reducing cells changes very little from log to stationary phase growth, but stationary phase iron-reducing cells have a significantly more negative charge (Figure 2-11b and d). All cells exhibited expected behavior with increasing ionic strength: the apparent surface charge approaches zero due to charge screening by double-layer compression.

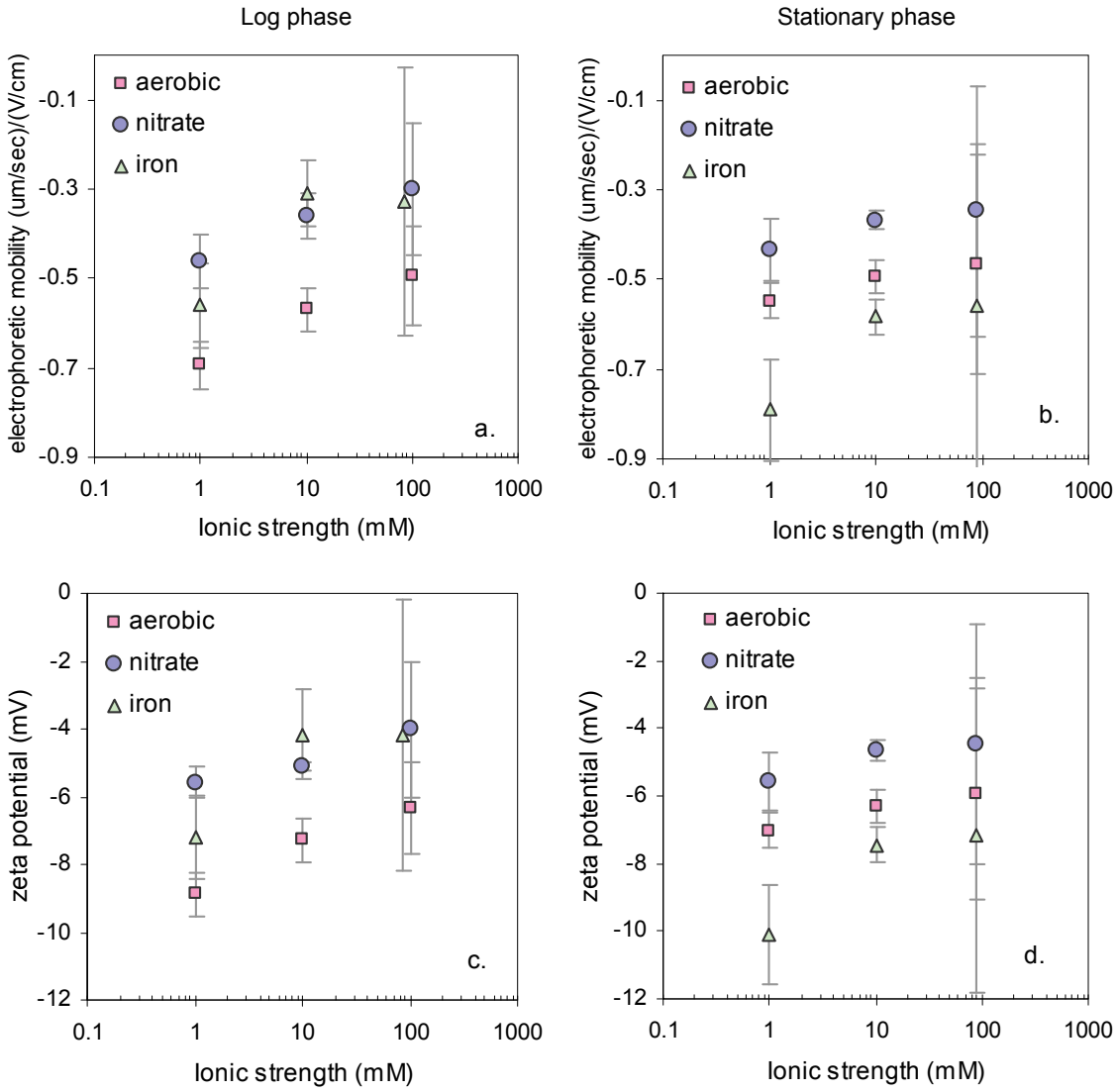

Figure 2-11. Electrophoretic mobility (a, b) and zeta potential (c, d) of S. oneidensis cells at log (a, c) and stationary (b, d) growth phase under aerobic, nitrate-reducing and iron-reducing conditions

Iron-reducing cultures present a particular challenge for electrokinetic analysis. Ferric iron precipitates readily under aerobic conditions, and charged iron (oxy)hydroxide particles will interfere with electrokinetic mobility measurements, as the instrument cannot distinguished them from the bacterial cells of interest. Ferrozine analysis of unfiltered samples revealed total iron levels below 5 μM in all cell suspensions and

controls subjected to electrokinetic analysis with the exception of one (which had 18 μM total Fe), indicating a general absence of iron particle contamination.

The electrophoretic mobilities observed for nitrate-reducing *S. oneidensis* MR-1 were in good agreement with those reported by other researchers [71], but that study did not examine aerobic or iron-reducing cultures. Although the organism is a well-known iron reducer [41], we are unaware of any prior zeta potential analyses of *S. oneidensis* MR-1 under iron-reducing conditions. A study of a different species, *S. putrefaciens 200R*, reported electrophoretic mobilities for stationary phase cells that were approximately an order of magnitude greater than our data at similar pH and ionic strength, with aerobic cells more negatively charged than iron-reducing cells [72].

Results from experiments with *E. coli* O157:H7 and *Yersinia enterolitica* corroborate our findings that aerobic versus anaerobic conditions affect cell surface properties. A careful study of these pathogens indicated that dissolved oxygen levels during growth or acclimation influenced titratable cell surface charge and the expression of surface macromolecules [73], as well as zeta potential and attachment behavior in column studies [74]. The effects, however, were organism dependent: while the net changes in surface properties brought about by anaerobic growth conditions enhanced *E. coli* transport, they decreased *Y. enterolitica* transport.

Inconclusive though the EPS data were (Figure 2-9), they suggested relative dominance of neutral carbohydrates over acidic carbohydrate functional groups for log phase nitrate-reducing cultures, whereas acidic and neutral carbohydrates might be more evenly balanced in log-phase aerobic cultures. These results were in qualitative

agreement with the electrokinetic findings that nitrate-reducing cultures had lower net surface charge than aerobic cultures at log phase.

By a traditional interpretation of the MATH assay, cells with greater hydrophobicity and lower surface charge should adhere to a greater extent at the hydrocarbon interface. Such qualitative agreement between the results of cell surface characterization by MATH and electrokinetic analyses was not observed. At log phase, nitrate- and iron-reducing cultures had low and statistically indistinguishable net surface charge (-5.1 ± 0.1 and -4.2 ± 1.3 mV in 10 mM KCl, respectively), but the iron-reducing cells adhered to the greatest degree (46 ± 3 % adherence in 10 mM KCl) at the hydrocarbon interface, while nitrate-reducing cells adhered the least (13 ± 5 %). Aerobic cells, with the greatest net surface charge (-7.3 ± 0.6 mV) exhibited intermediate adherence (29 ± 9 %). At stationary phase, aerobic cells exhibited intermediate surface charge (-6.3 ± 0.5 mV) but low adherence (17 ± 6 %) while the least-charged cells (nitrate-reducing, -4.7 ± 0.03 mV) and the most-charged cells (iron-reducing, -7.5 ± 0.5 mV) had similar high adherence around 30%.

Non-charge-based interactions may have contributed to the adhesion behavior observed in the MATH results. Local charge heterogeneity on the surface of bacterial cells is an important factor affecting their attachment behavior in transport studies [75]; heterogeneity in the distribution and physical conformation of charged and hydrophobic functional groups in the EPS matrix could equally affect adhesion in the MATH test. Conversely, the electrophoretic mobility or zeta potential of a bacterial cell is a spatially averaged “macro” property that reflects the charge contributions of dissociable functional groups. It will not be affected by local heterogeneity or by the presence of hydrophobic

moieties, nor by steric interactions (bridging or hindrance) accessible to long polymers extending from the cell surface [64, 76], although the hydrodynamic permeability of "soft" cell surface polymer layers does effect their electrophoretic behavior. All of these interactions – local, average, hydrophobic, steric, and electrostatic – contribute to attachment behavior, and our results indicate that their individual and net contributions can change under different microbial redox conditions, suggesting that further study of similar properties in biofilm systems are merited if we are to improve our understanding of bioparticle transport in the subsurface.

2.4.4 Biofilm culture results

Representative images of microscope slides (coupons) from sterile control biofilm reactors are shown in Figure 2-12. Two fields of view at 10x magnification from the same microscope slide are given side-by-side for each sampling point. The sterility of each of these control samples was independently confirmed by plate count; these images do not show bacterial growth.

Overall, control slides images show dark fields of view with a few specks of dust or particulate matter and occasional streaking, presumably from the air drying of residual medium after the slide was briefly rinsed. Figure 2-12a shows controls sampled over a 71.5 hour time series in a single reactor; no biofilm growth is present over the course of the experiment. Figure 2-12b and c show the control reactor for a separate experiment, with samples taken at 13.3 and 20.15 hours. The right-hand field of view for each of the two samples in Figure 2-12b was taken from the bottom end of the microscope slide as per its orientation in the bioreactor and during air drying. We sometimes saw this sort of

accumulation of particulate "crud" at the bottom of the slide, which was always the last portion to dry.

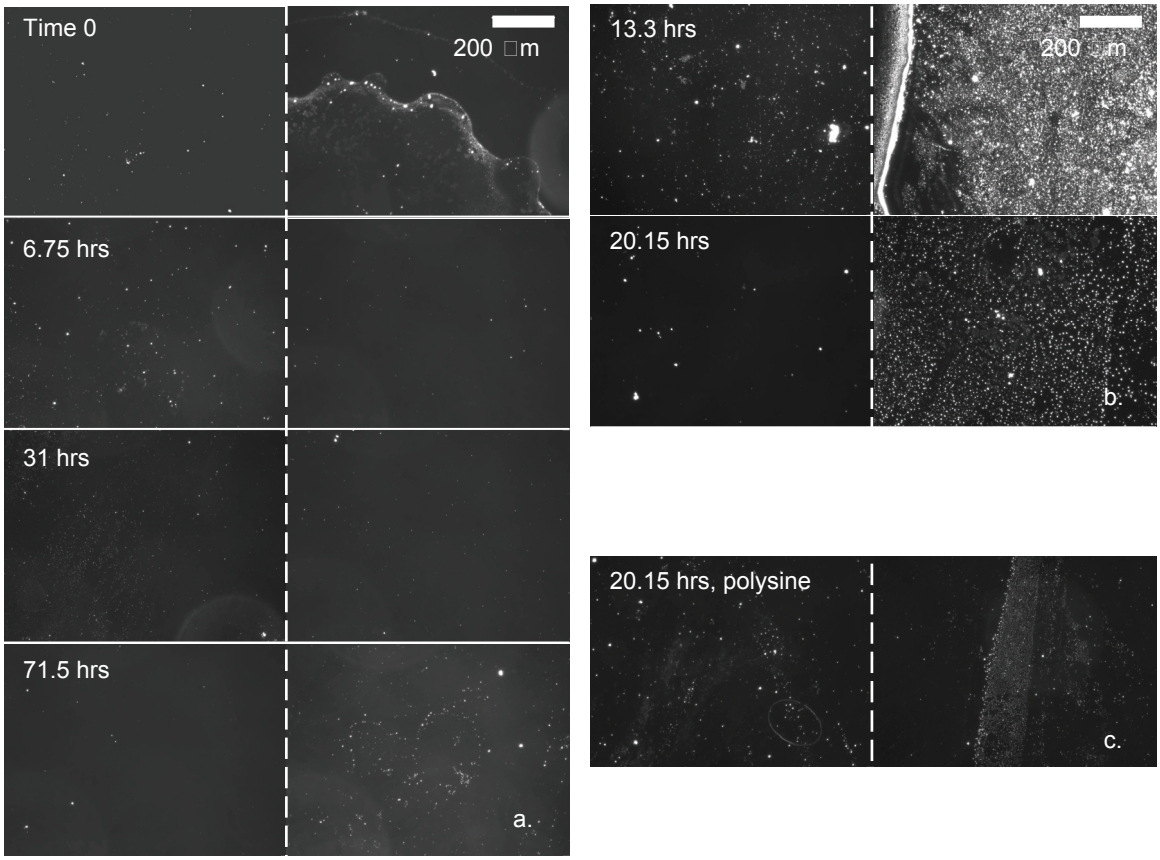

Figure 2-12. Sterile control coupons from biofilm reactor. (a) and (b) standard microscope slides, (c) poly-L-lysine coated slides. Two fields of view are shown per slide.

We tested both standard soda lime glass slides and poly-L-lysine coated slides in our control reactors, expecting that the positively-charged poly-L-lysine slides might attract enhanced particulate deposition. The slides in Figure 2-12b, like those in Figure 2-12a, are standard soda lime glass. The slide in Figure 2-12c, by comparison, is poly-L-lysine coated. It was withdrawn from the same reactor and at the same time as the 20.5 hour sample in Figure 2-12b (the 13.3 hour poly-L-lysine sample is missing because of a coupon holder failure in the bioreactor). There did not seem to be any significant

difference in poly-L-lysine slides compared to standard slides in control samples. The absence of a zone with enhanced particulate matter at the bottom end of the slide for this particular sample was unremarkable, as such deposition was not always observed. Negative controls showed certain degree of variability; this background noise must be accounted for in analysis of any images of active biofilms.

Images of microscope slides (coupons) from active biofilm growth reactors are shown in Figure 2-13. Again, two fields of view at 10x magnification are given side-by-side for each sampled coupon. Figure 2-13a shows an active time series corresponding to the controls in Figure 2-12a. Two biofilm reactors were run and sampled in parallel, with one coupon removed from each reactor at each time point, so four fields of view are shown for each time. These reactors were inoculated with *S. oneidensis* for 18 hours in batch mode, with high stir for the first minute followed by low stir for the remainder of the inoculation and growth period. Initial attachment and early biofilm development is visible at the first time point, taken when the medium was refreshed at the end of the inoculation period. Thereafter, growth medium was pumped through the reactor with a residence time of 11 hours. After 6.75 hours, more growth was visible with a higher degree of surface coverage, but this biofilm was not stable and it sloughed off at later time points. When the experiment was repeated on two separate occasions to focus on earlier times, biofilm coverage at the ~6 hour point was not reproducible (data not shown). Note the significant variability in biofilm coverage and morphology that may be observed between two different regions on the same biofilm coupon (image pair separated by a dashed line), as well as the significant variability observed between duplicate reactors sampled at the same time (left and right columns of image pairs).

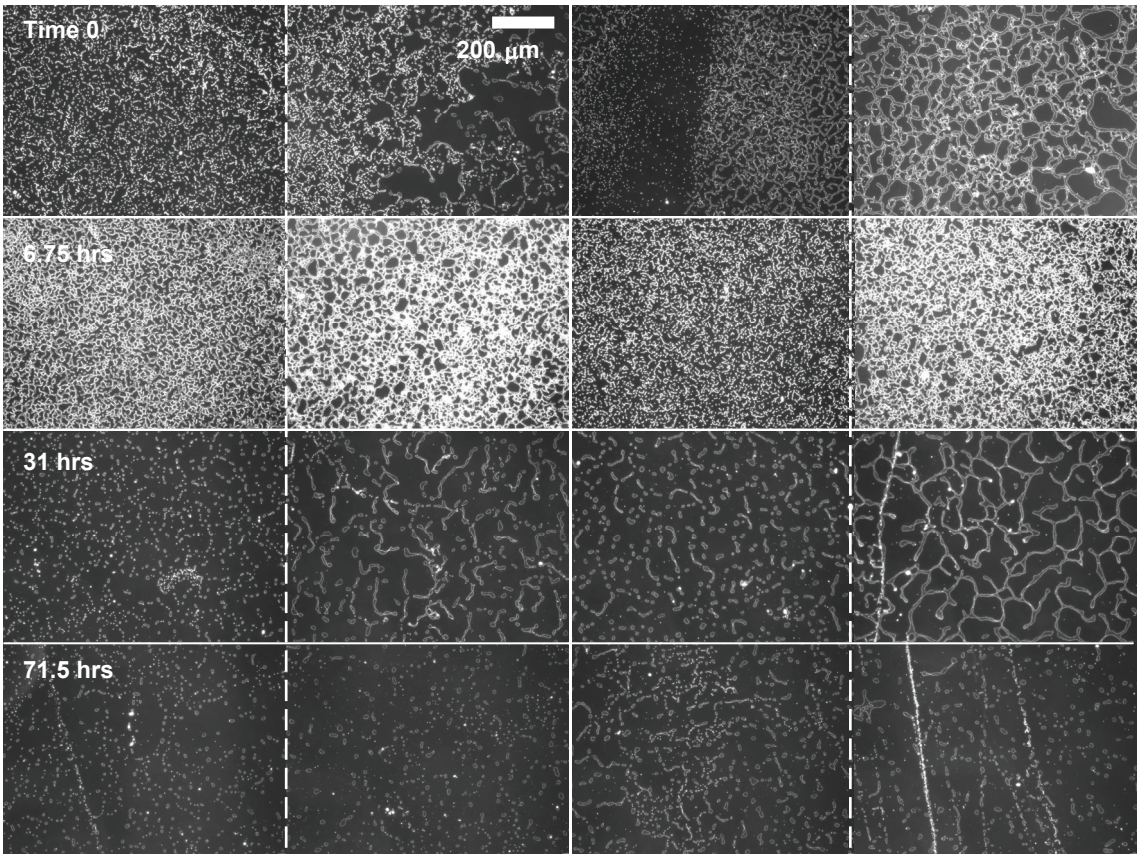

Figure 2-13. *S. oneidensis* biofilm evolution over 71.5 hours. Image pairs separated by a dashed line are two different regions on the same biofilm coupon. Left and right columns of image pairs represent duplicate reactors. Samples in a given row were collected at the same time point.

Images of *S. oneidensis* and *P. aeruginosa* growth on both poly-L-lysine and standard glass microscope slides are shown in Figure 2-14. Again, two fields of view at 10x magnification are given side-by-side for each sampled coupon. Duplicate reactors, differing only in the organism with which they were inoculated, contained both types of slides. The inoculation period was 13.5 hours with high stir for the first minute followed by low stir for the remainder of the experiment. Residence time in the reactor after the batch inoculation period was 11 hours. All samples in this figure were taken at 13.3 hours. *S. oneidensis* biofilm coverage (Figure 2-14a and b) was less extensive than that of *P. aeruginosa* (c and d), but significant variability was observed for both species. *S. oneidensis* coverage was notably far less than had been observed at either the 0 or 6.75

hour samples in Figure 2-13. Poly-L-lysine coated slides (b and d) did not provide significant improvements in biofilm coverage compared to regular glass (a and c). The coating's positive charge which could enhance initial attachment may be offset by its documented antimicrobial properties [77].

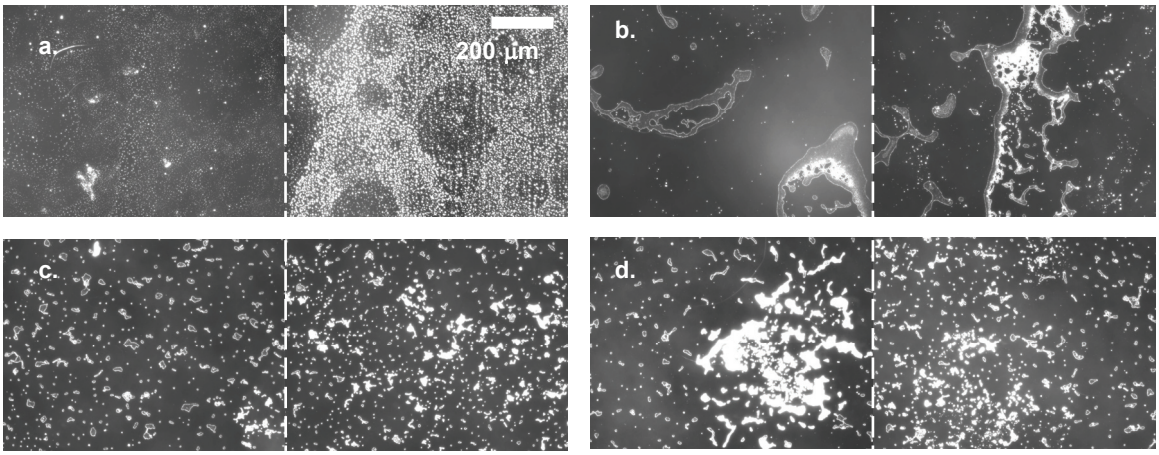

Figure 2-14. *S. oneidensis* (a, b) and *P. aeruginosa* (c, d) biofilms on soda lime glass (a, c) and poly-L-lysine coated (b, d) microscope slides. All samples taken at 13.3 hours.

Tests with poly-L-lysine coated slides, various stir regimes, shorter residence time, longer or shorter inoculation times and even with the good biofilm-former *P. aeruginosa* failed to generate a satisfactory biofilm growth method with sufficient yield and reproducibility to justify further characterization of biofilm EPS or surface properties. Low yields may be explained by competition between biofilms and planktonic growth. A hydraulic residence time of about 30 minutes, less than the doubling time of the organisms, would ensure selection of attached growth and perhaps increase biofilm yield, but the total volume of growth medium required (e.g., over 20 liters to run duplicate reactors and a sterile control for 12 hours) is prohibitive, not the least because it would be extremely difficult to manage such volumes under anaerobic conditions. The high stir of 230 rpm used in some tests was the maximum stable stir rate in the bioreactor vessel, but the amount of shear it provided would certainly be orders of

magnitude less than the shear forces applied during streaming potential measurements, which could have made it extremely difficult to obtain an electrokinetic-based estimate of biofilm surface charge. Difficulties with the biofilm reactor itself, including deformation of plastic parts after repeated autoclave sterilization, presented further challenges. Well-controlled hydrodynamics have been cited as important to the growth of reproducible biofilms [10, 78, 79], and the hydrodynamic control offered by our magnetically-driven stir vane may have been insufficient, particularly when coupon-holding rods failed and released their slides during the active growth period.

Flat-plate clamping-cell style bioreactors, with high surface-to-volume ratios, might be more appropriate: the small reactor volume and cross-flow design make it possible to achieve higher shear forces and extremely short hydraulic residence times, which would select for shear-resistant biofilm growth. However, clamping-cell designs generally accommodate only one or two microscope slide biofilm coupons, so they are not ideal for destructive time-series sampling, replicate samples, or for the production of large quantities of biomass.

2.5 Conclusions

The results of the planktonic studies confirm the influence of metabolic state, represented by electron acceptor conditions and growth phase, on the surface properties of planktonic *S. oneidensis* MR-1. Discernible differences in zeta potential and apparent hydrophobicity were detected between aerobic and anaerobic cultures, and comparison of these two data sets with each other and with the literature suggests that charge, non-polar interactions, and steric factors, all of which relate to the conformation of EPS macromolecules, contribute to adhesion and attachment behavior in complex ways. Data

collected under iron-reducing conditions demonstrated that it is possible to culture *S. oneidensis* with ferric citrate and characterize its surface properties without interference from iron particulate matter. Furthermore, a modified ferrozine assay may be used to demonstrate dissimilatory iron reduction, but is matrix-sensitive.

EPS extraction and purification from planktonic cultures for the purpose of surface property characterization present challenges. Most methods employed in the literature involve chemical extraction to achieve sufficient yields, but even the gentlest of these extractants, formaldehyde, can affect the chemical composition of the EPS. Starting with a higher cell density and harvesting and washing the cells by filtration, rather than low-speed centrifugation [80], may help reduce loss of loosely bound EPS polysaccharides while still ensuring the necessary removal of residual growth medium. Subsequent EPS extraction by ultracentrifugation, followed by filtration to remove any residual cells and potentially by dialysis to remove low molecular weight organics could provide a sufficient mass of high-quality EPS for characterization. It is probably desirable to avoid concentration by ethanol-precipitation and freeze-drying.

The original description of the MATH assay [53] used microscopic examination of the aqueous phase cell suspension to confirm that changes in OD post-partitioning cannot be attributed to e.g., aggregation or cell lysis, and observation of the oil phase itself confirmed that cells do not partition into the hydrocarbon. However, a recent study has demonstrated that hydrocarbon microdroplets persisting in the aqueous suspension after phase separation may artificially increase measured OD, an effect which can be avoided by replacing the OD measurement with direct cell counts under an inverted

microscope [52]. These proposed modifications may increase the accuracy and precision of the measurement.

Efforts to culture *S. oneidensis* biofilms failed to yield sufficiently reproducible and complete surface coverage of microscope slide coupons in a stirred bioreactor. Replacing *S. oneidensis* with *P. aeruginosa* improved yield somewhat but not reproducibility. Without a method that generated comparable biofilms every time, further analysis of biofilm surface properties (e.g., EPS composition, biofilm hydrophobicity, biofilm surface charge by streaming potential analysis or potentiometric titration) under different redox conditions would not have been meaningful. However, these results do not indicate that biofilm studies are pointless or unimportant. On the contrary, one laboratory study using biofilm-coated quartz sand has already demonstrated that biofilm surface properties affect bacterial transport behavior through complex surface interactions [17].

Further research is needed to improve biofilm cultivation techniques and refine characterization methods so that transport-relevant particle-biofilm interactions can be investigated systematically under environmentally relevant conditions. The presence of bacterial surface EPS has a profound impact not only on the overall retention of planktonic cells used in transport and deposition experiments, but also on the spatial variation of the deposition rate [64]. Similar effects may be expected when the surface where the bioparticles are deposited is also coated with biopolymers. Improved methods would allow researchers to approach questions such as:

- How do biofilm morphology, total biomass, cell counts, and EPS composition vary as a function of redox conditions?

- How do surface charge, surface hydrophobicity, and zeta potential of a biofilm vary as a function of redox conditions?
- Does the presence of biofilm under different redox conditions affect model particle removal in filtration systems?

Potentiometric titration and surface functional analysis by e.g., ATR-FTIR [73] would provide additional and complementary information about surface functional groups, whether of whole cells or biofilm. Unlike the protein and carbohydrate assays used in the present study, these methods do not require EPS extraction to characterize surface properties. This offers the double advantage of eliminating an experimental step and providing what is perhaps a more relevant and realistic picture of surface properties. One column study [21] has already shown that EPS-coated sand is not a good surrogate for biofilm-coated sand in microsphere deposition studies, a result which suggests that the process of extracting EPS for separate use or characterization influences its properties significantly. Deposition studies in packed columns or other porous media would quantify how biofilms affect reversible and irreversible attachment behavior of biocolloids, while studies under controlled hydrodynamics (e.g., radial stagnation point flow cells) shed light on irreversible attachment. A quartz crystal microbalance system could be used to probe the attachment properties of EPS extracted from biofilms with well-characterized particles (e.g., functionalized microspheres) or biocolloids of interest (e.g., pathogenic organisms or surrogates), although once again with the caveat that extracted EPS may be a poor surrogate for bulk biofilm [21].

Information about the roles of biofilms in virus or bacteria removal in the subsurface is relevant to engineered systems where such biofilms are likely to form.

Many of these systems involve some type of water reuse or reclamation, and they are likely to become more important in the face of future water scarcity. If microbially-induced subsurface redox conditions can be established to play a significant and predictable role in determining pathogen removal, well operation and water recharge management might be optimized to favor the development of redox conditions where removals are highest, and risk-assessment analysis could help indentify situations where regulation or practice may be insufficiently protective. But such advances in applications will rest on advances in fundamental understanding of biofilm properties and their influence on bioparticle transport.

2.6 References

1. Van der Wielen, P., W. Senden, and G. Medema, *Removal of Bacteriophages MS2 and Phi X174 during transport in a sandy anoxic aquifer.* Environmental Science & Technology, 2008. 42(12): p. 4589-4594.
2. Hunter, K.S., Y.F. Wang, and P. Van Cappellen, *Kinetic modeling of microbially-driven redox chemistry of subsurface environments: coupling transport, microbial metabolism and geochemistry.* Journal of Hydrology, 1998. 209(1-4): p. 53-80.
3. Lovley, D.R. and E.J.P. Phillips, *Novel mode of microbial energy metabolism: organic carbon oxidation coupled to dissimilatory reduction of iron or manganese.* Applied & Environmental Microbiology, 1988. 54(6): p. 1472-1480.
4. Chapelle, F.H., *Ground-water Microbiology and Geochemistry*. 2nd ed. 2001, New York: Wiley and Sons. 477.
5. Stewart, P.S. and M.J. Franklin, *Physiological heterogeneity in biofilms.* Nature Reviews Microbiology, 2008. 6(3): p. 199-210.
6. Cao, B., L.A. Shi, R.N. Brown, Y.J. Xiong, J.K. Fredrickson, M.F. Romine, M.J. Marshall, M.S. Lipton, and H. Beyenal, *Extracellular polymeric substances from Shewanella sp HRCR-1 biofilms: characterization by infrared spectroscopy and proteomics.* Environmental Microbiology, 2011. 13(4): p. 1018-1031.
7. D'Abzac, P., F. Bordas, E. Joussein, E. Van Hullebusch, P.N.L. Lens, and G. Guibaud, *Characterization of the mineral fraction associated to extracellular polymeric substances (EPS) in anaerobic granular sludges.* Environmental Science & Technology, 2010. 44(1): p. 412-418.
8. Flemming, H.C., J. Wingender, C. Mayer, V. Korstgens, and W. Borchard, *Cohesiveness in biofilm matrix polymers*, in *Community Structure and Co-operation in Biofilms*, D.G. Allison, et al., Editors. 2000, Cambridge University Press: Cambridge. p. 87-105.
9. Flemming, H.C., T.R. Neu, and D.J. Wozniak, *The EPS matrix: the "house of biofilm cells".* Journal of Bacteriology, 2007. 189(22): p. 7945-7947.
10. Besemer, K., G. Singer, R. Limberger, A.K. Chlup, G. Hochedlinger, I. Hödl, C. Baranyi, and T.J. Battin, *Biophysical controls on community succession in stream biofilms.* Applied and Environmental Microbiology, 2007. 73(15): p. 4966-4974.
11. Myszka, K. and K. Czaczyk, *Characterization of adhesive exopolysaccharide (EPS) produced by Pseudomonas aeruginosa under starvation conditions.* Current Microbiology, 2009. 6(58): p. 541-546.
12. Kim, H.Y., K.M. Yeon, C.H. Lee, S. Lee, and T. Swaminathan, *Biofilm structure and extracellular polymeric substances in low and high dissolved oxygen membrane bioreactors.* Separation Science and Technology, 2006. 41(7): p. 1213-1230.
13. Hunter, R.C., V.R. Phoenix, A. Saxena, and T.J. Beveridge, *Impact of growth environment and physiological state on metal immobilization by Pseudomonas aeruginosa PAO1.* Canadian Journal of Microbiology, 2010. 56(7): p. 527-538.

14. Thormann, K.M., R.M. Saville, S. Shukla, and A.M. Spormann, *Induction of rapid detachment in Shewanella oneidensis MR-1 biofilms.* Journal of Bacteriology, 2005. 187(3): p. 1014-1021.
15. Saville, R.M., S. Rakshe, J.A.J. Haagensen, S. Shukla, and A.M. Spormann, *Energy-dependent stability of Shewanella oneidensis MR-1 biofilms.* Journal of Bacteriology, 2011. 193(13): p. 3257-3264.
16. McLean, J.S., P.D. Majors, C.L. Reardon, C.L. Bilskis, S.B. Reed, M.F. Romine, and J.K. Fredrickson, *Investigations of structure and metabolism within Shewanella oneidensis MR-1 biofilms.* Journal of Microbiological Methods, 2008. 74(1): p. 47-56.
17. Liu, Y. and J. Li, *Role of Pseudomonas aeruginosa biofilm in the initial adhesion, growth and detachment of Escherichia coli in porous media.* Environmental Science & Technology, 2008. 42(2): p. 443-449.
18. Tong, M., J. Ding, Y. Shen, and P. Zhu, *Influence of biofilm on the transport of fullerene (C60) nanoparticles in porous media.* Water Research, 2010. 44(4): p. 1094-1103.
19. Janjaroen, D., F.Q. Ling, G. Monroy, N. Derlon, E. Morgenroth, S.A. Boppart, W.T. Liu, and T.H. Nguyen, *Roles of ionic strength and biofilm roughness on adhesion kinetics of Escherichia coli onto groundwater biofilm grown on PVC surfaces.* Water Research, 2013. 47(7): p. 2531-2542.
20. Majumdar, U., T. Alexander, M. Waskar, and M.V. Dagaonkar, *Effect of biofilm on colloid attachment in saturated porous media.* Water Science and Technology, 2014. 70(2): p. 241-248.
21. Tripathi, S., D. Champagne, and N. Tufenkji, *Transport behavior of selected nanoparticles with different surface coatings in granular porous media coated with Pseudomonas aeruginosa biofilm.* Environmental Science & Technology, 2012. 46(13): p. 6942-6949.
22. Wang, A.M., B. Lin, B.E. Sleep, and S.N. Liss, *The impact of biofilm growth on transport of Escherichia coli O157:H7 in sand.* Ground Water, 2011. 49(1): p. 20-31.
23. Paris, T., S. Skali-Lami, and J.C. Block, *Probing young drinking water biofilms with hard and soft particles.* Water Research, 2009. 43(1): p. 117-126.
24. Lovley, D.R., D.E. Holmes, and K.P. Nevin, *Dissimilatory Fe(III) and Mn(IV) reduction*, in *Advances in Microbial Physiology*. 2004. p. 219-286.
25. Krause, B. and K.H. Nealson, *Physiology and enzymology involved in denitrification by Shewanella putrefaciens.* Applied and Environmental Microbiology, 1997. 63(7): p. 2613-2618.
26. Lovley, D.R., E.J.P. Phillips, and D.J. Lonergan, *Hydrogen and formate oxidation coupled to dissimilatory reduction of iron or manganese by Alteromonas putrefaciens.* Applied and Environmental Microbiology, 1989. 55(3): p. 700-706.
27. DiChristina, T.J. and E.F. DeLong, *Isolation of anaerobic respiratory mutants of Shewanella putrefaciens and genetic analysis of mutants deficient in anaerobic growth on Fe3+.* Journal of Bacteriology, 1994. 176(5): p. 1468-1474.
28. Moser, D.P. and K.H. Nealson, *Growth of the facultative anaerobe Shewanella putrefaciens by elemental sulfur reduction.* Applied and Environmental Microbiology, 1996. 62(6): p. 2100-2105.

29. de Kerchove, A.J. and M. Elimelech, *Impact of alginate conditioning film on deposition kinetics of motile and nonmotile Pseudomonas aeruginosa strains.* Applied and Environmental Microbiology, 2007. 73(16): p. 5227-5234.
30. Taylor, S.W., C.R. Lange, and E.A. Lesold, *Biofouling of contaminated ground-water recovery wells: Characterization of microorganisms.* Ground Water, 1997. 35(6): p. 973-980.
31. Wingender, J. and H.C. Flemming, *Biofilms in drinking water and their role as reservoir for pathogens.* International Journal of Hygiene and Environmental Health, 2011. 214(6): p. 417-423.
32. Herzberg, M. and M. Elimelech, *Physiology and genetic traits of reverse osmosis membrane biofilms: a case study with Pseudomonas aeruginosa.* Isme Journal, 2008. 2(2): p. 180-194.
33. Hunter, R.C., A.P. Hitchcock, J.J. Dynes, M. Obst, and T.J. Beveridge, *Mapping the speciation of iron in Pseudomonas aeruginosa biofilms using scanning transmission X-ray microscopy.* Environmental Science & Technology, 2008. 42(23): p. 8766-8772.
34. Spormann, A.M., *Physiology of microbes in biofilms.* Bacterial Biofilms, 2008. 322: p. 17-36.
35. Kostka, J. and K.H. Nealson, *Isolation, cultivation and characterization of iron- and manganese-reducing bacteria*, in *Techniques in Microbial Ecology*, R.S. Burlage, et al., Editors. 1998, Oxford University Press: New York. p. 58-75.
36. Freeze, R.A. and J.A. Cherry, *Groundwater*. 1979, Englewood Cliffs, NJ: Prentice-Hall. 604.
37. Flynn, C.M., K.A. Hunt, J.A. Gralnick, and F. Srienc, *Construction and elementary mode analysis of a metabolic model for Shewanella oneidensis MR-1.* Biosystems, 2012. 107(2): p. 120-128.
38. Myers, C.R. and K.H. Nealson, *Respiration-linked proton translocation coupled to anaerobic reduction of Manganese(iv) and Iron(iii) in Shewanella putrefaciens MR-1.* Journal of Bacteriology, 1990. 172(11): p. 6232-6238.
39. Thormann, K.M., S. Duttler, R.M. Saville, M. Hyodo, S. Shukla, Y. Hayakawa, and A.M. Spormann, *Control of formation and cellular detachment from Shewanella oneidensis MR-1 biofilms by cyclic di-GMP.* Journal of Bacteriology, 2006. 188(7): p. 2681-2691.
40. Thormann, K.M., R.M. Saville, S. Shukla, D.A. Pelletier, and A.M. Spormann, *Initial phases of biofilm formation in Shewanella oneidensis MR-1.* Journal of Bacteriology, 2004. 186(23): p. 8096-8104.
41. Haas, J.R. and T.J. Dichristina, *Effects of Fe(III) chemical speciation on dissimilatory Fe(III) reduction by Shewanella putrefaciens.* Environmental Science & Technology, 2002. 36(3): p. 373-380.
42. Viollier, E., P.W. Inglett, K. Hunter, A.N. Roychoudhury, and P. Van Cappellen, *The ferrozine method revisited: Fe(II)/Fe(III) determination in natural waters.* Applied Geochemistry, 2000. 15(6): p. 785-790.
43. Stookey, L.L., *Ferrozine - a new spectrophotometric reagent for iron.* Analytical Chemistry, 1970. 42(7): p. 779-&.
44. Wingender, J., M. Strathmann, A. Rode, A. Leis, and H.C. Flemming, *Isolation and biochemical characterization of extracellular polymeric substances from*

Pseudomonas aeruginosa, in *Microbial Growth in Biofilms, Pt A*. 2001. p. 302-314.
45. Nichols, C.M., S.G. Lardiere, J.P. Bowman, P.D. Nichols, J.A.E. Gibson, and J. Guezennec, *Chemical characterization of exopolysaccharides from Antarctic marine bacteria.* Microbial Ecology, 2005. 49(4): p. 578-589.
46. Kim, H.N. and S.L. Walker, *Escherichia coli transport in porous media: Influence of cell strain, solution chemistry, and temperature.* Colloids and Surfaces B-Biointerfaces, 2009. 71(1): p. 160-167.
47. Dubois, M., K.A. Gilles, J.K. Hamilton, P.A. Rebers, and F. Smith, *COLORIMETRIC METHOD FOR DETERMINATION OF SUGARS AND RELATED SUBSTANCES.* Analytical Chemistry, 1956. 28(3): p. 350-356.
48. Rosenberg, M., *Bacterial Adherence to Hydrocarbons - a Useful Technique for Studying Cell-Surface Hydrophobicity.* Fems Microbiology Letters, 1984. 22(3): p. 289-295.
49. Rosenberg, M., D. Gutnick, and E. Rosenberg, *Adherence of Bacteria to Hydrocarbons - a Simple Method for Measuring Cell-Surface Hydrophobicity.* Fems Microbiology Letters, 1980. 9(1): p. 29-33.
50. Neu, T.R. and K.C. Marshall, *Microbial "footprints" - a new approach to adhesive polymers.* Biofouling, 1991. 3: p. 101-112.
51. Walker, S.L., J.E. Hill, J.A. Redman, and M. Elimelech, *Influence of growth phase on adhesion kinetics of Escherichia coli D21g.* Applied and Environmental Microbiology, 2005. 71(6): p. 3093-3099.
52. Zoueki, C.W., N. Tufenkji, and S. Ghoshal, *A modified microbial adhesion to hydrocarbons assay to account for the presence of hydrocarbon droplets.* Journal of Colloid and Interface Science, 2010. 344(2): p. 492-496.
53. Rosenberg, M. and J.R. Doyle, *Microbial cell surface hydrophobicity: history, measurement, and significance*, in *Microbial Cell Surface Hydrophobicity*, J.R. Doyle and M. Rosenberg, Editors. 1990, American Society for Microbiology: Washington, DC. p. 1-37.
54. Pembrey, R.S., K.C. Marshall, and R.P. Schneider, *Cell surface analysis techniques: What do cell preparation protocols do to cell surface properties?* Applied and Environmental Microbiology, 1999. 65(7): p. 2877-2894.
55. Hunter, R.J., *Zeta potential in Colloid Science: Principles and Applications*. 1981: Academic Press. 386.
56. Ling, F. and W.T. Liu, *Impact of chloramination on the development of laboratory-grown biofilms fed with filter-pretreated groundwater.* Microbes and Environments, 2013. 28(1): p. 50-57.
57. Humphreys, G., G.L. Lee, S.L. Percival, and A.J. McBain, *Combinatorial activities of ionic silver and sodium hexametaphosphate against microorganisms associated with chronic wounds.* Journal of Antimicrobial Chemotherapy, 2011. 66(11): p. 2556-2561.
58. Rasband, W.S., *ImageJ*. 1997-2012, U. S. National Institutes of Health: Bethesda, Maryland, USA. p. http://imagej.nih.gov/ij/.
59. Dobbin, P.S., A.K. Powell, A.G. McEwan, and D.J. Richardson, *The influence of chelating-agents upon the dissimilatory reduction of Fe(III) by Shewanella putrefaciens.* Biometals, 1995. 8(2): p. 163-173.

60. Chen, G.X. and S.L. Walker, *Role of solution chemistry and ion valence on the adhesion kinetics of groundwater and marine bacteria.* Langmuir, 2007. 23(13): p. 7162-7169.
61. Haznedaroglu, B.Z., C.H. Bolster, and S.L. Walker, *The role of starvation on Escherichia coli adhesion and transport in saturated porous media.* Water Research, 2008. 42(6-7): p. 1547-1554.
62. Zhang, X.Q., P.L. Bishop, and B.K. Kinkle, *Comparison of extraction methods for quantifying extracellular polymers in biofilms.* Water Science and Technology, 1999. 39(7): p. 211-218.
63. Nielsen, P.H., A. Jahn, and R. Palmgren, *Conceptual model for production and composition of exopolymers in biofilms.* Water Science and Technology, 1997. 36(1): p. 11-19.
64. Liu, Y., C.H. Yang, and J. Li, *Influence of extracellular polymeric substances on Pseudomonas aeruginosa transport and deposition profiles in porous media.* Environmental Science & Technology, 2007. 41(1): p. 198-205.
65. Gaboriaud, F., E. Dague, S. Bailet, F. Jorand, J. Duval, and F. Thomas, *Multiscale dynamics of the cell envelope of Shewanella putrefaciens as a response to pH change.* Colloids and Surfaces B-Biointerfaces, 2006. 52(2): p. 108-116.
66. Van der Mei, H.C., B. Van de Belt-Gritter, and H.J. Busscher, *Implications of microbial adhesion to hydrocarbons for evaluating cell-surface hydrophobicity 2. Adhesion mechanisms.* Colloids and Surfaces B-Biointerfaces, 1995. 5(3-4): p. 117-126.
67. Zoueki, C.W., S. Ghoshal, and N. Tufenkji, *Bacterial adhesion to hydrocarbons: Role of asphaltenes and resins.* Colloids and Surfaces B-Biointerfaces, 2010. 79(1): p. 219-226.
68. Busscher, H.J., B. Van de Belt-Gritter, and H.C. Van der Mei, *Implications of microbial adhesion to hydrocarbons for evaluating cell-surface hydrophobicity .1. Zeta-potentials of hydrocarbon droplets.* Colloids and Surfaces B-Biointerfaces, 1995. 5(3-4): p. 111-116.
69. Zangi, R. and J. Engberts, *Physisorption of hydroxide ions from aqueous solution to a hydrophobic surface.* Journal of the American Chemical Society, 2005. 127(7): p. 2272-2276.
70. Rosenberg, M., *Microbial adhesion to hydrocarbons: twenty-five years of doing MATH.* Fems Microbiology Letters, 2006. 262(2): p. 129-134.
71. Neal, A.L., S.N. Dublin, J. Taylor, D.J. Bates, L. Burns, R. Apkarian, and T.J. DiChristina, *Terminal electron acceptors influence the quantity and chemical composition of capsular exopolymers produced by anaerobically growing Shewanella spp.* Biomacromolecules, 2007. 8(1): p. 166-174.
72. Roberts, J.A., D.A. Fowle, B.T. Hughes, and E. Kulczycki, *Attachment behavior of Shewanella putrefaciens onto magnetite under aerobic and anaerobic conditions.* Geomicrobiology Journal, 2006. 23(8): p. 631-640.
73. Castro, F.D., J. Sedman, A.A. Ismail, B. Asadishad, and N. Tufenkji, *Effect of dissolved oxygen on two bacterial pathogens examined using ATR-FTIR spectroscopy, microelectrophoresis, and potentiometric titration.* Environmental Science & Technology, 2010. 44(11): p. 4136-4141.

74. Castro, F.D. and N. Tufenkji, *Role of oxygen tension on the transport and retention of two pathogenic bacteria in saturated porous media.* Environmental Science & Technology, 2008. 42(24): p. 9178-9183.
75. Walker, S.L., J.A. Redman, and M. Elimelech, *Influence of growth phase on bacterial deposition: Interaction mechanisms in packed-bed column and radial stagnation point flow systems.* Environmental Science & Technology, 2005. 39(17): p. 6405-6411.
76. Rijnaarts, H.H.M., W. Norde, J. Lyklema, and A.J.B. Zehnder, *DLVO and steric contributions to bacterial deposition in media of different ionic strengths.* Colloids and Surfaces B-Biointerfaces, 1999. 14(1-4): p. 179-195.
77. Colville, K., N. Tompkins, A.D. Rutenberg, and M.H. Jericho, *Effects of poly(L-lysine) substrates on attached Escherichia coli bacteria.* Langmuir, 2010. 26(4): p. 2639-2644.
78. Ramasamy, P. and X. Zhang, *Effects of shear stress on the secretion of extracellular polymeric substances in biofilms*, in *Water Science and Technology*. 2005. p. 217-223.
79. Jackson, G., H. Beyenal, W.M. Rees, and Z. Lewandowski, *Growing reproducible biofilms with respect to structure and viable cell counts.* Journal of Microbiological Methods, 2001. 47(1): p. 1-10.
80. Tazehkand, S.S., S. Torkzaban, S.A. Bradford, and S.L. Walker, *Cell preparation methods influence Escherichia Coli D21g surface chemistry and transport in saturated sand.* Journal of Environmental Quality, 2008. 37(6): p. 2108-2115.

3 Attachment sensitivity analysis and 1-D modeling of biofiltration heterogeneity in CXTFIT

3.1 Background and Motivation

A recent analysis [1] of published field data estimated the travel times that would be necessary to meet nationally-mandated microbial risk standards in seven sandy aquifers in The Netherlands. The results, summarized in

Table 3-1, indicated that five of the aquifers would achieve sufficient microbial removal in fewer than 10 days, and a sixth would meet standards in under 20 days. The seventh, however, would require over 100 days of subsurface travel time before viral concentrations were reduced below national water quality standards. The outlier was hydrologically similar to the other aquifers, but it was anoxic, suggesting the importance of biogeochemical factors.

The enhanced transport in the anoxic aquifer was consistent with inactivation studies that reported slower viral die-off in anaerobic microcosms [2, 3], with simulated slow sand filtration experiments that observed lower coliphage transport in an anaerobic enclosure [4], and with the idea that (oxy)hydroxide mineral coatings, likely to be less prevalent under anaerobic conditions, may contribute significantly to virus removal [5, 6]. The approach taken in the analysis of the anoxic Dutch aquifer [1] is typical when modeling field data: a small microcosm inactivation experiment was conducted to estimate the value of the first-order kinetic rate coefficient for inactivation, and an apparent attachment rate coefficient was fit from observed breakthrough curves.

Table 3-1: Characteristics of seven sandy aquifers, with travel times required to achieve sufficient reduction in viral concentrations that the annual risk threshold for microbial illness will not be exceeded if the water is used as drinking water. Data from [1].

Aquifer	Status	Travel time to achieve $1x10^{-4}$ annual microbial risk
A, B	aerobic	< 2 days
C	aerobic	2-3 days
D, E	aerobic	8-9 days
F	aerobic	16-17 days
G	anoxic	101 days

Previous work [7, 8] has shown that models of virus transport are sensitive to these parameters that quantify the attachment (filtration) and inactivation (die-off) of viral particles, yet the values of these parameters – representing the sum of all biological and physicochemical mechanisms responsible for virus removal – are often poorly constrained. Modeling studies have been used to interpret and explain observed microbial transport phenomena (e.g., [1, 6, 9-11]) and to predict vulnerable aquifers [8]. In these models, possibility of spatial heterogeneity in attachment and inactivation processes is lost in the macroscale treatment of "apparent" values used to quantify these biological removal mechanisms. And in the absence of documented, site-specific field values for attachment and inactivation, the predictive model [8] assumed a single constant value to represent biological removal processes when evaluating the vulnerability of several dozen real aquifers, despite having demonstrated the importance of the model's attachment parameter during sensitivity analysis. But a modeling approach that explicitly includes variability in attachment processes has the potential to help elucidate the role of biological heterogeneity in microbial transport.

3.1.1 What is heterogeneity?

The heterogeneities that pertain to microbial transport in the subsurface are varied. They include the physical and geochemical properties of porous media: the grain

size distribution, shape, sorting, porosity, and hydraulic conductivity of aquifer materials; the geologic material and mineral coatings of the aquifer grains and their corresponding surface properties; the hydraulic gradient, the degree of saturation. They also include the properties of the infiltrating groundwater, not only its chemistry, but also the possible presence of organic matter, particulate material, and surface-derived contaminants. Finally, they include biological heterogeneities both within the porous media and related to the microbes that are transported through the groundwater system: spatial and temporal variation in the presence and physicochemical nature of biofilms on aquifer mineral grains, the size and surface properties of microbial particles being transported, and rates of inactivation or die-off.

Furthermore, these heterogeneities are likely to be interrelated. A change in the pH or the ionic strength of infiltrating groundwater can alter the apparent surface charge of both aquifer materials and particulate contaminants [12-14], thus affecting the ability of aquifer grains to capture microbial particles by attachment. In addition to affecting particle-mineral grain interactions [15], dissolved organic matter can support significant biofilm growth in an aquifer, altering the pore structure and thus the hydraulic properties of the porous medium [16] even as the enhanced biological activity causes a cascade of geochemical shifts down gradient. Changes in groundwater chemistry and the activity of native microflora in the aquifer ecosystem may affect the die-off rates for microbes of interest (as reviewed in reference [14]).

Finally, many of these heterogeneities manifest themselves at multiple scales. Patchy surface coverage of biofilm or mineral coatings on granular aquifer materials can occur within a single pore, but zonation of surface coverage may also be observed on the

scale of centimeters or meters, as when oxyhydroxide minerals accumulate around a well-screen. While the characteristic aerobic-to-anoxic redox zonation of infiltrating organic-rich surface waters occurs on a scale of meters, anoxic microenvironments may exist even within aerobic areas and vice versa [17]. A discretized hydrologic model can resolve groundwater flow and aquifer properties at the scale of the model grid – provided the necessary supporting data are available – but the flow field also varies locally within a single pore or pore throat, and it is these micro-scale heterogeneities that determine whether a given particle collides with and has the opportunity to attach to an aquifer grain. Modeling of reactive solutes indicates the importance of the heterogeneity of the pore-size distribution when removal processes occur primarily within pore throats [18].

At the field scale, resolving the many superposed heterogeneities is often impractical, so researchers commonly resort to handling transport-relevant parameters as bulk properties, perhaps undertaking a more detailed treatment of one or two factors of interest. We too, adopt this approach, focusing our inquiries on the oft-ignored heterogeneities of biological origin.

3.1.2 Modeling approaches to breakthrough data and (sometimes) heterogeneity

Physicochemical filtration is considered the primary removal mechanism for colloidal particles in saturated porous media, so many studies have focused on the factors affecting microbial deposition. The results of laboratory column studies involving viruses and bacteriophages, as well as other non-biological colloids, are commonly interpreted with clean bed filtration theory (CBFT) [19], although this approach is recognized as an oversimplification of complex natural processes [20, 21]. CBFT assumes a spatially constant deposition rate coefficient and predicts an exponential

deposition profile, but power law [22], hypo- [23] and hyperexponential [24] profiles have been observed in the lab for a variety of colloids. Nonexponential behavior may be explained by several phenomena or a combination thereof, including failure of CBFT to account for the hydrodynamic field at mineral grain surfaces [25, 26], blocking [27], straining for larger particles [28], deposition in the secondary minimum [29, 30], and steric interactions [24]. The possibility of detachment may also be taken into account.

However, the most frequently-cited explanations for deviations from clean-bed filtration theory (e.g., [28, 31, 32]) involve different types of heterogeneities that may affect the attachment interaction between a microbe and the surface of a collector grain: microbial subpopulations that differ in size or in surface properties, local variations in surface chemistry, grain surface roughness, microscale variations in the surface potentials, patchy mineral surface coatings, and the like.

When traditional filtration-theory approaches are applied to analyze microbial transport from field breakthrough data, calculated collision efficiencies often decrease with travel distance. In an extensive review, Pang [33] reported that some 30% of the field datasets examined showed evidence of deviations from classic filtration behavior (typically power-law removal with distance), with corresponding decreases in α sometimes attributed to preferential removal of a "stickier" bacterial subpopulation. But the more considered examinations of this change in α have identified site-specific reasons for enhanced removals at short travel distance, e.g., the known spatial distribution of iron mineral coatings [6], and noted the possibility that a correlation between flow velocities and attachment in a heterogeneous system could generate apparent scale-dependency of transport parameters [9]. Predictions of filtration removals based on

α derived from laboratory or short field studies will likely overestimate concentration reductions if the underlying CBFT-based assumption of an exponential deposition profile is not accurate [9, 22].

Tufenkji *et al.* [34] demonstrated that introducing a distribution of deposition rate coefficients into CBFT in place of a single rate constant allowed prediction of non-exponential deposition behavior. Improved fits of non-ideal column breakthrough data also helped elucidate which mechanism was likely dominant in causing the observed deviation from CBFT.

At the field-scale, an entirely different modeling approach provided further evidence that the treatment of heterogeneity is important. Scheibe *et al.* [35] used a published correlation between grain size and hydraulic conductivity to generate correlated fields of hydraulic conductivity and corresponding attachment rate coefficients at constant α in a stochastic representation of a well-documented field site. They then compared predictions of bacterial transport in four scenarios: (1) fully homogeneous, (2) heterogeneous flow with homogeneous attachment, (3) correlated heterogeneous flow and attachment, and (4) uncorrelated heterogeneous flow and attachment. This last scenario was accomplished by "scrambling" the correlated attachment rate coefficient field. Only the third case predicted transport behavior where collision efficiencies – which were held constant during the model run – appeared to decrease with distance, demonstrating that apparent scale-dependence of the filtration parameter α may be explained by a failure to account for correlation between hydrodynamic and biofiltration-related heterogeneities.

Such observations lead us to ask how heterogeneity in biological parameters might affect estimations of microbial removal or uncertainty in aquifer risk assessments.

3.2 Objectives

The modeling investigations described in this chapter sought to contribute to understanding of the role of biological heterogeneity on the extent of transport of biological particles through porous media, with a focus on three specific objectives:

- To evaluate the interconnected sensitivities of a 1-D filtration model to biological and physical system parameters
- To identify system configurations – combinations of physical and biological factors – where performance (in terms of microbial removal) might be particularly sensitive to biological heterogeneity, as well as systems likely to be more robust
- To establish the impact on groundwater modeling results of including heterogeneity in biological parameters and evaluate the implications for future modeling and field applications

The filtration-theory model used in the sensitivity analysis allowed exploration of the physical and biological factors that can affect the removal rate constant for viral particles as they move through porous media. We then moved to a simple advection-dispersion model to explore the effects heterogeneity in removal rates on virus transport at field scale.

3.3 Methods

3.3.1 Sensitivity Analysis: Filtration-inactivation model

Two processes, attachment and inactivation, are generally considered to contribute to virus removal in porous aquifer materials.

As per the common approach, we framed attachment in terms of clean-bed filtration theory [19]. The attachment or deposition of a microorganism on a mineral grain surface requires that the two come in contact with each other and that the microorganism "stick" to the surface of the mineral grain as a result of this "collision." The collision itself depends on the particle's approach to the surface, described as a theoretical single-collector efficiency (η_0), while the probability of a collision resulting in attachment, known as the collision efficiency (α), depends on physicochemical interactions between the particle and the collector surface. Attachment, when it occurs, is treated as irreversible. For modeling purposes, we predicted the contribution of attachment to particle removal for a range of α values using the equation developed by Yao *et al.* [19]:

$$\ln\frac{C}{C_0} = -\frac{3}{2}\frac{(1-n)\alpha\eta_0}{d_c}L, \qquad \text{(Eqn. 3-1)}$$

where d_c is the diameter of the collector grain, n is the porosity, C_0 is the influent concentration, and C is the concentration at length L from the influent location.

The parameter η_0 may be evaluated from one of several theoretical models that sum the contributions of gravity, interception, and Brownian motion to particle deposition. For the viral-sized particles that were the focus of our analysis, the single

collector efficiency is dominated by the contributions of diffusion and was calculated as follows from a reduced form of the T&E equation [36]:

$$\eta_0 = 2.4 A_s^{1/3} N_R^{-0.081} N_{Pe}^{-0.715} N_{vdW}^{0.052}, \qquad \text{(Eqn. 3-2)}$$

where

$N_R = \frac{d_p}{d_c}$	Aspect ratio: d_p is the diameter of the particle (virus)
$N_{Pe} = \frac{U d_c}{D_\infty}$	Ratio of advective to diffusive transport: U is the approach velocity or Darcy flux, defined as the volumetric discharge per unit area, and D_∞ is the bulk diffusion coefficient calculated from the Stokes-Einstein equation
$N_{vdW} = \frac{A}{k_B T}$	Van der Waals number: A is the Hamaker constant, k is the Boltzman constant, and T is the temperature in Kelvin
$A_s = \frac{2(1-\gamma^5)}{2-3\gamma+3\gamma^5-2\gamma^6}$	Happel's porosity-dependent parameter for the effects of neighboring grains: $\gamma = (1-n)^{1/3}$.

At constant flow in porous media such that $L = \frac{Ut}{n}$, the contributions of attachment to microbe removal follow first-order kinetics:

$$\ln \frac{C}{C_0} = -k_{att} t$$

$$\text{where} \quad k_{att} = \frac{3}{2} \frac{(1-n)\alpha \eta_0 U}{n d_c}. \qquad \text{(Eqn. 3-3)}$$

Solution-phase viral inactivation was modeled as first-order process, a common simplification [14, 37]. Note that attached-phase viral inactivation rates are relevant only if viruses may later detach, whereas filtration theory treats attachment as irreversible. The expression for solution-phase inactivation was written in $\log_{10}$ form, so that

concentration reductions could be expressed as "log reductions," a 1-log reduction being equivalent to a ten-fold or 90% decrease in concentration:

$$\log_{10} \frac{C}{C_0} = -k_{inact} t \, .$$

The combined effect of these two removal processes, attachment and inactivation, was then represented in a combined filtration-inactivation model (retaining the $\log_{10}$ base for k_{inact}):

$$\ln \frac{C}{C_0} = -(k_{att} + 2.3 k_{inact}) t \, . \qquad \text{(Eqn. 3-4)}$$

Before proceeding any further, let us explicitly consider the simplifications of this model in the context of groundwater systems. As already mentioned, the model assumes a constant flow velocity. Constant velocity can be a reasonable description of groundwater flow at field scale under steady-state natural gradients, but it does not capture pore-scale velocity variations or transient conditions. The filtration model is one-dimensional, and does not include the effects of dilution or dispersion. All parameters have a single value, implying that physical characteristics like porosity and grain size are homogeneous, that interactions between the model microorganism and the mineral grain surfaces can be represented by a single α, that detachment of infective microorganisms does not occur, and that the model microbial population loses infectivity via first-order kinetics. In short, the model makes no attempt to represent the heterogeneity that characterizes the natural world.

And yet, (over)simplicity is not as useless as it may seem at first glance. Easily manipulated in Excel, such a model allows us to perform sensitivity analysis on the

various parameters, suggesting which real-world heterogeneities are likely to have the most impact on the system and thus merit further investigation.

We therefore assessed the time required for a 5-$\log_{10}$ decrease in virus concentration (99.999% removal) using a range of reasonable values for various input parameters. Other researchers [1] considered average concentrations of entero- and reoviruses in raw sewage and estimated the log reductions that would be required to avoid reduce the individual infection risk below 10^{-4} yr^{-1}. Allowing for a dilution factor of 1000 in a situation where e.g., a leaky sewer line contaminated an aquifer, they found that a further 5.8 - 6.3-$\log_{10}$ reduction in virus concentrations would still be required. U.S. regulation mandates 4-$\log_{10}$ virus removal for public drinking water systems that rely on groundwater [38].

We reiterate that this work focused on viral-sized particles and the analysis which follows, like the expression for single collector efficiency upon which it is based, is not valid for bacteria or protozoan cysts because it does not consider the contributions of interception or gravitational settling. These removal mechanisms are important for larger particles, but they do not contribute significant removal for viruses [36].

3.3.1.1 Sensitivity analysis: Input parameters

The values of the input parameters used for the sensitivity analysis are listed in Table 3-2. The flow velocity in our "default" simulation is a relatively quick 0.5 m/d and the grain size is 0.5 mm. We varied velocity over a range representing natural gradients to high-yield pumping well fields. Grain size and porosity were varied over typical ranges for sandy aquifers.

Table 3-2: Default values of parameters for sensitivity analysis

Symbol	Parameter	Default Value	Range
ε	porosity	0.37	0.25-0.49
T	temperature	10 °C	5 – 25 °C
d_p	particle (virus) diameter	50 nm	20 – 100 nm
d_c	grain size	0.5 mm	0.0625 - 5 mm
U	approach velocity	0.5 m/d	0.01-100 m/d
A	Hamaker constant	1E-20 J	-
k_{inact}	log inactivation rate constant	0.01 or 0.05 d^{-1}	0.001 – 0.1 d^{-1}
α	collision efficiency	-	3.0E-6 – 2.2E-2

Collision efficiencies and inactivation rate constants reported in the literature vary enormously, reflecting a huge range of experimental conditions, methods, and objectives. Researchers have observed viruses or phages that stick to everything or nothing, that die off in a few hours or that retain their infectivity for months. Establishing "typical" behavior is difficult.

For our analysis, we focus our attention on groundwater systems that may allow significant virus transport. Values considered for the constant α represent a realistic range for subsurface systems where attachment is unfavorable. Researchers commonly report alphas from field studies involving ϕX174, MS2, and other surrogates ranging on the order of 10^{-5} to 10^{-2} [1, 6, 39], with many observations from clean, sandy aquifers falling in the lower end of that range.

Inactivation data from different studies can be hard to compare, as die-off may be measured or calculated differently, but values reported for clean, sandy aquifers in The Netherlands [1, 11] suggest that k_{inact} in the range of 10^{-2} to 10^{-1} d^{-1} is reasonable. Higher inactivation rate constants have certainly been observed in other systems, as reviewed elsewhere [40], but we are interested in conservative cases with slower inactivation.

Although we have chosen realistic parameter values, the removal times plotted in the figures that follow do not represent a real-world system. This is not an advection-dispersion model, but a 1-D filtration-inactivation model for the purpose of sensitivity analysis. Direct comparison to natural or engineered groundwater systems is inappropriate; the results here are valid for internal comparison only.

3.3.2 CXTFIT studies

3.3.2.1 Modifications to CXTFIT

Harvey and Garabedian [10] coupled colloid filtration theory and one-dimensional advection-dispersion to build a model for bacterial transport during an injection experiment in a sandy aquifer. Many subsequent studies have adopted and expanded upon this approach with varying degrees of complexity (see [32, 33] for reviews). In its simplest form, the steady-state, one-dimensional local scale advection-dispersion equation for a reactive solute subject to first-order degradation may be written in terms of time t and travel distance x as

$$\frac{\partial C}{\partial t} = D\frac{\partial^2 C}{\partial x^2} - v\frac{\partial C}{\partial x} - \mu C \qquad \text{(Eqn. 3-5)}$$

where C is concentration, v is the average linear flow velocity (related to the approach velocity as $v = \frac{U}{n}$), D is the hydrodynamic dispersion coefficient (equal to the product of the longitudinal dispersivity, α_L, and the velocity, v), and μ is the first-order removal rate constant. The simplified equation presented here represents a homogeneous, saturated porous medium where adsorption is not a factor. Describing microbial attachment as a

first-order removal process, as per colloid filtration theory, makes virus transport amenable to analysis via Eqn. 3-5.

One may introduce detachment into this model by including a detachment rate coefficient and a second equation with the mass balance on the attached particles. However, several field studies of virus and phage transport have reported detachment to be small or insignificant compared to attachment and inactivation [11, 15, 41], so we omit detachment here for the purpose of simplicity.

The summed effects of attachment (k_{att}) and inactivation (k_{inact}, reported as before on a $\log_{10}$ basis) are thus represented in Eqn. 3-5 by the "biofiltration" removal rate coefficient μ:

$$\mu = k_{att} + 2.3k_{inact} . \qquad \text{(Eqn. 3-6)}$$

CXTFIT v2.1 [42] is a public-domain transport model that solves the steady-state, 1-D advection-dispersion equation analytically subject to various boundary and initial conditions. It includes solutions for chemical non-equilibrium (kinetic adsorption), first order degradation and zero-order production. It runs both forwards, to predict concentrations, and backwards, to fit observed concentration data, and is commonly used to extract transport parameters (notably D and α_L) from columns and field tracer studies [e.g., 1, 43, 44].

Although analytical solutions exist only for homogeneous conditions, stochastic methods can approximate a heterogeneous subsurface. CXTFIT may also be run stochastically. In forward mode, the user specifies the ensemble average velocity $<v>$ and the standard deviation σ_v of a log-normal probability density function (PDF) for velocity:

$$F(v) = \frac{1}{v\sigma_v\sqrt{2\pi}} \exp\left[-0.5Y_v^2\right] \qquad \text{where} \quad Y_v = \frac{\ln(v) - \bar{v}}{\sigma_v}.$$

The mean, $\bar{v}$, of the log-normal distribution is related to the ensemble average velocity [42] as

$$\bar{v} = \ln(< v >) - 0.5\sigma_v^2.$$

The modeling domain is divided into a series of independent 1-D stream tubes, each with values for velocity and any other stochastic parameters randomly assigned according to the user-defined distributions. The transport equation is solved deterministically for each stream tube and the results averaged across all stream tubes to give the mean concentration. The stream tube approach is represented schematically in Figure 3-1. CXTFIT can also run backwards in stochastic mode, fitting the mean and standard deviation of distributions for transport parameters from an appropriate field or laboratory data set.

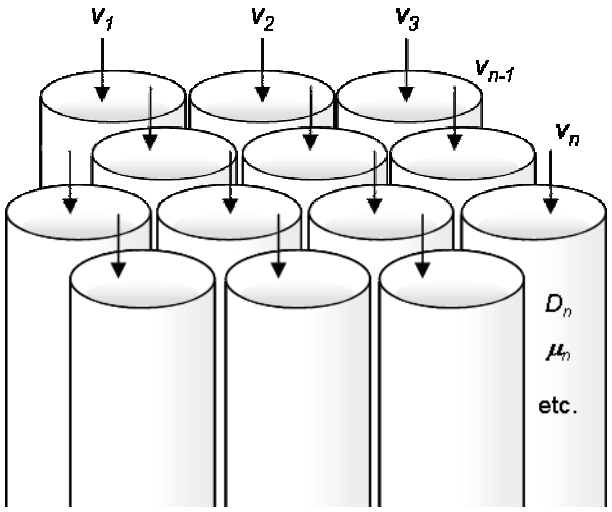

Figure 3-1. Conceptual diagram of the 1-D stream tube model. Adapted from [42].

As explored in the sensitivity analysis, k_{att} exhibits non-linear dependence on both physical and biological parameters. Pore-scale velocity, porosity n, and grain size d_c of

the porous media are notably heterogeneous at field scales. We might also expect spatial variation in the collision efficiency, α, reflecting biogeochemical heterogeneity. Although the public release of CXTFIT was capable of incorporating D or an adsorption-related parameter into the stochastic model, it could not accommodate heterogeneity in the first order removal rate constant. We therefore modified the CXTFIT code to introduce the biofiltration removal rate coefficient μ as a stochastic parameter.

The code does not use Eqn. 3-3 to account explicitly for the contribution of velocity to attachment, nor are the parameters n and d_c involved in the solution to the advection-dispersion equation. Instead, the general nature of the relationship between velocity and removal is captured by calculating the stochastic parameters v and μ from a bivariate log-normal joint PDF [42]:

$$F(v,\mu) = \frac{1}{2\pi\sigma_v\sigma_\mu v\mu\sqrt{1-\rho_{v\mu}^2}} \exp\left[-\frac{Y_v^2 - 2\rho_{v\mu}Y_vY_\mu + Y_\mu^2}{2(1-\rho_{v\mu}^2)}\right]$$

with

$$Y_v = \frac{\ln(v)-\overline{v}}{\sigma_v} \quad ; \; Y_\mu = \frac{\ln(\mu)-\overline{\mu}}{\sigma_\mu} \quad ; \; \rho_{v\mu} = \int_0^\infty\int_0^\infty Y_vY_\mu f(v,\mu)\,dv\,d\mu\,.$$

The correlation coefficient $\rho_{v\mu}$ represents the strength of association between μ and v. If $\rho_{v\mu} = 0$, the log-normal distributions for v and μ vary independently: flow field heterogeneity and removal rate constant heterogeneity are unrelated, and the joint PDF is the product of two single log-normal distributions. Positive values of $\rho_{v\mu}$ signify that higher biofiltration rate constants correlate with higher flow velocities, while negative values of $\rho_{v\mu}$ mean that lower biofiltration rate constants correspond with higher flow velocities.

A value of $\rho_{v\mu} = \pm 1$ reflects an absolute correlation between the two stochastic parameters [42] such that

$$\mu(v) = \left(\frac{v}{< v >} \right)^{\frac{\rho_{v\mu}\sigma_\mu}{\sigma_v}} < \mu > \exp\left(0.5\rho_{v\mu}\sigma_v\sigma_\mu - 0.5\sigma_\mu^2\right).$$

One or two additional parameters may be varied in addition to v and μ, but not independently: instead, each is tied to velocity through a bivariate log-normal joint PDF with a correlation coefficient of ±1.

3.3.2.2 Forward implementation

The modified CXTFIT code was run deterministically in stochastic mode, in which parameter values are assigned and the solution to Eqn. 3-5 is evaluated for each stream tube. The results are subsequently averaged to provide the field-scale resident concentration as a function of time at a particular location, thus simulating a breakthrough curve.

We considered two hypothetical cases: (a) a relatively slow flow velocity and longer travel time, and (b) a relatively high flow velocity and shorter travel time. Simulation parameters are listed in Table 3-3. Although these are idealized and hypothetical settings, it is helpful to contextualize them. Case (a) may be thought of as a sandy aquifer with moderate flow. The average linear velocity of 30 cm/d could reflect an artificial gradient due to one or more small pumping wells, as for a cluster of houses without a public water connection or a small family farm with domestic and limited agricultural water usage. Wells located at 10 and 20 meters from the hypothetical contamination source, corresponding to average travel times of approximately 1 and 2

months, allow examination of the effects of travel distance. Relative homogeneity of the aquifer materials is parameterized by smaller values of σ_v and by a longitudinal dispersivity in line with that reported from a homogeneous sandy field site at similar travel distances [1]. By contrast, the higher dispersion, velocity and σ_v assigned to case (b) describe a comparatively heterogeneous, high-yield formation, such as a municipal production well in a sand and gravel alluvial aquifer. The set-back distance of 30 m with an average travel time of ~6 days is similar to several wells at riverbank filtration facilities in the American Midwest [45].

We modeled the propagation of a 2-day pulse input of a microbial contaminant through the system. This example contamination event could represent a spike in viral concentrations in infiltrating surface waters due to e.g., sanitary sewer overflows or runoff from animal agriculture after a storm event. All concentrations were in normalized form (i.e., $C_o = 1$ for the pulse input). Selection of biofiltration rate constants for these cases is discussed in more detail below.

Table 3-3: Input parameters for a two hypothetical situations: case (a), a small domestic well in a sandy aquifer, and case (b), a municipal production well in an alluvial aquifer.

Symbol	Parameter	case (a)	case (b)	unit
$<v>$	average velocity	30	500	cm/d
$<D>$	dispersion*	500	15000	cm^2/d
σ_v	std. dev. of ln v	0.05, 0.1	0.1, 0.2	-
μ	biofiltration rate constant	0.03, 0.1, 0.2, 0.8	0.03, 0.1, 0.2, 0.5	d^{-1}
σ_μ	std. dev. of ln μ	0.1, 0.5, 1.0	0.1, 0.5, 1.0	-
$\rho_{v\mu}$	correlation coefficient	0, ±0.5, ±1	0, ±0.5, ±1	-
x	travel distance	10, 20	30	m
-	model time step	1	0.25	d

* Longitudinal dispersivity was held constant at $D/v = 17$ cm for case (a) and $D/v = 30$ cm for case (b). In stochastic implementations of CXTFIT, this is accomplished by allowing D to vary with a standard deviation $\sigma_D = \sigma_v$ and a correlation coefficient $\rho_{vD} = 1$.

To guide the parameterization of the removal rate constant ($<\mu>$ and σ_μ) for forward modeling studies, the theoretical value of the biofiltration removal rate constant was evaluated via Eqn. 3-6 with k_{att} estimated from the T&E equation (Eqn. 3-2) for a viral-sized particle. Values for select porosity, grain size, and collision efficiency (α) are reported in Table 3-4. Certain combinations, such as high porosity and granule grain size (d_c = 2 mm), or a 5 m/d average linear velocity in a low-porosity fine sand (d_c = 0.2 mm), are perhaps improbable, and the highest collision efficiencies are more likely to occur in fine materials than coarse, factors we took into consideration when choosing our parameterization. Noting that different combinations of α and k_{inact} often generated similar overall biofiltration rate constants, and considering the effects of σ_μ on the range of values applied in modeling realizations, we selected $<\mu>$ = 0.03 d^{-1} to represent a worse-case, low removal scenario, $<\mu>$ = 0.1 and 0.2 d^{-1} for intermediate removals, and $<\mu>$ = 0.5 or 0.9 d^{-1} to represent high removals at $<v>$ = 500 or 30 cm/d, respectively.

Table 3-4: Biofiltration rate constant μ (d^{-1}) for select combinations of porosity, grain size, and α at the average velocities used in CXTFIT forward case studies.

	porosity, n = 0.25				porosity, n = 0.30				porosity, n = 0.35			
grainsize (mm):	0.2	0.5	1.1	2	0.2	0.5	1.1	2	0.2	0.5	1.1	2
velocity, v = 30 cm/d												
k_{inact} = 0.01 d^{-1}												
α = 1.E-05	0.061	0.032	0.025	0.024	0.050	0.029	0.025	0.024	0.043	0.027	0.024	0.023
1.E-04	0.404	0.108	0.047	0.032	0.295	0.084	0.040	0.029	0.223	0.068	0.035	0.028
1.E-03	3.834	0.876	0.258	0.112	2.741	0.631	0.191	0.086	2.026	0.471	0.147	0.070
k_{inact} = 0.05 d^{-1}												
α = 1.E-05	0.153	0.124	0.117	0.116	0.142	0.121	0.117	0.116	0.135	0.119	0.116	0.115
1.E-04	0.496	0.200	0.139	0.124	0.387	0.176	0.132	0.121	0.315	0.160	0.127	0.120
1.E-03	3.926	0.968	0.350	0.204	2.833	0.723	0.283	0.178	2.118	0.563	0.239	0.162
velocity, v = 500 cm/d												
k_{inact} = 0.01 d^{-1}												
α = 1.E-05	0.108	0.042	0.028	0.025	0.084	0.037	0.027	0.024	0.068	0.033	0.026	0.024
1.E-04	0.873	0.213	0.075	0.043	0.629	0.159	0.060	0.037	0.470	0.123	0.051	0.033
1.E-03	8.522	1.924	0.547	0.220	6.083	1.379	0.397	0.164	4.489	1.022	0.298	0.127
k_{inact} = 0.05 d^{-1}												
α = 1.E-05	0.200	0.134	0.120	0.117	0.176	0.129	0.119	0.116	0.160	0.125	0.118	0.116
1.E-04	0.965	0.305	0.167	0.135	0.721	0.251	0.152	0.129	0.562	0.215	0.143	0.125
1.E-03	8.614	2.016	0.639	0.312	6.175	1.471	0.489	0.256	4.581	1.114	0.390	0.219

Default values from the sensitivity analysis, reported in Table 3-2, were used for all parameters not specified above.

3.3.2.3 Inverse modeling

Van der Wielen *et al.* [1] injected bromide and MS2 bacteriophage into a sandy aquifer and measured breakthrough concentrations at three down-gradient locations. They fit the bromide breakthrough data using CXTFIT to estimate the average flow velocity and the dispersivity, but they did not consider possible subsurface heterogeneity. After "correcting" the MS2 breakthrough concentrations for dilution and dispersion by applying the dilution factor obtained from the conservative tracer data, the researchers attributed all additional removal to the combination of attachment and inactivation. They made separate, batch-study measurements of k_{inact} and then calculated k_{att} from an approximate solution of the 1-D advection-dispersion equation [11]:

$$k_{att} = \frac{\left[1 - 2\alpha_L \frac{2.3}{x} \log\left(\frac{C_{\max}}{C_0}\right)\right]^2 - 1}{4\alpha_L} v - 2.3k_{inact}. \qquad \text{(Eqn. 3-7)}$$

Finally, they reported the corresponding collision efficiency (α) for MS2 at their study site from Eqn. 3-3.

We re-analyzed the results of this published field study using our modified CXTFIT code to investigate the possible influence of biological heterogeneity. Conservative tracer data from two monitoring wells (MW1 and MW2) were fit using stochastic mode in CXTFIT. The resulting distributions for velocity and dispersivity were applied to fit the biofiltration removal rate constant from the published MS2 breakthrough curves using both deterministic and stochastic models. Field breakthrough data were treated as flux-averaged concentrations [46], with longitudinal dispersivity once again held constant. As per CXTFIT recommendations, fitting was performed

several times with both constrained and unconstrained parameter values to obtain the best results.

3.4 Results and Discussion

3.4.1 Sensitivity Analysis

Sensitivity analysis reveals the paramount importance of the two biological factors – inactivation, and the role of collision efficiency in attachment – for the removal of virus-sized particles. The compounding influence of physical system characteristics is also in evidence. As we examine the results of the sensitivity analysis, we consider several guiding questions:

1. For realistic combinations aquifer characteristics, how sensitive is 5-log removal time to changes in α and inactivation?
2. Which sensitivities are likely to be operationally relevant once translated into a field situation?
3. Which configurations are likely most vulnerable to adverse affects caused by changes in (or mis-estimation of) α and k_{inact}?

3.4.1.1 Sensitivity to "biological" parameters: k_{inact} and α

Figure 3-2a shows the effects of attachment and inactivation on the removal of a virus-sized particle in our default simulation. For a hypothetical virus that cannot be inactivated, represented by the solid line, the time necessary to achieve a 5-$\log_{10}$ reduction in virus concentration is determined entirely by the degree to which the viral particles attach (irreversibly) to the aquifer materials. Comparatively "sticky" interactions between virus and porous medium are represented by higher alpha values and

result in relatively rapid reductions in virus concentrations. Lower alphas, which are often relevant in oligotrophic groundwater systems, may require hundreds of days for 5-log virus removal through attachment alone. A full groundwater flow model would be necessary to assess removals in a field situation, but we note that long travel times which might be feasible in the context of aquifer storage and recovery would likely be unrealistic for a standard drinking-water production field in a riverbank filtration-type setting.

Clearly, inactivation must also play a role if groundwater systems are to offer non-hydrodynamic advantages for virus removal compared to surface water supply. Dotted lines in Figure 3-2a show removal times for a realistic range of viral inactivation, with k_{inact} given on a $\log_{10}$ basis. The addition of inactivation as a removal mechanism decreases removal times significantly. Although these reductions are most dramatic at low alpha, they are not irrelevant in sticky systems, where already quick removal times may be shortened by an additional 15% or more for higher inactivation rate constants (Figure 3-2b), making such conditions even more appealing for engineering applications.

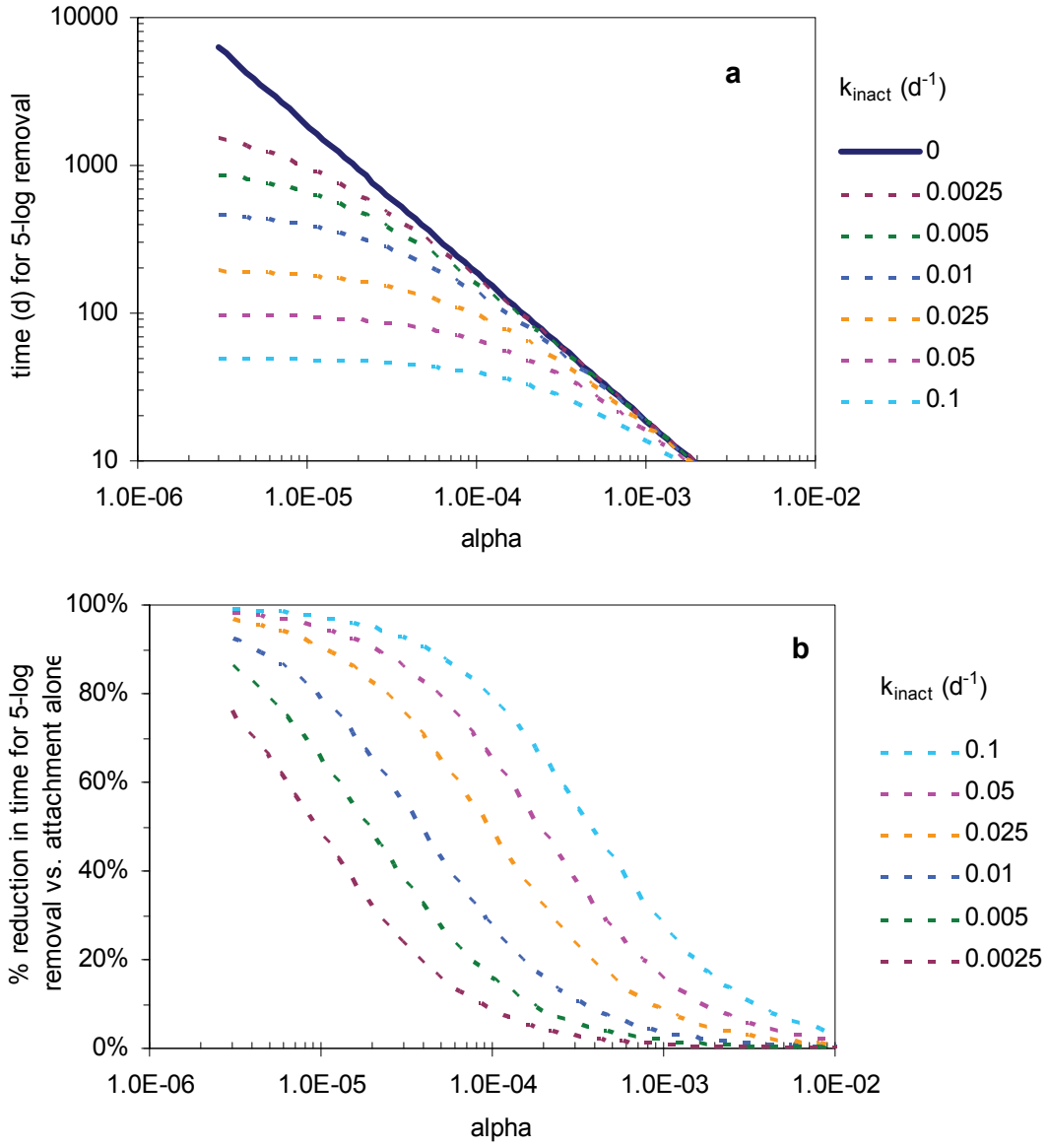

Figure 3-2. (a) Time required for 5-$\log_{10}$ removal as a function of collision efficiency, α. and inactivation rate constant, k_{inact}. Default values used for all other transport parameters. (b) Percent reduction, compared to a system with no inactivation, in the number of days required for 5-log removal at a various k_{inact}.

Unfortunately, inactivation rate constants for viral particles in natural systems are poorly characterized. Inactivation depends not only on the type of virus [47, 48], but also on factors such as temperature, solution chemistry, and the presence of other microorganisms [2, 49, 50]. Environmental conditions are dynamic, so *in situ* inactivation

rates could change over time or along a groundwater flow path. Figure 3-2a suggests that changes in inactivation could result in huge differences in virus removal, particularly in systems with low or intermediate "stickiness." Figure 3-2a also demonstrates that changes in alpha will result in significant differences in virus removal, with the greatest differences occurring in slow inactivation systems. And like inactivation rate constants, alphas for microbial particles in natural systems are poorly characterized and depend on a number of dynamic environmental factors including solution chemistry and the physico-chemical properties of the aquifer materials [32]. It is clear from our analysis and from other studies [7, 8] that virus removal in the subsurface is very sensitive to changes in "biological" factors – both inactivation and stickiness – and yet these parameters are among the least well-known. Spatial and temporal heterogeneity in these biological factors is likely to generate significant variability in virus removal, and the degree to which biological factors are under-characterized may thus contribute uncertainty that cannot be ignored.

The rest of our sensitivity analysis will examine several physical parameters of the aquifer system that affect the removal rate constant, k_{att}. (In this model, and in the absence of a reliable parameterization, inactivation is treated as a constant independent of the physical characteristics of the system.) Figure 3-2 hints at what we may expect: the relative importance of attachment or inactivation in a given system will greatly affect sensitivity to changes in the values of the physical parameters that contribute to k_{att}. We will therefore consider both faster (k_{inact} = 0.05 d^{-1}) and slower (k_{inact} = 0.01 d^{-1}) inactivation constants throughout the sensitivity analysis. We will likewise consider

three alpha values: a relatively low α of 1.0 x 10^{-5}, a mid-range α of 1.0 x 10^{-4}, and a high or "sticky" α of 1.0 x 10^{-3}.

3.4.1.2 Sensitivity to grain size, d_c

An examination of the terms in Eqn. 3-3 reveals an inverse correlation of $k_{att} \propto d_c^{-1.634}$ between the attachment rate coefficient and the grain size of the porous aquifer materials. We see elevated sensitivity to grain size with slow inactivation (k_{inact} = 0.01 d^{-1}), because attachment is responsible for a larger proportion of removal when inactivation is slow. Variations in grain size explain differences of up to 450 days in the time required for 5-log removal with slow k_{inact} (Figure 3-3b). However, sensitivity can be concentrated in certain grain sizes. Consider an "unsticky" system (α = 1E-5): with slow inactivation, attachment is the primary removal mechanism. Fine grain sizes provide more surface area for attachment by diffusive mechanisms, so a loss of fine materials dramatically increases removal times. However, the system is largely insensitive to changes in grain size on the coarser end of the spectrum. Increasing α to 1E-4 not only increases the overall magnitude of the effect grain size has on removal time, it also causes sensitivity over a larger range of sizes, from very fine sand to granules and pebbles. Finally, the enhanced attachment seen in sticky systems (α = 1E-3) can largely outweigh a slow inactivation rate as long as the aquifer materials are coarse-grained or finer; only in the coarsest materials does performance decline markedly.

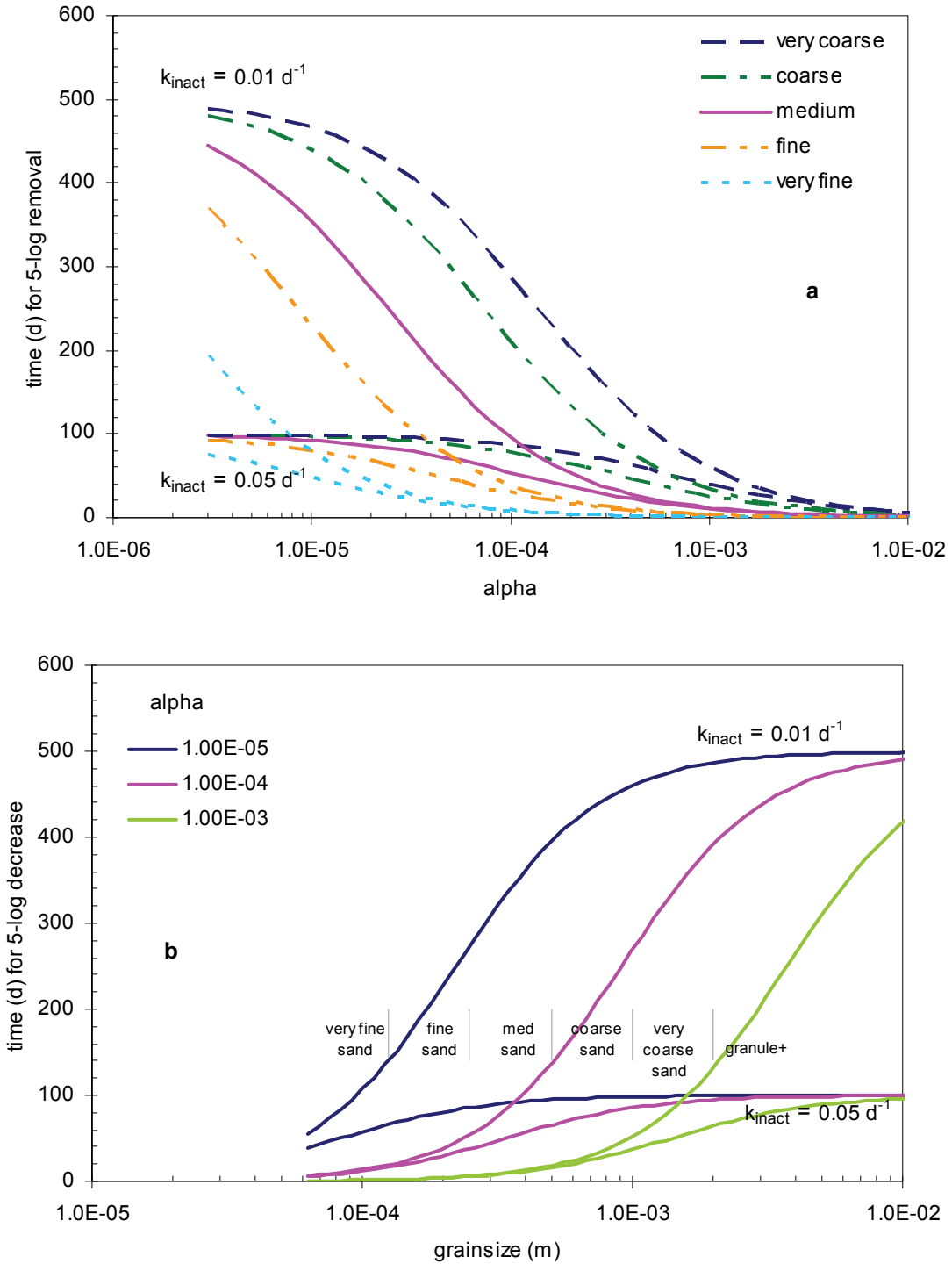

Figure 3-3. Time for 5-log removal (a) as a function of alpha for selected grain sizes (d_c = 0.08, 0.20, 0.38, 0.75 and 1.1 mm) and (b) as a function of grain size for α = 1E-5, 1E-4 and 1E-3 in both slow (k_{inact} = 0.01d^{-1}) and fast (k_{inact} = 0.05d^{-1}) inactivation systems. All other transport parameters at default values. Grain size divisions are by Wentworth class.

In contrast, the absolute magnitude of the sensitivity to grain size is much smaller when inactivation is fast (k_{inact} = 0.05 d^{-1}), because attachment contributes proportionally less to virus removal. Variations in grain size generate differences of 50-100 days, with maximum sensitivity over the widest range of grain sizes occurring once again in systems with intermediate stickiness ($\alpha \sim$ 1E–4). Though less dramatic in fast-inactivation systems, grain size is likely still relevant in that it can cause large relative increases or decreases in the amount of virus removal achieved by filtration.

Overall, the results suggest that the presence of zones of coarser materials where removals are low would contribute enhanced virus transport in sandy aquifer materials, an observation documented by others [37]. More relevant to this project, grain size heterogeneity could explain significant differences in virus removal in most of the biological space we are considering: only systems with high inactivation and low alpha are relatively insensitive to changes in d_c, because removals are controlled by inactivation in all but the finest media. The stickiest systems also show limited sensitivity to d_c, this time focused in the coarser size ranges. Zones with gravel, silt, or clay, which we have not considered explicitly, will generate even more extreme differences in virus removal by filtration, not only due to their grain size, but also because they may differ geochemically, with corresponding changes in α.

3.4.1.3 Sensitivity to velocity, *U*

Our simplified first order model assumes that the flow velocity is constant. The resulting dependence of attachment on velocity scales as $k_{att} \propto U^{0.285}$. Systems with slower flow offer fewer opportunities for virus particles to collide with and stick to

porous aquifer materials, so the contributions of attachment to virus removal are lower. A comparison of exponents reveals that the filtration of virus-sized particles is less sensitive to velocity than to grain size.

As shown in Figure 3-4, slow inactivation systems with low and intermediate alphas (α < ~1E-4) show the greatest sensitivity to velocity, illustrating the dramatic decrease in removal time that is generated by a transition from an inactivation-dominated removal mechanism (at low velocity) to an attachment-dominated one (at high velocity). Long removal times, however, suggest systems that will need significant dilution to be operationally relevant, thus decreasing the influence of the biological factors that are the focus of this work.

Variations in flow velocity over three orders of magnitude, as in Figure 3-4, would be unlikely in the producing layers of a natural gradient water-bearing formation, but a mixture of coarse and fine aquifer materials could give single-order-of-magnitude velocity variations. Furthermore, sticky systems with natural gradient velocities (below ~0.5 m/d) are in fact sensitive to velocity, showing 30-40% decreases in removal times as velocities increase by a factor of ten. This suggests that velocity heterogeneity in slow-flow systems (e.g., soil aquifer treatment or small domestic wells) could generate significant variability in virus removals if α is high. Higher-flow systems, above 1 m/d, with intermediate α show similar sensitivity to a factor of ten increase in velocity, suggesting that velocity heterogeneities – as well as the increase in velocity along a single streamline as groundwater flows towards a pumping well – could generate variability in virus removal in contexts like municipal well fields. Once again, we note the importance

of biological factors: the stickiness of the system determines the sensitivity to changes in velocity.

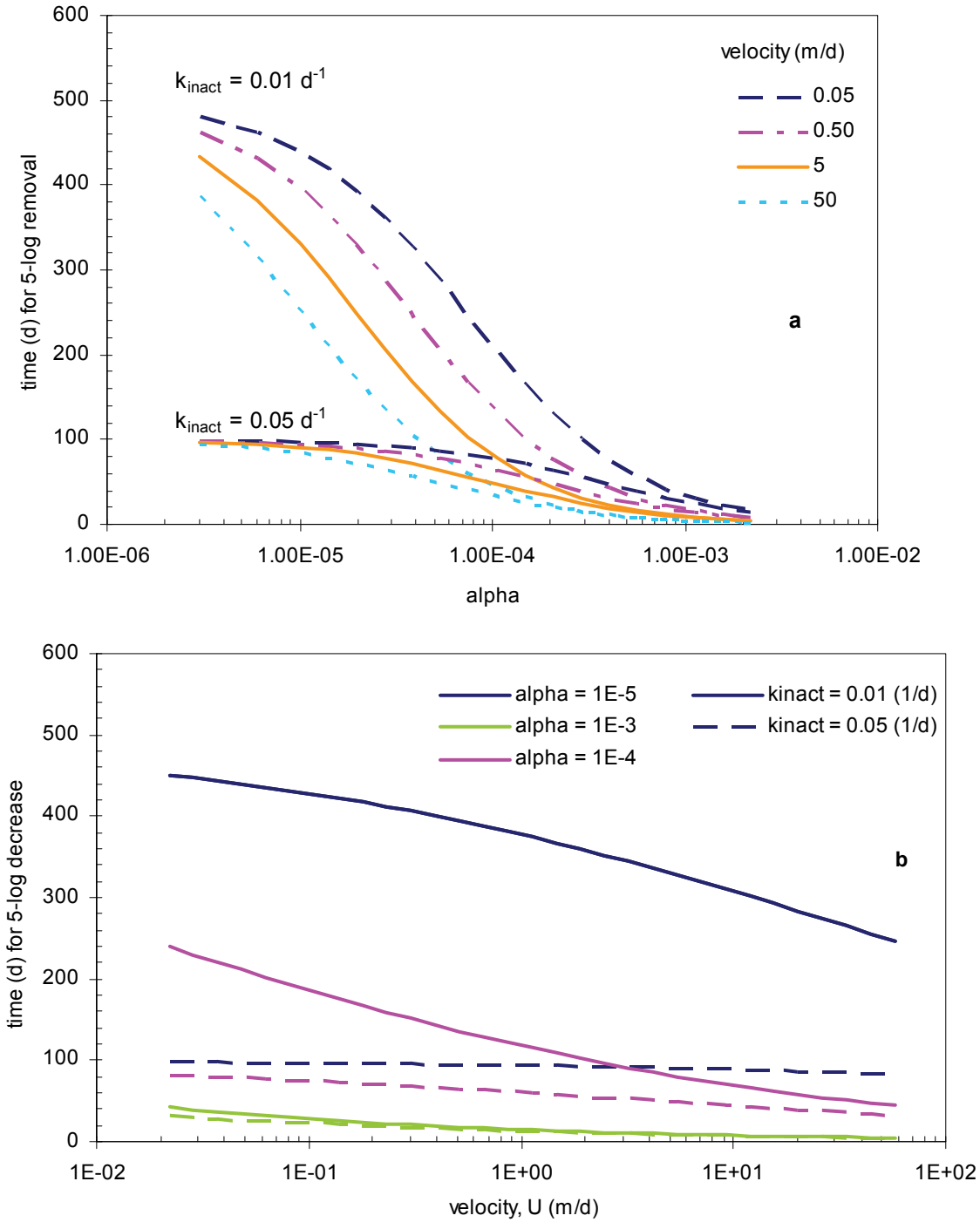

Figure 3-4. Time for 5-log removal (a) as a function of alpha for selected velocities, and (b) as a function of velocity for α = 1E-5, 1E-4 and 1E-3 in both slow (k_{inact} = 0.01d^{-1}) and fast (k_{inact} = 0.05d^{-1}) inactivation systems. All other transport parameters at default values.

This analysis of the role of velocity is deceptive for two reasons: first, it appears to imply that high flow velocities are preferable to low velocities for virus removal, and second, it evokes unrealistic systems. The first shortcoming is one of perception. Mathematically, higher velocities decrease the single collector efficiency η_0, but the negative impact on virus removal is more than offset by the fact that fast flow velocities cover more distance in a given amount of time. Attachment is a surface phenomenon, and the total available surface area of the porous media increases with travel distance. As a result, higher flow velocities do achieve the benchmark 5-log reduction in virus concentration faster than slow velocities would, thanks to the increase in travel distance. However, the location of a groundwater well is typically fixed in space. Longer travel distances are not accessible, so higher flow velocities between a source and the well not only reduce the efficiency of the filtration process along that flow path, they also decrease amount of time during which inactivation may reduce the concentration of a microbial contaminant.

The second shortcoming regards the extremely high velocities included in Figure 3-4. Local groundwater velocities on the order of 50 m/d can and do occur in the zone immediately around the screens of high-yield municipal wells, but they cannot be maintained over large distances. Even the shortest removal times shown in Figure 3-4 – five or six days for systems with $\alpha = 10^{-3}$ – imply induced velocities of 50 m/d along flow paths of 250 meters or more in length. This is operationally unrealistic.

3.4.1.4 Sensitivity to porosity, *n*

Attachment is inversely related to porosity, but the dependency cannot be expressed as a simple power law due to the polynomial nature of the expression relating the single collector efficiency to porosity. Higher porosities at constant grain size correspond to a lower surface area per unit volume of porous aquifer materials as well as to flow paths that are less affected by the media grains themselves, which together result in decreased attachment of virus-sized particles and correspondingly longer travel times required to achieve 5-log removal (Figure 3-5). Over a typical range of porosity values for sand and gravel aquifer systems, the effect of porosity on removal is of similar magnitude to that of varying velocity over three orders of magnitude.

As is the case for velocity, the greatest sensitivity to porosity in terms of absolute magnitude occurs for viruses with slow inactivation in systems of low or intermediate stickiness. Removal times are relatively short (under 100 d) in sticky systems, so absolute changes are correspondingly smaller. However, changes in porosity over the range shown can alter expected removal times by a factor of 5-6 in these systems, suggesting that spatial heterogeneity in porosity could contribute significant variability when biogeochemical conditions (summarized by α) make filtration a significant removal mechanism. Porosity is less important if inactivation is rapid, with sensitivity limited to stickier systems.

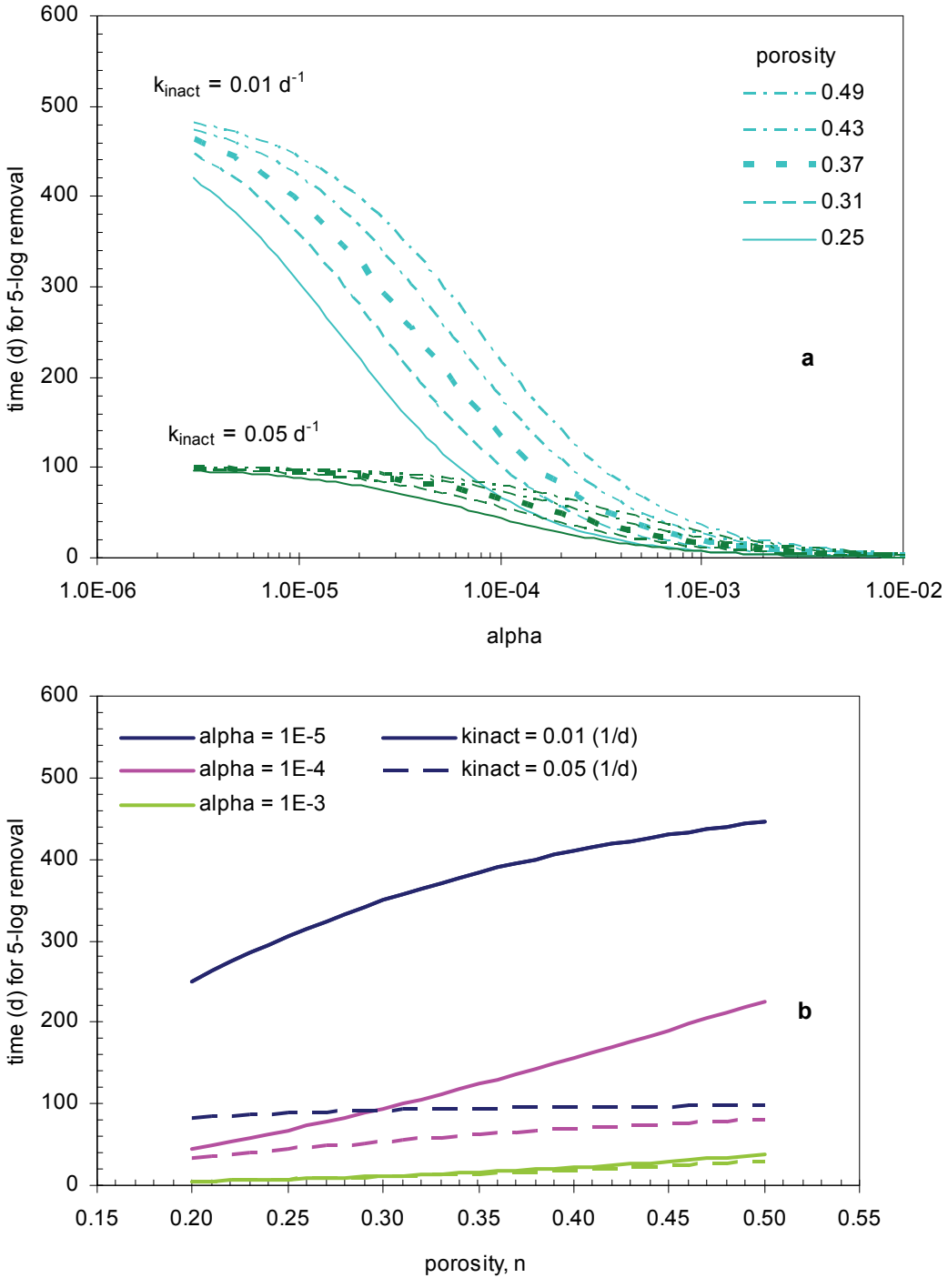

Figure 3-5. Time for 5-log removal (a) as a function of alpha for selected porosities, and (b) as a function of porosity for α = 1E-5, 1E-4 and 1E-3 in both slow (k_{inact} = 0.01d^{-1}) and fast (k_{inact} = 0.05d^{-1}) inactivation systems. All other transport parameters at default values.

3.4.1.5 Combined effects

As we have seen, velocity has the opposite influence on removal compared to grain size or porosity: removal times decrease with increasing velocity, but rise with increasing grain size or porosity. However, velocity, grain size, and porosity are unlikely to be entirely independent in the subsurface. In heterogeneous aquifer materials, areas with coarser grain size or higher porosity offer less resistance to flow, so while slow flow velocities can occur anywhere, the fastest velocities typically occur in the coarsest media. At the same time, the highest porosities are typically observed only in well-sorted media; a mixture of grain sizes tends to decrease porosity. Likewise, the highest porosities are not typically observed in coarser media [51].

Figure 3-6 shows the combined effects of velocity, porosity, and grain size in our simple filtration-inactivation model. This plot underscores how the degree of virus removal can vary enormously: a large swathe of removal-time "space" is accessible just through different combinations of system characteristics. Removal times are shown for two grain sizes: very coarse sand (d_c = 1.1 mm) printed in shades of blue, and fine sand (d_c = 0.2 mm) printed in shades of orange, as labeled on the plot area. Four velocities are shown for each grain size, with the darkest colors corresponding to the slowest flows, regardless of grain size. Each velocity-grain size combination is also shown at three different porosities, represented by the pattern of the line.

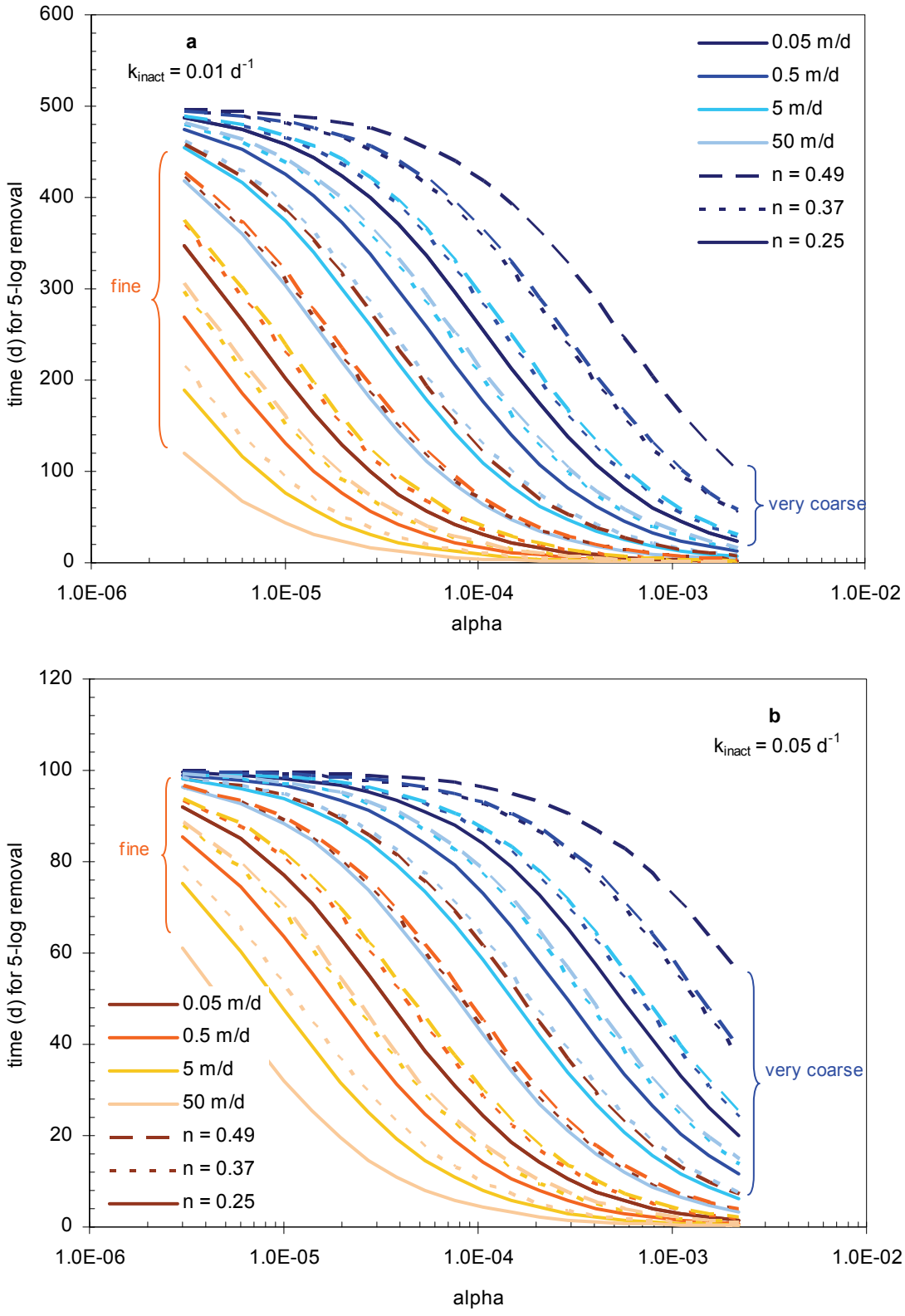

Figure 3-6. Combined effects of velocity, porosity, and grain size on time for 5-log removal under (a) slow (k_{inact} = 0.01d^{-1}) and (b) fast (k_{inact} = 0.05d^{-1}) inactivation conditions. All other transport parameters at default values.

We start by examining the slow-inactivation case (Figure 3-6a). Under intermediate alpha conditions (α ~ 1E-4), the removal-time spread for coarse media (blue) is larger than that for fine media (orange), so a co-occurrence of faster flows and coarse media will somewhat increase sensitivity to velocity variations. Comparing the slopes of the removal lines in coarse and fine media, we further note an increase in sensitivity to α in the event of fast/coarse co-occurrence. Furthermore, the spread in removal times generated by changes in porosity is larger in fast/coarse systems than it is in fast/fine systems, so a co-occurrence of faster flows and coarser media will also increase sensitivity to porosity variation. Conversely, co-occurrence of slow flows and finer grain sizes would decrease sensitivity to velocity, α, and porosity (although this effect would be somewhat mitigated in the case of high porosity).

Similar analysis for α ~ 1E-3 suggests that fast/coarse co-occurrence will have little effect in sticky systems, providing only small enhancements in sensitivity to velocity, α, and porosity. Under high-alpha conditions, it is coarse systems with slow flow that will show the greatest sensitivity to all parameters, particularly if they also have higher porosities.

Under low alpha conditions (α ~ 1E-5), fast/coarse co-occurrence will enhance sensitivity to variations in velocity and α only if the porosity is low; sensitivity will be somewhat dampened at intermediate and high porosity. However, fine systems with slow flow will also show enhanced sensitivity to velocity, α, and porosity.

As shown in Figure 3-6b, an increased inactivation rate constant not only decreases overall removal times (note the change in y-axis scale) but also shifts all the removal curves along the horizontal axis: higher α is required before the contributions of

attachment become significant, with corresponding implications for sensitivity to physical, attachment-related parameters.

At intermediate alpha ($\alpha \sim$ 1E-4), the steepest slopes are observed for fast/coarse systems with low porosity and slow/fine ones with high porosity. These co-occurrences will increase sensitivity to α, velocity, and porosity. An absence of the highest flows from the finest materials will further enhance the overall sensitivity of systems with intermediate stickiness.

Sticky conditions ($\alpha \sim$ 1E-3) at high inactivation look much like intermediate alpha conditions at lower inactivation. A co-occurrence of faster flows and coarse media will somewhat increase the system's sensitivity to velocity variations, though to a lesser degree than at $\alpha \sim$ 1E-4. The higher slopes of the fast/coarse removal lines indicate a marked increase in sensitivity to α compared to what we would expect if fast flows tended to occur in fine media. Likewise, fast/coarse co-occurrence will increase sensitivity to porosity variation.

In all cases, the potential natural associations that we've been examining – faster flows in coarser media and, possibly, slower flows in finer grain sizes – have a normalizing effect, eliminating the most extreme removal times. But as we have seen, whether they enhance or depress sensitivity to variation in system characteristics depends on the specific system configuration.

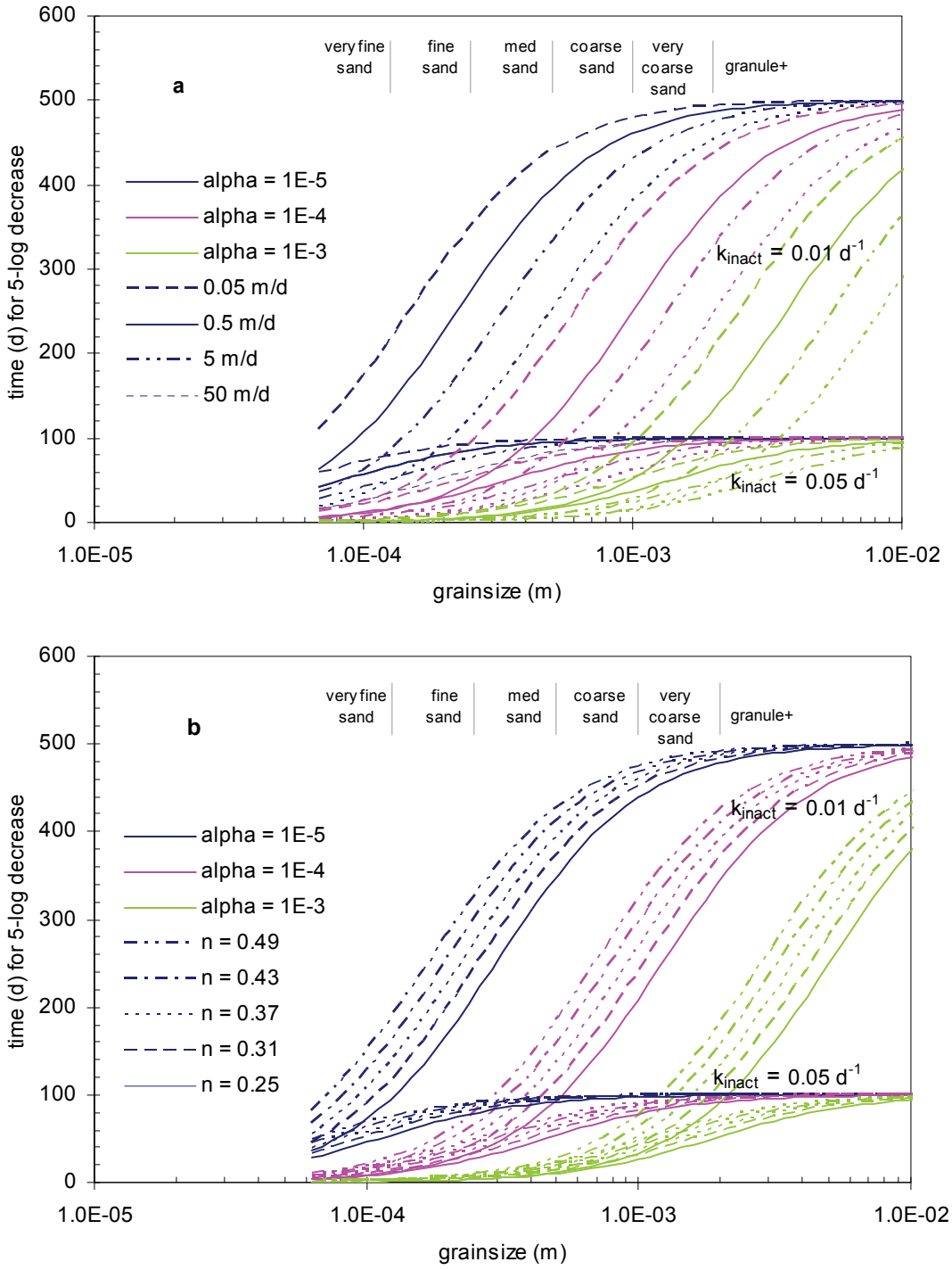

Figure 3-7. Combined effects of alpha and (a) velocity or (b) porosity on time for 5-log removal as a function of grain size. All other transport parameters at default values.

Higher flow velocities shift the d_c range where maximum sensitivity occurs toward coarser grain sizes (Figure 3-7a). As a result, a co-occurrence of fast flows and coarse materials will make systems with low α more sensitive over a larger range of grain sizes, while systems with high α will become even less sensitive to changes in grain size than they already were. These effects hold for both slow and rapid inactivation conditions. Low porosities, too, shift the d_c range of maximum sensitivity toward coarser grain sizes (Figure 3-7b). As result, the increased sensitivity to grain size brought about by fast/coarse co-occurrence under low α conditions will be further enhanced if porosities are low, and the high α systems will become more insensitive.

3.4.1.6 Sensitivity to temperature (T) and viral particle size (d_p)

A contamination source could contain several types of viruses, each with a different particle size, not to mention differences in shape, surface properties, and viability. Furthermore, the profile of potential viral contamination could vary from source to source and site to site. However, the effect of particle size on removal by filtration has been well-studied in the literature, as reviewed by Tufenkji and Elimelech [36] in their development of a new collector efficiency correlation equation. In the viral size range, the efficacy of attachment as a removal mechanism decreases for larger viruses, with $k_{att} \propto d_p^{-0.796}$.

Regions with cold climates have colder groundwaters than warmer locales, and shallow groundwater temperatures can swing seasonally [52], but these heterogeneities occur at spatial and temporal scales far larger than those of the parameters we have considered so far. Furthermore, the range of relevant temperatures is limited, about 5 -

25°C. Warmer temperatures enhance attachment of viral-sized particles because they enhance convective diffusion. For any given combination of aquifer and particle properties, k_{att} at 25°C will be 34% higher than the same system at 5°C (data not shown). The corresponding decrease in removal time, which may approach but never exceed 34%, will depend on the contribution of inactivation. Since inactivation rates also usually increase at higher temperatures, warmer climates and seasons will be more conducive to viral concentration reductions during subsurface passage. The extent that warmer temperatures would affect α by enhancing biological activity in the subsurface is unknown.

3.4.1.7 Sensitivity implications

As we have demonstrated throughout the sensitivity analysis, the overall effect of changing a physical characteristic that contributes to k_{att} depends on the balance between attachment and inactivation. Inactivation-dominated systems are comparatively insensitive to changes that affect attachment unless those shifts are big enough to make attachment become a significant contributor to virus removal. Conversely, attachment-dominated systems will be relatively insensitive to variations in the inactivation rate constant.

The filtration-only framework of our sensitivity analysis is not an operational model. It ignores the hydrodynamic effects of advection, dispersion, and dilution, and its assumption of constant and uniform parameter values does not accurately represent a natural system. It can, however, guide our attention. Riverbank filtration, dune filtration, artificial recharge, and the like are systems with engineered travel distances and/or travel times. To state the obvious, if changing biological conditions cause the time necessary

for a desired n-log removal to increase from 12 d to 20 d when the design subsurface residence time is 30 d, this is not an operational problem. For any given design travel time, high porosity, low velocity, and coarse grain size all bring about enhanced sensitivity to biofiltration: it is in these aquifer materials that shifts in α and/or k_{inact} are most likely to cause virus removal performance to decline from acceptable to unacceptable, and it is in these aquifer materials that changing biofiltration efficiency will have the least ability to remedy poor removals.

3.4.2 CXTFIT studies

3.4.2.1 Forward modeling: case comparisons with uncorrelated heterogeneity

Predicted breakthrough patterns for two hypothetical aquifers allow assessment of the relative significance of heterogeneity in different types of situations. The results of our simplified CXTFIT study cannot be interpreted as quantitative predictions of microbial breakthrough in real aquifers, but we did parameterize our hypothetical cases as idealized representations of two distinct systems.

Modeling results for cases (a) and (b) are summarized in Table 3-5 in terms of both $\log_{10}$ removal at maximum breakthrough and the time at which C_{max} occurred. Breakthrough statistics for case (a) are reported at two travel distances from the contamination source, while breakthrough for case (b) is reported at a single location. As the value of $<\mu>$ increases, removals improve significantly in aquifer (a), where changes in $<\mu>$ can cause system performance to shift by several log units. But aquifer (b) is comparatively insensitive to $<\mu>$, with removal at peak breakthrough never exceeding ~1.5 log units over the entire range of biofiltration rate constants considered.

Physical heterogeneity (parameterized as $\sigma_v = \sigma_D$) decreases maximum breakthrough concentrations, the timing of the earliest breakthrough and t_{Cmax} at a given location, and it increases late breakthrough concentrations ("tailing"). Since spreading of the contaminant plume is greater at longer travel distances and in systems with fast flow, high D, and/or large σ_v , t_{Cmax} effects will be more likely to appear there.

Overall, a higher average biofiltration rate constant provides greater removal. It also shifts the timing of maximum breakthrough (t_{Cmax}) earlier, because the falling leg of the breakthrough curve represents longer residence times which afford greater concentration reductions. Biological heterogeneity (σ_μ), by extending the range of μ to include lower values that contribute disproportionately in first order removal, increases maximum breakthrough concentrations and thus shifts t_{Cmax} later compared to a more homogeneous case. These effects are more pronounced at longer travel time and at greater $<\mu>$. In other words, configurations where removal would be high under homogeneous conditions have the greatest potential to be adversely affected under heterogeneous ones.

For example, the expected removal is 2.9 log for the case (a) sandy aquifer at 10 m ($\sigma_v = 0.1$) with elevated but heterogeneous biofiltration ($<\mu> = 0.8$ d^{-1}, $\sigma_\mu = 1.0$, $\rho_{v\mu} = 0$), a mere 0.7 $\log_{10}$ units better than the predicted removal of 2.2 log under significantly less efficient and more homogeneous biofiltration conditions ($<\mu> = 0.1$ d^{-1}, $\sigma_\mu = 0.1$, $\rho_{v\mu} = 0$). At 20 m, the difference falls to 0.1 log units (3.8 vs. 3.7 $\log_{10}$ removal). These results underscore the importance of the small μ values in a distribution with a large σ_μ and suggest that the distribution of biological heterogeneity, particularly the low tail of the distribution, may have a significant impact on microbial transport.

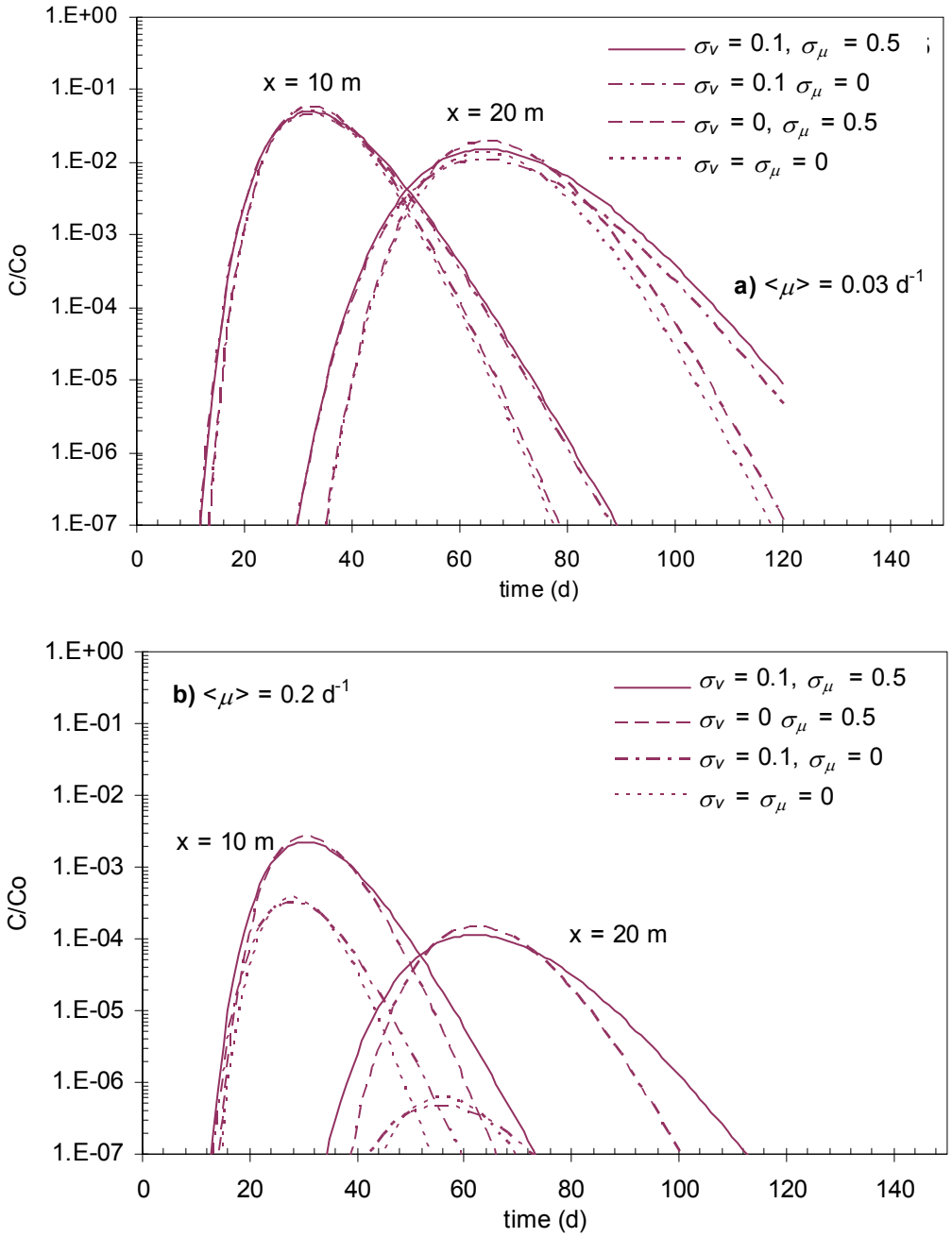

Figure 3-8. Breakthrough versus time at 10 m and 20 m in a hypothetical sandy aquifer with (a) $<\mu> = 0.03\ d^{-1}$ and (b) $<\mu> = 0.2\ d^{-1}$. Other parameters : $<v> = 30$ cm/d, $<D> = 500\ cm^2/d$, $\rho_{v\mu} = 0$.

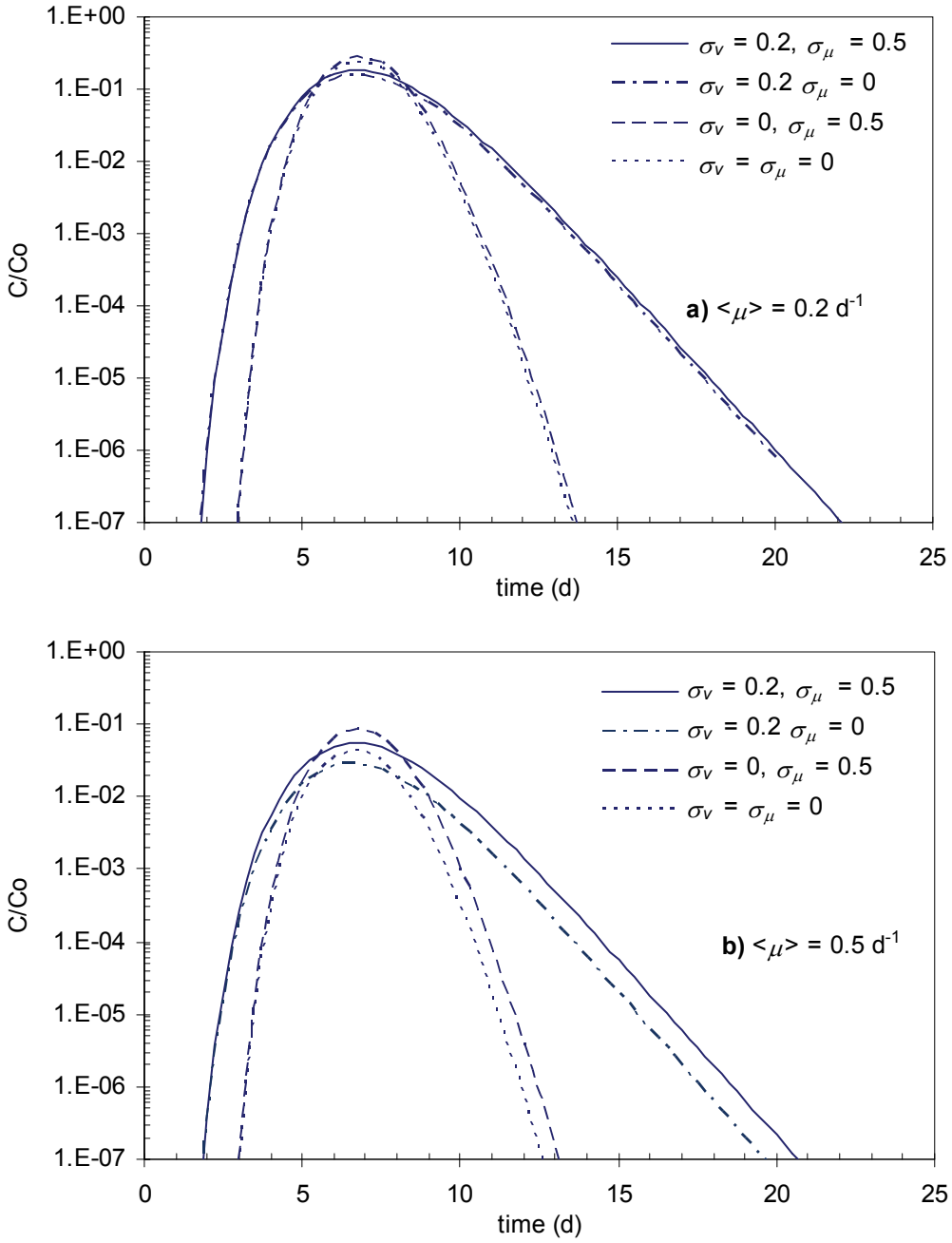

Figure 3-9. Breakthrough versus time at 30 m in a hypothetical alluvial aquifer with (a) $<\mu> = 0.2$ d^{-1} and (b) $<\mu> = 0.5$ d^{-1}. Other parameters : $<v> = 500$ cm/d, $<D> = 1500$ cm^2/d, $\rho_{v\mu} = 0$.

If the combined effects of biological and physical heterogeneity are uncorrelated ($\rho_{v\mu} = 0$), log removal at maximum breakthrough is set by the combination of $<\mu>$ and σ_μ, with C_{max} then reduced somewhat by physical heterogeneity. The plots in Figure 3-8

and Figure **3-9** show select model realizations from cases (a) and (b) to help illustrate the varying impact of including provisions for heterogeneity. In each figure, the y-axis gives normalized concentration on a log scale in order to facilitate interpretation of concentration in terms of log removal, e.g., C/C_o = 1E-2 corresponds to 2-$\log_{10}$ removal.

Consider breakthrough in a well 20 m from the contamination source in a case (a) hypothetical sandy aquifer with $<\mu>$ = 0.2 d^{-1} (Figure 3-8b). The homogeneous case is represented by a fine dotted line, with about 6.2 log removal at peak breakthrough. Adding biological heterogeneity (σ_μ = 0.5) increases the maximum breakthrough concentration by more than two orders of magnitude. Regardless of σ_μ , the addition of velocity heterogeneity (σ_v = 0.1) causes some flattening of the breakthrough curve, with earlier breakthrough, a small decrease of about 0.08 log in C_{max}, and an increase in concentrations at later times ("tailing") relative to the homogeneous velocity realization. If the well is located only 10 m from the contamination source, or if biological removal is less efficient ($<\mu>$ = 0.03 d^{-1}, Figure 3-8a), these effects are still present but their influence on $\log_{10}$ removal is less pronounced. At $<\mu>$ = 0.03 d^{-1}, the combined effects of uncorrelated physical and biological heterogeneity increase C_{max} only a little, shaving just 0.3 units off of log removal at peak breakthrough, compared to a 2.3 unit decrease in log removal for $<\mu>$ = 0.2 d^{-1}.

A similar analysis of a well 30 m down gradient from a hypothetical contamination source in the case (b) alluvial aquifer is illustrated in Figure 3-9. At $<\mu>$ = 0.2 d^{-1}, the adverse impact of biological heterogeneity (σ_μ = 0.5) on log removal is less than 0.02 log units, fully outweighed by the 0.2 log improvement in removals brought about by physical heterogeneity (σ_v = 0.2), which is greater in case (b) than it was in case

(a). Even at $<\mu> = 0.5\ d^{-1}$, the adverse effects of biological heterogeneity on removal are almost completely reversed by the beneficial effects of physical heterogeneity. System performance as measured by peak breakthrough is essentially unchanged compared to the homogeneous case, but the physical heterogeneities of the system lead to the extended tailing which is enhanced at higher $<\mu>$ (see Figure 3-9b) and σ_μ (data not shown).

The timing of maximum breakthrough, t_{Cmax}, is determined by $<\mu>$, shifted later by σ_μ, and possibly pulled earlier again by σ_v. In case (b), v and D are high and travel times are short, so the effects of σ_μ are reduced and those of σ_v amplified, with the result that biological heterogeneity has little effect on t_{Cmax} (i.e., t_{Cmax} increases little or not at all as σ_μ, rises). In case (a), travel times are longer, so the effects of σ_μ are more significant in establishing log removal. The relative physical homogeneity of this case (v, D, and σ_v are lower) means σ_v has much less effect on t_{Cmax}, and indeed the shift of peak breakthrough towards later times with the addition of biological heterogeneity is easily visible in Figure 3-8b. Note that effects on t_{Cmax} reported in Table 3-5 are partially obscured by the size of the model time step.

3.4.2.2 Forward modeling: correlated physical and biological heterogeneities

If biological (σ_μ) and physical (σ_v) heterogeneities are correlated, represented by $\rho_{v\mu} \neq 0$, the effects on system performance reflect a complex interplay of factors. Building on the independent heterogeneities of Figure 3-8 and Figure **3-9**, the plots in Figure 3-10 and Figure 3-10 show the influence of the correlation parameter $\rho_{v\mu}$ on select model realizations from Table 3-5. The solid lines, representing $\rho_{v\mu} = 0$, are common to all the figures. Overall, log removals and time to peak breakthrough show the greatest

sensitivity to correlated heterogeneities in the case (a) aquifer, particularly at longer (20 m) travel distance.

The breakthrough curves in Figure 3-10 illustrate how a negative correlation between biological and physical heterogeneity can generate earlier breakthrough, a higher C_{max}, and a faster drop in virus concentrations after peak breakthrough. Higher velocities and lower μ each independently increase maximum breakthrough concentrations, so coupling them results in even higher breakthrough peaks. The stronger the inverse correlation between v and μ, the worse the log removal at C_{max}. These effects are greatest in more heterogeneous systems and at longer travel times, so the ~0.2 log decrease in removal at the 20 m travel distance shown in Figure 3-10a represents one of the larger impacts observed among our many model realizations.

Poor removal in the fastest flow zones shifts the timing of maximum breakthrough earlier, with the greatest shifts occurring as $\rho_{v\mu}$. approaches -1. The pull towards earlier times that inversely correlated heterogeneities exert on t_{Cmax}, strongest when biological heterogeneity is large (high σ_μ), can counterbalance or even entirely reverse the usual trend of increasing t_{Cmax} with increasing σ_μ , particularly if $<\mu>$ is low (e.g., see case (a) at 20 m in Table 3-5). These model results are particularly interesting in light of field studies where the breakthrough of microbes or microspheres is observed to precede that of a conservative tracer. This commonly-reported phenomenon (reviewed in [32, 53]) is generally attributed to size exclusion effects, reflecting the idea that particles cannot access the smallest pore spaces in granular media and thus "see" a lower apparent porosity than a solute does. However, our model indicates that negatively

correlated heterogeneities could cause similar behavior, suggesting that it may be difficult to distinguish between the two without a conservative particle tracer.

If, however, the correlation between biological and physical heterogeneity is positive, the consequences are markedly different. The longer travel times of slow flow zones can partially compensate lower rate constants that tend to occur there, while the association of higher μ values with faster flow helps offset shorter travel times. With zones of high and low velocity contributing more equal concentrations than they do for $\rho_{v\mu} \leq 0$, the overall breakthrough curve at a given location is flatter, wider, and delayed: maximum breakthrough occurs later (t_{Cmax} increases), and tailing is enhanced.

This result, too, presents interesting features. Field injection experiments generally observe tailing of particulate contaminants: an extended period of persistent if decreasing microbe concentrations long after peak breakthrough. The mathematics of detachment and attached-phase inactivation, factors we have omitted from our simple 1-D model, generate tailing behavior. Certainly detachment is likely to play a role in the field. However, others have shown that the inclusion of these parameters in a homogeneous CXTFIT model was still insufficient to fully explain observed breakthrough patterns [11]. Our results suggest that a positive correlation between flow field heterogeneity and the biofiltration removal rate constant could contribute to tailing behavior while partially offsetting size exclusion effects.

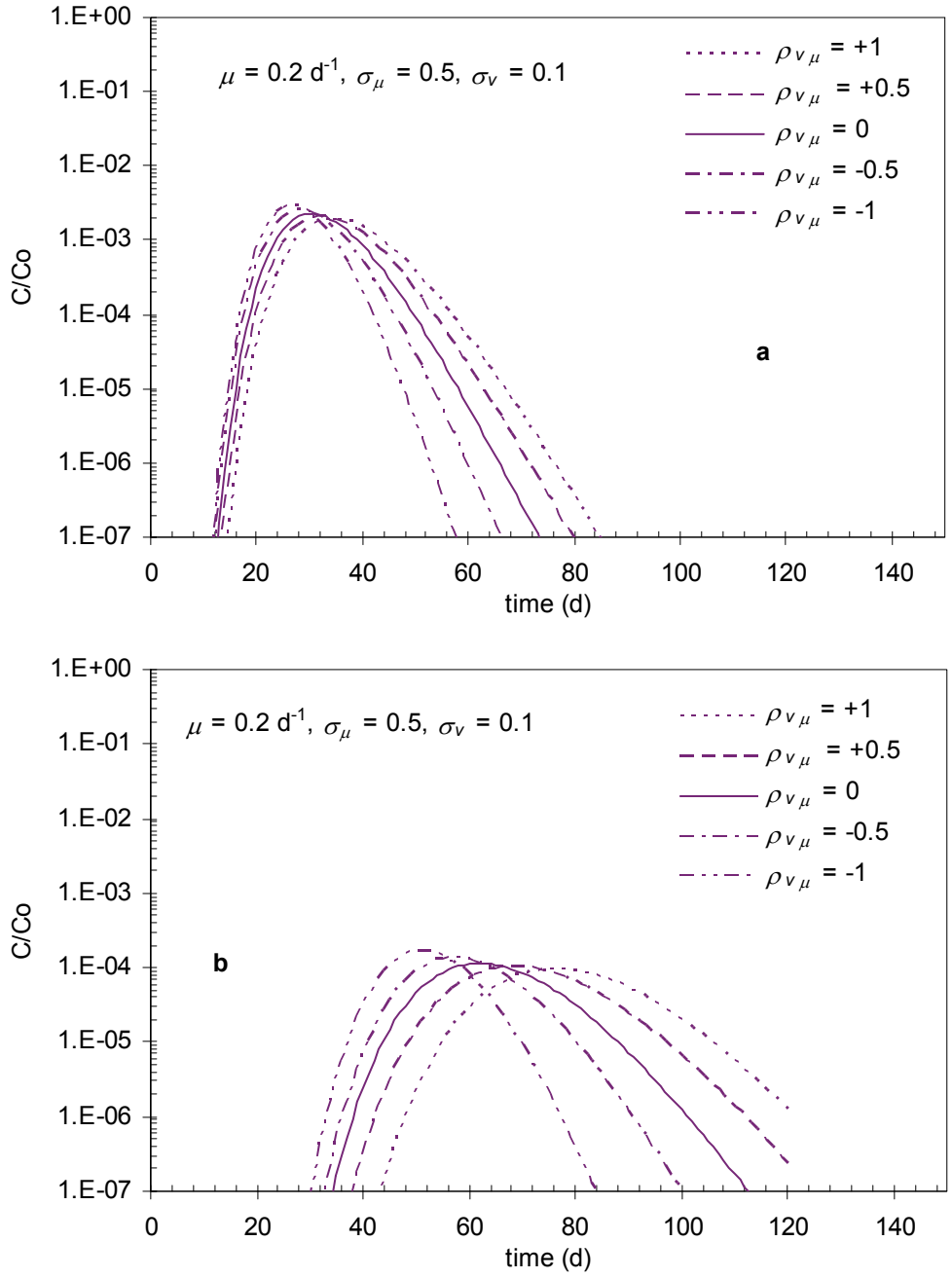

Figure 3-10. Breakthrough versus time at (a) 10 m and (b) 20 m in a hypothetical sandy aquifer for different degrees of correlation between physical and biological heterogeneity, as represented by $\rho_{v\mu}$. Other parameters : $\langle v \rangle$ = 30 cm/d, $\langle D \rangle$ = 500 cm^2/d.

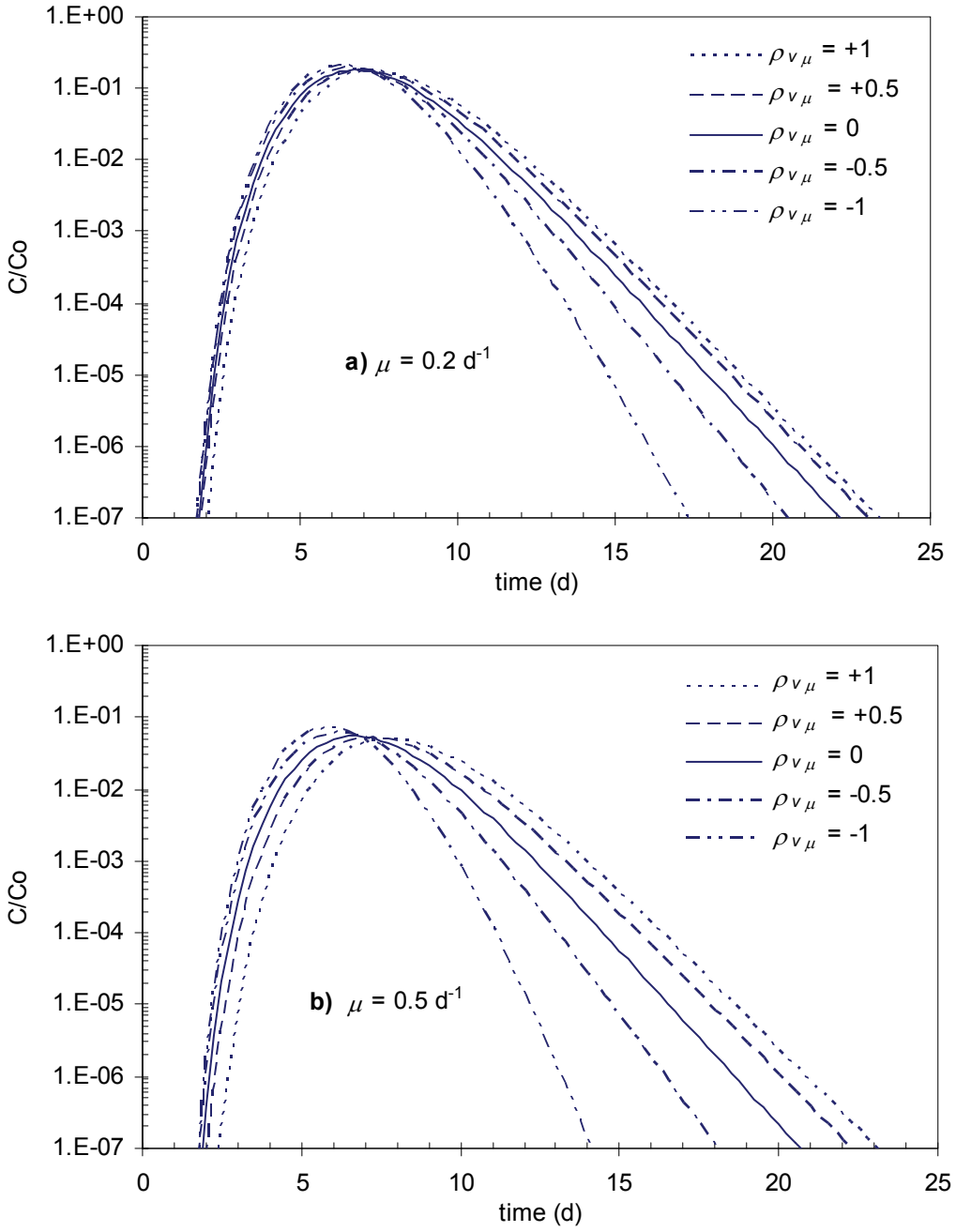

Figure 3-11. Breakthrough versus time at 30 m with (a) $<\mu>$ = 0.2 d^{-1} and (b) $<\mu>$ = 0.5 d^{-1} in a hypothetical alluvial aquifer for different degrees of correlation between physical and biological heterogeneity, as represented by $\rho_{v\mu}$. Other parameters : $<v>$ = 500 cm/d, $<D>$ = 1500 cm^2/d, $\sigma_v = \sigma_D = 0.2$, $\sigma_\mu = 0.5$.

For many of the model realizations with $\rho_{v\mu} > 0$, log removal at peak breakthrough improves (lower C_{max}) as $\rho_{v\mu}$ becomes increasingly positive, but the opposite pulls of v and μ can give rise to an interesting phenomenon as the balance

between their effects shifts. Removals can improve as $\rho_{v\mu}$ rises from 0 to +0.5 only to fall again as $\rho_{v\mu}$ approaches +1. Incomplete positive correlation between μ and v allows some faster removal constants even in slower flow zones, resulting in lower concentrations there. When the concentrations contributed by mid-range and slow velocity stream tubes represent a significant portion of total breakthrough (which is most likely to occur at small μ and large σ_μ), overall C_{max} can actually be lower at incomplete correlation. We observe this in many of the case (b) realizations with high biological heterogeneity ($\sigma_\mu = 1$), as well as in the most sensitive ($\mu = 0.03$ d^{-1}, $\sigma_\mu = 1$, $\sigma_v = 1$) case (a) realization at 20 meters.

Because breakthrough contributions of the fastest stream tubes are reduced while those of more average flow zones are enhanced when $\rho_{v\mu} > 0$, t_{Cmax} shifts later. The effect is magnified by greater degrees of heterogeneity (higher σ_μ and σ_v) and at longer distance, although the resolution of the t_{Cmax} values reported in Table 3-5 is limited by the size of the model time step, so sometimes no change in t_{Cmax} is observed, particularly for realizations with the lowest σ_μ . We note that the effect of positively correlated heterogeneities on t_{Cmax} reinforces the delay in breakthrough caused by elevated σ_μ..

In light of these differing impacts on system performance, the question arises whether positive or negative correlations are more likely to be a realistic representation of the subsurface environment.

A negative value of $\rho_{v\mu}$. arises if higher flow velocities tend to correspond to lower biofiltration removal rate constants. Several factors indicate that negative values of $\rho_{v\mu}$. may be more realistic than positive ones. Although our sensitivity analysis predicted higher k_{att} at higher velocities, the dependency on grain size was even stronger, with

lower k_{att} in coarser media. In a physically heterogeneous aquifer, elevated velocities are likely to occur in zones with coarser grain sizes, so a net negative correlation between μ and v is plausible based on physical parameters alone. Furthermore, transport studies in columns packed with uniform glass beads have found apparent decreases in the attachment rate coefficient (k_{att}) and the collision efficiency (α) with increasing flow velocity under unfavorable attachment conditions [25]. The presence of (oxy)hydroxide mineral coatings has been shown to be inversely correlated to grain size [54], and if other potentially favorable attachment surfaces, including sticky biofilm coatings and clay-type minerals, are also less prevalent in potentially coarser, high-flow zones in the subsurface, the corresponding decrease in α would reinforce any negative correlations between velocity and removal that arise from purely physical phenomena. An extensive review of published field data also found an inverse relationship between microbial removal rates and flow velocity [33].

Conversely, a positive value of $\rho_{v\mu}$. describes the situation where higher flow velocities correspond to higher biofiltration removal rate constants. Although it is harder to explain the co-occurrence of high flow and high removal by an analysis of physical factors, our sensitivity analysis demonstrated the importance of biological factors – α and k_{inact} – in determining μ. If organic matter and dissolved oxygen are replenished by infiltrating surface waters, high flow areas may be more likely to be aerobic, which at least in some cases (as we saw in the Introduction) may translate to higher α and better removal, so a positive value of $\rho_{v\mu}$. may not be entirely unconceivable.

Thus the simple 1-D CXTFIT model is sensitive not only the distribution chosen to represent μ, but also to the correlation (or lack thereof) between biological and physical heterogeneities.

The rationale behind using a log-normal distribution for μ lies in DLVO theory, which describes an electrostatic repulsive energy barrier as a colloid comes into close proximity with a similarly-charged surface. If the kinetic energy of the approaching microbial particle exceeds the energy barrier, the microbe may be deposited onto the sediment grain surface, so the attachment rate constant is related to the energy barrier by an Arrhenius-type exponential relationship [55]. The energy barrier is determined by the size and surface charge of the microbial particles and the sediment grains. If these properties are normally distributed, the deposition rate constant implied by DLVO theory is log-normally distributed. From a physical perspective, the log-normal distribution can be thought of as a trend of gradually increasing deposition from the largest to the smallest zones of pore space [56]. It also avoids implying the existence of negative rates of attachment or inactivation.

However, there are both micro and macro phenomena which may contribute to non-DLVO attachment behavior, so other distributions for μ are also possible. Hydrophobic and steric factors at the level of an individual particle-grain surface interaction (discussed in Ch.2) are joined by potential blocking of favorable attachment sites and straining of microbial colloids in the smallest pore throats. Redman *et al.*[22] posited a power-law function to describe microscale heterogeneity and found good agreement with the results of column studies of norovirus deposition. Tufenkji *et al.* [34] compared normal, log-normal, bimodal normal and power law distributions both

theoretically and to analyze viral and bacterial deposition profiles from short laboratory column studies. These researchers found that the choice of heterogeneity distribution does affect predicted system performance, although the optimum model depends on the experimental data set. They emphasized the impossibility of determining which representation of heterogeneity is most appropriate from solution-phase breakthrough curves in the absence of spatial deposition profile data and noted that in some cases, differentiation between heterogeneity regimes is only evident at longer travel distances.

Table 3-5: Timing of peak breakthrough and corresponding log removal at 10 m travel distance in case (a): $\langle v \rangle$ = 30 cm/d, $\langle D \rangle$ = 500 cm^2/d

	$\langle \mu \rangle$ = 0.03 d^{-1}				$\langle \mu \rangle$ = 0.1 d^{-1}				$\langle \mu \rangle$ = 0.2 d^{-1}				$\langle \mu \rangle$ = 0.8 d^{-1}			
σ_μ :	0	0.1	0.5	1	0	0.1	0.5	1	0	0.1	0.5	1	0	0.1	0.5	1
Log removal at peak breakthrough:																
σ_v = 0	1.29	1.29	1.25	1.16	2.21	2.19	1.90	1.52	3.43	3.37	2.59	1.86	9.37	8.88	4.99	2.87
σ_v = 0.05																
$\rho_{v\mu}$ = -1		1.30	1.24	1.15		2.19	1.88	1.50		3.37	2.55	1.83		8.84	4.92	2.82
-0.5		1.30	1.25	1.16		2.20	1.90	1.52		3.38	2.58	1.85		8.87	4.97	2.86
0	1.30	1.30	1.26	1.17	2.23	2.21	1.91	1.54	3.45	3.39	2.60	1.87	9.39	8.90	5.01	2.89
+0.5		1.30	1.27	1.18		2.21	1.93	1.55		3.40	2.63	1.89		8.93	5.04	2.91
+1		1.31	1.27	1.19		2.22	1.94	1.56		3.41	2.64	1.90		8.95	5.08	2.94
σ_v = 0.10																
$\rho_{v\mu}$ = -1		1.34	1.27	1.17		2.23	1.88	1.50		3.39	2.54	1.81		8.85	4.86	2.78
-0.5		1.34	1.29	1.19		2.24	1.92	1.55		3.42	2.60	1.87		8.91	4.97	2.86
0	1.35	1.34	1.30	1.21	2.27	2.25	1.96	1.58	3.50	3.43	2.65	1.92	9.45	8.96	5.05	2.93
+0.5		1.35	1.31	1.23		2.26	1.98	1.60		3.45	2.69	1.95		9.00	5.12	2.98
+1		1.35	1.32	1.23		2.27	2.00	1.62		3.47	2.72	1.96		9.05	5.17	3.01
Time (d) to peak breakthrough:																
σ_v = 0	32	32	32	33	30	30	31	32	28	28	30	32	21	22	28	31
σ_v = 0.05																
$\rho_{v\mu}$ = -1		32	32	32		30	30	31		28	29	30		20	25	28
-0.5		32	32	32		30	31	32		28	29	31		21	26	30
0	32	32	32	33	30	30	31	32	28	28	30	32	21	22	28	31
+0.5		32	33	33		31	32	33		29	31	33		22	30	33
+1		32	33	34		31	33	34		29	33	34		23	32	34
σ_v = 0.10																
$\rho_{v\mu}$ = -1		32	31	31		29	29	30		27	27	28		19	22	26
-0.5		32	32	32		30	30	31		27	28	30		20	25	28
0	32	32	32	33	30	30	31	32	28	28	30	32	21	21	28	31
+0.5		32	33	33		31	33	34		29	32	34		23	32	34
+1		32	34	34		31	34	35		30	35	36		24	36	38

Table 3-5 cont'd: Log removal and timing of peak breakthrough at 20 m travel distance in case (a): $\langle v \rangle$ = 30 cm/d, $\langle D \rangle$ = 500 cm^2/d

	$\langle \mu \rangle$ = 0.03 d^{-1}				$\langle \mu \rangle$ = 0.1 d^{-1}				$\langle \mu \rangle$ = 0.2 d^{-1}				$\langle \mu \rangle$ = 0.8 d^{-1}			
σ_μ :	0	0.1	0.5	1	0	0.1	0.5	1	0	0.1	0.5	1	0	0.1	0.5	1
Log removal at peak breakthrough:																
σ_v = 0	1.87	1.86	1.72	1.50	3.74	3.66	2.79	2.03	6.21	5.97	3.84	2.48	18.2	16.4	7.20	3.77
σ_v = 0.05																
$\rho_{v\mu}$ = -1		1.89	1.72	1.50		3.67	2.76	2.00		5.97	3.79	2.44		16.4	7.11	3.71
-0.5		1.89	1.74	1.52		3.69	2.79	2.04		5.99	3.83	2.48		16.4	7.17	3.76
0	1.90	1.89	1.75	1.53	3.77	3.70	2.82	2.06	6.25	6.01	3.87	2.51	18.2	16.4	7.23	3.80
+0.5		1.90	1.76	1.54		3.71	2.84	2.07		6.03	3.90	2.53		16.5	7.28	3.83
+1		1.90	1.77	1.54		3.72	2.86	2.08		6.05	3.93	2.54		16.5	7.32	3.85
σ_v = 0.10																
$\rho_{v\mu}$ = -1		1.95	1.76	1.52		3.73	2.80	2.04		6.01	3.77	2.43		16.3	7.05	3.67
-0.5		1.96	1.80	1.57		3.75	2.84	2.08		6.05	3.87	2.52		16.4	7.20	3.79
0	1.97	1.97	1.82	1.60	3.85	3.77	2.89	2.13	6.33	6.09	3.94	2.58	18.3	16.5	7.30	3.87
+0.5		1.97	1.84	1.62		3.79	2.93	2.16		6.12	3.99	2.61		16.6	7.39	3.92
+1		1.98	1.85	1.61		3.81	2.95	2.16		6.15	4.02	2.63		16.7	7.45	3.94
Time (d) to peak breakthrough:																
σ_v = 0	65	65	65	66	60	61	64	65	56	57	62	65	41	44	59	64
σ_v = 0.05																
$\rho_{v\mu}$ = -1		64	63	63		59	59	61		54	56	60		39	50	56
-0.5		64	64	65		60	61	63		55	59	62		41	54	60
0	64	64	65	66	60	61	63	65	56	57	62	65	41	44	59	64
+0.5		65	66	67		61	66	67		58	65	67		47	65	68
+1		65	67	68		62	68	69		59	69	70		50	71	73
σ_v = 0.10																
$\rho_{v\mu}$ = -1		63	61	61		57	58	58		51	51	55		34	42	50
-0.5		64	63	63		59	59	61		54	56	59		39	50	56
0	64	64	65	65	60	60	63	65	55	56	62	64	40	44	59	64
+0.5		65	67	68		62	68	69		59	69	70		50	70	72
+1		65	69	71		64	73	74		62	75	77		58	82	82

Table 3-5 cont'd: Log removal and timing of peak breakthrough at 30 m travel distance in case (b): $\langle v \rangle$ = 500 cm/d, $\langle D \rangle$ = 1500 cm^2/d

	$\langle \mu \rangle$ = 0.03 d^{-1}				$\langle \mu \rangle$ = 0.1 d^{-1}				$\langle \mu \rangle$ = 0.2 d^{-1}				$\langle \mu \rangle$ = 0.5 d^{-1}			
σ_μ :	0	0.1	0.5	1	0	0.1	0.5	1	0	0.1	0.5	1	0	0.1	0.5	1
Log removal at peak breakthrough:																
σ_v = 0	0.19	0.19	0.19	0.18	0.37	0.37	0.36	0.31	0.63	0.63	0.57	0.45	1.37	1.36	1.08	0.74
σ_v = 0.1																
$\rho_{v\mu}$ = -1		0.25	0.25	0.23		0.43	0.40	0.34		0.68	0.59	0.47		1.40	1.09	0.74
-0.5		0.25	0.25	0.24		0.43	0.41	0.36		0.68	0.61	0.49		1.41	1.12	0.77
0	0.25	0.25	0.25	0.24	0.43	0.43	0.42	0.37	0.69	0.68	0.62	0.51	1.43	1.42	1.14	0.79
+0.5		0.25	0.25	0.25		0.43	0.42	0.37		0.69	0.63	0.51		1.42	1.16	0.81
+1		0.25	0.25	0.24		0.44	0.42	0.37		0.69	0.64	0.51		1.43	1.17	0.81
σ_v = 0.2																
$\rho_{v\mu}$ = -1		0.37	0.36	0.34		0.54	0.50	0.43		0.79	0.68	0.54		1.50	1.15	0.78
-0.5		0.37	0.37	0.35		0.55	0.52	0.47		0.80	0.72	0.59		1.52	1.21	0.86
0	0.37	0.37	0.37	0.36	0.55	0.55	0.53	0.49	0.81	0.80	0.74	0.62	1.55	1.53	1.26	0.91
+0.5		0.37	0.37	0.37		0.55	0.54	0.50		0.81	0.76	0.64		1.55	1.29	0.94
+1		0.37	0.37	0.36		0.56	0.54	0.49		0.81	0.76	0.63		1.56	1.30	0.93
Time (d) to peak breakthrough:																
σ_v = 0	7	7	7	7	7	7	7	7	6.75	6.75	6.75	7	6.75	6.75	6.75	6.75
σ_v = 0.1																
$\rho_{v\mu}$ = -1		7	7	6.75		6.75	6.75	6.75		6.75	6.5	6.5		6.5	6.25	6.5
-0.5		7	7	7		6.75	6.75	6.75		6.75	6.75	6.75		6.5	6.5	6.5
0	7	7	7	7	6.75	6.75	7	7	6.75	6.75	6.75	7	6.75	6.75	6.75	6.75
+0.5		7	7	7		7	7	7		6.75	7	7		6.75	7	7
+1		7	7	7		7	7	7		6.75	7	7.25		6.75	7.25	7.5
σ_v = 0.2																
$\rho_{v\mu}$ = -1		6.75	6.75	6.75		6.75	6.5	6.5		6.5	6.25	6.25		6.25	5.75	6
-0.5		6.75	6.75	6.75		6.75	6.75	6.75		6.75	6.5	6.5		6.5	6.25	6.25
0	6.75	6.75	6.75	6.75	6.75	6.75	6.75	6.75	6.75	6.75	6.75	6.75	6.5	6.5	6.75	6.75
+0.5		6.75	7	7		6.75	7	7		6.75	7	7.25		6.75	7.25	7.25
+1		6.75	7	7		6.75	7	7.25		6.75	7.25	7.5		6.75	7.75	8

3.4.2.3 Inverse modeling: field tracer data

Model fits to observed bromide breakthrough at monitoring wells 1 and 2 are plotted in Figure 3-12, with parameter values listed in Table 3-6.

At the first monitoring well (MW1), the 1-D model fits the data reasonably well. A small deformation of the falling limb of the observed breakthrough data, visible in Figure 3-12a, suggests the possibility of a dual permeability formation, with superposition of two breakthrough curves, but CXTIFT cannot capture this feature, and the qualitative description of the field site indicates that both the injection well and MW1 are screened entirely within the same coarse sand layer of the aquifer. Regardless, good agreement with published values and an identical velocity with an extremely low fitted standard deviation (σ_v = σ_D = 1.2E-5) in the heterogeneous model suggest that the authors' assumption of a physically homogeneous subsurface is acceptable between the injection point and MW1.

MW2 is quite different. Visual inspection of the observed tracer breakthrough reveals clear non-ideal behavior with shouldering on either side of *Cmax*. The published description of the field site indicates that layering of aquifer materials does generate a dual-permeability formation between MW1 and MW2, and that while the majority of the well screen at MW2 lies in the main coarse sand zone, the top of the screen intersects a fine sand layer. This macro-scale heterogeneity is not accounted for in the 1-D model. Assumptions about pulse-input boundary conditions may also be inaccurate if flow patterns allow MW2 to be influenced by uncontaminated groundwater that did not travel through the injection area.

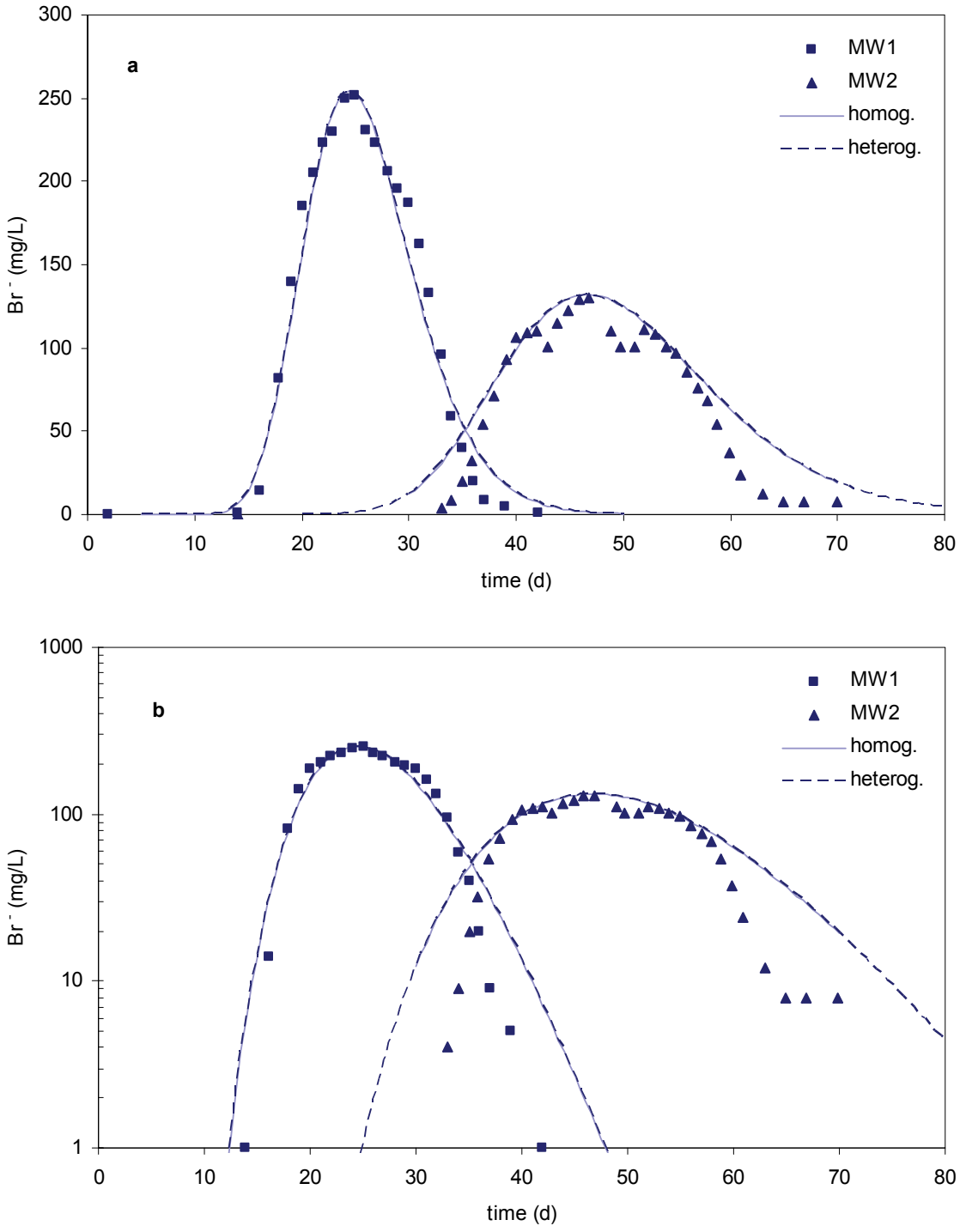

Figure 3-12. (a) Linear and (b) semi-log plots of observed bromide tracer concentrations at MW1 (squares), located 7.8 m down gradient from the injection well, and at MW2 (triangles), located 17.2 m down gradient from the injection point. Fits from homogeneous (solid line) and heterogeneous (dashed line) models are shown.

Fitting with CXTFIT fails to match the tails of the distribution, over-predicting concentrations both before and after maximum breakthrough. Attempts to improve the fit by allowing for heterogeneity were unsuccessful: although R^2 rose slightly to 0.8364, the results were unrealistic: CXTFIT's fitting routine minimized dispersion and maximized σ_v (data not shown). Since longitudinal dispersivity should be reasonably consistent at a single field site, we constrained $<D>$ for MW2 to the fitted value from MW1. The resulting fitted $<v>$ and R^2 were identical to the homogeneous case, with a low σ_v. Velocity and dispersivity results are close to those published with the study; minor discrepancies may be attributed to the inaccuracies introduced when reconstructing raw breakthrough data from a published plot. The authors apparently settled for the homogeneous fit of v and D, although the mismatch between fitted and observed tracer data suggests that the 1-D CXTFIT model may not be appropriate for modeling transport to MW2.

3.4.2.4 Inverse modeling: phage field data

Observed bacteriophage MS2 breakthrough concentrations and model fits are plotted in Figure 3-13 for both monitoring wells, with fitting results for $<\mu>$, σ_μ, and $\rho_{v\mu}$ reported in Table 3-6. The 1-D CXTFIT model was unable to fit the breakthrough curves adequately using either homogeneous or heterogeneous assumptions, likely due to inaccuracy of model assumptions about the underlying processes, including the deliberate omission of detachment.

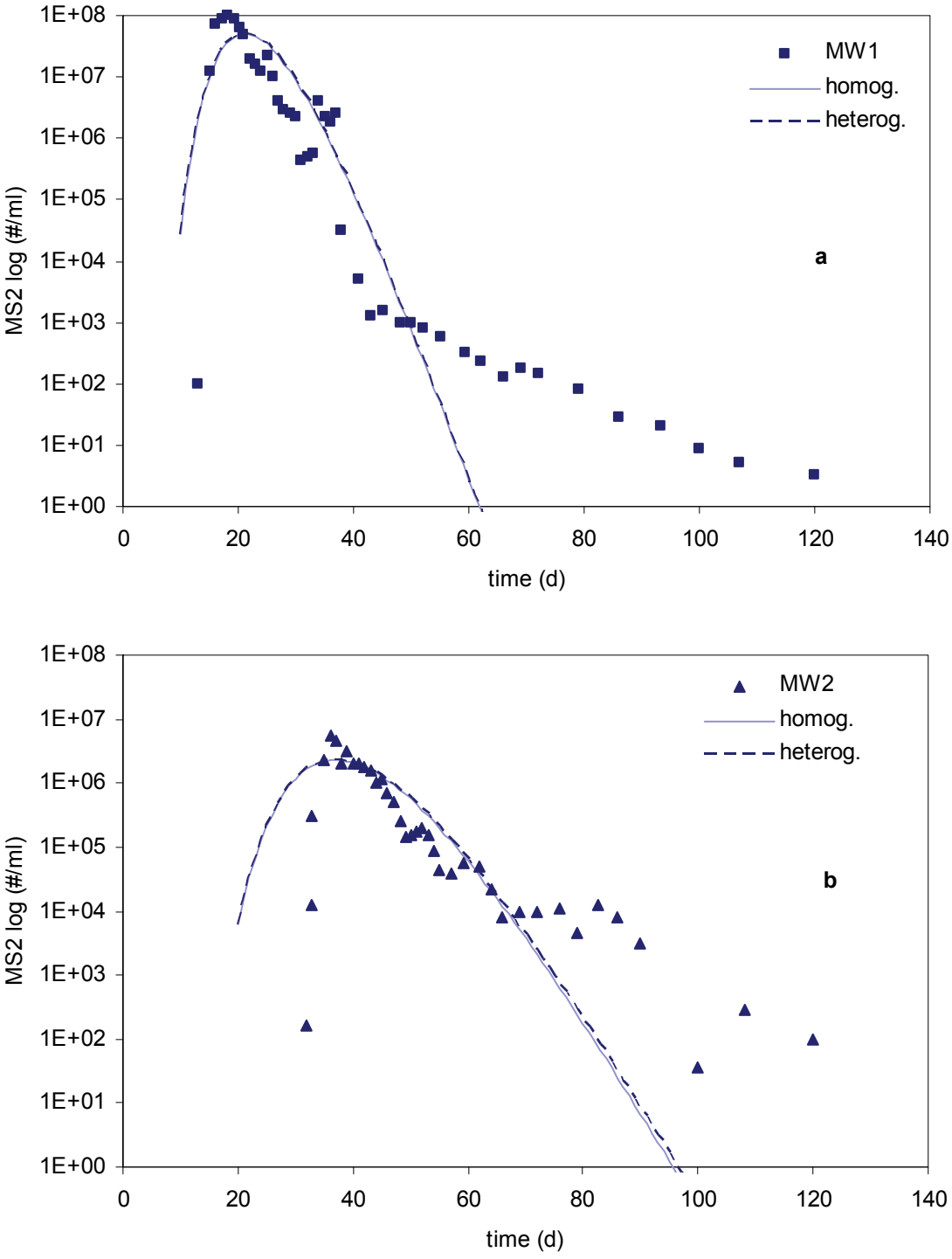

Figure 3-13. MS2 bacteriophage breakthrough observations and model fits for (a) MW1 and (b) MW2.

As is commonly observed in field studies, phage breakthrough precedes predictions based on the average linear velocity from the tracer data. Without adjustments to increase the apparent average velocity of the phage particles in the model, CXTFIT must underestimate the peak breakthrough and overestimate falling concentrations soon after the peak in its attempts to fit the phage data. As noted before, a 1-D model without detachment is likewise unable to capture long-term tailing, which was observed in the field results. Homogeneous fits, using constant v and D from the bromide tracer results, none-the-less returned biofiltration rate constants of ~0.18 d^{-1} at MW1 and ~0.16 d^{-1} at MW2, a result not dissimilar from the study's findings.

We have seen that heterogeneity in the biofiltration rate constant increases peak breakthrough concentrations, retards t_{Cmax}, and enhances tailing. The homogeneous model was already overestimating both t_{Cmax} and the early falling leg of the breakthrough curve, so significant heterogeneity in μ would hardly be an improvement. Since σ_v fitted from the tracer data was so small, the physical heterogeneity allowed in the heterogeneous fitting of the phage breakthrough was negligible, essentially forcing the "heterogeneous" case to near-homogeneity in terms of flow velocity. With a low σ_v, correlations between physical and biological heterogeneity could play only a limited role in improving the model. Consequently, the heterogeneous fitting for $<\mu>$ also returned results nearly identical to the homogeneous model.

Applying the authors' reported inactivation rate measurements and field site characteristics in conjunction with our own model estimates of v and μ allows us to calculate collision efficiencies from Eqn. 3-3 to compare with the published results. The small discrepancy in velocity and 30% increase in our model estimate of k_{att} compared to

the authors' leads to a two-fold difference in estimates of collision efficiency. For example, the authors report α = 3.4E-5 for MW1, but analyzing the same data with CXTFIT, we estimate α at 6.5E-5 (homogeneous) or 6.6E-5 (heterogeneous). We emphasize that both our approach and that of the published paper rely upon the same 1-D approximation, yet yield somewhat different results.

A sensitivity analysis (data not shown) of the fitting procedure revealed that different parameter combinations can yield very similar R^2 values. The CXTFIT non-linear least squares fitting algorithm is known to be sensitive to initial guesses and to the presence or absence of fitting constraints [42], and other researchers have asserted that the tails of the distribution may be inappropriately underweighted during the fitting procedure [11]. We conclude that the apparent absence of physical heterogeneity according to the CXTFIT model fits likely indicates that the field site is in fact relatively homogeneous, but artifacts in the fitting procedure and the inapplicability of the over-simplified 1-D model at MW2 make it difficult to quantify the limited physical heterogeneity that is present, which in turn prevents meaningful estimation of biological heterogeneity.

This inverse modeling case study underscores the difficulties in extracting fundamental parameters from field breakthrough curves. Filtration theory and the α it invokes were developed for homogeneous, clean, spherical porous media, not aquifers. To avoid overanalysis and overinterpretation of field results, some researchers have advocated quantifying field removal in terms of a filter factor, defined empirically as the slope of the plot of $\log(C_{max}/C_o)$ vs. distance, or alternatively as k_{att}/v [57]. However, collision efficiencies extracted from field data abound in the literature, often calculated

via different approaches. In light of the sensitivity of α to variations in estimation technique and the potential confounding effects of heterogeneity, we question the comparability of collision efficiencies from different sources. The inverse study likewise demonstrates the impracticability of optimizing models of heterogeneity, let alone correlated heterogeneities, without a full understanding of the underlying fundamental processes.

Table 3-6: Transport parameters fit from Br^- and MS2 breakthrough data in CXTFIT inverse study.

Parameter	MW1			MW2		
	published*	**homogen.**	**heterogen.**	**published***	**homogen.**	**heterogen.**
From Br^- tracer:						
v or $<v>$ (m/d)	0.33	0.3251	0.3251	0.38	0.3596	0.3596
D or $<D>$ (m^2/d)		0.05960	0.05959	-	0.1415	[0.1415]
dispersivity, α_L (m)	0.19	(0.18)	(0.18)	0.26	(0.39)	(0.39)
$\sigma_v = \sigma_D$	-	–	0.1214E-4	-	-	0.01336
R^2	-	0.9675	0.9675	-	0.8351	0.8352
From MS2 phage:						
μ or $<\mu>$ (d^{-1})	(0.1393)	0.1813	0.1813	(0.1265)	0.1576	0.1583
σ_μ		–	0.02165	-	-	0.03161
$\rho_{v\mu}$		–	–1	-	-	+0.9448
R^2		0.4809	0.4808	-	0.5657	0.5650
collision efficiency, α	3.4E-5	(6.55E-5)	(6.53E-5)	2.9E-5	(5.17E-5)	(5.22E-5)

Parenthesis indicate calculated values, square brackets indicate values fixed during fitting.
CXTFIT reports fitted parameters to 4 significant figures, a convention we reproduce here.
*Source: reference [1]

3.5 Conclusions

From an operational perspective, options to alter the physical characteristics of an existing well field are limited. Turning pumping wells on or off or controlling wet/dry cycling in infiltration basins for induced recharge will affect flow paths and water table levels, as might a flooding event at a riverbank filtration installation. Site-specific knowledge about subsurface formations may allow optimal exploitation of those heterogeneities. Otherwise, the physical properties of a given production field are more or less static; it is the biological ones that may vary dynamically.

The results of our analysis demonstrate the sensitivity of the 1-D filtration model to these biological parameters. The effects of heterogeneity in physical parameters contributing to k_{att} – notably velocity, grain size and porosity – play out in a space whose contours are established by biological and biogeochemical phenomena: the rate constant representing die-off or inactivation of microbial contaminants, and the apparent "stickiness" of these particles and of the sediment grain surfaces to which they may attach. Through their influence on the surface phenomena involved in k_{att}, high porosity, low velocity, and coarse grain size all bring about enhanced sensitivity to biofiltration. All but the stickiest formations benefit from increases in inactivation.

The simplifying assumptions associated with a CBFT approach to filtration processes are not realistic in the natural subsurface environment: velocity, grain size, porosity, stickiness, and inactivation are not single, constant values. The relative importance of different variables suggested by our sensitivity analysis may be emphasized or obscured as additional layers of complexity and scales of heterogeneity are taken into account. Since complete physical characterization of a field site is

impractical, further research is needed to link physical properties (represented stochastically, if need be) with biological ones to facilitate the estimation of biofiltration performance in heterogeneous, 3D space.

Introducing a stochastic first-order biofiltration removal rate constant in conjunction with the advection-dispersion equation allowed us to use a set of hypothetical CXTFIT case studies to examine the possible influence of biological heterogeneity on microbial removal in groundwater systems. Biological heterogeneity, represented by a log-normal distribution of biofiltration removal rate constants, had notably adverse impacts on system performance. The simplistic 1D model further demonstrated the potential for correlations between biogeochemical and geophysical heterogeneities to influence virus breakthrough in complex, varied, and sometimes counterintuitive ways due to the competing influences of different transport-related factors.

However, we were unable to improve interpretation of an existing field data set by applying our modified CXTFIT model. It is likely that the 1-D assumption did not represent the physical reality of the system, particularly at the second monitoring well. Furthermore, our model was too simplistic. With detachment omitted and the velocity and dispersion assumed to be the same for phage and tracer, including provisions for heterogeneity did little to improve the fit. The exercise revealed both the inapplicability of the 1D model and the limitations its fitting procedure.

While the filtration-theory approach from the sensitivity analysis focuses on attachment and fails to account for advection-dispersion effects, CXTFIT incorporates advection-dispersion but loses all the resolution of attachment behavior by treating all first-order removal processes (both attachment and inactivation) in terms of a simple rate

constant. Our modified code, expanding that parameterization to a stochastic variable optionally correlated with velocity, reintroduced a small amount of detail to the treatment of biological removal process, but further work is needed.

Stochastic approaches that separate attachment, detachment, and inactivation and re-calculate the contributions of each stepwise in a heterogeneous flow field will decouple time-based removal mechanisms (inactivation) from surface-based filtration phenomena that scale with time only under constant velocity assumptions. The more realistic framework of such approaches may yield insights about the nature and magnitude of the effects of biological heterogeneity. However, such theoretical investigations into the potential effects of physical and biological heterogeneities, let alone correlations between them, will be hard to validate at field scale because deposition profiles are rarely available for field transport studies. Improved methods for the collection and analysis of solution-phase breakthrough concentrations may help compensate for missing attached-phase concentrations data. Finally, more research is needed into the parameterization and possible correlation of biological and physical heterogeneities at multiple length scales within the same system.

3.6 References

1. Van der Wielen, P., W. Senden, and G. Medema, *Removal of Bacteriophages MS2 and Phi X174 during transport in a sandy anoxic aquifer.* Environmental Science & Technology, 2008. 42(12): p. 4589-4594.
2. Gordon, C. and S. Toze, *Influence of groundwater characteristics on the survival of enteric viruses.* Journal of Applied Microbiology, 2003. 95(3): p. 536-544.
3. Hunter, K.S., Y.F. Wang, and P. Van Cappellen, *Kinetic modeling of microbially-driven redox chemistry of subsurface environments: coupling transport, microbial metabolism and geochemistry.* Journal of Hydrology, 1998. 209(1-4): p. 53-80.
4. Holzbecher, E., H. Dizer, Grutzmacher, J. Lopez-Pila, and G. Nutzmann, *The influence of redox conditions on phage transport - Enclosure experiments and modeling.* Environmental Engineering Science, 2006. 23(4): p. 623-630.
5. Abudalo, R.A., Y.G. Bogatsu, J.N. Ryan, R.W. Harvey, D.W. Metge, and M. Elimelech, *Effect of ferric oxyhydroxide grain coatings on the transport of bacteriophage PRD1 and Cryptosporidium parvum oocysts in saturated porous media.* Environmental Science & Technology, 2005. 39(17): p. 6412-6419.
6. Schijven, J.F., G. Medema, A.J. Vogelaar, and S.M. Hassanizadeh, *Removal of microorganisms by deep well injection.* Journal of Contaminant Hydrology, 2000. 44(3-4): p. 301-327.
7. van der Wielen, P., M. Blokker, and G.J. Medema, *Modelling the length of microbiological protection zones around phreatic sandy aquifers in The CD Netherlands.* Water Science and Technology, 2006. 54(3): p. 63-69.
8. Schijven, J.F., S.M. Hassanizadeh, and A.M.D. Husman, *Vulnerability of unconfined aquifers to virus contamination.* Water Research, 2010. 44(4): p. 1170-1181.
9. Dong, H.L., T.D. Scheibe, W.P. Johnson, C.M. Monkman, and M.E. Fuller, *Change of collision efficiency with distance in bacterial transport experiments.* Ground Water, 2006. 44(3): p. 415-429.
10. Harvey, R.W. and S.P. Garabedian, *Use of colloid filtration theory in modeling movement of bacteria through a contaminated sandy aquifer.* Environmental Science & Technology, 1991. 25(1): p. 178-185.
11. Schijven, J.F., W. Hoogenboezem, S.M. Hassanizadeh, and J.H. Peters, *Modeling removal of bacteriophages MS2 and PRD1 by dune recharge at Castricum, Netherlands.* Water Resources Research, 1999. 35(4): p. 1101-1111.
12. Loveland, J.P., J.N. Ryan, G.L. Amy, and R.W. Harvey, *The reversibility of virus attachment to mineral surfaces.* Colloids and Surfaces A-Physicochemical and Engineering Aspects, 1996. 107: p. 205-221.
13. Ryan, J.N., M. Elimelech, R.A. Ard, R.W. Harvey, and P.R. Johnson, *Bacteriophage PRD1 and silica colloid transport and recovery in an iron oxide-coated sand aquifer.* Environmental Science & Technology, 1999. 33(1): p. 63-73.
14. John, D.E. and J.B. Rose, *Review of factors affecting microbial survival in groundwater.* Environmental Science & Technology, 2005. 39(19): p. 7345-7356.

15. Pieper, A.P., J.N. Ryan, R.W. Harvey, G.L. Amy, T.H. Illangasekare, and D.W. Metge, *Transport and recovery of bacteriophage PRD1 in a sand and gravel aquifer: effect of sewage-derived organic matter.* Environmental Science & Technology, 1997. 31(4): p. 1163-1170.
16. Kone, T., F. Golfier, L. Orgogozo, C. Oltean, E. Lefevre, J.C. Block, and M.A. Bues, *Impact of biofilm-induced heterogeneities on solute transport in porous media.* Water Resources Research, 2014. 50(11): p. 9103-9119.
17. Larentis, M., K. Hoermann, and T. Lueders, *Fine-scale degrader community profiling over an aerobic/anaerobic redox gradient in a toluene-contaminated aquifer.* Environmental Microbiology Reports, 2013. 5(2): p. 225-234.
18. Gharasoo, M., F. Centler, P. Regnier, H. Harms, and M. Thullner, *A reactive transport modeling approach to simulate biogeochemical processes in pore structures with pore-scale heterogeneities.* Environmental Modelling & Software, 2012. 30: p. 102-114.
19. Yao, K.M., M.M. Habibian, and C.R. O'Melia, *Water and Waste Water Filtration - Concepts and Applications.* Environmental Science & Technology, 1971. 5(11): p. 1105-1112.
20. Tufenkji, N., *Modeling microbial transport in porous media: Traditional approaches and recent developments.* Advances in Water Resources, 2007. 30(6-7): p. 1455-1469.
21. Ginn, T.R., B.D. Wood, K.E. Nelson, T.D. Scheibe, E.M. Murphy, and T.P. Clement, *Processes in microbial transport in the natural subsurface.* Advances in Water Resources, 2002. 25(8-12): p. 1017-1042.
22. Redman, J.A., S.B. Grant, T.M. Olson, and M.K. Estes, *Pathogen filtration, heterogeneity, and the potable reuse of wastewater.* Environmental Science & Technology, 2001. 35(9): p. 1798-1805.
23. Tong, M., X. Li, C.N. Brow, and W.P. Johnson, *Detachment-influenced transport of an adhesion-deficient bacterial strain within water-reactive porous media.* Environmental Science & Technology, 2005. 39(8): p. 2500-2508.
24. Tong, M., T.A. Camesano, and W.P. Johnson, *Spatial variation in deposition rate coefficients of an adhesion-deficient bacterial strain in quartz sand.* Environmental Science and Technology, 2005. 39(10): p. 3679-3687.
25. Johnson, W.P., X.Q. Li, and S. Assemi, *Deposition and re-entrainment dynamics of microbes and non-biological colloids during non-perturbed transport in porous media in the presence of an energy barrier to deposition.* Advances in Water Resources, 2007. 30(6-7): p. 1432-1454.
26. Torkzaban, S., S.A. Bradford, and S.L. Walker, *Resolving the coupled effects of hydrodynamics and DLVO forces on colloid attachment in porous media.* Langmuir, 2007. 23(19): p. 9652-9660.
27. Ren, J.H., A.I. Packman, and C. Welty, *Correlation of colloid collision efficiency with hydraulic conductivity of silica sands.* Water Resources Research, 2000. 36(9): p. 2493-2500.
28. Li, X.Q., T.D. Scheibe, and W.P. Johnson, *Apparent decreases in colloid deposition rate coefficients with distance of transport under unfavorable deposition conditions: A general phenomenon.* Environmental Science & Technology, 2004. 38(21): p. 5616-5625.

29. Yuan, H. and A.A. Shapiro, *A mathematical model for non-monotonic deposition profiles in deep bed filtration systems.* Chemical Engineering Journal, 2011. 166(1): p. 105-115.
30. Tufenkji, N. and M. Elimelech, *Deviation from the classical colloid filtration theory in the presence of repulsive DLVO interactions.* Langmuir, 2004. 20(25): p. 10818-10828.
31. Mailloux, B.J., M.E. Fuller, T.C. Onstott, J. Hall, H.L. Dong, M.F. DeFlaun, S.H. Streger, R.K. Rothmel, M. Green, D.J.P. Swift, and J. Radke, *The role of physical, chemical, and microbial heterogeneity on the field-scale transport and attachment of bacteria.* Water Resources Research, 2003. 39(6).
32. Schijven, J.F. and S.M. Hassanizadeh, *Removal of viruses by soil passage: Overview of modeling, processes, and parameters.* Critical Reviews in Environmental Science and Technology, 2000. 30(1): p. 49-127.
33. Pang, L.P., *Microbial removal rates in subsurface media estimated from published studies of field experiments and large intact soil cores.* Journal of Environmental Quality, 2009. 38(4): p. 1531-1559.
34. Tufenkji, N., J.A. Redman, and M. Elimelech, *Interpreting deposition patterns of microbial particles in laboratory-scale column experiments.* Environmental Science & Technology, 2003. 37(3): p. 616-623.
35. Scheibe, T.D., H.L. Dong, and Y.L. Xie, *Correlation between bacterial attachment rate coefficients and hydraulic conductivity and its effect on field-scale bacterial transport.* Advances in Water Resources, 2007. 30(6-7): p. 1571-1582.
36. Tufenkji, N. and M. Elimelech, *Correlation equation for predicting single-collector efficiency in physicochemical filtration in saturated porous media.* Environmental Science & Technology, 2004. 38(2): p. 529-536.
37. Azadpour-Keeley, A., B.R. Faulkner, and J.-S. Chen, *Movement and Longevity of Viruses in the Subsurface*. 2003, US EPA National Risk Management Research Laboratory, Cincinnati, Ohio. p. 24.
38. EPA, *Ground Water Rule: A Quick Reference Guide*. 2008, Office of Water (4606M).
39. Schijven, J.F. and S.M. Hassanizadeh, *Virus removal by soil passage at field scale and groundwater protection of sandy aquifers.* Water Science and Technology, 2002. 46(3): p. 123-129.
40. Pedley, S., Yates, M., Schijven, J. F., West, J., Howard, G. & Barrett, M., *Pathogens: Health relevance, transport and attenuation*, in *Protecting Groundwater for Health*, O. Schmoll, et al., Editors. 2006, WHO.
41. Pang, L., M. McLeod, J. Aislabie, J. Simunek, M. Close, and R. Hector, *Modeling transport of microbes in ten undisturbed soils under effluent irrigation.* Vadose Zone Journal, 2008. 7(1): p. 97-111.
42. Toride, N., F. Leij, and M.T. van Genuchten, *The CXTFIT Code for Estimating Transport Parameters from Laboratory of Field Tracer Experiments, Version 2.1, Research Report No. 137*. 1995, U.S. Salinity Laboratory, USDA, ARS, Riverside, CA.
43. Hall, J.A., B.J. Mailloux, T.C. Onstott, T.D. Scheibe, M.E. Fuller, H. Dong, and M.F. DeFlaun, *Physical versus chemical effects on bacterial and bromide*

transport as determined from on site sediment column pulse experiments. Journal of Contaminant Hydrology, 2005. 76(3-4): p. 295-314.
44. Weaver, L., L.W. Sinton, L.P. Pang, R. Dann, and M. Close, *Transport of microbial tracers in clean and organically contaminated silica sand in laboratory columns compared with their transport in the field.* Science of the Total Environment, 2013. 443: p. 55-64.
45. Weiss, W.J., E.J. Bouwer, W.P. Ball, C.R. O'Melia, M.W. Lechevallier, H. Arora, and T.F. Speth, *Riverbank filtration - fate of DBP precursors and selected microorganisms.* Journal American Water Works Association, 2003. 95(10): p. 68-81.
46. Parker, J.C. and M.T. van Genuchten, *Flux-averaged and volume-averaged concentrations in continuum approaches to solute transport.* Water Resources Research, 1984. 20(7): p. 866-872.
47. Jansons, J., L.W. Edmonds, B. Speight, and M.R. Bucens, *Survival of viruses in groundwater.* Water Research, 1989. 23(3): p. 301-306.
48. Keswick, B.H. and C.P. Gerba, *Viruses in groundwater.* Environmental Science & Technology, 1980. 14(11): p. 1290-1297.
49. Hurst, C.J., C.P. Gerba, and I. Cech, *Effects of environmental variables and soil characteristics on virus survival in soil.* Applied and Environmental Microbiology, 1980. 40(6): p. 1067-1079.
50. Nasser, A.M., R. Glozman, and Y. Nitzan, *Contribution of microbial activity to virus reduction in saturated soil.* Water Research, 2002. 36(10): p. 2589-2595.
51. Freeze, R.A. and J.A. Cherry, *Groundwater*. 1979, Englewood Cliffs, NJ: Prentice-Hall. 604 pp.
52. Kasenow, M., *Applied Ground-Water Hydrology and Well Hydraulics*. 2nd ed. 2001, Denver, CO: Water Resources Publications. 835 pp.
53. Bradford, S.A. and S. Torkzaban, *Colloid transport and retention in unsaturated porous media: A review of interface-, collector-, and pore-scale processes and models.* Vadose Zone Journal, 2008. 7(2): p. 667-681.
54. Dong, H.L., T.C. Onstott, M.F. Deflaun, M.E. Fuller, T.D. Scheibe, S.H. Streger, R.K. Rothmel, and B.J. Mailloux, *Relative dominance of physical versus chemical effects on the transport of adhesion-deficient bacteria in intact cores from South Oyster, Virginia.* Environmental Science & Technology, 2002. 36(5): p. 891-900.
55. Elimelech, M., *Predicting collision efficiencies of colloidal particles in porous media.* Water Research, 1992. 26(1): p. 1-8.
56. Bradford, S.A. and N. Toride, *A stochastic model for colloid transport and deposition.* Journal of Environmental Quality, 2007. 36(5): p. 1346-1356.
57. Pang, L.P., M. Close, M. Goltz, M. Noonan, and L. Sinton, *Filtration and transport of Bacillus subtilis spores and the F-RNA phage MS2 in a coarse alluvial gravel aquifer: Implications in the estimation of setback distances.* Journal of Contaminant Hydrology, 2005. 77(3): p. 165-194.

4 A stochastic, 3-D modeling approach to resolve correlated physical and flow heterogeneities and their influence on microbial transport in a riverbank filtration setting

4.1 Background and Motivation

Porous, granular aquifer materials are a natural filter, so subsurface passage has the potential to provide significant removal of microbial contaminants and general buffering capacity against surface-derived contamination. Growing pressures on water resources [1] and the ever-present threat of waterborne disease [2] underscore the importance of understanding the processes that control the movement of viruses and other microbial pathogens in groundwater. Significant progress has been made in this area through the contributions of well-controlled laboratory experiments in columns and flow-cell systems (e.g., references [3-5], [6] and data referenced therein), including studies of more complex, heterogeneous media (e.g., references [7-10]). Advances have also been made through field-scale modeling efforts that combine a porous media transport equation with a filtration model for microbial attachment (e.g., references [11, 12]).

But natural aquifer materials vary widely, and flow patterns – be they natural or engineered – can have a significant effect on microbial removals. Field data about microbial attenuation are therefore more relevant and reliable than laboratory estimates [13] when it comes to estimating microbial contamination risks at drinking water production wells, establishing good practices for effluent disposal and other potential contamination sources, or identifying suitable locations for artificial recharge or wastewater reclamation projects. However, the complexity and expense of conducting

field experiments means that they are much less numerous than laboratory studies of microbial transport in porous media.

Field scale models that combine a realistic representation of microbial attenuation with a realistic parameterization of aquifer and flow heterogeneity can help to fill this gap, but there are few such studies (e.g., references [14-18]), and none have focused on a riverbank filtration (RBF) context. This project lays out a method for constructing a modeling study of virus removal in a heterogeneous RBF setting and highlights some of the potential limitations of common approaches to interpreting results using the coupled flow-filtration model of microbial transport.

4.1.1 One-dimensional models leave room for improvement

Modeling microbial removals observed in field transport experiments presents challenges. Faced with breakthrough curves that clearly reveal non-ideal and heterogeneous aquifer conditions [19], given unknown travel time distributions that render it impossible to determine the relevant source concentration [20], or explicitly recognizing that a simple transport model is inappropriate for the site in question [21], a number of researchers have just reported observed log removals without attempting any model-based interpretation of field results.

However, coupled transport-attachment models have been developed for a handful of field sites where flow is approximately one-dimensional. In particular, a deep-well injection site [22] and a dune recharge operation [12, 23], both in The Netherlands, and an artificial recharge basin in California [24] have all been modeled using the 1D advection-dispersion equation coupled with a kinetic formulation for microbial removal based on filtration theory, following the approach pioneered by Harvey and Garabedian

[11]. The same approach was applied to breakthrough data for wells spaced over a distance of 7 m from the injection point in a forced gradient bacterial transport study conducted at the South Oyster focus site in Virginia [25].

Variations in velocity were ignored in these studies, although velocities likely increased along ~1D flow paths due to the influence of an extraction well in both the dune recharge and deep well injection operations, while velocities decreased with distance from the injection well at the Virginia site. No attempt was made to represent the physical heterogeneity of the subsurface, although in the dune recharge case, there was known vertical layering of fine and coarse sand intersecting the screens of both the injection and the withdrawal wells.

There is even at least one published report that has gone so far as to take the same 1D approach to model riverbank filtration field data. In an otherwise thorough and practical analysis of a "sand abstraction system" – a term used in arid southern Africa to describe what is essentially a riverbank filtration well with a single lateral arm extending across the entire width of the sandy riverbed of an ephemeral stream – the study authors applied the same one-dimensional transport-attachment model to extract an apparent attachment rate constant for filtration and use it to predict coliform removals over a 500 m travel distance approaching the production well [26].

Apparent attachment rate coefficients derived from the models of these various sites reflect the lumped effects of both physical and biological influences. Apparent collision efficiencies generally decreased with transport distance. As demonstrated convincingly by Scheibe *et al.* [18], this seeming scale-dependence of transport

properties can arise from a failure to account for correlation between filtration/attachment processes and flow heterogeneity.

4.2 Objectives

The modeling investigations described in this chapter sought to contribute to understanding of the role of aquifer heterogeneity on the extent of transport of biological particles through porous media, with a focus on three specific objectives:

- To lay out a modeling framework for assessing the relative roles of attachment and hydrodynamics in contributing to the removal of virus-sized particles for riverbank filtration systems
- To extend previous modeling work on the role of physical heterogeneity to a riverbank filtration setting
- To apply a sophisticated 3D groundwater flow model coupled with a contaminant transport code to investigate the influence of correlation between heterogeneous aquifer properties and filtration/attachment processes

In applying a general approach to a hypothetical, idealized model domain, we focused on what models can reveal about underlying processes. We do not attempt to represent a particular field site or to predict actual system performance. Instead, our approach demonstrates the use of a consistent basis for comparison to examine the origins of relative differences between RBF systems with varying characteristics.

4.3 Theory

4.3.1 Dimensionless formulation of RBF flow fields

Derived from Darcy's law in radial coordinates, the Thiem equation [27] describes the drawdown associated with a pumping well under steady-state conditions. In a homogeneous, isotropic, confined aquifer, the drawdown s at a distance r from the pumping well is given by:

$$s = h_0 - h = \frac{Q}{2\pi KB}\ln\left(\frac{r}{R}\right), \qquad \text{(Eqn. 4-8)}$$

where h is the head at radius r, h_0 is the background head at the limit of the radius of influence R, Q is the volumetric pumping rate, K is the hydraulic conductivity, and B is the thickness of the aquifer.

The drawdown due to two pumping wells, A and B, may be determined by linear superposition. Designating well A as a virtual "mirror" well with an injection rate of equal magnitude and opposite sign to the withdrawal rate at well B ($Q_B = -Q_A$), it is possible to simulate a linear groundwater divide situated exactly half way between the two wells. This system can therefore be used to approximate the groundwater table in a riverbank filtration system, shown in Figure 4-1. Well B is the production well, located at (0,L); the river is a line at (x,0), and the virtual mirror well A is located at (0,-L).

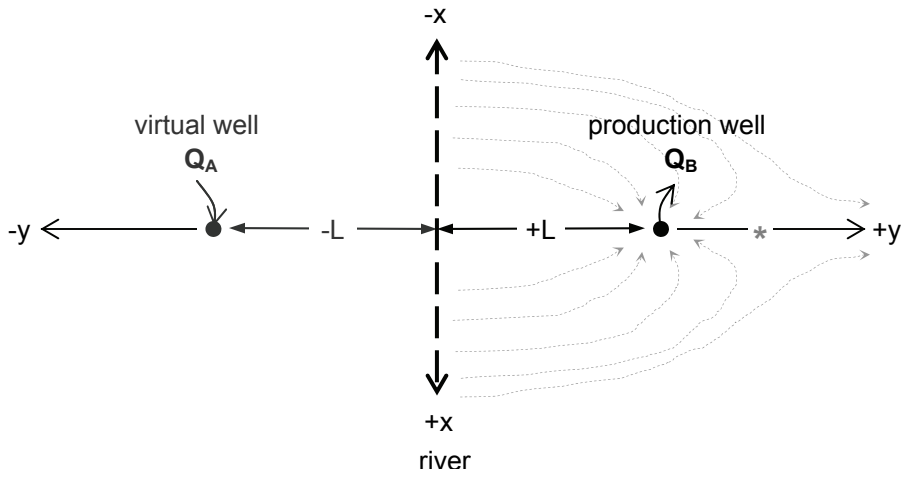

Figure 4-1 Plan view of a simulation domain for a hypothetical riverbank filtration system approximated with the Thiem equation. The river, denoted by a thick dashed line, falls along the x-axis. The direction of river flow is not important. The general shape of the flow field is sketched with grey dashed lines; the critical or stagnation point is marked with a small star. The underlying bedrock slopes away from the river on both sides; this slope is aligned with the y-axis.

Converting from a radial to an orthogonal coordinate system, the net drawdown, s_{TOT}, at location (x, y) in the well field is given by

$$s_{TOT} = s_A + s_B = \frac{Q}{4\pi KB} \ln\left(\frac{x^2 + (y + L^2)}{x^2 + (y - L^2)}\right). \qquad \text{(Eqn. 4-9)}$$

The head in an aquifer system is the sum of the water table elevation z, the pressure head Ψ, and the contribution of the slope S of the system. In our hypothetical riverbank filtration aquifer, the slope of the underlying bedrock is oriented along the y-axis with positive values of S corresponding to a naturally losing stream:

$$h(x, y) = z(x, y) + \Psi(x, y) - yS\,.$$

Since Ψ is zero at the water table for an unconfined aquifer and head $h(x,y)$ is merely the aquifer thickness minus the drawdown, we may use Eqn. 4-9 to approximate the elevation of the water table as follows:

$$z(x,y) = B - \frac{Q}{4\pi KB}\ln\left(\frac{x^2 + (y+L^2)}{x^2 + (y-L^2)}\right) - yS\,. \qquad \text{(Eqn. 4-10)}$$

To facilitate the analysis of the system, we rewrite Eqn. 4-10 in non-dimensional form:

$$z'(x,y) = 1 - \alpha y' \frac{Q'}{4\pi}\ln\left(\frac{x'^2 + (y'+1^2)}{x'^2 + (y'-1^2)}\right), \qquad \text{(Eqn. 4-11)}$$

where

$$z' = \frac{z}{B}$$

$$x' = \frac{x}{L},\ y' = \frac{y}{L}$$

$$L' = \frac{LS}{B}$$

$$Q' = \frac{Q}{KB^2}$$

$$\alpha = \frac{L'}{Q'}\,.$$

For our losing stream in a sloped system with a pumping well located at distance L from the river, we expect the formation of a stagnation point down gradient in the axis of the well, sketched in Figure 4-1. It defines the limit of the well's capture zone in the y-direction. The first derivative of z' with respect to y' gives the flux vector in the y-direction, so the dimensionless location of the critical point, y'_{crit}, may be found by setting $dz'/dy' = 0$ and solving for y':

$$y'_{crit} = \sqrt{1 + \frac{1}{\pi\alpha}} \qquad \text{(Eqn. 4-12)}$$

This parameter, y'_{crit}, may be thought of as representing the plan view organization of flow paths between the river and the well. Smaller y'_{crit} values correspond to systems where flow is more linear. In effect, y'_{crit} reflects the areal extent of the pumping well's zone of influence relative to the size of the system as a whole. Logically, high pumping rates and low hydraulic conductivities enhance the impacts of an RBF installation on natural aquifer flow patterns, as reflected in higher values of y'_{crit}. Perhaps less intuitively, locating a well close to the river or in an aquifer with a water table that has only a shallow natural slope will also increase y'_{crit}, because the influence of the pumping in the zone connecting the well to the river is enhanced in the former case, while the influence of the well on local flow patterns extends farther down gradient in the latter case.

The parameter Q' is a dimensionless pumping rate. Like a vertical profile through the domain, it represents the magnitude of the effects of pumping within the well's zone of influence. Thick aquifers, low (dimensional) pumping rates, and high hydraulic conductivities all contribute to lesser drawdown relative to the vertical extent of the aquifer, which translates to smaller values of Q'.

Taking these two dimensionless parameters together, $y'_{crit} - Q'$ space is a useful construct to organize comparative modeling studies of RBF systems. Appropriate selection of system parameters makes it possible to distinguish between effects on system performance that relate to the distribution of flow paths lengths induced by horizontal flow convergence at the well vs. those which relate to the acceleration of flow towards the well due to vertical flow convergence. Since filtration theory describes particle removal in terms of both distance travelled and attachment processes that depend on such

parameters as velocity and grain size, it is essential to consider both the organization of flow paths and the conditions on a given flow path when applying filtration theory to RBF-type systems. The $y'_{crit} - Q'$ framework partially decouples these effects: all length-based effects are captured in y'_{crit}, but velocity-based effects figure in both parameters.

4.3.2 A (re-)clarification of filtration models: the importance of velocity

As discussed in previous chapters, laboratory and field studies of microbial removal by porous aquifer materials are commonly interpreted through the lens of clean bed filtration theory (CBFT). Aqueous phase microbial concentrations decline with distance from the contamination source as collisions between the microbial particles and aquifer sand grains along each flow path result in the attachment and immobilization of microbes at mineral surfaces. The microbe-sand grain collision rate is described as a theoretical single-collector efficiency, η_0, while the probability of a given collision resulting in attachment (known as the collision efficiency, α) depends on physicochemical interactions between the particle and the collector surface.

In this section, we wish to highlight a common conceptual and mathematical error in the application of CBFT to field data and field-scale modeling studies. The confusion arises from the introduction of flow velocity into the original equation proposed by Yao *et al.* [28] to quantify particle removal in clean filter beds:

$$\ln\frac{C}{C_0} = -\frac{3}{2}\frac{(1-n)\alpha\eta_0}{d_c}L, \qquad \text{(Eqn. 4-13)}$$

where d_c is the diameter of the collector grain, n is the porosity, C_0 is the influent concentration, and C is the concentration at length L from the influent location.

Substituting $L = vt$ transforms this expression into a kinetic rate law with a first-order coefficient k:

$$k = \frac{3}{2}\frac{(1-n)\alpha\eta_0}{d_c}v. \qquad \text{(Eqn. 4-14)}$$

The velocity v in question is the pore velocity, as it is the pore velocity that determines the transport distance L through porous media. Moreover, it is the pore velocity that can be estimated from tracer studies in the field. The rate constant k may then be conveniently inserted in the advection-dispersion equation to describe microbial removal by attachment as a first-order process.

Researchers who wish to use an apparent attachment rate constant k fit from field or column breakthrough data to quantify the apparent collision efficiency (α) must first estimate (η_0). Like the rate constant k itself, the single-collector efficiency η_0 exhibits velocity dependence. However, selecting the appropriate velocity for a calculation of η_0 is a potential pitfall. It is easy – but generally incorrect – to assume that one should use the pore velocity v, for the sake of consistency with the $L = vt$ substitution performed to transform Eqn. 4-13 into a first-order kinetic expression.

As clarified by Logan *et al.* in 1995 [29], the derivations of two early theoretical models for η_0 were based not on the pore velocity, but on the approach velocity. Also known as a superficial velocity or a Darcy flux, the approach velocity U is defined as the ratio of the volumetric flux (Q) to the cross sectional area (A). It is related to the pore velocity (v) by the porosity of the medium (n):

$$U = \frac{Q}{A} = vn. \qquad \text{(Eqn. 4-15)}$$

However, simplifying assumptions in these early derivations presented inconsistencies when applied to porous media. One model was based on isolated collector grains that do not actually exist in packed beds, while the other depended on a Peclet number that did not properly represent the flow around spherical grains in packed media. As a result of these inherent limitations, Logan *et al.* concluded that it made little difference whether an approach velocity or a pore velocity was used when evaluating η_0 from the two early models. Either way, the model was an imperfect approximation.

Subsequently, the 1976 R&T equation [30] and in 2004 the T&E equation [6] addressed the shortcomings of earlier theoretical models for η_0. These more recent, improved models are the ones generally applied today. Critically, both were derived in an internally consistent fashion using the approach velocity U. It is therefore inappropriate to use the pore velocity v for velocity in the R&T or T&E equation when evaluating η_0. The correct substitution is not v but the product vn, as maybe seen from Eqn. 4-15.

Despite the clarifications published two decades ago, this continues to be a common error that we have noted in several published studies (e.g., [18], [31], [32]). The confusion may stem in part from typographical errors and an editorial shortcut in the original R&T manuscript (although these were none-the-less noted explicitly by Logan *et al.* [29]), perhaps compounded by a seminal 1991 paper [11] which used v when evaluating η_0 from one of the two early equations for which the choice between v and U was indifferent.

4.3.2.1 Filter factors and attachment rate constants

For the viral-sized particles that were the focus of our analysis, the single collector efficiency is dominated by the contributions of diffusion. It may be calculated as follows from a reduced form of the T&E equation [6]:

$$\eta_0 = 2.4 A_s^{1/3} N_R^{-0.081} N_{Pe}^{-0.715} N_{vdW}^{0.052} \qquad \text{(Eqn. 4-16)}$$

where

$N_R = \frac{d_p}{d_c}$	Aspect ratio: d_p is the diameter of the particle (virus)
$N_{Pe} = \frac{U d_c}{D_\infty}$	Ratio of advective to diffusive transport: U is the approach velocity or Darcy flux, defined as the volumetric discharge per unit area, and D_∞ is the bulk diffusion coefficient calculated from the Stokes-Einstein equation
$N_{vdW} = \frac{A}{k_B T}$	Van der Waals number: A is the Hamaker constant, k is the Boltzman constant, and T is the temperature in Kelvin
$A_s = \frac{2(1-\gamma^5)}{2-3\gamma+3\gamma^5-2\gamma^6}$	Happel's porosity-dependent parameter for the effects of neighboring grains: $\gamma = (1-n)^{1/3}$.

Substituting Eqn. 4-15 and Eqn. 4-16 into Eqn. 4-13, the removal of viral-sized particles by clean-bed filtration processes may be expressed as

$$\ln \frac{C}{C_0} = -\left[\frac{3}{2} d_p^{-0.081} D_\infty^{+0.715} N_{VdW}^{+0.052}\right]\left[\frac{2.4 A_s^{1/3}(1-n)}{n^{+0.715}}\right]\left[\frac{\alpha}{v^{+0.715} d_c^{+1.634}}\right] L \,. \qquad \text{(Eqn.4-17)}$$

The first term in square brackets on the right hand side reflects properties of the viral population, the second bracketed term groups all porosity-dependent effects, and the third bracketed term captures flow and aquifer grain effects. The product of these three terms

is known as a filter factor (*f*); it is the removal rate constant in units of inverse length rather than inverse time:

$$f = \left[\frac{3}{2} d_p^{-0.081} D_\infty^{+0.715} N_{VdW}^{+0.052}\right]\left[\frac{2.4 A_s^{1/3}(1-n)}{n^{+0.715}}\right]\left[\frac{\alpha}{v^{+0.715} d_c^{+1.634}}\right] \qquad \text{(Eqn. 4-18)}$$

While a viral population may present a distribution of properties, particularly when multiple types of viruses are present, heterogeneity in the first bracketed term is unlikely to be spatially organized. Certainly porosity, captured in the second bracketed term, will vary spatially in heterogeneous aquifer materials, and likely in a fashion that correlates with hydraulic conductivity, although such a relationship is difficult to quantify. Heterogeneity in the third bracketed term will have a strong spatial organization, as it arises directly from the hydraulic conductivity of heterogeneous aquifer materials and from the organization of the flow field. The collision efficiency α may also exhibit spatially-organized heterogeneity, because the "stickiness" of a collision is governed not only by the properties of the microbial particle but also by those of the aquifer materials. But despite efforts by others (e.g., [33]), a robust basis for parameterizing heterogeneity in α is lacking.

When using filtration theory to quantify attachment in microbial transport models based on the advection-dispersion equation, the final substitution of $L = vt$ allows Eqn.4-17 to be rewritten in a form with an attachment rate constant in units of inverse time:

$$\ln\frac{C}{C_0} = -fvt \ , \qquad \text{(Eqn. 4-19)}$$

thus

$$k_{att} = -fv = -\left[\frac{3}{2} d_p^{-0.081} D_\infty^{+0.715} N_{VdW}^{+0.052}\right]\left[\frac{2.4 A_s^{1/3}(1-n)}{n^{+0.715}}\right]\left[\frac{\alpha}{v^{+0.715} d_c^{+1.634}}\right] v \,. \quad \text{(Eqn. 4-20)}$$

The product of the filtration factor f and the velocity v is the attachment rate coefficient k describing first-order removal by filtration processes. We note that use of an incorrect reference velocity would have resulted in an inaccuracy proportional to $n^{-0.715}$ in estimates of the apparent filter factor or attachment rate coefficient from the T&E equation, and thus also in subsequent estimates of the apparent α.

The time-dependence of microbial removal by attachment processes arises only from the $L = vt$ substitution. Filtration is a surface process, so the fundamental control on removal by attachment is the length traveled through the porous media, not the time spent doing so. Since we do not consider inactivation in the present study – which as a first-order kinetic process would add time-dependent removal – we frame our discussion from this point forward in terms of the filter factor, f, rather than the attachment rate constant, k_{att}.

4.4 Methods

4.4.1 Modeling software

4.4.1.1 ParFlow

Flow simulations were performed in ParFlow [34-37] on the Maryland Advanced Research Computer Cluster (MARCC). ParFlow is a finite difference code capable of modeling surface and subsurface flow under saturated or variably saturated conditions. Designed to run in a parallel computing environment, it is capable of large-scale, high-resolution, three-dimensional watershed simulations. Given system geometry, internal

features, sources, sinks, boundary conditions and initial conditions, ParFlow simulates steady state flow. To describe a layered alluvial aquifer, the model domain was assigned small-scale variation in hydraulic conductivity (K) following a correlated Gaussian random field. This heterogeneity was generated numerically using the "turning bands" approach [38].

4.4.1.2 Slimfast and modifications

Tracer and virus transport simulations through the flow domain were conducted in SLIM [39], which takes a Lagrangian random walk, particle-tracking approach to model the subsurface transport of reactive and unreactive constituents. SLIM is an open-source research code designed to integrate with ParFlow. Briefly, SLIM transforms the advection-dispersion equation and linked mass balance on attached or adsorbed contaminants into a cloud of "particles," each of which is a numerical construct representing a small portion of the total solute mass in the system. These "particles," which have no physical equivalent, can then be moved through the simulation subject to advection, dispersion, sorption, radioactive decay, chemical reaction, etc., in order to model the transport of a neutrally-buoyant aqueous species. As described by the developers [15], attachment and detachment rates are represented as probability functions, so that for each particle time step the probability that a particle representing, say, a free-moving aqueous phase virus will be transformed into a stationary attached-phase virus (or vice versa) is given by the product of the rate constant and the duration of the time step.

SLIM was capable of applying constant attachment and detachment rate coefficients to model contaminant transport. We modified the code to add a formulation

for attachment consistent with microbial removal by filtration theory. The filter factor in m^{-1} was calculated from Eqn. 4-18 for every grid cell in the domain. The velocity for this calculation was taken as the average velocity in that grid cell from the ParFlow steady-state flow field, and the grain size (d_c in meters) was calculated from the hydraulic conductivity of the grid cell (K in m/d) by inverting the Hazen relationship [40] (Eqn. 4-21):

$$d_c = 10^{-4} e^{\log\left(\frac{K}{86400}\right)}. \qquad \text{(Eqn. 4-21)}$$

The values of the other parameters used in the calculation of the filter factor are given in Table 4-1. Note that the collision efficiency α was at all times held constant at 1×10^{-4}. This calculation generates a spatial field of filter factors predicted by the T&E equation and correlated with the both the flow field and, for heterogeneous domains, the hydraulic conductivity field.

To calculate removals by attachment at every particle time step, SLIM multiplied the filter factor in the current grid cell by the distance L travelled during the current time step, which was the product of the locally interpolated velocity and the duration of that time step.

We wish to emphasize the deliberate use of two different pore velocities in this calculation: the grid cell average pore velocity in the estimation of the filter factor, and the ultra-local interpolated velocity for each small time step in the "conversion" of the filter factor into an attachment rate constant. In effect, the only purpose of the final multiplication by velocity is to express the distance travelled L as vt in order to express filtration as a kinetic process for integration into the advection-dispersion equation. Thus

the relevant velocity for the final multiplication is the one that determines the distance travelled over that time step. While one could also argue that this ultra-local, interpolated time step velocity is likewise relevant for the virus-sand grain interactions quantified in η_0, the rest of the parameters involved in the η_0 calculation are available only at the coarser, grid-scale resolution, so using a grid cell average velocity to calculate η_0 is internally consistent. Additionally, calculating the filter factor on a grid cell scale offers computational advantages in SLIM.

We further modified the SLIM code to optionally scramble the field of filter factors using an implementation of the Fisher-Yates shuffling algorithm [41]. We thus removed correlation between the attachment field and the hydraulic conductivity field without altering the statistical properties of the distribution of filter factor values, the organization of the pumping-induced flow regime, or the spatial correlation of the heterogeneous hydraulic conductivity field (for heterogeneous domain simulations). Only the saturated zone filter factors were scrambled; inactive and unsaturated grid cells were left in place.

Simulation results from ParFlow and SLIM were visualized in two and three dimensions using the public domain software package VisIt [42].

Table 4-1. Parameter values used for evaluation of the filter factor

d_p	particle diameter	50 nm
A	Hamaker constant	1.0×10^{-20} J
T	groundwater temperature	10 °C
k_b	Boltzman constant	1.3806×10^{-23} J/K
n	porosity	0.30
α	collision efficiency	1.0×10^{-4}

4.4.2 Construction of the modeling domain

4.4.2.1 ParFlow model domain

As an example application of the dimensionless approach described above, two sets of hypothetical RBF systems are shown in $y'_{crit} - Q'$ space in Figure 4-2, with values of key parameters summarized in Table 4-2. For a given set of cases, hydraulic conductivity and aquifer thickness are constant, so that Q' is determined entirely by the dimensional pumping rate. To study the effect of well location for these different systems in a consistent way, the slope S was adjusted to maintain uniform values of y'_{crit} for each setback distance L. Values for Q, K, L, and B were all chosen from a range representing the characteristics of real RBF sites [20, 43-45]. Information about the system slope S is difficult to find in the literature, but we expect that the lower values considered here may reasonably occur at RBF field sites. Another published simulation of RBF in a similarly simplified domain used S = 0.003 [46]. Higher values of S, representing a steeply sloping water table, are harder to validate in the context of realistic RBF installations. They may be thought of as hypothetical systems.

We constructed four of these systems, identified with open squares in Figure 4-2, as full modeling domains in ParFlow. Each domain was built in dimensional form, with the river at y = 0, and a fully-penetrating pumping well located at y = 50 m or y = 75 m. Grid cells on the bottom of the domain were inactivated as required to generate the desired system slope. So that boundaries would not affect the flow field in undesirable ways, the extent of the domain in x and y was set at 3 and 1.5 times the distance from the river to the critical point, respectively. Domain geometry is summarized in Table 4-3 and sketched schematically in vertical section in Figure 4-3. Analytically predicted velocity

fields and water table elevations are plotted in dimensionless space in Figure 4-4 and Figure 4-5.

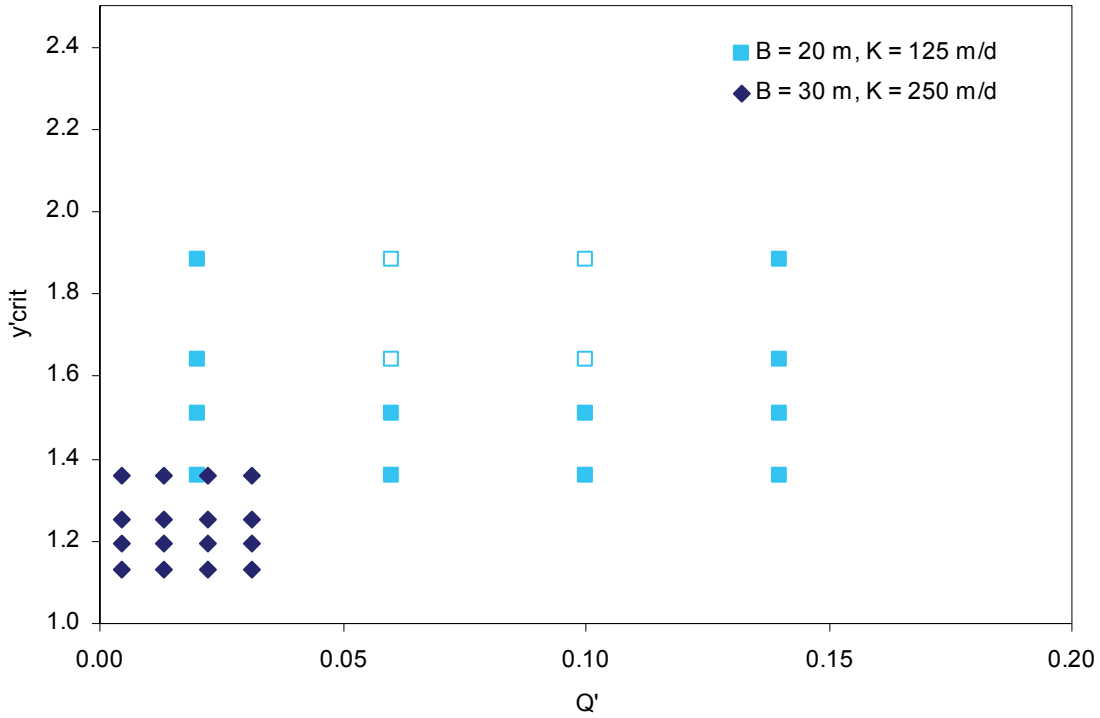

Figure 4-2. Example of $y'_{crit} - Q'$ space showing the effects of well location and pumping rate for two hypothetical aquifers: a thinner, lower-conductivity aquifer (squares) and a thicker, higher-conductivity formation (diamonds). Open symbols represent systems selected as examples for further analysis. See Table 4-2 for parameter values.

Table 4-2. Aquifer parameters for the two hypothetical aquifers shown in Figure 4-2. See Eqn. 4-8, Eqn. 4-11, and Eqn. 4-12 for variable definitions. An asterisk denotes systems selected for further analysis.

Q'	y'_{crit}	S (-)	Q (m^3/d)	L (m)	y_{crit} (m)
K = 125 m/d, B = 20 m					
0.020	1.88	0.001	1000	50	94.2
	1.64			75	123.2
	1.51			100	150.8
	1.36			150	204.0
0.060	1.88*	0.003	3000	50	94.2
	1.64*			75	123.2
	1.51			100	150.8
	1.36			150	204.0
0.100	1.88*	0.005	5000	50	94.2
	1.64*			75	123.2
	1.51			100	150.8
	1.36			150	204.0
0.140	1.88	0.007	7000	50	94.2
	1.64			75	123.2
	1.51			100	150.8
	1.36			150	204.0
K = 250 m/d, B = 30 m					
0.004	1.36	0.001	1000	50	68.0
	1.25			75	93.9
	1.19			100	119.3
	1.13			150	169.9
0.013	1.36	0.003	3000	50	68.0
	1.25			75	93.9
	1.19			100	119.3
	1.13			150	169.9
0.022	1.36	0.005	5000	50	68.0
	1.25			75	93.9
	1.19			100	119.3
	1.13			150	169.9
0.031	1.36	0.007	7000	50	68.0
	1.25			75	93.9
	1.19			100	119.3
	1.13			150	169.9

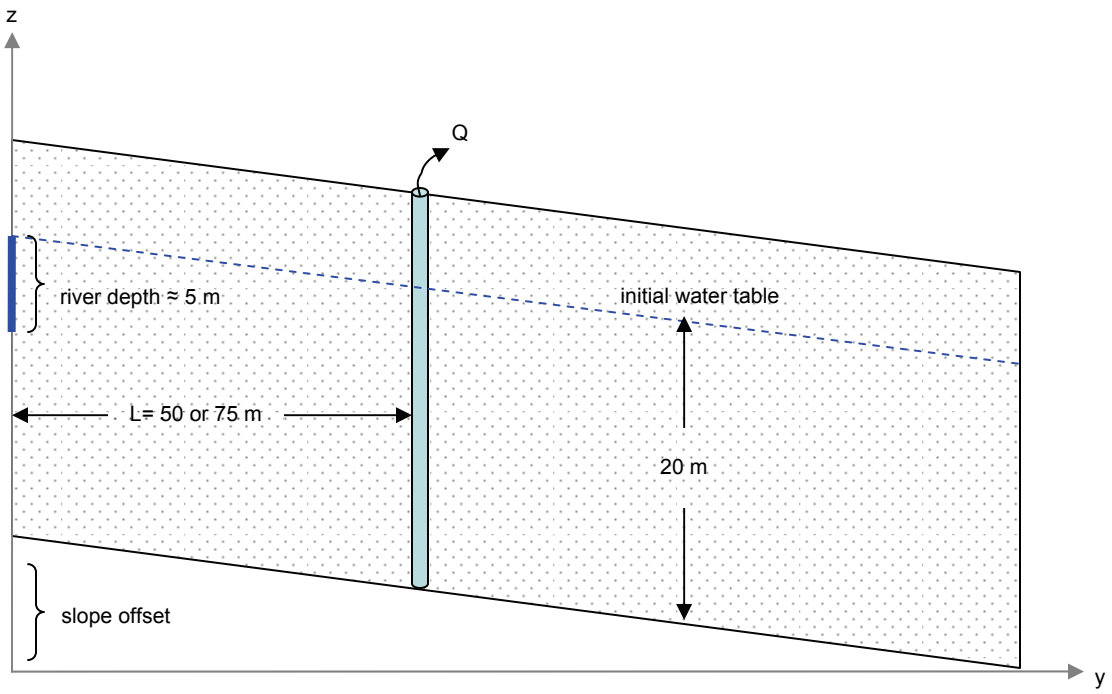

Figure 4-3. Vertical section of the domain geometry, showing the general layout of the sloped bedrock, the river boundary, the initial water table (dashed line), and the pumping well. Cartoon not drawn to scale.

The river at y = 0 was represented by a constant head boundary condition corresponding to a saturated aquifer thickness of 20 m. The river was assumed to be approximately 5 m deep (snapped to the model grid), so a no-flux boundary was specified at y = 0 for the ~15 m below the river. The down gradient boundary condition at the y-limit of the domain was set at a constant head calculated from Eqn. 4-10. No-flux boundary conditions were specified for all other surfaces.

The top of the domain was approximately 5 meters above the water table under no pumping conditions, ensuring the presence of an unsaturated zone that was assigned a residual saturation of 0.00001 and Van Genuchten soil parameters [47] $\alpha = 35\ m^{-1}$ and n = 2. These values ensure a sharp transition between the saturated zone and the unsaturated zone; for the purposes of modeling virus transport in RBF systems, we are not interested in the capillary fringe above the water table.

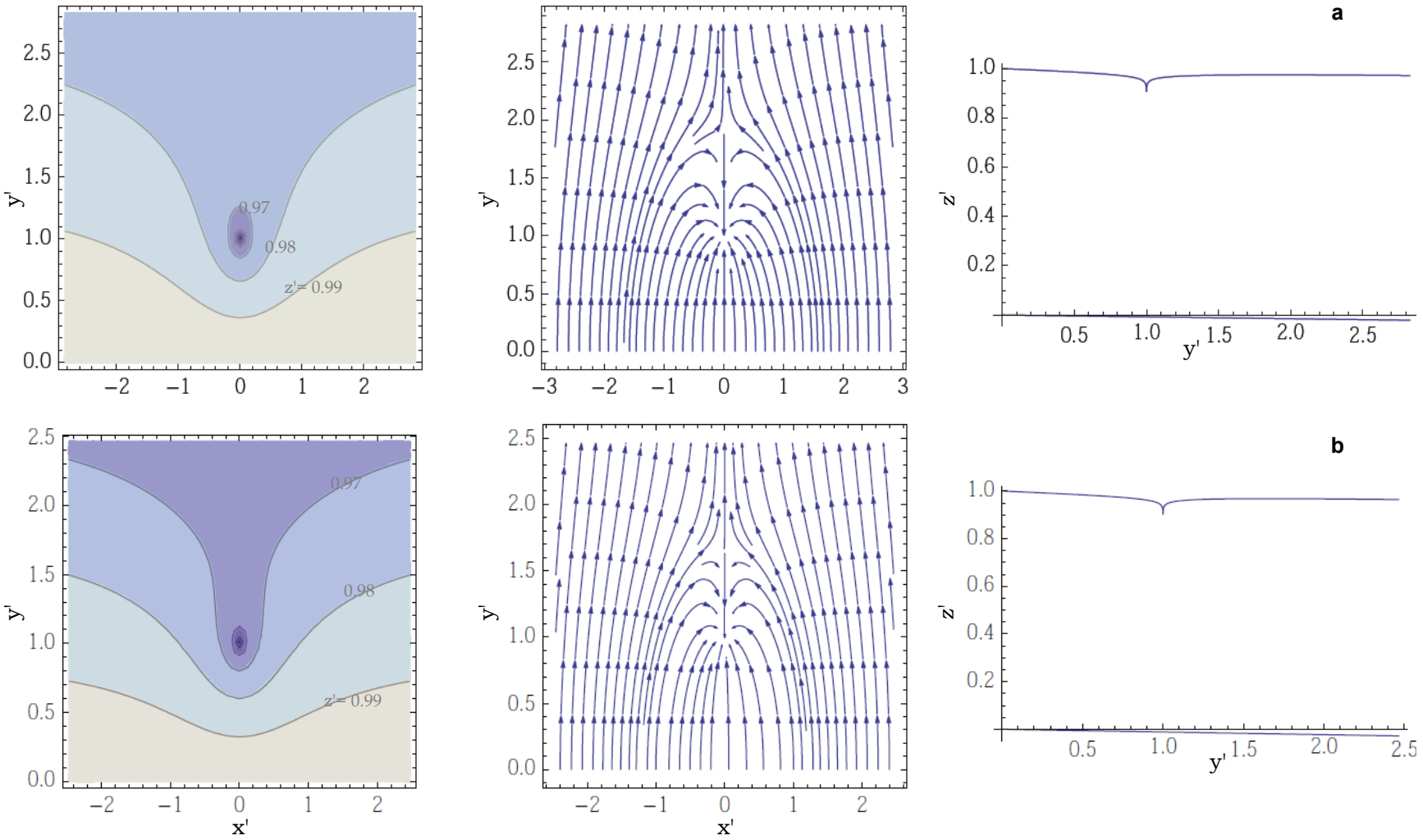

Figure 4-4. Water table contours, velocity field, and water table vertical profile for the Q' = 0.060 (low pumping rate) case with (a) y'_{crit} =1.88 (50 m well setback) and (b) y'_{crit} = 1.64 (75 m well setback).

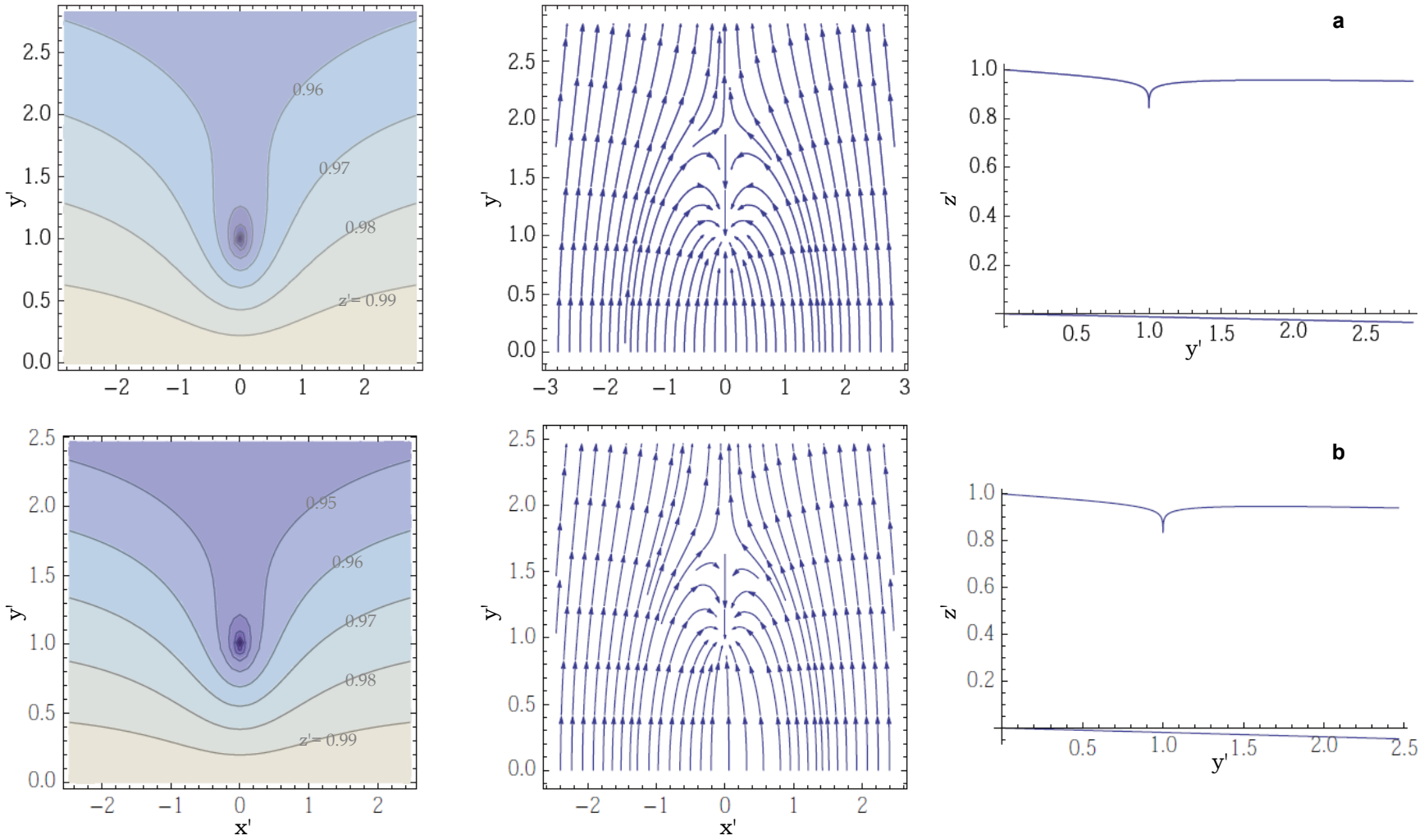

Figure 4-5. Water table contours, velocity field, and water table vertical profile for the Q' = 0.10 (high pumping rate) case with (a) y'_{crit} =1.88 (50 m well setback) and (b) y'_{crit} = 1.64 (75 m well setback).

For each of the four systems, one homogeneous realization of the model domain was generated with K = 125 m/d everywhere. Additionally, 10 random heterogeneous realizations were created using a log-normal distribution of hydraulic conductivity with a geometric mean of 125 m/d and a standard deviation of 0.4. To simulate the horizontal layering and lenses typical of alluvial systems, a correlation length scale of γ = 6 m was set for x and y, with γ = 2 m for z. Grid size was 2 m in x and y, and ranged from 0.355 to 0.558 m in z depending on the system slope.

The domain was initialized with a constant head of 20 m relative to the sloped bottom and the simulation was run in ParFlow until the water table had reached steady state under pumping conditions, with a stable head profile. The pressure and hydraulic conductivity fields from ParFlow were subsequently fed to SLIM for virus transport calculations.

Table 4-3. Domain geometry for ParFlow and SLIM

Q':	0.060	0.060	0.100	0.100
y'_{crit}:	1.88	1.64	1.88	1.64
domain origin:	(0,0,0)	(0,0,0)	(0,0,0)	(0,0,0)
extent of domain (m)				
x_{max}	284	372	284	372
y_{max}	142	186	142	186
z_{max}	25.135	25.110	25.205	25.575
grid cell size (m)				
dx	2	2	2	2
dy	2	2	2	2
dz	0.426	0.558	0.355	0.465
domain size	595k grid cells	778k grid cells	710k grid cells	951k grid cells
river position, vertical coordinates (m)				
riverbed	15.336	15.624	15.620	15.810
river surface	20.462	20.558	20.710	20.930
river depth	5.126	4.934	5.090	5.120
location (m) of fully penetrating well				
coordinates (x,y)	(142,50)	(186,75)	(142,50)	(186,75)

4.4.2.2 SLIM model domain

The model grid declared in SLIM matched that of ParFlow exactly. Numerical "particles" used for transport calculations were launched in a pulse input from the river. Due to model limitations, particles cannot be initialized at the outer limit of the domain, so our initial particles were located in a vertical plane, snapped to the grid, in the 2nd y grid cell extending from the water table down to the riverbed. We later applied a correction factor to account for the fact that the flow model placed the river at y = 0.

4.4.3 Cases

For each of the eleven realizations – one homogeneous, ten heterogeneous – of the four systems selected for demonstration, we simulated four breakthrough curves using SLIM. Detachment was specified at 5% of attachment, consistent with other studies [12, 18]:

case 1: conservative tracer

case 2: virus with constant attachment

case 3, "correlated:" virus with a spatially-variable filter factor calculated from filtration theory as described in section 4.4.1.2 and including the influence of heterogeneity in flow and hydraulic conductivity

case 4, "scrambled:" virus with a randomly variable filter factor as described in section 4.4.1.2

It is helpful to represent the removal due to attachment processes (ln C/C_0) for each of these cases in mathematical shorthand. As can be seen, case 2 is not a relevant basis of comparison, so we will not examine it further:

case 1: $removal = 0$

case 2: $removal = kt$

where k is a constant

case 3: $removal = f(v, K) * vt$

case 4: $removal = f(v', K') * vt$

where v' and K' represent values from a different random grid cell.

The 132 breakthrough curves from SLIM were then analyzed as follows. Each tracer breakthrough curve was fitted using CXTFIT v2.1 [48] in one-site kinetic non-equilibrium mode (described in the previous chapter) to obtain an estimate for the average pore velocity and the longitudinal dispersivity in that particular realization of the model domain. These macro-scale values for velocity and dispersivity were then applied to fit apparent macro-scale filter factors for the virus breakthrough curves from each domain using CXTFIT.

From the apparent macro-scale filter factors, apparent macro-scale collision efficiencies (α) were calculated using Eqn. 4-14. Note that the true, micro-scale value of α was held constant at 1×10^{-4} for cases 3 and 4. As reviewed previously, this general one-dimensional modeling approach to breakthrough curves from a three-dimensional system reflects common practice for field studies at sites where full subsurface characterizations and calibrated flow models are unavailable, although many of these are small monitoring studies with limited disruption of the natural groundwater flow pattern and for which the assumption of one-dimensional flow is expected to be a reasonable

approximation. As demonstrated by Scheibe *et al.* [18] for the case of a field injection and transport experiment, this approach also offers the opportunity to elucidate the relative contributions of attachment and flow heterogeneity in determining overall virus removal.

However, Scheibe *et al.* [18], like many researchers, worked on the basis of attachment rate constants rather than filter factors, so they scrambled k_{att} and not f to generate their fourth set of breakthrough curves. This approach is less realistic because it is equivalent to scrambling not only the CBFT-derived quantification of the attachment process (f), but also the distance each particle travels through the aquifer (v from the product $L = vt$). The flow field is thus scrambled as well, but only for the calculation of first-order removal by attachment processes, and not for the remainder of the advection-dispersion equation. In the present study, we avoid such an inconsistent treatment of the flow field by scrambling the filter factor alone.

4.5 Results and discussion

4.5.1 Domain and flow field

The steady-state water tables simulated in ParFlow for each of the RBF systems were in good agreement with the analytical solution from Eqn. 4-10. Figure 4-6 shows the simulated water table and the analytically predicted one for the homogeneous realization of each domain. The largest deviations were in the area around the river boundary, where simulated heads were as much as 28 cm lower than predicted analytically. However, the analytical solution was only an approximation, as it was derived for a confined aquifer. The water table profile was generally beginning to stabilize within 2-3 days of model time, but these simulations ran for 21 days of model

time, at which point the maximum rate of change in head at any point in the domain had decreased to less than 1 mm/d.

As expected, head profiles from heterogeneous realizations were not as smooth as those in Figure 4-6, but they were otherwise very consistent with the homogeneous profiles. A cutaway of a single realization of a heterogeneous hydraulic conductivity field is shown in Figure 4-7.

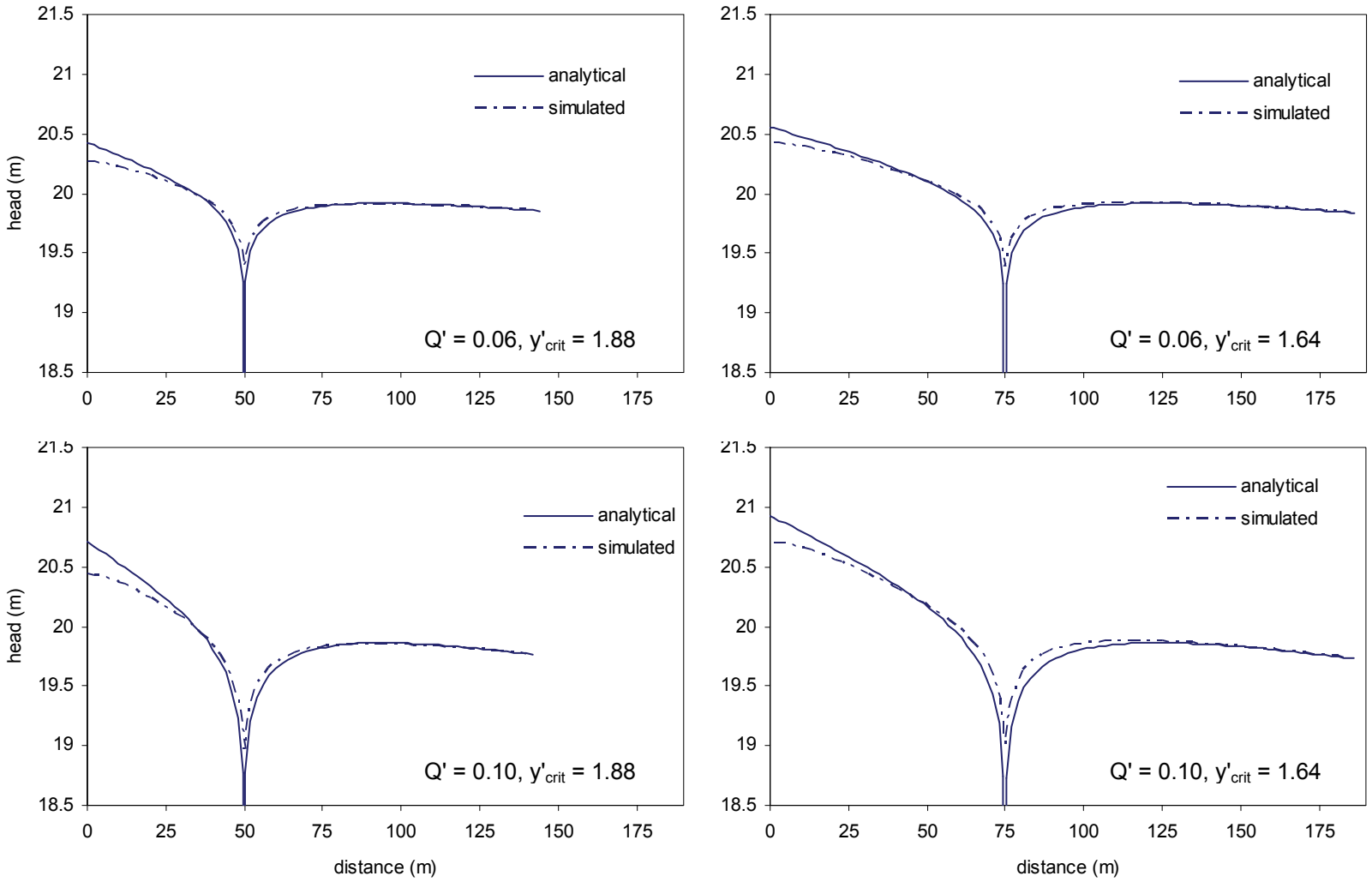

Figure 4-6. Simulated and theoretical water table elevations for the homogeneous realizations of four simulated riverbank filtration systems. The analytical solution is undefined at the well.

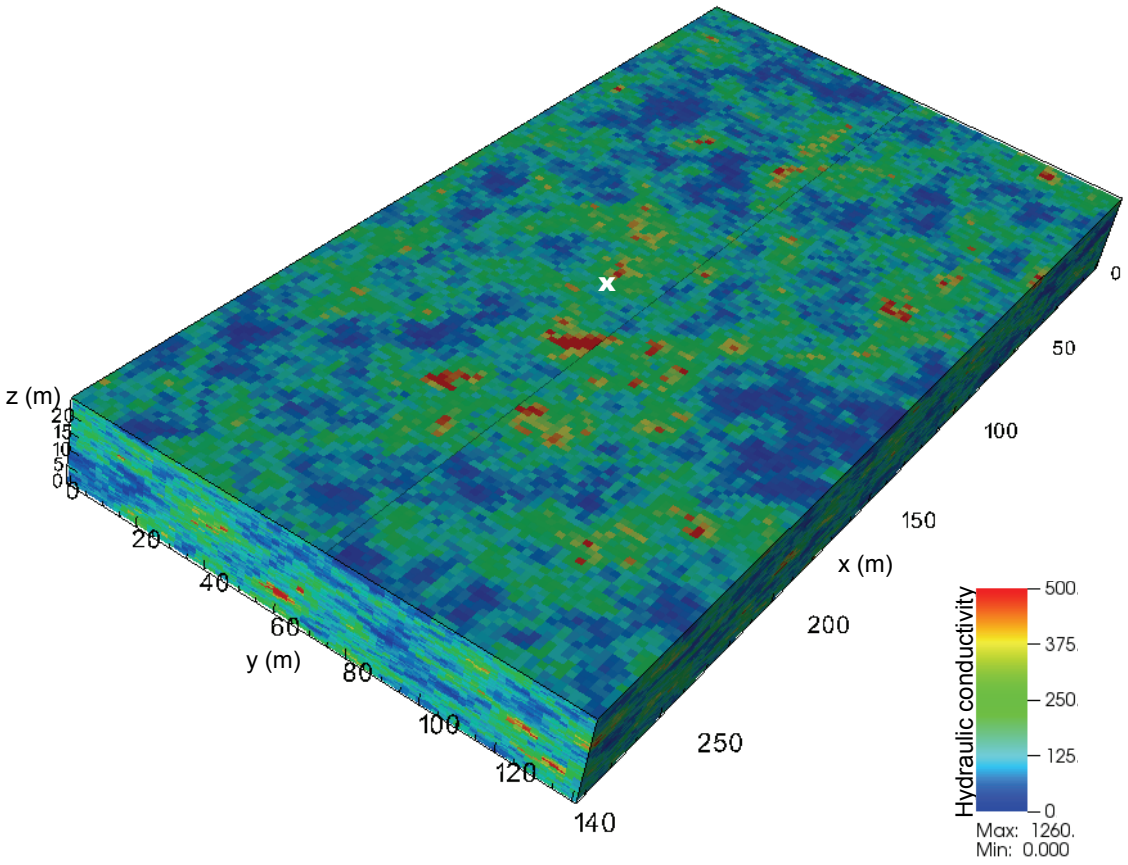

Figure 4-7. The heterogeneous hydraulic conductivity field for a single realization of the $Q' = 0.06$, $y'_{crit} = 1.88$ domain. Average $K = 125$ m/d, $\sigma_{lnK} = 0.4$. A small x denotes the location of the well at y = 50 m, centered in x at 142 m. The minimum value ($K = 0$) exists only in inactive grid cells, which are not shown.

4.5.2 Breakthrough curves

The simulated breakthrough curves for each of the four RBF domains are plotted in Figure 4-8, Figure 4-9, Figure 4-10, and Figure 4-11. The homogeneous realization of the domain (constant K) is shown with solid symbols, while an example of a single heterogeneous realization is plotted with open symbols. Virus breakthrough (b) was lower than tracer breakthrough (a) due to removal by filtration processes. As expected, a larger well setback distance and smaller pumping rate both contributed to lower virus breakthrough concentrations. Scrambling the field of filter factors to remove spatial correlation with flow and hydraulic conductivity further enhanced removals (c).

One-dimensional fits from CXTFIT are also shown for the simulated breakthrough curves. While the 1D model generally captures the timing of breakthrough, it often fails to match the peak concentration. For example, removals are over-estimated in the $Q' = 0.10$ case with the well at 50 m (y'_{crit} =1.88). Failure to capture the trailing edge of breakthrough reflects the distribution of travel times unaccounted for in a 1D model. The low levels of persistent virus ($C/C_0 \sim$ 5E-5) observed in all cases, and notably visible "growing in" in the scrambled simulation, are due to the combination of a specified low level of detachment and numerical noise. One-dimensional fits are particularly poor for these scrambled cases, so apparent filter factors in these systems are likely even higher than those estimated using CXTFIT.

To illustrate the variability of the heterogeneous domain, simulated breakthrough curves for all runs in a single system ($Q' = 0.10$, $y'_{crit} = 1.88$) are plotted in Figure 4-12. Compared to the homogeneous domain, physical heterogeneity introduces notable variability in the timing and magnitude of tracer or virus breakthrough.

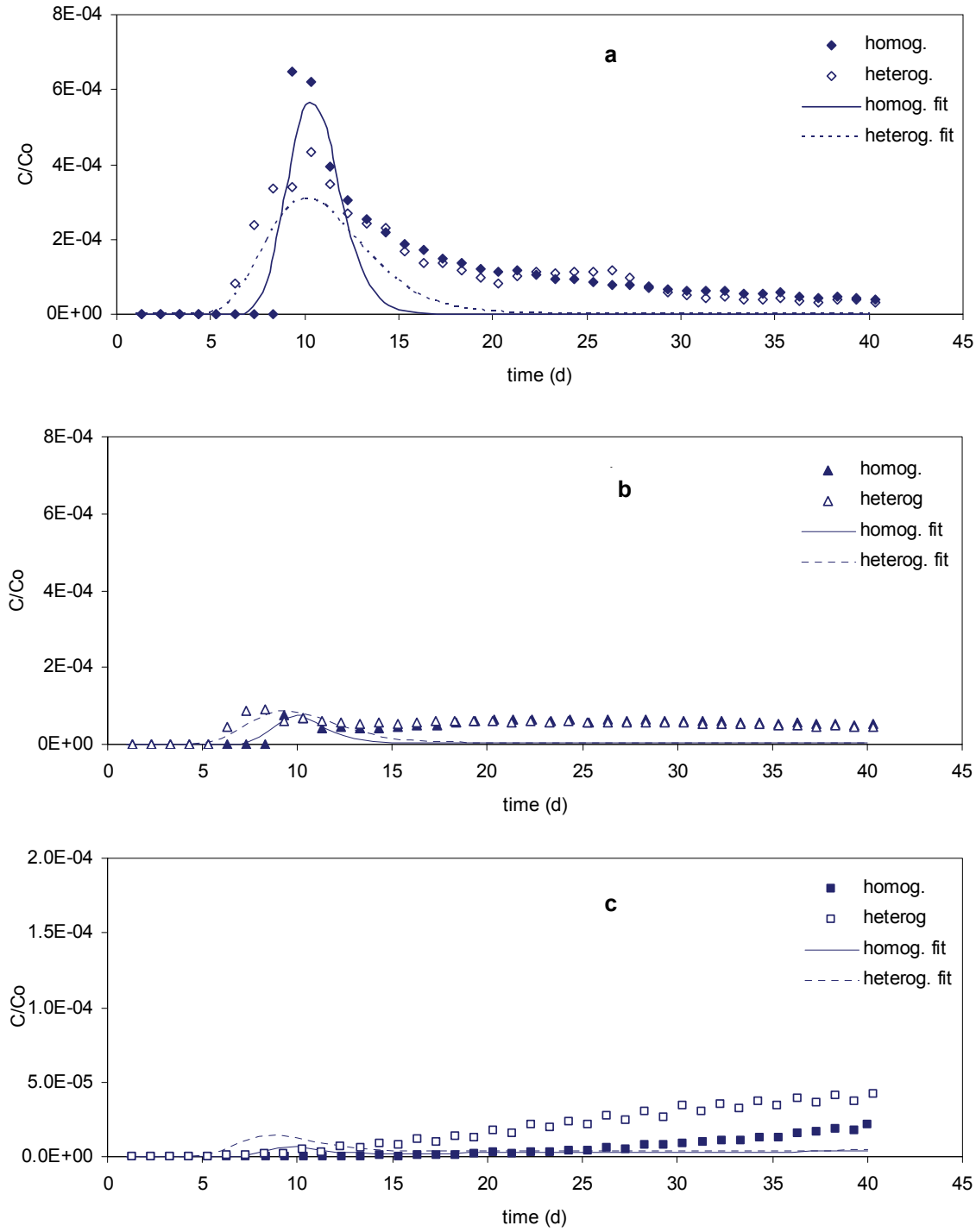

Figure 4-8. Simulated breakthrough curves and 1D model fits for (a) conservative tracer, (b) correlated filtration factor and (c) scrambled filtration factor in the Q' = 0.060, y'_{crit} =1.88 domain (low pumping rate, 50 m well setback). Results are shown for the homogeneous domain (K = 125 m/d) and for a single heterogeneous realization. Note the change in y-axis scale for (c).

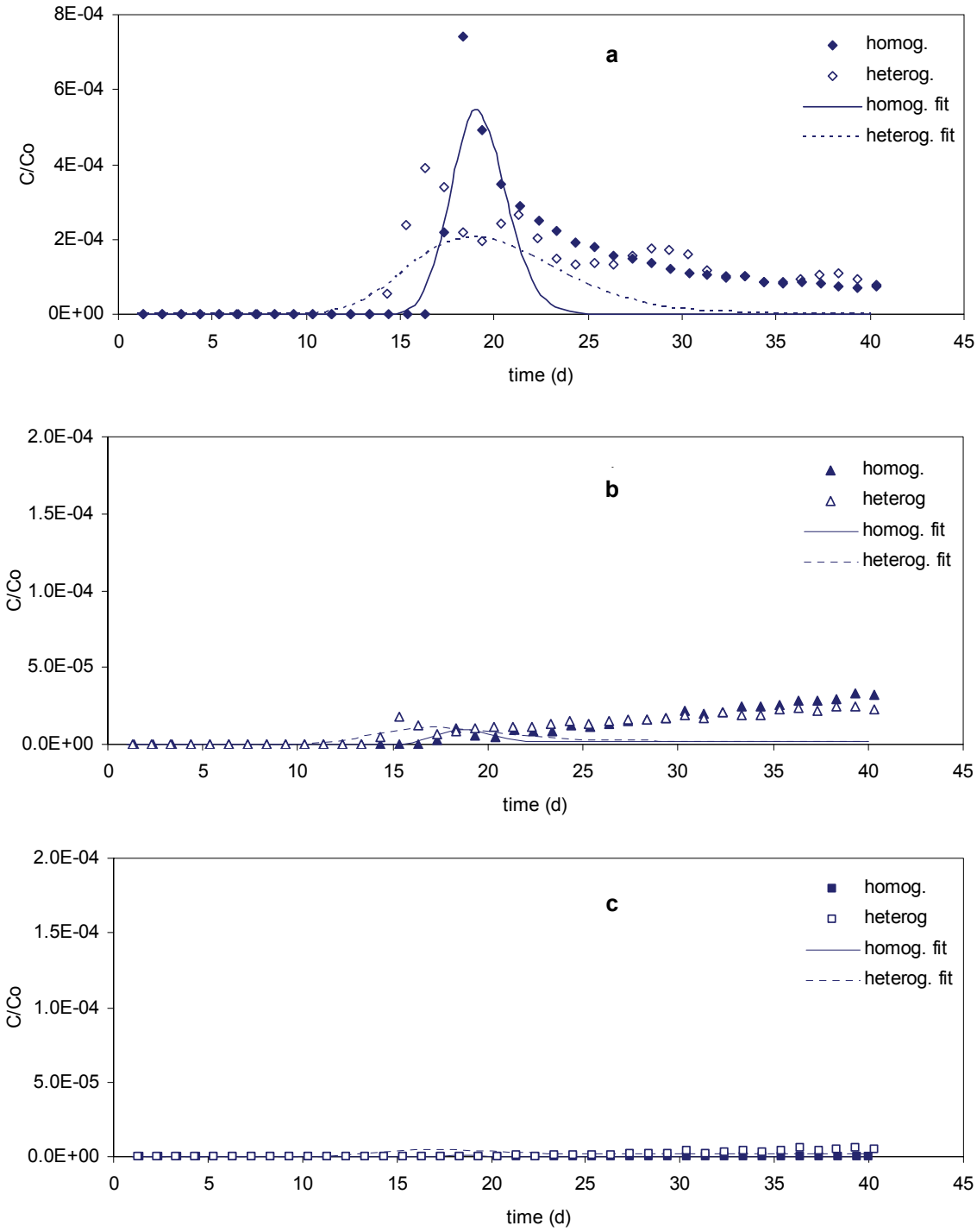

Figure 4-9. Simulated breakthrough curves and 1D model fits for (a) conservative tracer, (b) correlated filtration factor and (c) scrambled filtration factor in the Q' = 0.060, y'_{crit} =1.64 domain (low pumping rate, 75 m well setback). Results are shown for the homogeneous domain (K = 125 m/d) and for a single heterogeneous realization. Note the change in y-axis scale for (b) and (c).

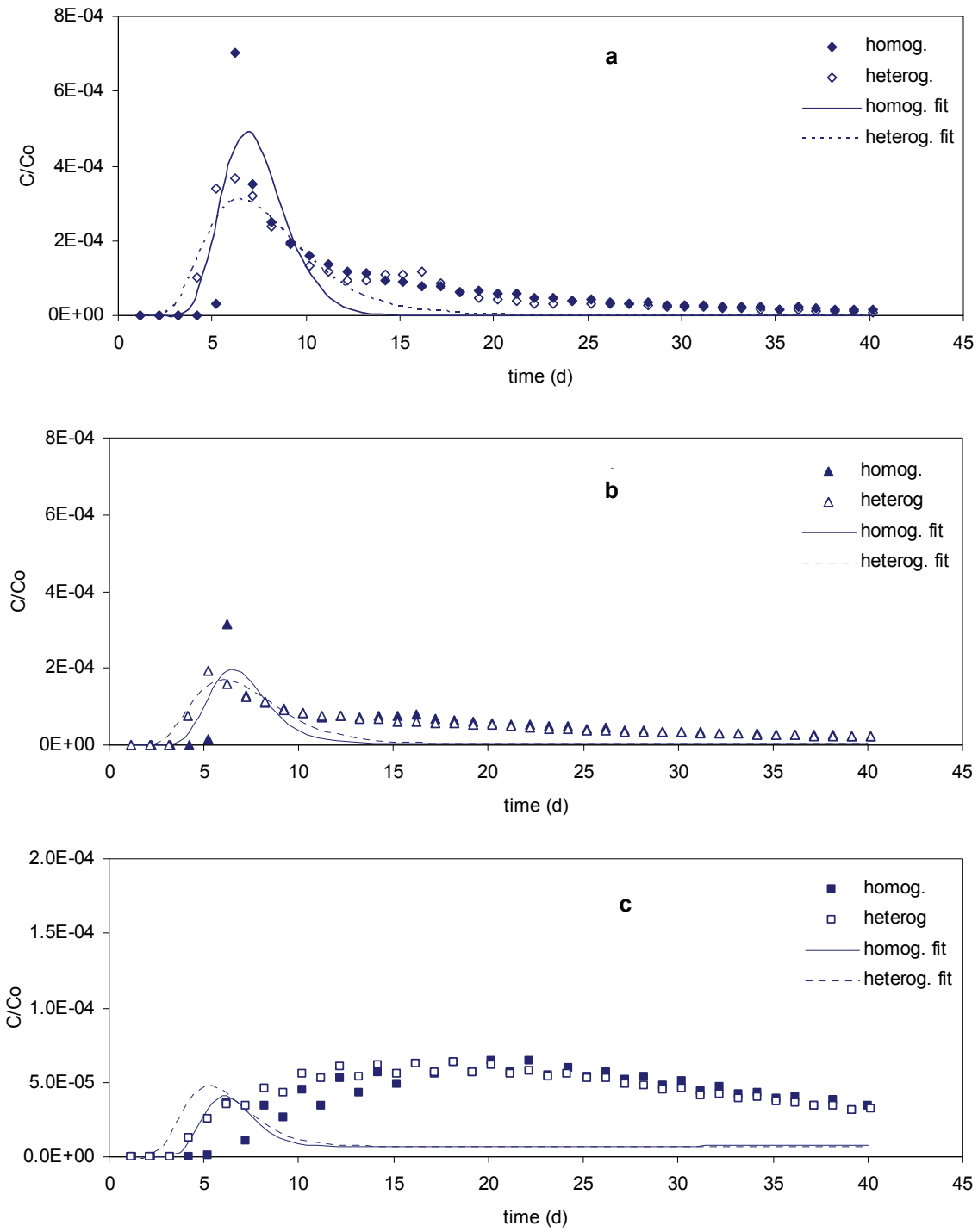

Figure 4-10. Simulated breakthrough curves and 1D model fits for (a) conservative tracer, (b) correlated filtration factor and (c) scrambled filtration factor in the Q' = 0.10, y'_{crit} =1.88 domain (high pumping rate, 50 m well setback). Results are shown for the homogeneous domain (K = 125 m/d) and for a single heterogeneous realization. Note the change in y-axis scale for (c).

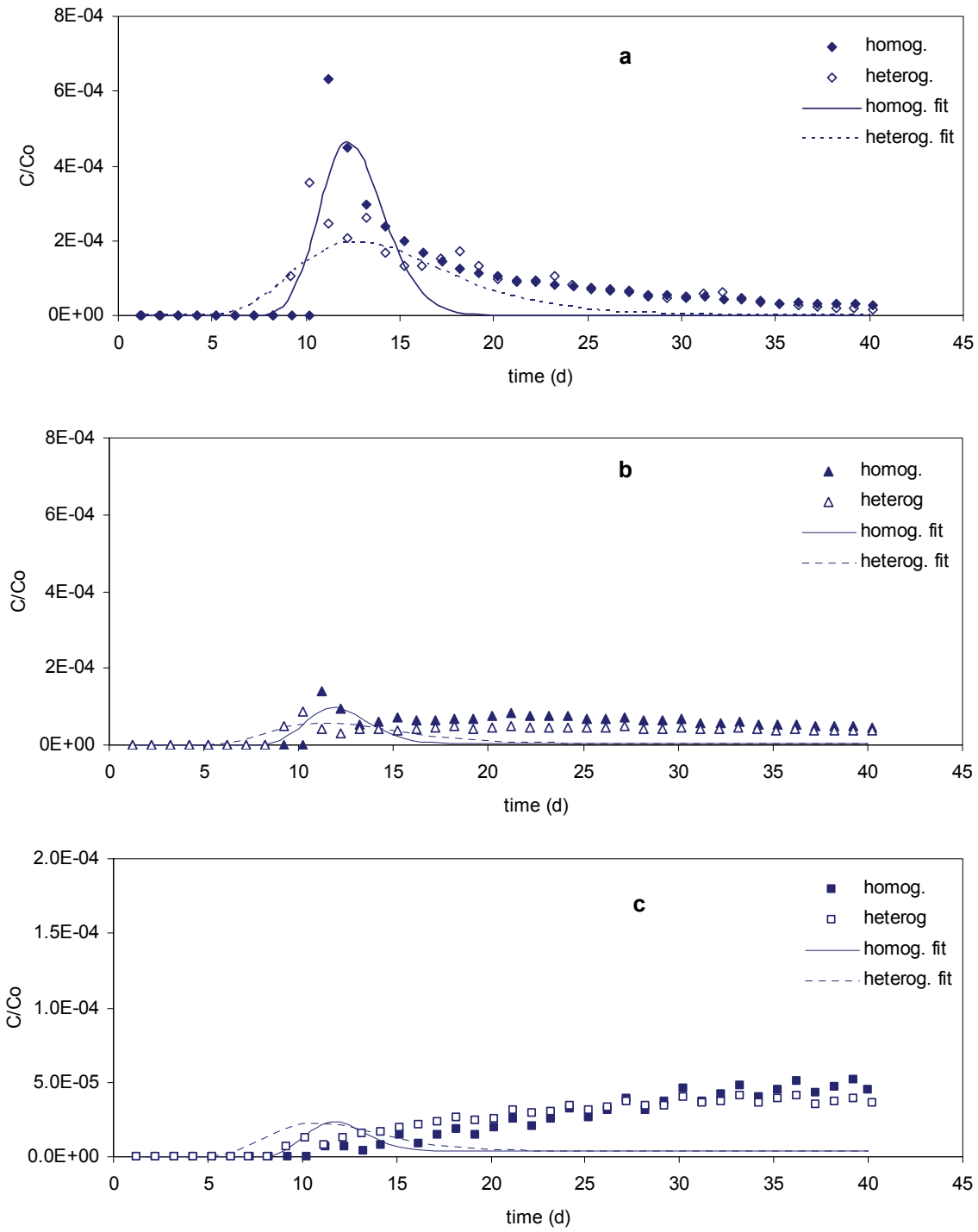

Figure 4-11. Simulated breakthrough curves and 1D model fits for (a) conservative tracer, (b) correlated filtration factor and (c) scrambled filtration factor in the Q' = 0.10, y'_{crit} =1.64 domain (high pumping rate, 75 m well setback). Results are shown for the homogeneous domain (K = 125 m/d) and for a single heterogeneous realization. Note the change in y-axis scale for (c).

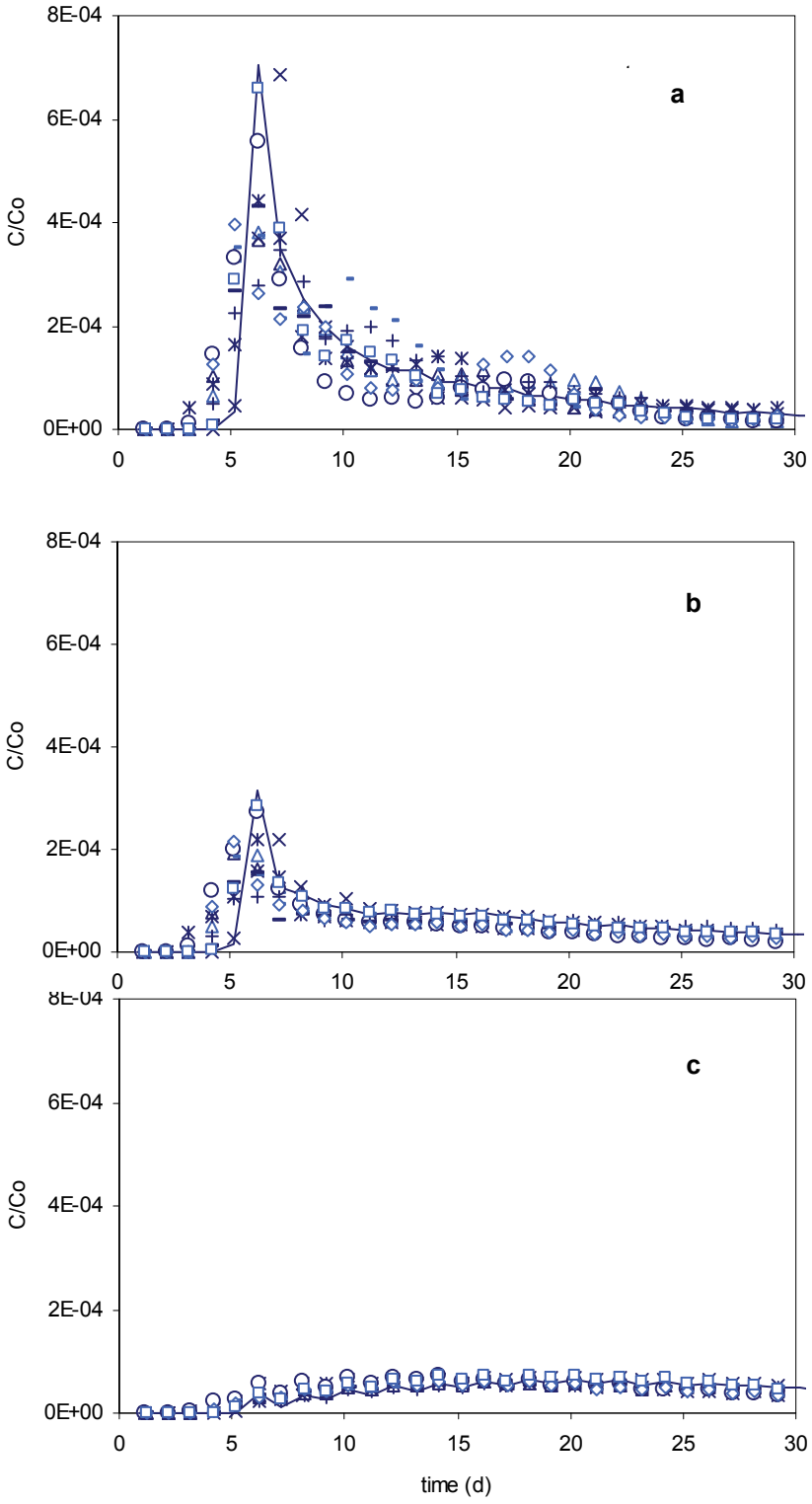

Figure 4-12. Simulated breakthrough curves for (a) conservative tracer, (b) virus with correlated *f*, and (c) virus with scrambled *f*. The homogeneous domain is represented with a solid line (not to be confused with a fit), while the ten heterogeneous realizations are each plotted with a different symbol.

4.5.3 Filter factor, *f*

Velocity, longitudinal dispersivity, normalized maximum breakthrough concentration (expressed as $\log_{10} C_{max}/C_0$), fitted filter factors, and calculated collision efficiencies for each case in each domain are listed in

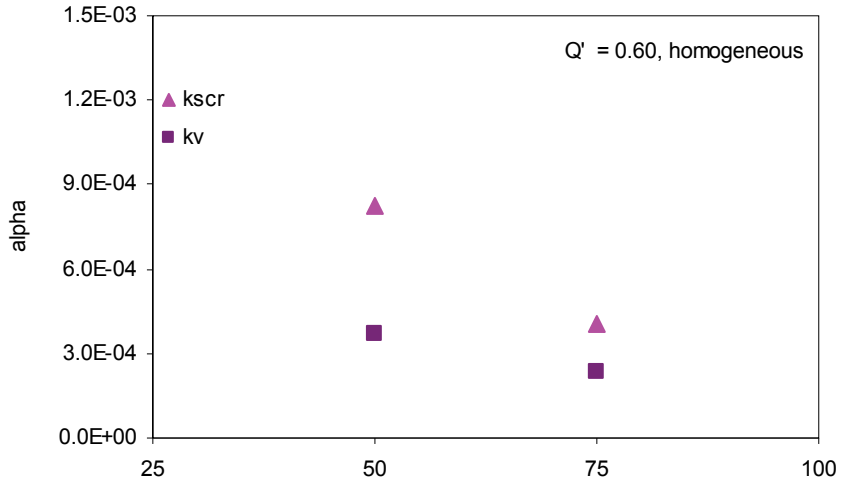

Figure 4-14. Apparent collision efficiency as a function of well setback for homogeneous (a, c) and heterogeneous (b, d) realizations of the low (a, b) and high (c, d) pumping domains. Solid symbols in (b) and (d) represent the average of the heterogeneous realizations. The y'crit values for systems with 50 m and 75 m well setback were 1.88 and 1.64, respectively.

Table 4-4. As expected, average pore velocities were lower for smaller pumping rates (lower Q') and larger setback distances (smaller y'_{crit}). Fitted dispersivity values (α_L) were appropriately smaller for homogeneous realizations than for heterogeneous ones, and largest where the flows were elevated and travel distances short.

4.5.3.1 Correlated filter factor

As expected, apparent filter factors were larger under lower pumping conditions ($f \sim 4\text{x}10^{-2}$, $Q' = 0.06$) than they were for domains with higher pumping ($f \sim$ 2-3 $\text{x}10^{-2}$, $Q' = 0.10$), reflecting the improved filtration efficiency of slower fluid flow (Figure 4-13). These apparent filter factors calculated from our hypothetical simulations are in agreement with those published in an extensive literature review of existing field transport studies, which gave the order of magnitude for length-based removal rates in RBF settings as typically 10^{-1} to 10^{-2} on a log per meter basis [13].

The solid square symbols in Figure 4-13 also illustrate the small decrease in apparent filter factor with increasing well setback that we observed consistently across all simulations. Filter factors increase wherever local velocities decrease, due to the inverse relationship between η_0 and v (see Eqn. 4-16), so the lower overall velocities in systems with greater well setbacks would logically lead to an increase in the apparent filter factor with distance. However, the observed effect was exactly the opposite. As explained below, this discrepancy is a consequence of using a 1D model to characterize a 3D system where f correlates spatially with flow.

The extent to which a system is defined by direct or circuitous flow is quantified by y'_{crit}. Larger values correspond to systems where flow is less direct. With a wider distribution of flow path lengths (and velocities and travel times), these high-y'_{crit} systems look less one-dimensional: the combination of the well setback, the pumping rate, and the hydrological characteristics of the system ensure that the areal extent of the well's zone of influence makes up a significant portion of the overall flow pattern that delivers river water to the well. Many of these flow paths take long, curved lines through the domain. Approximating high-y'_{crit} systems with a 1D model consequently underestimates actual flow velocities, because the circuitous flow pattern is ignored.

The underestimation of velocity for systems with high-y'_{crit} results in an overestimation of the apparent filter factor. Because the magnitude of this error depends primarily on the organization of the flow field, it is largely independent of Q'.

We might further expect lower y'_{crit} systems to exhibit reduced sensitivity to a change in Q', because the filtration efficiency of these systems (measured by f) is determined to a greater extent by removals in the relatively 1D portion of the flow field. However, this effect was not immediately apparent; a greater range of systems would need to be simulated.

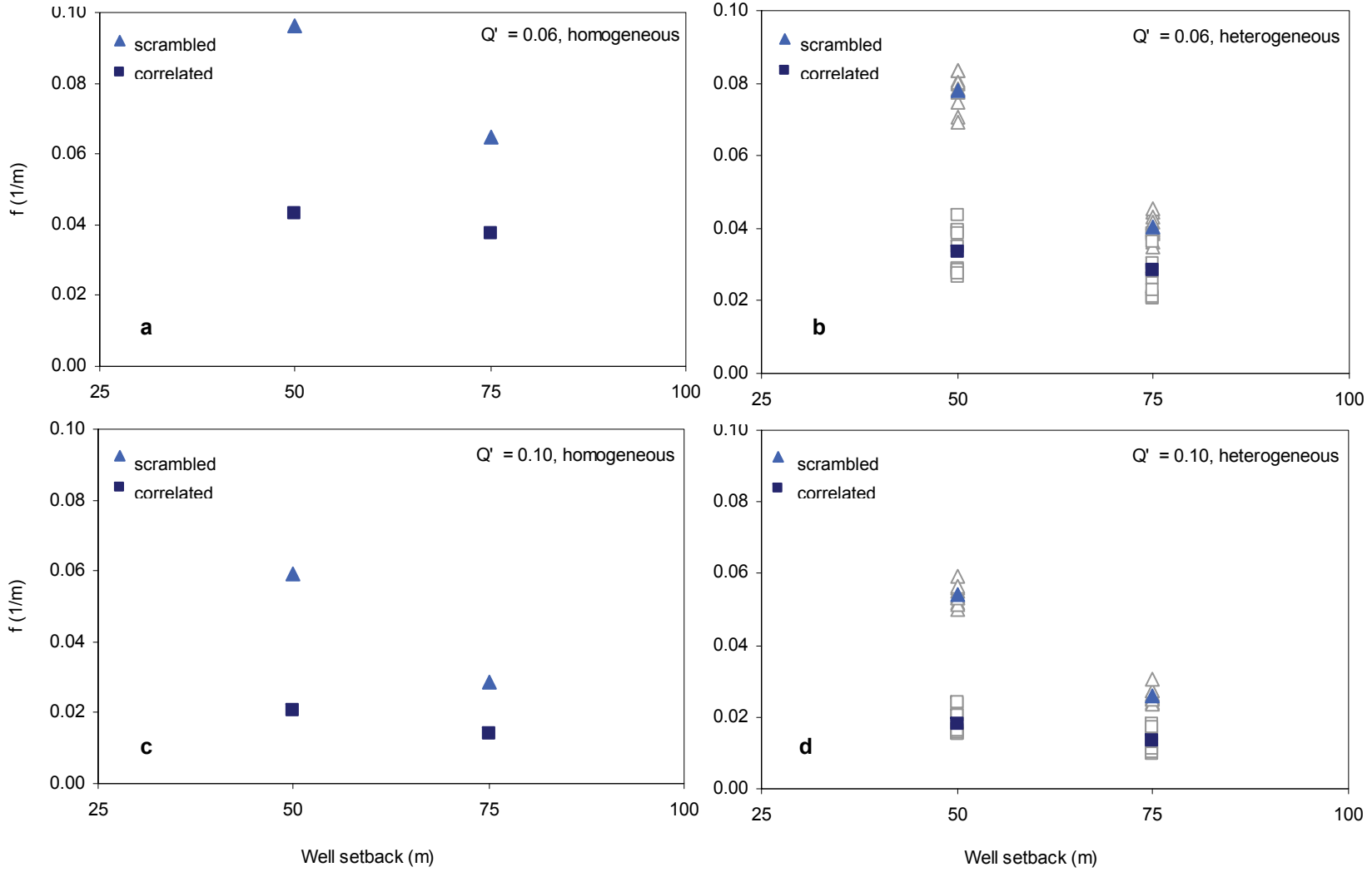

Figure 4-13. Apparent filter factor as a function of well setback for homogeneous (a, c) and heterogeneous (b, d) realizations of the low (a, b) and high (c, d) pumping domains. Solid symbols in (b) and (d) represent the average of the heterogeneous realizations. The y'crit values for systems with 50 m and 75 m well setback were 1.88 and 1.64, respectively.

If the hydraulic conductivity field is heterogeneous (Figure 4-13b and d), lower y'_{crit} values – here due to longer travel distances – slightly enhance sensitivity to heterogeneity for the correlated case. This is because the pumping-induced flow field samples a smaller portion of the domain in systems that look more one-dimensional.

In a heterogeneous domain, coarser grain sizes estimated from Eqn. 4-21 will decrease local *f* in areas with higher hydraulic conductivity. And because a local increase in *K* also corresponds to a local increase in velocity, the impact on local *f* is magnified. Since removal by filtration is an exponential function of length, not a linear one, local areas with low filter factors can contribute disproportionally to transport, so for the correlated case, the introduction of physical heterogeneity into the system must necessarily have an adverse effect on removals and thus on apparent macro-scale *f*. Indeed, the average apparent *f* from ten heterogeneous realizations of a given domain is invariably lower than the apparent *f* from the corresponding homogeneous domain. The change in average macro-scale *f* from homogeneous to heterogeneous simulations of a given RBF system is thus an indicator of the importance of local-scale filtration behavior in determining overall virus removal, regardless of the flow pattern.

The performance of a system with good overall virus removal can be hurt by a few low-removal areas which contribute significant virus breakthrough at the well, but a system where removal is already poor is little affected by either a further decrease in *f* or the presence of a few higher-*f* zones. As a result, systems with higher apparent filtration efficiency at a given y'_{crit} are expected to show greater sensitivity to physical heterogeneity. Furthermore, slower velocities in systems with lower pumping rates (lower Q') allow for greater relative influence of grainsize in the local *f*. For these

reasons, the heterogeneity-induced spread in apparent f is greater in the low pumping-rate system (Q' = 0.06) shown Figure 4-13b in than in the Q' = 0.10 system represented in Figure 4-13d.

Finally, we note that the effects of physical heterogeneity on system performance are at least equal in magnitude to those of the organization of the flow field (y'_{crit}) and very nearly as large as those due to the extent of pumping (Q'), underscoring the difficulty of predicting or even understanding the origins of RBF performance in the field without a site-specific characterization, at least for this portion of $y'_{crit} - Q'$ space.

4.5.3.2 Scrambled filter factor

That it is the correlation which matters between variability in f and variability in the fields of flow and hydraulic conductivity – and not merely the presence of a distribution of f values – is demonstrated by the scrambled case. Here, the spatial arrangement of filter factors was rearranged randomly without altering the actual "population" of values. The results of these scrambled simulations are plotted with diamond-shaped symbols in Figure 4-13.

Apparent f is significantly larger than it was in the correlated case across the board, because the lower filtration efficiency that was previously localized within the cone of depression and on the most direct flow paths to the well has now been randomly spread throughout the entire domain, replaced by systematically higher f values that were previously located in slower flow areas that have less influence on breakthrough. This increase in apparent f is naturally lesser in the heterogeneous realizations of domain, because variable hydraulic conductivity gives rise to both high and low filter factors independent of the spatial organization of the flow field, so the f values which replace

those within the cone of depression and on the most direct flow paths include some lower ones.

The general influence of y'_{crit} is similar in the scrambled case and the correlated one. The filter factor still appears to decrease with travel distance, but this time the change is far more dramatic. The underestimation of flow velocities and consequent artificial elevation of f at larger y'_{crit} still causes the apparent filter factor to seem to fall with distance, but this systematic error is no longer offset by the increase in the true local filter factors that arose from slower velocities at greater well setback in the correlated case. The decreased influence of y'_{crit} for the correlated case compared to the scrambled case is a measure of the scale-dependency introduced into apparent f by the 1D assumption.

The effect of Q' is, however, unaffected by scrambling: the $Q' = 0.10$ system still has a smaller apparent f and a reduced sensitivity to heterogeneity compared to the $Q' = 0.06$ system. The organization of the flow field, not the depth of the cone of depression, is what controls the relative influence of correlated heterogeneities in different systems.

4.5.4 Collision efficiency, α

The collision efficiency, α, is sometimes presented as a way "to exclude the effects of flow and diffusion" [12] from the attachment rate coefficient, thus focusing on the influence of the surface properties of the microbial particles and the aquifer grains. While this conceptualization of α is accurate in theory, it often falls short in practice. The necessity of back-calculating α from the apparent f or k_{att}, the average velocity, and an estimated grain size renders the collision efficiency little more than a fitted fudge factor. What role biological heterogeneity and surface interactions may play in particle

transport is buried in apparent α under the artifacts of inadequate modeling assumptions, oversimplification of physical/flow heterogeneity, and, in the case of field studies, the inherent scatter in field data. Indeed, the CBFT approach from which α is derived is recognized to be an oversimplification of complex natural processes [49, 50], especially when applied to field data. The assumptions it requires about such things as constant porosity, constant velocity, and the hydrodynamic field around spherical, uniform sand grains are unrealistic for field settings.

We report apparent collision efficiencies calculated from Eqn. 4-18 in

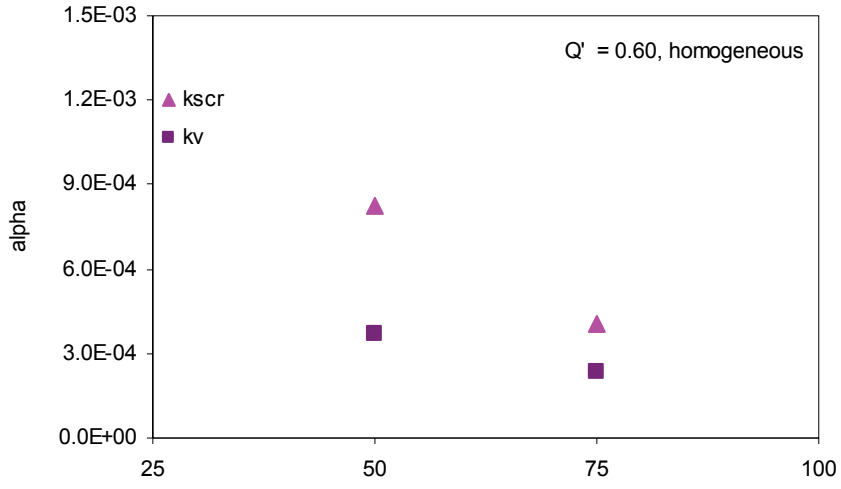

Figure 4-14. Apparent collision efficiency as a function of well setback for homogeneous (a, c) and heterogeneous (b, d) realizations of the low (a, b) and high (c, d) pumping domains. Solid symbols in (b) and (d) represent the average of the heterogeneous realizations. The y'crit values for systems with 50 m and 75 m well setback were 1.88 and 1.64, respectively.

Table 4-4 and in Figure 4-14 not to suggest a meaningful analysis of these numbers, but rather to add to the body of literature, e.g., references [18, 32], that has questioned the utility of extracting α from field breakthrough curves. The apparent collision efficiencies in our simulations were invariably higher than the constant value of $1x10^{-4}$ that we had specified for every grid cell in every realization. The mismatch depended strongly on y'_{crit} and, to a lesser extent, on Q'. Unsurprisingly, the discrepancy was minimized in systems that more closely approached the 1D behavior assumed for the calculation of apparent values.

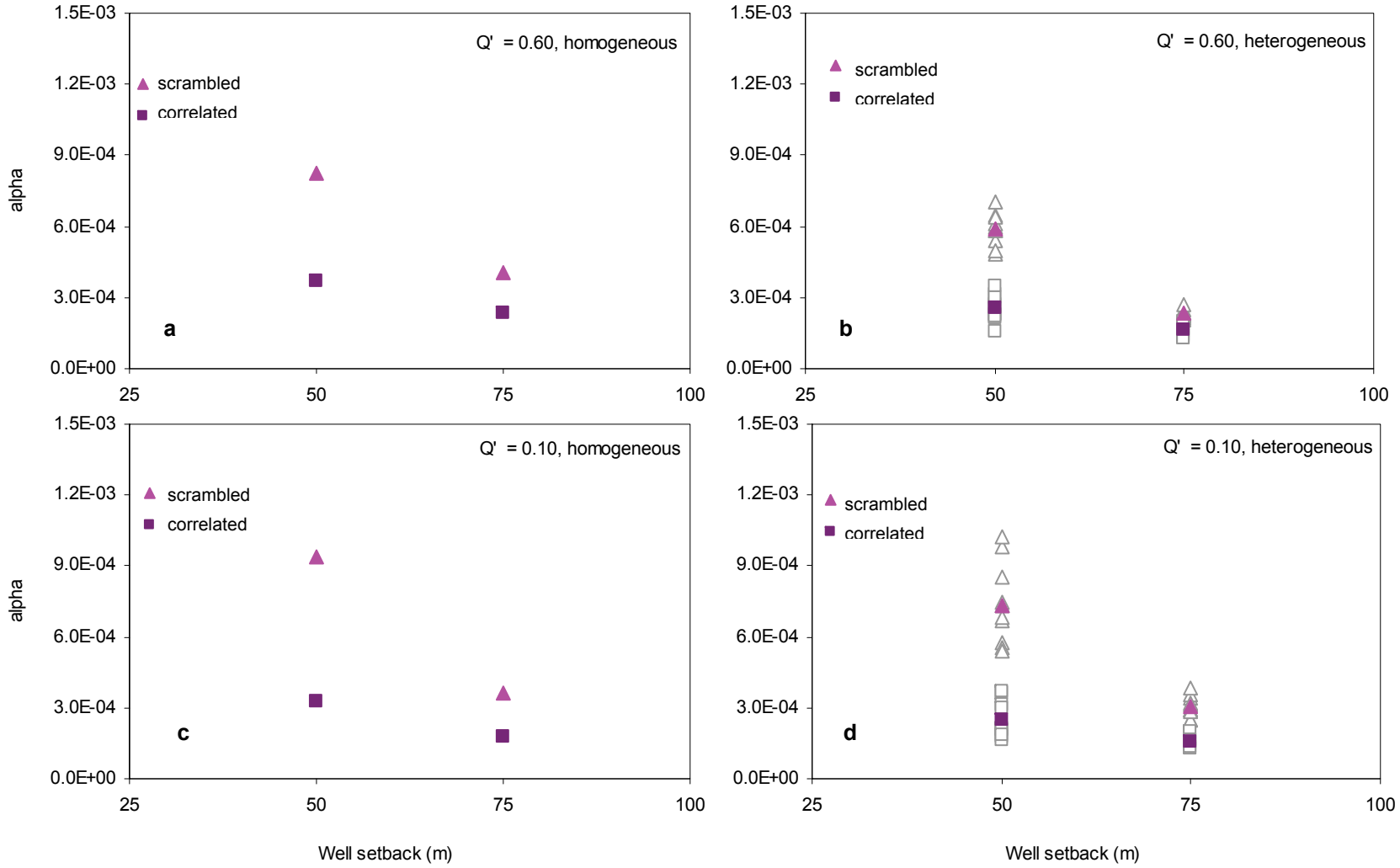

Figure 4-14. Apparent collision efficiency as a function of well setback for homogeneous (a, c) and heterogeneous (b, d) realizations of the low (a, b) and high (c, d) pumping domains. Solid symbols in (b) and (d) represent the average of the heterogeneous realizations. The y'crit values for systems with 50 m and 75 m well setback were 1.88 and 1.64, respectively.

Table 4-4. Transport parameters derived from simulated breakthrough curves including apparent velocity, filter factor and collision efficiency.

	homog.	**heterog.**										
	1	2	3	4	5	6	7	8	9	10	11	avg
Q' = 0.06, y'_{crit} =1.88												
tracer												
V (m/d)	4.71	4.51	4.42	4.25	4.41	4.96	3.76	3.82	4.35	4.50	4.84	4.38
D (m^2/d)	2.10	7.06	7.03	1.39	4.63	3.36	8.46	11.13	6.55	10.52	2.05	6.22
R^2	0.5562	0.4982	0.3388	0.7848	0.3510	0.7427	0.1761	0.2211	0.4760	0.2607	0.6864	
log C_{max}/C_o	-3.19	-3.36	-3.40	-3.15	-3.33	-3.24	-3.44	-3.33	-3.30	-3.40	-3.18	-3.31
α_L (m)	0.45	1.57	1.59	0.33	1.05	0.68	2.25	2.91	1.50	2.34	0.42	1.46
correlated												
log C_{max}/C_o	-4.12	-4.05	-3.91	-4.16	-4.16	-3.91	-4.43	-4.09	-4.19	-4.03	-4.01	-4.09
f	0.0433	0.0291	0.0282	0.0438	0.0349	0.0285	0.0390	0.0266	0.0394	0.0277	0.0384	0.0336
α	3.72E-4	2.31E-4	2.16E-4	3.14E-4	2.67E-4	2.66E-4	2.27E-4	1.59E-4	2.95E-4	2.20E-4	3.45E-4	2.54E-4
scrambled												
log C_{max}/C_o	-6.33	-5.15	-5.40	-5.82	-5.10	-4.91	-5.54	-5.42	-5.24	-5.27	-5.51	-5.34
f	0.0964	0.0749	0.0800	0.0809	0.0706	0.0692	0.0836	0.0833	0.0776	0.0803	0.0783	0.0779
α	8.27E-4	5.95E-4	6.13E-4	5.80E-4	5.41E-4	6.47E-4	4.86E-4	4.98E-4	5.81E-4	6.37E-4	7.04E-4	5.88E-4

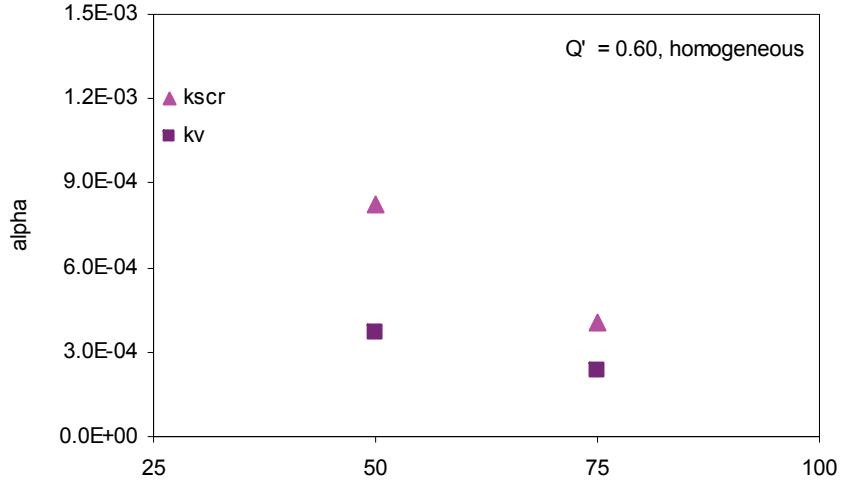

Figure 4-14. Apparent collision efficiency as a function of well setback for homogeneous (a, c) and heterogeneous (b, d) realizations of the low (a, b) and high (c, d) pumping domains. Solid symbols in (b) and (d) represent the average of the heterogeneous realizations. The y'crit values for systems with 50 m and 75 m well setback were 1.88 and 1.64, respectively.

Table 4-4 cont'd.

	homog.	heterog.										
	1	2	3	4	5	6	7	8	9	10	11	avg
Q' = 0.06, y'_{crit} =1.64												
tracer												
V (m/d)	3.90	3.74	4.00	3.91	4.13	3.78	3.29	3.65	3.40	3.60	3.99	3.75
D (m^2/d)	0.86	5.67	4.62	4.19	3.05	3.52	3.62	4.63	1.54	1.98	1.98	3.48
R^2	0.5341	0.2147	0.3495	0.4838	0.6592	0.4155	0.4056	0.4680	0.6075	0.5629	0.5151	
log C_{max}/C_o	-3.13	-3.41	-3.49	-3.50	-3.38	-3.48	-3.43	-3.45	-3.35	-3.40	-3.35	-3.42
α_L (m)	0.22	1.52	1.16	1.07	0.74	0.93	1.10	1.27	0.45	0.55	0.50	0.93
correlated												
log C_{max}/C_o	-4.96	-4.74	-4.46	-4.48	-4.36	-4.73	-5.29	-4.62	-5.23	-5.11	-4.72	-4.77
f	0.0374	0.0302	0.0207	0.0205	0.0212	0.0263	0.0385	0.0228	0.0380	0.0363	0.0281	0.0283
α	2.32E-4	1.74E-4	1.34E-4	1.28E-4	1.45E-4	1.54E-4	1.78E-4	1.26E-4	1.86E-4	1.96E-4	1.81E-4	1.60E-4
scrambled												
log C_{max}/C_o	-7.33	-6.00	-6.17	-6.04	-5.73	-6.17	-6.82	-6.22	-6.82	-6.65	-6.12	-6.28
f	0.0649	0.0394	0.0390	0.0360	0.0349	0.0399	0.0443	0.0385	0.0452	0.0432	0.0417	0.0402
α	4.02E-4	2.27E-4	2.52E-4	2.24E-4	2.38E-4	2.35E-4	2.05E-4	2.13E-4	2.21E-4	2.33E-4	2.69E-4	2.32E-4

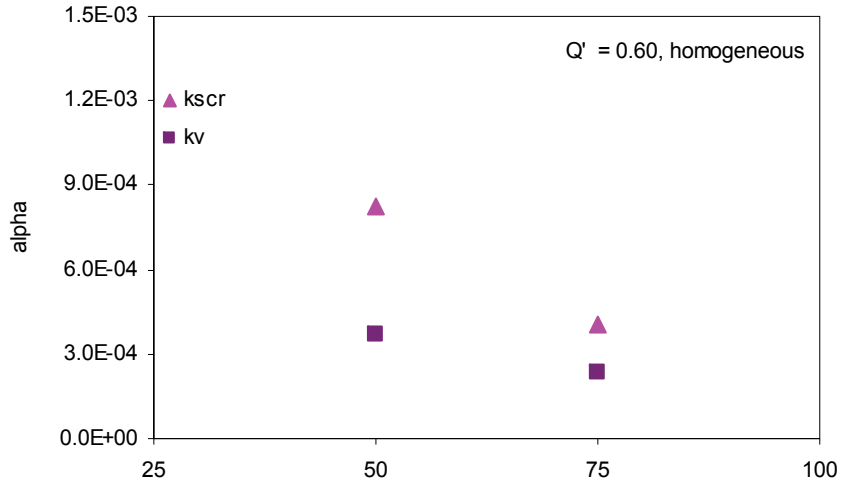

Figure 4-14. Apparent collision efficiency as a function of well setback for homogeneous (a, c) and heterogeneous (b, d) realizations of the low (a, b) and high (c, d) pumping domains. Solid symbols in (b) and (d) represent the average of the heterogeneous realizations. The y'crit values for systems with 50 m and 75 m well setback were 1.88 and 1.64, respectively.

Table 4-4 cont'd

	homog.	heterog.										
	1	2	3	4	5	6	7	8	9	10	11	avg
Q' = 0.10, y'_{crit} =1.88												
tracer												
V (m/d)	6.75	6.23	6.13	6.59	5.62	7.48	5.24	5.32	5.86	5.62	7.28	6.14
D (m^2/d)	9.06	21.71	21.28	4.96	25.05	13.54	21.14	22.82	20.61	32.00	8.86	19.20
R^2	0.6148	0.8067	0.7460	0.8919	0.5981	0.7845	0.7636	0.6777	0.7352	0.6548	0.7703	
log C_{max}/C_o	-3.15	-3.44	-3.42	-3.16	-3.35	-3.26	-3.46	-3.43	-3.37	-3.40	-3.18	-3.35
α_L (m)	1.34	3.49	3.47	0.75	4.46	1.81	4.04	4.29	3.51	5.69	1.22	3.27
correlated												
log C_{max}/C_o	-3.50	-3.71	-3.69	-3.66	-3.66	-3.56	-3.96	-3.74	-3.81	-3.67	-3.55	-3.70
f	0.0205	0.0152	0.0154	0.0238	0.0153	0.0167	0.0203	0.0157	0.0239	0.0161	0.0205	0.0183
α	3.25E-4	2.11E-4	2.08E-4	3.62E-4	1.77E-4	3.16E-4	2.09E-4	1.65E-4	2.98E-4	1.86E-4	3.70E-4	2.50E-4
scrambled												
log C_{max}/C_o	-4.35	-4.26	-4.30	-4.31	-4.18	-4.17	-4.34	-4.34	-4.31	-4.27	-4.24	-4.27
f	0.0591	0.0530	0.0553	0.0562	0.0419	0.0518	0.0538	0.0512	0.0533	0.0592	0.0565	0.0532
α	9.39E-4	7.33E-4	7.45E-4	8.55E-4	4.86E-4	9.81E-4	5.53E-4	5.41E-4	6.65E-4	6.86E-4	1.02E-3	7.26E-4

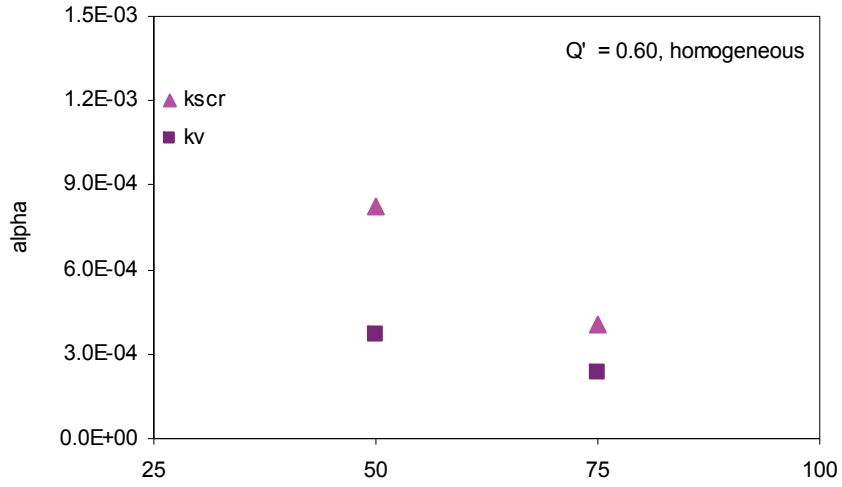

Figure 4-14. Apparent collision efficiency as a function of well setback for homogeneous (a, c) and heterogeneous (b, d) realizations of the low (a, b) and high (c, d) pumping domains. Solid symbols in (b) and (d) represent the average of the heterogeneous realizations. The y'crit values for systems with 50 m and 75 m well setback were 1.88 and 1.64, respectively.

Table 4-4 cont'd

	homog.	heterog.										
	1	2	3	4	5	6	7	8	9	10	11	avg
Q' = 0.10, y'_{crit} =1.64												
tracer												
V (m/d)	5.95	5.13	6.01	5.97	6.55	5.50	5.04	5.67	5.33	5.64	5.91	5.67
D (m^2/d)	4.26	18.12	13.07	14.72	7.79	14.29	8.00	10.59	4.02	5.29	11.55	10.74
R^2	0.6369	0.6334	0.6927	0.7370	0.8658	0.6395	0.7711	0.8069	0.8719	0.8087	0.5698	
log C_{max}/C_o	-3.20	-3.45	-3.50	-3.50	-3.36	-3.44	-3.43	-3.44	-3.34	-3.40	-3.40	-3.43
α_L (m)	0.72	3.54	2.18	2.46	1.19	2.60	1.59	1.87	0.75	0.94	1.96	1.91
correlated												
log C_{max}/C_o	-3.85	-4.06	-3.98	-4.00	-3.77	-4.10	-4.20	-4.01	-4.21	-4.21	-4.00	-4.05
f	0.0141	0.0147	0.0099	0.0100	0.0104	0.0124	0.0168	0.0112	0.0182	0.0172	0.0131	0.0134
α	1.80E-4	1.46E-4	1.28E-4	1.28E-4	1.57E-4	1.38E-4	1.61E-4	1.32E-4	1.92E-4	2.01E-4	1.65E-4	1.55E-4
scrambled												
log C_{max}/C_o	-4.83	-4.71	-4.60	-4.48	-4.34	-4.67	-4.83	-4.58	-4.86	-4.80	-4.72	-4.66
f	0.0286	0.0249	0.0263	0.0243	0.0236	0.0260	0.0256	0.0248	0.0271	0.0273	0.0305	0.0260
α	3.66E-4	2.47E-4	3.42E-4	3.12E-4	3.56E-4	2.90E-4	2.46E-4	2.92E-4	2.87E-4	3.18E-4	3.86E-4	3.08E-4

4.6 Conclusions

The interpretation of microbial removals in riverbank filtration settings is complicated by the complexity of the flow field relative to typical column studies or injection tests. While flow in such systems can often be reasonably represented as one-dimensional, the pumping wells of an RBF production field induce flow patterns that are definitely three-dimensional. Comparing different RBF systems is particularly troublesome unless they are carefully chosen to control which factors are held constant. We therefore developed a dimensionless framework to guide modeling simulations of RBF, using $y'_{crit} - Q'$ space to separate out the contribution of the pumping-induced distribution of flow path lengths to the overall filtration behavior of the system.

We demonstrated the application of this framework, selecting just four systems for further study. The results of our simulations underscore how a failure to fully account for correlations between physical/flow heterogeneities and attachment processes produces artificial scale dependency in macroscale estimates of parameters like f and α, which are commonly used to quantify the performance of subsurface passage as a process for microbial removal. We know of one other study [18] that has made such a demonstration, but it was not conducted in an RBF setting, and the nature of the scale-dependency was therefore different.

Despite a very limited number of realizations (ten), our stochastic approach suggested that flow heterogeneity from a pumping well field and physical heterogeneity from aquifer properties can counteract each other: while a less linear flow field improves removals and apparent filtration efficiency, heterogeneity in hydraulic conductivity hurts filtration performance on average. In the four systems in our study, the pumping rate

mattered more than well setback for determining the apparent filter factor, but the variability between individual heterogeneous realizations of the domain was almost as great as the differences between 3000 and 5000 m^3/d pumping rates.

The apparent lesser influence of the organization of the flow field – for which the well setback was a surrogate – on filter efficiency was due in part to the inaccuracies introduced by the 1D approximation of an apparent, macroscale *f*. A study involving a larger range of y'_{crit} values than we considered would further clarify the extent of the 1D inaccuracy. For a y'_{crit} controlled by varying the well setback, we hypothesize a U-shaped dip in the curve of apparent *f* vs. y'_{crit}. The small end of the y'_{crit} range represents lower-velocity, long setback systems with comparatively 1D flow patterns that could be well-approximated by an apparent *f*. The increase in average velocity as y'_{crit} rises should at first cause apparent *f* to fall, but as the 1D approximation becomes less and less accurate, underestimation of local velocities would cause apparent *f* to increase again, as we saw in our simulations.

A more exhaustive investigation, including not only a larger number of heterogeneous realizations, but also more study systems would help clarify the importance of pumping rate and well setback. Further work is need to investigate different aquifer configurations (slope, thickness) and hydraulic conductivity, including the distribution of *K* in heterogeneous domains. Comparison with a constant *f* case could also provide additional evidence to support the idea that scale-dependency of apparent filter parameters can be a modeling artifact.

The collision efficiency α was held constant in this study, but the importance of physical heterogeneity, particularly in the lower-y'_{crit} system we simulated, suggests that

heterogeneity in the biological characteristics reflected in α could have a significant impact on system performance. Future studies might consider the effect of a distribution of collision efficiencies. Other researchers have proposed the possibility of a spatial correlation between α and hydraulic conductivity [15, 33], with higher collision efficiencies associated with lower conductivity zones. Such a correlation would magnify the scale-dependency of the apparent filter factor estimated from 1D fitting of breakthrough curves. Further expansion of the simulation to include virus inactivation, commonly represented as a kinetic first-order process, would allow for a more complete investigation of the role of biological heterogeneity, which has the potential to be significant in at least some cases.

Use of the $y'_{crit} - Q'$ framework to guide these modeling studies should help to establish a typology of systems where e.g., simplifying 1D assumptions are less problematic, or the effects of biological heterogeneity will have little effect on filtration performance. An expansion and generalization of the dimensionless framework to include more types of flow patterns – including RBF sites with wells located in meander bends, on islands, or where regional flow patterns align with the river bed – would make it possible to contextualize the simulations by pinning a wide variety of real field sites to the model space.

4.7 References

1. UNESCO, *United Nations World Water Developement Report 4: Managing Water Under Uncertainty and Risk*. 2012, Paris: UNESCO CLD.
2. Hilborn, E.D., T.J. Wade, L. Hicks, L. Garrison, J. Carpenter, E. Adam, B. Mull, J. Yoder, V. Roberts, and J.W. Gargano, *Surveillance for waterborne disease outbreaks associated with drinking water and other nonrecreational water -- United States, 2009-2010.* MMWR Surveillance summaries: Morbidity and mortality weekly report. Surveillance summaries / CDC, 2013. 62(35): p. 714-720.
3. Penrod, S.L., T.M. Olson, and S.B. Grant, *Deposition kinetics of two viruses in packed beds of quartz granular media.* Langmuir, 1996. 12(23): p. 5576-5587.
4. Hahn, M.W. and C.R. O'Melia, *Deposition and reentrainment of Brownian particles in porous media under unfavorable chemical conditions: some concepts and applications.* Environmental Science & Technology 2004. 38(1): p. 210-220.
5. Walker, S.L., J.A. Redman, and M. Elimelech, *Influence of growth phase on bacterial deposition: Interaction mechanisms in packed-bed column and radial stagnation point flow systems.* Environmental Science & Technology, 2005. 39(17): p. 6405-6411.
6. Tufenkji, N. and M. Elimelech, *Correlation equation for predicting single-collector efficiency in physicochemical filtration in saturated porous media.* Environmental Science & Technology, 2004. 38(2): p. 529-536.
7. Abudalo, R.A., Y.G. Bogatsu, J.N. Ryan, R.W. Harvey, D.W. Metge, and M. Elimelech, *Effect of ferric oxyhydroxide grain coatings on the transport of bacteriophage PRD1 and Cryptosporidium parvum oocysts in saturated porous media.* Environmental Science & Technology, 2005. 39(17): p. 6412-6419.
8. Dong, H.L., T.C. Onstott, M.F. Deflaun, M.E. Fuller, T.D. Scheibe, S.H. Streger, R.K. Rothmel, and B.J. Mailloux, *Relative dominance of physical versus chemical effects on the transport of adhesion-deficient bacteria in intact cores from South Oyster, Virginia.* Environmental Science & Technology, 2002. 36(5): p. 891-900.
9. Foppen, J.W.A., S. Okletey, and J.F. Schijven, *Effect of goethite coating and humic acid on the transport of bacteriophage PRD1 in columns of saturated sand.* Journal of Contaminant Hydrology, 2006. 85(3-4): p. 287-301.
10. Walshe, G.E., L. Pang, M. Flury, M.E. Close, and M. Flintoft, *Effects of pH, ionic strength, dissolved organic matter, and flow rate on the co-transport of MS2 bacteriophages with kaolinite in gravel aquifer media.* Water Research, 2010. 44(4): p. 1255-1269.
11. Harvey, R.W. and S.P. Garabedian, *Use of colloid filtration theory in modeling movement of bacteria through a contaminated sandy aquifer.* Environmental Science & Technology, 1991. 25(1): p. 178-185.
12. Schijven, J.F., W. Hoogenboezem, S.M. Hassanizadeh, and J.H. Peters, *Modeling removal of bacteriophages MS2 and PRD1 by dune recharge at Castricum, Netherlands.* Water Resources Research, 1999. 35(4): p. 1101-1111.

13. Pang, L.P., *Microbial removal rates in subsurface media estimated from published studies of field experiments and large intact soil cores.* Journal of Environmental Quality, 2009. 38(4): p. 1531-1559.
14. Bhattacharjee, S., J.N. Ryan, and M. Elimelech, *Virus transport in physically and geochemically heterogeneous subsurface porous media.* Journal of Contaminant Hydrology, 2002. 57(3-4): p. 161-187.
15. Maxwell, R.M., C. Welty, and R.W. Harvey, *Revisiting the Cape Cod bacteria injection experiment using a stochastic modeling approach.* Environmental Science & Technology, 2007. 41(15): p. 5548-5558.
16. Maxwell, R.M., C. Welty, and A.F.B. Tompson, *Streamline-based simulation of virus transport resulting from long term artificial recharge in a heterogeneous aquifer.* Advances in Water Resources, 2003. 26(10): p. 1075-1096.
17. Rehmann, L.L.C., C. Welty, and R.W. Harvey, *Stochastic analysis of virus transport in aquifers.* Water Resources Research, 1999. 35(7): p. 1987-2006.
18. Scheibe, T.D., H.L. Dong, and Y.L. Xie, *Correlation between bacterial attachment rate coefficients and hydraulic conductivity and its effect on field-scale bacterial transport.* Advances in Water Resources, 2007. 30(6-7): p. 1571-1582.
19. Weaver, L., L.W. Sinton, L. Pang, R. Dann, and M. Close, *Transport of microbial tracers in clean and organically contaminated silica sand in laboratory columns compared with their transport in the field.* Science of The Total Environment, 2013. 443(0): p. 55-64.
20. Weiss, W.J., E.J. Bouwer, W.P. Ball, C.R. O'Melia, M.W. Lechevallier, H. Arora, and T.F. Speth, *Riverbank filtration - fate of DBP precursors and selected microorganisms.* Journal American Water Works Association, 2003. 95(10): p. 68-81.
21. Woessner, W.W., P.N. Ball, D.C. DeBorde, and T.L. Troy, *Viral transport in a sand and gravel aquifer under field pumping conditions.* Ground Water, 2001. 39(6): p. 886-894.
22. Schijven, J.F., G. Medema, A.J. Vogelaar, and S.M. Hassanizadeh, *Removal of microorganisms by deep well injection.* Journal of Contaminant Hydrology, 2000. 44(3-4): p. 301-327.
23. Schijven, J.F. and J. Šimůnek, *Kinetic modeling of virus transport at the field scale.* Journal of Contaminant Hydrology, 2002. 55(1-2): p. 113-135.
24. Anders, R. and C.V. Chrysikopoulos, *Virus fate and transport during artificial recharge with recycled water.* Water Resources Research, 2005. 41(10): p. W10415.
25. Dong, H.L., T.D. Scheibe, W.P. Johnson, C.M. Monkman, and M.E. Fuller, *Change of collision efficiency with distance in bacterial transport experiments.* Ground Water, 2006. 44(3): p. 415-429.
26. Mutsvangwa, C., B. Mutaurwa, M. Mazhandu, and M. Kubare, *Application of Harvey-Garabedian model for describing bacterial removal in Sand Abstraction Systems associated with ephemeral rivers.* Journal of Contaminant Hydrology, 2006. 88(1-2): p. 55-68.
27. Fitts, C.R., *Groundwater Science*. 2nd ed. 2013, Oxford: Elsevier.

28. Yao, K.M., M.M. Habibian, and C.R. O'Melia, *Water and waste water filtration - concepts and applications.* Environmental Science & Technology, 1971. 5(11): p. 1105-1112.
29. Logan, B., D. Jewett, R. Arnold, E. Bouwer, and C. O'Melia, *Clarification of clean-bed filtration models.* Journal of Environmental Engineering, 1995. 121(12): p. 869-873.
30. Rajagopalan, R. and C. Tien, *Trajectory analysis of deep-bed filtration with the sphere-in-cell porous media model.* AIChE Journal, 1976. 22(3): p. 523-533.
31. Van der Wielen, P., W. Senden, and G. Medema, *Removal of Bacteriophages MS2 and Phi X174 during transport in a sandy anoxic aquifer.* Environmental Science & Technology, 2008. 42(12): p. 4589-4594.
32. Pang, L.P., M. Close, M. Goltz, M. Noonan, and L. Sinton, *Filtration and transport of Bacillus subtilis spores and the F-RNA phage MS2 in a coarse alluvial gravel aquifer: Implications in the estimation of setback distances.* Journal of Contaminant Hydrology, 2005. 77(3): p. 165-194.
33. Ren, J.H., A.I. Packman, and C. Welty, *Correlation of colloid collision efficiency with hydraulic conductivity of silica sands.* Water Resources Research, 2000. 36(9): p. 2493-2500.
34. Ashby, S.F. and R.D. Falgout, *A parallel multigrid preconditioned conjugate gradient algorithm for groundwater flow simulations.* Nuclear Science and Engineering, 1996. 124: p. 145-159.
35. Jones, J.E. and C.S. Woodward, *Newton-Krylov-multigrid solvers for large-scale, highly heterogeneous, variably saturated flow problems.* Advances in Water Resources, 2001. 24(7): p. 763-774.
36. Kollet, S.J. and R.M. Maxwell, *Integrated surface-groundwater flow modeling: A free-surface overland flow boundary condition in a parallel groundwater flow model.* Advances in Water Resources, 2006. 29(7): p. 945-958.
37. Maxwell, R.M., *A terrain-following grid transform and preconditioner for parallel, large-scale, integrated hydrologic modeling.* Advances in Water Resources, 2013. 53: p. 109-117.
38. Tompson, A.F.B., R. Ababou, and L.W. Gelhar, *Implementation of the three-dimensional turning bands random field generator.* Water Resources Research, 1989. 25(10): p. 2227-2243.
39. Maxwell, R.M., *SLIM-FAST: A User's Manual V.4.* . 2010: GWMI 2010-01. 49 p.
40. Hazen, A., *Discussion of "Dams on sand foundations" by A.C. Koenig.* Transactions of the American Society of Civil Engineers, 1911. 73: p. 199-203.
41. Fisher, R.A. and F. Yates, *Statistical tables for biological, agricultural and medical research* 1938, London: Oliver & Boyd.
42. Childs, H., E. Brugge, B. Whitlock, J. Meredith, S. Ahern, D. Pugmire, K. Biagas, M. Miller, C. Harrison, G.H. Weber, H. Krishnan, T. Fogal, A. Sanderson, C. Garth, E.W. Bethel, D. Camp, O. Rübel, M. Durant, J.M. Favre, and P. Navrátil, *VisIt: An end-user tool for visualizing and analyzing very large data*, in *High Performance Visualization: Enabling Extreme-Scale Scientific Insight*. 2012, Chapman and Hall/CRC Press: Boca Raton. p. 357-372.

43. Schubert, J., *German experience with riverbank filtration systems*, in *Riverbank Filtration: Improving Source-water Quality*, C. Ray, G. Melin, and R.B. Linsky, Editors. 2002, Kluwer Academic Publishers: Dordrecht, the Netherlands. p. 364.
44. Hunt, H., J. Schubert, and C. Ray, *Conceptual design of riverbank filtration systems*, in *Riverbank Filtration: Improving Source-water Quality*, C. Ray, G. Melin, and R.B. Linsky, Editors. 2002, Kluwer Academic Publishers: Dordrecht, the Netherlands. p. 19-27.
45. Hubbs, S., K. Ball, D.L. Hass, and M.J. Robison, *Riverbank filtration construction options considered at Lousiville, Kentucky*, in *Riverbank Filtration: Improving Source-water Quality*, C. Ray, G. Melin, and R.B. Linsky, Editors. 2002, Kluwer Academic Publishers: Dordrecht, the Netherlands. p. 49-59.
46. Derx, J., A.P. Blaschke, A.H. Farnleitner, L. Pang, G. Blöschl, and J.F. Schijven, *Effects of fluctuations in river water level on virus removal by bank filtration and aquifer passage - A scenario analysis.* Journal of Contaminant Hydrology, 2013. 147: p. 34-44.
47. van Genuchten, M.T., *A closed-form equation for predicting the hydraulic conductivity of unsaturated soils.* Soil Science Society of America Journal, 1980. 44(5): p. 892-898.
48. Toride, N., F. Leij, and M.T. van Genuchten, *The CXTFIT Code for Estimating Transport Parameters from Laboratory of Field Tracer Experiments, Version 2.1, Research Report No. 137*. 1995, U.S. Salinity Laboratory, USDA, ARS, Riverside, CA.
49. Ginn, T.R., B.D. Wood, K.E. Nelson, T.D. Scheibe, E.M. Murphy, and T.P. Clement, *Processes in microbial transport in the natural subsurface.* Advances in Water Resources, 2002. 25(8-12): p. 1017-1042.
50. Tufenkji, N., *Modeling microbial transport in porous media: Traditional approaches and recent developments.* Advances in Water Resources, 2007. 30(6-7): p. 1455-1469.

5 Conclusion

5.1 The continuing concern of pathogens in drinking water

Thankfully, a combination of good sanitation practices and appropriate technologies for the production of drinking water preserves most of the modern, developed world from the waterborne epidemics which plagued cities in the 1800s, and which are still all too common in the developing world today. According to the U.S. Food and Drug Administration, the last major cholera outbreak in the US was in 1911, although sporadic cases have been recorded since [1].

However, this public health success story does not mean that waterborne pathogens are no longer of concern. Quite to the contrary, providing safe, pathogen-free drinking water is still a challenge, as evidenced by the 28 drinking water-associated disease outbreaks recorded in the United States by the CDC during the 2009-10 reporting period, the most recent for which data is available [2]. Cholera and yellow fever have been replaced – on a much smaller scale, fortunately – by such pathogens as the bacteria *E. coli* and *Campylobacter jejuni*, the protozoa *Giardia lamblia* and *Cryptosporidium parvum*, as well as Noroviruses and Rotaviruses. All are responsible for symptoms generally described as gastroenteritis. The gravity of the illness can range from minor discomfort to possible death, and immunocompromised individuals are generally considered to be at the greatest risk.

The control of waterborne pathogens in drinking water thus remains the subject of evolving legislation, and a constant concern for drinking water utilities. Drinking water treatment, including routine chlorination with the appropriate contact time, is effective in

removing bacterial pathogens, *Giardia*, and most viruses. *Cryptosporidium*, on the other hand, seems relatively resistant to all disinfection except UV irradiation [1]. All of these pathogens are ubiquitous in surface waters: sources include wastewater discharges, agricultural runoff, and storm water runoff [3]. Since surface waters frequently serve as a source of drinking water, improved processes for pathogen removal in water treatment as well as means of reducing pathogen concentrations in source water are naturally the subject of continuing research.

5.1.1 Riverbank filtration

Riverbank filtration (RBF) and a family of related processes fall somewhat in the category of a treatment technology and somewhat in the category of a means to improve source water quality. The principle of RBF is simple. Rather than treating surface water directly, a set of production wells is installed adjacent to the river. Pumping from these wells induces flow from the river, through the banks and alluvial aquifer system, and into the well, with the subsurface materials acting as a "natural" filter. As the water infiltrates, physicochemical, biological, and geochemical processes result in a reduction of contaminant concentrations compared to the raw surface water, thus improving water quality if and when the infiltrated water is subsequently recovered. Dilution of the infiltrating water with (generally higher-quality) groundwater can bring about further reductions in the concentrations of surface-derived contaminants [4].

RBF is widely recognized as an efficient and low-cost technology [5], with a track record of nearly 150 years in Europe [6]. More recent development of RBF sites in the US and, increasingly, in a number of Asian and South American countries, attests to the technology's versatility and global appeal. Research that contributes to understanding of

microbial transport in such coupled surface water–groundwater systems, particularly focusing on situations where enhanced pathogen transport may occur, has obvious relevance to engineering and water resources management decisions with public health implications in the US and abroad.

5.1.2 Research methodology

This dissertation took three different approaches to the same underlying question: how does heterogeneity of physical or biological origin affect microbial transport? Through laboratory studies characterizing microbial surface properties, an exploration of biological heterogeneity in a 1D model system, and simulations of virus transport in a heterogeneous 3D riverbank filtration setting, this thesis sought to contribute to the understanding of microbial transport through porous media in a drinking water supply context.

5.2 Results and applications

5.2.1 The influence of metabolic state on microbial surface properties

Laboratory studies of planktonic *S. oneidensis* MR-1 cultures confirmed the influence of metabolic state, represented by electron acceptor conditions and growth phase, on the surface properties of the organism. Discernable differences in zeta potential and apparent hydrophobicity (as measured by the MATH test) were detected between aerobic and anaerobic cultures. Results of extracellular polymeric substance (EPS) analysis were in qualitative agreement with the electrokinetic findings that nitrate-reducing cultures had lower net surface charge than aerobic cultures at log phase.

However, similar qualitative agreement between the results of cell surface characterization by MATH and electrokinetic analyses was not observed.

Comparison of these two data sets with each other and with the literature suggests that charge, non-polar interactions, and steric factors, all of which relate to the conformation of EPS macromolecules, contribute to adhesion and attachment behavior in complex ways. Many interactions – local, average, hydrophobic, steric, and electrostatic – contribute to attachment behavior, and our results indicate that their individual and net contributions can change under different microbial redox conditions, suggesting that further study of similar properties in biofilm systems are merited if we are to improve our understanding of bioparticle transport in the subsurface.

Data collected under iron-reducing conditions demonstrated that it is possible to culture *S. oneidensis* with ferric citrate and characterize its surface properties without interference from iron particulate matter. Furthermore, a modified ferrozine assay may be used to demonstrate dissimilatory iron reduction, but is matrix-sensitive.

Efforts to culture *S. oneidensis* and *P. aeruginosa* in a modified biofilm reactor failed to yield sufficiently reproducible biofilms for further analysis of biofilm surface properties under different redox conditions.

The results of our laboratory investigations highlight the importance of biological processes in microbial transport. They suggest that it is essential for researchers performing column transport studies to control the metabolic state of their organisms carefully to ensure the reproducibility of their results. Furthermore, that conducting such studies – complete with appropriate surface characterizations – using organisms grown under different redox conditions or held at different metabolic states could yield insights

about the complex matrix of factors controlling transport behavior. Nothing we observed refutes the hypothesis that biofilm coatings in porous media may likewise exhibit different surface characteristics under different redox conditions, and that the dynamics of the system could affect pathogen transport. Despite the difficulty of characterizing undisturbed biofilm growth in porous media, further research is clearly needed in this area.

Our findings that metabolic state affects transport-relevant bacterial surface properties have implications not only in RBF settings, but also in lakebank filtration, dune filtration, and soil aquifer treatment, as the levels of organic matter present in the infiltrating surface water in all of these systems can be high enough to allow the development of redox zonation in the subsurface. In contrast, engineered recharge operations such as aquifer storage and recovery (ASR) that involve high quality waters are less likely to be affected by microbial redox processes, although injection of oxic water into an anoxic formation could produce biological and geochemical changes relevant to pathogen transport.

5.2.2 Attachment sensitivity analysis and 1-D modeling of biofiltration heterogeneity

A sensitivity analysis of filtration theory's parameterization of attachment behavior demonstrated that the effects of heterogeneity in physical parameters contributing to k_{att} – notably velocity, grain size and porosity – play out in a space whose contours are established by biological and biogeochemical phenomena: the rate constant representing die-off or inactivation of microbial contaminants, and the apparent "stickiness" of these particles and of the sediment grain surfaces to which they may attach. Through their influence on the surface phenomena involved in k_{att}, high porosity,

low velocity, and coarse grain size all bring about enhanced sensitivity to biofiltration. All but the stickiest formations are expected to benefit from increases in inactivation.

Introducing a stochastic first-order biofiltration removal rate constant in conjunction with the advection-dispersion equation allowed us to use a set of hypothetical 1-dimensional CXTFIT case studies to examine the possible influence of biological heterogeneity on microbial removal in groundwater systems. Biological heterogeneity, represented by a log-normal distribution of biofiltration removal rate constants, had notably adverse impacts on system performance. The simplistic 1D model further demonstrated the potential for correlations between biogeochemical and geophysical heterogeneities to influence virus breakthrough in complex, varied, and sometimes counterintuitive ways due to the competing influences of different transport-related factors. Reapplying the recoded stochastic model to an existing field data set revealed both the inapplicability of the 1D model formulation and the limitations of CXTFIT's fitting algorithm.

To the extent that filtration theory can approximate microbial removal by attachment processes in a complex natural system – and this point is debatable, due to the simplifying assumptions built into filtration theory – the results of our sensitivity analysis underscore the critical role of the "biological" parameters (collision efficiency and inactivation) that contribute to microbial removal during subsurface passage. Our hypothetical 1D modeling exercise further demonstrated the potential for heterogeneity in biological parameters to affect microbial removals. These findings have implications for the characterization of field site performance, because biological processes are dynamic and may be affected by changes in hydrodynamics (pumping, river stage) and in the

quality of the infiltrating surface water, thus contributing uncertainty to overall system performance. When a network of monitoring wells is available to track conditions in a production well field, monitoring redox conditions and groundwater microbial community indicators may help to identify biological patterns that correlate with system performance over time.

5.2.3 Correlated physical and flow heterogeneities in a 3D RBF filtration model

We developed a dimensionless framework to guide 3-dimensional modeling simulations of RBF, using $y'_{crit} - Q'$ space to separate out the contribution of the pumping-induced distribution of flow path lengths to the overall filtration behavior of the system. We demonstrated the application of this framework, selecting four systems for further study. The results of our simulations underscore how a failure to fully account for correlations between physical/flow heterogeneities and attachment processes produces artificial scale dependency in macroscale estimates of parameters like f and α, which are commonly used to quantify the performance of subsurface passage as a process for microbial removal.

Our stochastic approach suggested that flow heterogeneity from a pumping well field and physical heterogeneity from aquifer properties can counteract each other: while a less linear flow field improves removals and apparent filtration efficiency, heterogeneity in hydraulic conductivity hurts filtration performance on average. In the four systems in our simulations, the variability between individual heterogeneous realizations of the domain was almost as great as the differences between 3000 and 5000 m^3/d RBF pumping rates.

The importance of physical heterogeneity in these simulations, particularly in the lower-y'_{crit} system we simulated, suggests that heterogeneity in biological characteristics affecting filtration could have a significant impact on system performance, particularly if biofiltration efficiency correlates with flow-field heterogeneity. Model simulations such as these thus have the potential to guide costly field studies by allowing researchers and water utilities to asses whether microbial performance at a given RBF site is likely to be particularly susceptible to swings in biofiltration, thus meriting a more extensive site characterization. And in situations where more extensive site monitoring does take place, the complementary use of a calibrated, site-specific model could help RBF operators to optimize pumping rates spatially in different portions of the well field so as to reduce the probability of pathogen breakthrough in wells that are most sensitive to changing biofiltration efficiency.

While the $y'_{crit} - Q'$ space is specific to RBF – and moreover to a specific and idealized RBF configuration where the pumping well is set back from a losing stream in an aquifer where the natural gradient can be approximated as sloping away from the river – the dimensionless approach outlined could be adapted and expanded to other RBF site configurations, as well as to contexts that involve a distribution of flow path lengths and travel times. These include non-steady-state operations, some dune filtration contexts, and systems like deep well injection and AS(T)R that involve a withdrawal- or injection-induced flow pattern. However, when the flow field between a potential source of microbial contamination and a down gradient receptor can be reasonably represented as one-dimensional, a non-dimensionalization that separates out the effect of flow path length will be unnecessary.

Our modifications to the SLIM particle-tracking code are applicable to a wide range of numerical simulations of microbial transport through porous media based on clean bed filtration theory (CBFT). The nature of the flow field is not important, so this approach is not limited to RBF contexts; it could also be applied to all sorts of column, pilot, field, or modeling studies where flow and hydraulic conductivity information can be represented at the scale of the model grid. The ability to calculate expected attachment locally could be used to study the effects of heterogeneity in the porous medium on microbial transport, and even to shed light on the shortcomings of the CBFT model. When properly calibrated, such a coupled flow and transport model is also suitable for risk assessment applications.

5.3 A regulatory perspective

Several published field experiments with bacteriophages have indicated that standard local well-siting practices may not be sufficient to protect drinking water wells from microbial contamination.

Investigations of MS2 and ϕX174 transport in an anoxic Dutch aquifer found that attenuation was lower than expected based on hydrologically similar but aerobic aquifers [7]. A rough risk-assessment calculation indicated that Dutch regulations requiring 60 days of subsurface travel would not be sufficiently protective if pathogenic viruses behave like MS2 in terms of transport and inactivation under anoxic conditions. This study came on the heels of a previous risk assessment for Dutch aquifers that concluded subsurface travel times would need to be extended to 1-2 years in order for the 95% confidence interval for the risk of pathogen infection due to drinking water consumption to remain below the legislated threshold of 10^{-4} per person per year [8].

A risk assessment analysis for a septic-influenced aquifer in Montana indicated that the state's minimum water supply well setback of 100 ft (30.5 m) would need to be increased by ~50% to be protective in this setting, assuming that pathogenic viruses behave like MS2 in the seeding study [9]. Similarly, Florida law requires only 0.6 m vertical distance between a septic drain field and the water table below, but a field study of bacteriophage PRD1 transport found hydraulic loading dependent removals of just 1.4-2.2 log units at a monitoring depth 0.6 m below a septic drain field located in well-sorted fine and very fine sand. Rainfall events during the study period reduced these removals by at least 1 log unit, indicating a the potential for transport of sewage-derived pathogens into groundwater when the water table is shallow [10].

The U.S. EPA has no regulatory authority over the siting of private wells or small community systems serving fewer than 25 individuals or 15 connections, so the minimum 50-ft well setback from septic tanks and drainfields (250 ft from manure stacks) listed on its website [11] are merely recommendations. Regulation of private wells falls to the states. As summarized in reference [12], 47 states specify minimum well setback distances from potential sources of microbial contaminants, ranging from 10 to 300 ft (3-91 m). Just over a third use a minimum setback of 50 ft (15.2 m), while another 30% use 75-100 ft (23-30.5 m). Twenty-nine states also add hydrologic criteria to guide well construction. Lest it go unmentioned, three states do not regulate the siting of wells with respect to potential sources of microbial contamination. Furthermore, siting rules with respect to microbial contamination sources do not address setback from surface water sources (i.e., RBF-type settings).

In light of the results of the hypothetical heterogeneity simulations conducted in this thesis, the results of numerous field studies published in the scientific literature, and the damning prevalence of illness traced to private groundwater wells in CDC statistics on drinking-water borne disease outbreaks [2, 13, 14], it is evident that the regulation of private wells in the U.S. provides at best patchy protection of human health. Careful site characterizations and ongoing monitoring are not feasible for private wells, yet the expense of drilling means that these wells are more likely to be installed in the shallow, unconfined aquifers that are most susceptible to contamination with surface-derived contaminants. Our modeling studies suggest that local heterogeneities could have a significant effect on microbial transport to drinking-water wells, and that dynamic biological conditions in the subsurface add further uncertainty, reinforcing the argument for conservative practices for the siting of private drinking water wells.

Regulation of municipal drinking water production falls with the remit of the U.S. EPA, so nationwide rules exist. The 1989 EPA Surface Water Treatment Rule (SWTR) required most plants producing drinking water from surface water or "groundwater under the influence of surface water" to provide 3-log (99.9%) removal/inactivation of *Giardia* protozoan cysts and 4-log (99.99%) removal/inactivation of enteric viruses. These rules include RBF facilities. The Long Term 2 Enhanced Surface Water Treatment Rule (LT2ESWTR, commonly called the LT2 rule) added further monitoring and treatment requirements, particularly concerning removal of *Cryptosporidium* oocysts.

EPA regulations establish removal credits for different types of treatment processes, and drinking water plants use these guidelines to combine different processes in order to achieve the required removal. Engineered filters generally receive between

1.0 and 2.5 log removal credit for *Giardia* and/or viruses, depending on the system. The LT2 rule established *Cryptosporidium* removal credits of 0.5 and 1.0 log for RBF systems with 25 and 50 ft groundwater flow path lengths, respectively [15]. The flow path length for vertical wells is defined as the distance between the limit of the 100 year flood plain and the well screen, while for horizontal wells it is shortest linear distance between the river bed and the closest lateral under normal flow conditions. To be eligible for these credits, the RBF well must be installed in a granular aquifer. A single core is required to establish the suitability of the formation: grains less than 1 mm in diameter must be present in at least 1% of the material and over 90% of the core length. Facilities must also monitor turbidity in finished water every 4 hours while riverbank filtration is in operation. Based on the results of a demonstration of performance study, states may grant removal credits to systems that would not otherwise meet the standard criteria. Similarly, states may grant additional credits to RBF systems that demonstrate better removals.

The LT2 rule's consideration of RBF does not address virus removal, so municipal drinking water providers must meet the SWTR's 4-log removal requirement via processes such as sand filtration, membrane treatment, and/or disinfection. That the LT2 criteria are length-based rather than travel-time based focuses on filtration and attachment processes, rather than inactivation, which makes sense for inactivation-resistant *Cryptosporidium* oocysts. The overall federal approach to regulation of RBF is thus quite conservative. Concerns about pathogen removal under all infiltration conditions – particularly during high-flow events that may simultaneously mobilize elevated levels of surface-derived contaminants, shorten flow paths, and disturb the

riverbed – mean that the high (3-5 log) microbial removal efficiencies often reported by researchers do not to translate to equivalent removal credits.

If the discretionary room for states to grant additional performance-based removal credits to RBF systems extended beyond *Cryptosporidium*, municipal RBF facilities might have more incentive to determine operational practices and site conditions (perhaps including biological characteristics) that optimized removal of viruses and bacteria. Decreased disinfectant dosing is probably unrealistic, but such site-specific knowledge would afford plant operators greater certainty in avoiding natural or pumping-induced scenarios that elevate the risk of microbial breakthrough in a production well.

In the absence of regulatory policies that create incentives for RBF site development, characterization, and optimization, American water utilities will have fewer reasons to pursue riverbank filtration and U.S. researchers may have fewer funded opportunities to advance understanding of the underlying processes. Despite growing global interest and the technology's long history in Europe, it seems unlikely that microbial removal performance will inspire further domestic RBF development. Ironically, a different quirk of the American regulatory system may make RBF more appealing in the arid southwest, where allocations of limited surface and groundwater resources do not always recognize the existence of a direct hydrologic connection between the two.

Work on microbial transport in the subsurface, however, is likely to be increasingly relevant as demands on water resources lead to the exploitation of lower quality supplies and even necessitate improved water reuse technologies. A more sophisticated understanding of the controls that physical and biological heterogeneity

exert on microbial transport should facilitate responsible, sustainable, and publicly acceptable development of water resources in the future.

5.4 Research needs

5.4.1 Groundwater biofilms and bioparticle transport

Information about the roles of biofilms in virus or bacteria removal in the subsurface is relevant to engineered systems where such biofilms are likely to form. Many of these systems involve some type of water reuse or reclamation, and they are likely to become more important in the face of future water scarcity. If microbially-induced subsurface redox conditions do play a significant role in determining pathogen removal, well operation and water recharge management might be optimized to favor the development of redox conditions where removals are highest, and risk-assessment analysis could help identify situations where regulation/practice may be insufficiently protective.

Other researchers have already demonstrated that biofilm surface properties can affect bacterial transport behavior via complex surface interactions [16]. Further research is needed to improve biofilm cultivation techniques and refine characterization methods so that transport-relevant particle-biofilm interactions can be investigated systematically under environmentally relevant conditions.

The presence of bacterial surface EPS has a profound impact not only on the overall retention of planktonic cells used in transport and deposition experiments, but also on the spatial variation of the deposition rate [17]. Similar effects may be expected when the surface where the bioparticles are deposited is also coated with biopolymers. Improved methods would allow researchers to approach questions such as:

- How do biofilm morphology, total biomass, cell counts, and EPS composition vary as a function of redox conditions?
- How do surface charge, surface hydrophobicity, and zeta potential of a biofilm vary as a function of redox conditions?
- Does the presence of biofilm under different redox conditions affect model particle removal in filtration systems?

Information about the roles of biofilms in virus or bacteria removal in the subsurface is relevant to engineered systems where such biofilms are likely to form. Many of these systems involve some type of water reuse or reclamation, and they are likely to become more important in the face of future water scarcity. If microbially-induced subsurface redox conditions can be established to play a significant and predictable role in determining pathogen removal, well operation and water recharge management might be optimized to favor the development of redox conditions where removals are highest, and risk-assessment analysis could help identify situations where regulation or practice may be insufficiently protective. Such advances in applications will rest on advances in fundamental understanding of biofilm properties and their influence on bioparticle transport.

5.4.2 Heterogeneity modeling

Since complete physical characterization of a field site is impractical, further research is needed to link physical properties (represented stochastically, if need be) with biological ones to facilitate the estimation of biofiltration performance in heterogeneous, 3D space.

Stochastic approaches that separate attachment, detachment, and inactivation and re-calculate the contributions of each stepwise in a heterogeneous flow field can decouple time-based removal mechanisms (inactivation) from surface-based filtration phenomena that scale with time only under constant velocity assumptions. The more realistic framework of such approaches may yield insights about the nature and magnitude of the effects of biological heterogeneity. However, such theoretical investigations into the potential effects of physical and biological heterogeneities, let alone correlations between them, will be hard to validate at field scale because deposition profiles are rarely available for field transport studies. Improved methods for the collection and analysis of solution-phase breakthrough concentrations may help compensate for missing attached-phase concentrations data. Finally, more research is needed into the parameterization and possible correlation of biological and physical heterogeneities at multiple length scales within the same system.

Ultimately, modeling – and indeed engineering – exercises must find a compromise between the inaccuracies of oversimplification and the expense of exhaustive complexity. Further work is needed in sensitivity analysis of RBF-type systems to determine when simplifying assumptions and effective parameters can be used, and when heterogeneities of physical and/or biological origin will need to be accounted for if model results are to be useful. Cross-fertilization between filtration-type models and approaches developed in the hydrologic sciences to characterize complex watersheds and uncertain travel times may also yield insights about microbial removal processes and associated uncertainties.

5.5 References

1. USFDA, *Bad Bug Book, Foodborne Pathogenic Microorganisms and Natural Toxins*. 2nd ed. 2012.
2. Hilborn, E.D., T.J. Wade, L. Hicks, L. Garrison, J. Carpenter, E. Adam, B. Mull, J. Yoder, V. Roberts, and J.W. Gargano, *Surveillance for waterborne disease outbreaks associated with drinking water and other nonrecreational water -- United States, 2009-2010.* MMWR Surveillance summaries: Morbidity and mortality weekly report. Surveillance summaries / CDC, 2013. 62(35): p. 714-720.
3. Azadpour-Keeley, A., B.R. Faulkner, and J.-S. Chen, *Movement and Longevity of Viruses in the Subsurface*. 2003, US EPA National Risk Management Research Laboratory, Cincinnati, Ohio. p. 24.
4. Kuehn, W. and U. Mueller, *Riverbank filtration - An overview.* Journal American Water Works Association, 2000. 92(12): p. 60-69.
5. Tufenkji, N., J.N. Ryan, and M. Elimelech, *The promise of bank filtration.* Environmental Science & Technology, 2002. 36(21): p. 422A-428A.
6. Schubert, J., *Hydraulic aspects of riverbank filtration - field studies.* Journal of Hydrology, 2002. 266(3-4): p. 145-161.
7. Van der Wielen, P., W. Senden, and G. Medema, *Removal of Bacteriophages MS2 and Phi X174 during transport in a sandy anoxic aquifer.* Environmental Science & Technology, 2008. 42(12): p. 4589-4594.
8. Schijven, J.F., J.H.C. Mulschlegel, S.M. Hassanizadeh, P.F.M. Teunis, and A.M. de Roda Husman, *Determination of protection zones for Dutch groundwater wells against virus contamination - uncertainty and sensitivity analysis.* Journal of Water and Health, 2006. 4(3): p. 297-312.
9. DeBorde, D.C., W.W. Woessner, B. Lauerman, and P.N. Ball, *Virus occurrence and transport in a school septic system and unconfined aquifer.* Ground Water, 1998. 36(5): p. 825-834.
10. Nicosia, L.A., J.B. Rose, L. Stark, and M.T. Stewart, *A field study of virus removal in septic tank drainfields.* Journal of Environmental Quality, 2001. 30(6): p. 1933-1939.
11. U.S. EPA. *Private Wells: Basic Information*. [Accessed July 21, 2015]; Available from: http://water.epa.gov/drink/info/well/basicinformation.cfm.
12. Job, C.A., *Groundwater Economics*. 2010, Boca Raton: CRC Press.
13. Blackburn, B.G., G.F. Craun, J.S. Yoder, V. Hill, R.L. Calderon, N. Chen, S.H. Lee, D.A. Levy, and M.J. Beach, *Surveillance for waterborne-disease outbreaks associated with drinking water--United States, 2001-2002.* MMWR Surveillance summaries: Morbidity and mortality weekly report. Surveillance summaries / CDC, 2004. 53(8): p. 23-45.
14. Brunkard, J.M., E. Ailes, V.A. Roberts, V. Hill, E.D. Hilborn, G.F. Craun, A. Rajasingham, A. Kahler, L. Garrison, L. Hicks, J. Carpenter, T.J. Wade, M.J. Beach, and J.S. Yoder, *Surveillance for waterborne disease outbreaks associated with drinking water -- United States, 2007-2008.* MMWR Surveillance

summaries: Morbidity and mortality weekly report. Surveillance summaries / CDC, 2011. 60(SS12): p. 38-68.
15. U.S. EPA, *The Long Term 2 Enhanced Surface Water Treatment Rule (LT2ESWTR) Implementation Guidance, EPA 816-R-07-006*. 2007, Office of Water.
16. Liu, Y. and J. Li, *Role of Pseudomonas aeruginosa biofilm in the initial adhesion, growth and detachment of Escherichia coli in porous media.* Environmental Science & Technology, 2008. 42(2): p. 443-449.
17. Liu, Y., C.H. Yang, and J. Li, *Influence of extracellular polymeric substances on Pseudomonas aeruginosa transport and deposition profiles in porous media.* Environmental Science & Technology, 2007. 41(1): p. 198-205.

Appendix I. Bacteriophage MS2 studies

I.1 Background

The male-specific (F+) coliphage MS2 is frequently used as a surrogate in laboratory and field transport investigations, because its low attachment in sandy soils, similar size to pathogenic noroviruses, and low inactivation rates at pH and temperature conditions typical of groundwater make it relatively conservative (as reviewed in [1]).

MS2 is a small, single-stranded RNA virus with a diameter of 26 nm [2]. Its icosahedral capsid has no envelope, and is formed from 180 copies of a coat protein, plus one copy of the A protein, which is essential for infectivity. The 3-dimensional structure of the coat protein is known [3, 4], and measured electrophoretic mobilities agree well with model predictions of surface charge based on the presence of lysine, glutamic acid and aspartic acid residues in the two α-helices that form the exposed outer surface of the coat protein [5]. The zeta potential of MS2 calculated from electrophoretic mobility measurements in 0.01M NaCl has been reported at -17.7±2.3 mV (at pH 7), with the isoelectric point at pH 3.5 [6]. Furthermore, the electrophoretic mobility is essentially constant at pH above 5, indicating that MS2 has a negative charge that does not change much over the pH range that is environmentally relevant. Two hairpin loop structures that project from the surface of the MS2 capsid have hydrophobic qualities and have been suggested to be involved in "steric" interactions that could explain why MS2 deposition can be less than expected under conditions favorable to attachment [5]. Other researchers have also noted MS2's relative hydrophobicity and demonstrated increased deposition when hydrophobic attachment sites are available [7].

Reported inactivation rates vary over several orders of magnitude and are not always directly comparable. Typical inactivation rate constants in groundwater microcosms at cool temperatures (below 10°C) are on the order of 10^{-2} to 10^{-1} day^{-1}. Contrary to the suggestion that reversible attachment may be protective, made by some researchers in an attempt to explain long persistence in field experiments, a study designed to compare surface and solution inactivation rates found that surface-associated inactivation rates for MS2 were at least an order of magnitude higher than those in solution, at least when iron oxides were present [8].

As reviewed in the introductory chapter, the literature is inconclusive on the magnitude and significance of many factors influencing viral inactivation. On average, warmer temperature and the presence of native microorganisms seem to increase viral inactivation, but reviewers have highlighted the need for research into interactive factors affecting virus survival, notably the linked effects of native microorganisms, dissolved oxygen levels, and mineral matrices [9].

In preparation for planned work investigating the influence of microbially-induced redox conditions on the inactivation rates, surface properties, and transport behavior of MS2 bacteriophage, we tested methods for culture and enumeration of MS2. Finding the precision of the enumeration protocol inadequate for our needs, we did not pursue the studies further. The protocol and an inactivation study done as a method test are documented in this appendix.

I.2 Methods

I.2.1 Generation of MS2 stock

Our laboratory stock of MS2 was propagated from a sample donated by Kellogg Schwab's lab (JHSPH) using a protocol adapted from that lab and based on EPA Method 1602. The bacterial host, *E. coli* F_{amp}, was purchased from the American Type Culture Collection (ATCC strain 700891). This strain exhibits resistance to both streptomycin and ampicillin and carries the "male" F plasmid. The host was inoculated into an Erlenmeyer flask containing 25 ml of Tryptic Soy Broth (Bacto) with 1% streptomycin (Sigma Aldrich) and 1% ampicillin (Fisher Biotech) and grown to log phase at 37°C with gentle shaking (110 rpm). A small volume (75 µl) of log-phase host was then combined with 100 µl of high-titer phage (~1.4E9 PFU/ml), mixed into 5 ml of molten 0.7% tryptic soy agar (TSA) with 1% strep/amp. The soft agar was poured onto a "hard" 1.5% TSA plate with 1% strep/amp and incubated at 37°C for 16-18hrs without inversion, to encourage confluent growth of the host and complete infection with phage. Several such plates were prepared in parallel.

The top layer of agar from each plate was harvested by scraping into a 50 ml conical tube, to which 23 ml each of sterile phosphate-buffered saline (PBS) and chloroform were added to lyse cell walls and release the phage. Tubes were vortexed for 5 minutes and then centrifuged (4000x *g*) for 30 minutes at 10°C. The supernatant containing phage particles was collected and filtered sequentially through 0.22 and 0.1 µm filters pre-treated with 0.1% Tween80 detergent (Sigma) to prevent phage attachment, and rinsed with PBS. A portion of the filtrate was set aside for enumeration

and the rest was distributed into portions of 1ml or less, and stored at -80°C until further use. Standard practices of sterile technique were applied at all times, with appropriate controls to verify the absence of contamination.

I.2.2 Enumeration

Whether to establish the titer of a stock solution or the concentration of phage in an experimental sample, enumerations were performed using a modified version of the double agar layer (DAL) procedure outlined in section 11 of EPA Method 1602. The method is very similar to the one used to generate MS2 stock. After serial dilution, a sample containing phage is mixed with a small volume of log-phase *E. coli* F_{amp} host in molten 0.7% TSA containing selective antibiotics (1% strep/amp). This soft agar layer is poured onto a "hard" 1.5% TSA plate with selective antibiotics and allowed to solidify, then inverted (to preserve separated viral plaques) and incubated overnight at 37°C. Each lysis zone in the bacterial lawn is assumed to represent an infection caused by a single phage particle. These plaques are counted by hand, and the phage titer of the original sample is reported as plaque-forming units (PFU) per ml. Samples are plated in triplicate at several dilutions to ensure that at least one dilution will be countable, with somewhere between 30 and 300 plaques per plate.

Our modifications to the DAL procedure were as follows:

- The 1:10 dilution series of samples for enumeration were done in PBS instead of TSB.
- Sample dilution series were prepared in polypropylene microcentrifuge tubes rather than in borosilicate glass test tubes.

- Dilutions were made in a total volume of 1 ml (100 μl sample + 900 μl PBS) for each member of the dilution series. When original sample volume was particularly limited, the initial dilution in the series was made in a total volume of 0.5 ml (50 μl sample + 450 μl PBS). The original protocol called for a total volume of 10 ml for each member of the dilution series.
- The volume of soft agar layer was reduced from 5 ml to 3 ml to improve mixing.
- The volumes of host and phage-containing sample added to the soft agar layer were reduced to 75 and 100 μl respectively.

I.2.3 Inactivation study

Three identical microcosms of MS2 phage in PBS were prepared in polypropylene tubes. The initial concentration was on the order of 10^6 PFU/ml. Each microcosm was stored in the dark at a different temperature (4, 23.5, or 30°C), and samples were removed and enumerated over the course of 12 days to monitor changes in MS2 concentration. For each time point, a single sample was withdrawn and serially diluted. Reported concentrations reflect the average of triplicate plating of a given dilution.

I.3 Results and discussion

I.3.1 Precision of the enumeration method

To quantify the precision of the DAL procedure, we calculated the relative standard deviation of the plaque count for each of 105 separate enumerations. Each enumeration is based on triplicate plates of the countable dilution, so the relative standard deviation of a given enumeration is the quotient of the average plaque count ($\bar{x}$) and the sample standard deviation (s_N) for three plates. The results are reported in Figure I-15.

The 95% confidence interval for the relative standard deviation of the DAL enumeration procedure was 0.16 ± 0.02 (i.e., about 16%).

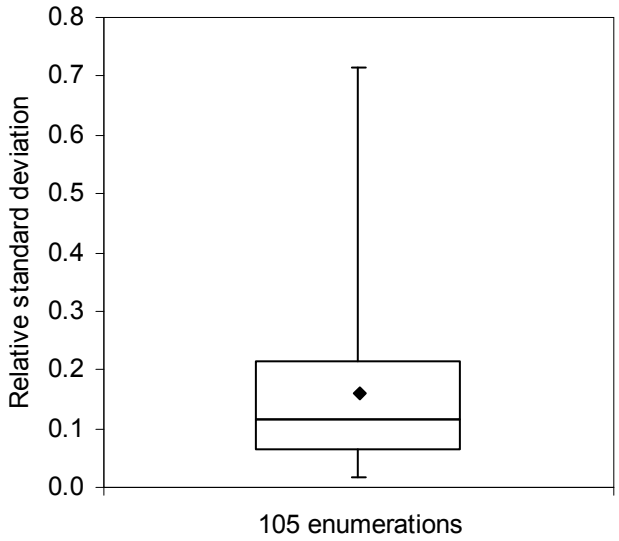

Figure I-15. Box-and-whisker plot of relative standard deviation across 105 triplicate enumerations. Mean (solid diamond): 0.16; Median: 0.12; Min: 0.02; Max: 0.71; Q1: 0.07; Q3: 0.21.

There were no obvious trends in relative standard deviation as a function of the number of dilutions required for enumeration (Figure I-16a), although the subset of data used to analyze the effects of dilution number had higher error on average (about 22%) compared to the full data set. It is likely that the accuracy of an enumeration is adversely affected by high dilution number, but there is no reason the precision should be, so these results were as expected.

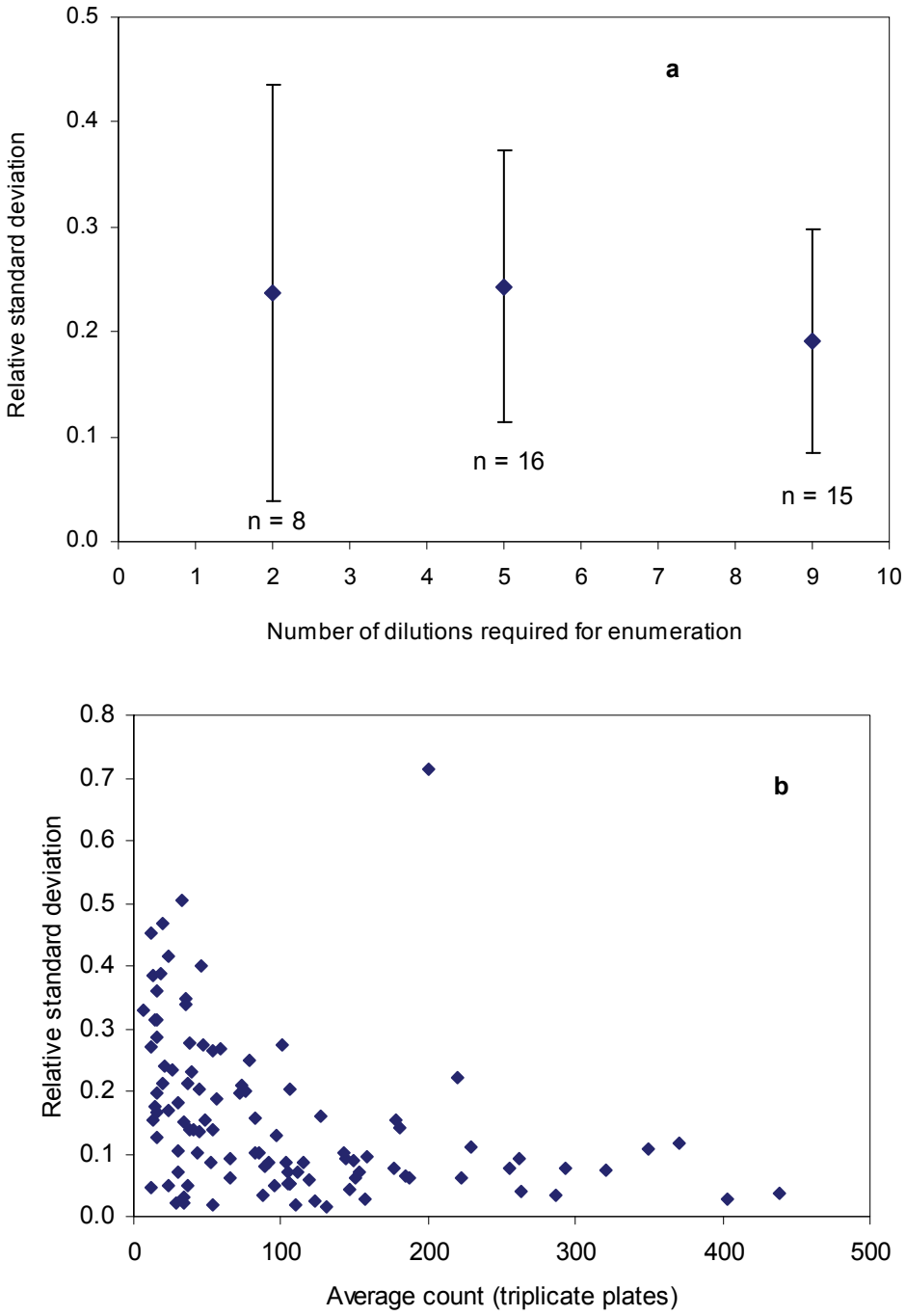

Figure I-16. Relative standard deviation as a function of (a) the number of serial dilutions required for enumeration or (b) the average number plaques across triplicate plates at the countable dilution. Error bars represent 95% confidence intervals with the number of observations noted at each dilution noted on the plot.

There was a clear relationship between relative error and the number of viral plaques counted: enumerations based on dilutions that yielded more than ~125 plaques

per plate on average across triplicate plates were more precise than those based on dilutions that plated out with smaller numbers of plaques (Figure I-15b). Unfortunately it is difficult to optimize the number of plaques that will form in the countable dilution of a sample of unknown concentration.

I.3.2 Inactivation study

Solution phase inactivation results are shown in Figure I-17. As reviewed in the introductory chapter, solution-phase inactivation is often observed to follow first-order kinetics, allowing estimation of the inactivation rate constant from the slope of the regression line through a plot of ln (C/C_o) versus time. A rate constant of 0.36 day^{-1} was observed at 22.5°C, in reasonable agreement with another solution-phase PBS study which found an initial inactivation rate constant of 0.12 day^{-1} at 25°C. As expected, inactivation was faster at 30°C, with a rate constant of 0.48 d^{-1}. However, the inactivation coefficient observed at 4°C (0.69 day^{-1}) was inexplicably faster still, and differed from the corresponding value reported in the literature (0.026 day^{-1} at 4°C) by more than an order of magnitude [10]. These inconsistent results are difficult to interpret, and all the more so because statistical testing indicates that all three of the slopes – and thus the inactivation rate coefficients – are statistically different at the P = 0.01 level. We cannot offer an explanation for why inactivation was apparently most rapid at the coldest temperature tested.

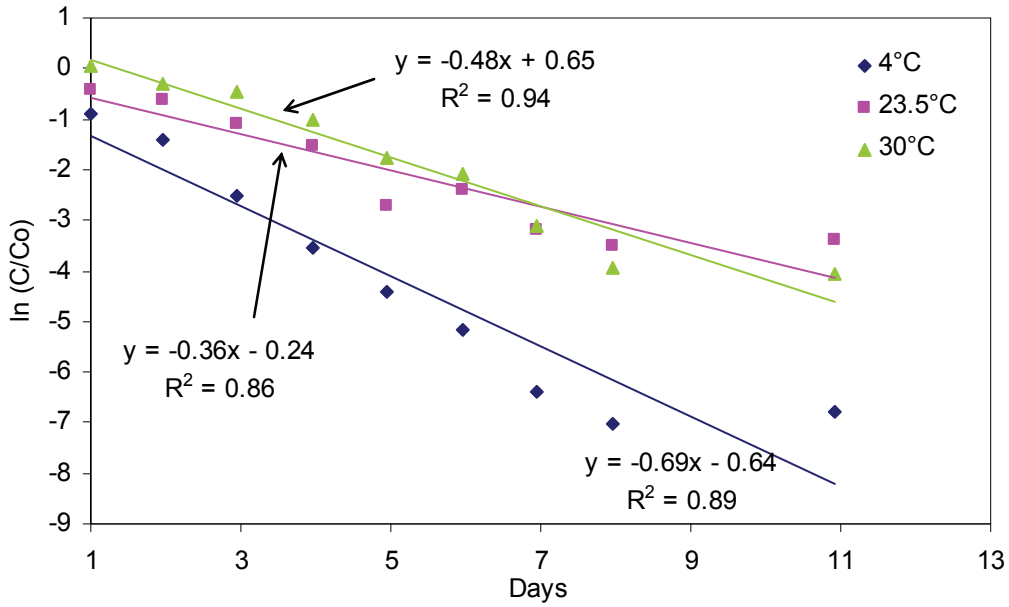

Figure I-17. Inactivation of MS2 in PBS at three temperatures.

Recent literature indicates that MS2 aggregates in PBS (pH 7.4, I ~160mM) but not in $NaHCO_3$ buffer solution [11]. Furthermore, insufficient purification of the phage stock may have contributed to aggregation. Instability of the solution-phase phage particles affects enumeration not only due to the potential inapplicability of the assumption that each plaque originates from a single phage, but also because phage aggregates may exhibit enhanced settling. Furthermore, aggregation could potentially be protective with respect to inactivation. As solution chemistry affects surface properties and potentially inactivation rates, additional purification steps (e.g., dialysis) may be necessary to generate a phage stock that is sufficiently homogeneous and well-controlled to be suitable for transport studies.

We determined that the low throughput and inherent variability of the DAL method made it unsuitable for the purposes our intended studies, which were likely to see only small shifts in count-based outcomes in response to experimental variables. When it

is possible to adapt them to the experimental design, quantitative molecular methods (e.g., qrtPCR) or even mass-based methods (e.g., QCMB) may offer better performance for transport and characterization studies of bacteriophages.

I.4 References

1. Schijven, J.F. and S.M. Hassanizadeh, *Removal of viruses by soil passage: Overview of modeling, processes, and parameters.* Critical Reviews in Environmental Science and Technology, 2000. 30(1): p. 49-127.
2. Strauss, J.H. and R.L. Sinsheimer, *Purification and properties of bacteriophage MS2 and of its ribonucleic acid.* Journal of Molecular Biology, 1963. 7(1): p. 43-54.
3. Golmohammadi, R., K. Valegard, K. Fridborg, and L. Liljas, *The refined structure of bacteriophage MS2 at 2.8 angstrom resolution.* Journal of Molecular Biology, 1993. 234(3): p. 620-639.
4. Valegard, K., L. Liljas, K. Fridborg, and T. Unge, *The three-dimensional structure of the bacterial virus MS2.* Nature, 1990. 345(6270): p. 36-41.
5. Penrod, S.L., T.M. Olson, and S.B. Grant, *Deposition kinetics of two viruses in packed beds of quartz granular media.* Langmuir, 1996. 12(23): p. 5576-5587.
6. Redman, J.A., S.B. Grant, T.M. Olson, M.E. Hardy, and M.K. Estes, *Filtration of recombinant Norwalk virus particles and bacteriophage MS2 in quartz sand: Importance of electrostatic interactions.* Environmental Science & Technology, 1997. 31(12): p. 3378-3383.
7. Bales, R.C., S.M. Li, K.M. Maguire, M.T. Yahya, and C.P. Gerba, *MS-2 and poliovirus transport in porous media - hydrophobic effects and chemical perturbations.* Water Resources Research, 1993. 29(4): p. 957-963.
8. Ryan, J.N., R.W. Harvey, D. Metge, M. Elimelech, T. Navigato, and A.P. Pieper, *Field and laboratory investigations of inactivation of viruses (PRD1 and MS2) attached to iron oxide-coated quartz sand.* Environmental Science & Technology, 2002. 36(11): p. 2403-2413.
9. John, D.E. and J.B. Rose, *Review of factors affecting microbial survival in groundwater.* Environmental Science & Technology, 2005. 39(19): p. 7345-7356.
10. Anders, R. and C.V. Chrysikopoulos, *Evaluation of the factors controlling the time-dependent inactivation rate coefficients of bacteriophage MS2 and PRD1.* Environmental Science & Technology, 2006. 40(10): p. 3237-3242.
11. Yuan, B.L., M. Pham, and T.H. Nguyen, *Deposition kinetics of bacteriophage MS2 on a silica surface coated with natural organic matter in a radial stagnation point flow cell.* Environmental Science & Technology, 2008. 42(20): p. 7628-7633.

Curriculum Vitae

Jessica's interest in the environmental engineering and the human relationship with the natural world dates to her childhood in the Rockies. Born in Montana in 1981, she grew up a few miles from Glacier National Park. After completing her bachelor's degree in environmental engineering at Yale University, she was awarded a Rotary Ambassadorial Fellowship to the University of Paris VIII Vincennes–St-Denis, where she earned a *licence* in geography with a focus on environmental management. A move from Paris to Baltimore brought Jessica to the Department of Geography and Environmental Engineering at Johns Hopkins University, where she completed first her MSE and then her dissertation under the guidance of Dr. Edward J. Bouwer.